

THE DESIGN OF NOVEL STRONG, STIFF AND
TOUGH COMPOSITE SYSTEMS USING THE
SHEAR-LAG ANALYSIS AND HALPIN-TSAI
MODELS

ISAIAH FASANYA

A thesis submitted in partial fulfilment of the requirements of Nottingham
Trent University for the degree of Doctor of Philosophy

February 2021

Abstract

Composite materials have gained wide applications, including advanced technology and engineering applications. This is primarily due to many advantages composite materials provides which include specific strength and specific modulus. Strength, stiffness (modulus) and toughness are often desired in composite materials. However, strength and toughness are mutually exclusives; therefore, the challenge to retain these trio-mechanical properties in composite materials without sacrificing one for another have proved daunting. Contrary to human-made material is nacre which is a natural existing type of composite material that have been able to circumvent the challenge and retained the trio mechanical properties. Taking into consideration existing composite reinforcement technologies, fibre reinforcement and nanocomposite which have evolved and adapted to various applications yet to achieve composite material that is sufficiently strong and stiff while maintaining toughness. Therefore, through modelling analysis, this research assesses the feasibility of fabricating composite material with enhanced strength and stiffness while maintaining toughness. An approach which involves identifying an ideal type of reinforcement filler with adequate strength and stiffness to enhance composite material which could be manoeuvred such that the reinforcement filler aspect ratio is within proximity to the composite material system critical aspect ratio for toughness to be maintained.

Acknowledgements

I would like to show my unreserved thanks to my supervisors, Dr Fengge Gao and Prof Carl Brown for their input, guidance, advice and support towards this research.

Also, I would like to thank Prof Mary O'Neill and Dr Karen Moss for your support, I do appreciate.

To you Dad, like you knew that I will need those encouraging words which you often encourage me with, I never knew it will be sooner than expected but no doubt that those words give me needed strength every time I remember, THANK YOU, DAD.

To my Mum and siblings, your encouragement and constant support mean so much to me.

My unreserved appreciation to Mr Tubo Okusanya and family, your support and kind gesture means a lot to me.

To my fiancée, Motolani Sobanwa and family, thank you for the care, encouragements and support.

I would like to thank the technical staff and my colleagues for all the help and support.

To friends and colleagues who have not been mentioned, thank you.

Above all, my uttermost appreciation to God Almighty for His grace and preservation.

Table of Contents

List of Figure	vi
List of Tables	xiv
1.0 Introduction	1
1.1 Background of the research	1
1.2 Research aims	7
2.0 Literature survey	9
2.1 Polymer and its composite system	10
2.1.1 Polymer matrices	11
2.2 Reinforcement fibres and fillers	19
2.2.1 Carbon fibre	19
2.2.2 Glass fibre.....	26
2.2.3 Glass flakes.....	31
2.2.4 Graphene	34
2.2.5 Carbon nanotubes.....	36
2.2.6 Clay – montmorillonite (MMT)	39
2.3 Reinforcement of composite systems and limitations associated with current technologies... 41	
2.3.1 Limitation of fibre reinforcement technology to develop strong, stiff and tough composite material	42
2.3.2 Shortfall of nanocomposite technology in developing strong, stiff, and tough composite material.....	49

2.3.3 Current progress on toughness enhancement mechanism to develop strong, stiff, and tough materials	53
2.4 Bio-inspired composite in developing strong, stiff and tough materials such as nacre	56
2.5 Composite modelling	59
3.0 Methodology.....	62
3.1 Material characterisation – Glass flakes	62
3.1.1 Size Characterisation – Thickness Measurement	63
3.1.2 Size Distribution – Length Measurement	63
3.2 Modelling Work	64
3.2.1 Glass fibre/glass flakes tensile strength and tensile modulus	65
3.2.2 Carbon fibre tensile strength and modulus	70
3.2.3 Investigated nanofillers tensile strength and tensile modulus.....	73
3.2.4 Polymer tensile strength and tensile modulus	73
3.2.5 Interfacial shear strength (IFSS)	74
4.0 Result and Discussion.....	77
4.1 Investigation of suitable fillers for the new composite in practical application.....	79
4.1.1 Glass flakes thickness measurement	79
4.1.2 Glass flakes Length measurement	84
4.2 Computation of modelling work and analysis	95
4.2.1 Determination of critical aspect ratio for various glass flakes used as reinforcement filler for different composite material systems	101

4.2.2 Modelling of mechanical properties of glass flake reinforced polymer composites with tough fracture	105
4.2.3 Modelling analysis of fibre reinforced composites.....	145
4.2.4 Modelling analysis of composites reinforced with nanofillers	152
5.0 Conclusion.....	162
6.0 Future work.....	164
References	165

List of Figures

Figure 1: (a) Typical reactive epoxy group, (b) an idealised epoxy resin chemical structure. Adapted from ref [59].....	12
Figure 2: Nylon 6 chemical structure illustrates ring opening of caprolactam. Adapted from Ref [73]	16
Figure 3: Chemical structure illustration for polyethylene. Adapted from Ref [86].....	16
Figure 4: Illustration of polymer chain structure for different types of polypropylene, adapted from ref [94]	19
Figure 5: Illustration of process involved in fabrication of carbon fibre	22
Figure 6: (a) Tensile strength and (b) tensile modulus as a function of heat treatment temperature of PAN and pitch carbon fibre during carbonisation and graphitisation processes. Adapted from Ref [104]	23
Figure 7: Progressive development of aromatic sheets during carbonisation/graphitisation with increase in heating treatment temperature for carbon fibre fabrication. Adapted from Ref [100]	25
Figure 8: Melt process of producing glass fibre	30
Figure 9: Schematic illustration of (a) an armchair nanotube, (b) a zig-zag nanotube, and (c) a chiral nanotube. Adapted from Ref [135].....	37
Figure 10: Schematic model illustration of (A) Russian doll multi-walled carbon nanotube (B) sketch of Russian doll layer arrangement and (C) Parchment model layer arrangement of multi-walled carbon nanotube. Adapted from Ref [140].....	38
Figure 11: Schematic illustration of octahedral and tetrahedral sheets arrangement of montmorillonite nanoclay layer. Adapted and modified from Ref [147]	41
Figure 12: Illustration of embedded silicate clay layers for polymer reinforcement. Adapted from Ref [147].....	52
Figure 13: Schematic structure of nacre showing its brick and mortar arrangement aragonite platelets in organic matrix. Adapted from Ref [206]	57

Figure 14: (a) Stress-strain curve of fractured hydrated and dried nacre, (b) debonding of polygonal aragonite platelet at the boundary with the organic matrix without platelet fracture and (c) pulled out platelets. Adapted from Ref [206]	58
Figure 15: FT-IR profile for investigated glass flakes (350nm milled).....	66
Figure 16: FT-IR analysis of E glass (a) nonsilanised (surface untreated) and (b) silane treated. Adapted from Ref [222].....	66
Figure 17: E-glass strength plotted against fibre diameter. Adapted from Ref [224]	68
Figure 18: E-glass modulus plotted against fibre diameter. Adapted from Ref [225]	68
Figure 19: Log-plot for E-glass strength plotted against fibre diameter.....	69
Figure 20: Log-plot for E-glass modulus plotted against fibre diameter	69
Figure 21: Log-plot for carbon fibre strength plotted against fibre diameter.....	71
Figure 22: Log-plot for carbon fibre modulus plotted against fibre diameter	72
Figure 23: Interfacial shear strength value for specified matrix systems with E-glass.....	75
Figure 24: Interfacial shear strength value for specified matrix systems with carbon fibre	76
Figure 25: SEM image illustration of 2.3 - 3.3 μ m glass flakes.....	80
Figure 26: SEM image illustration of 0.8-1.3 μ m glass flakes	80
Figure 27: SEM image illustration of 850nm unmilled glass flakes.....	81
Figure 28: SEM image illustration of 850nm milled glass flakes.....	81
Figure 29: SEM image illustration of 350nm unmilled glass flakes.....	82
Figure 30: SEM image illustration of 350nm milled glass flakes.....	82
Figure 31: SEM image illustration of 100nm milled glass flakes.....	83
Figure 32: Image illustration of dispersed glass flakes on microscope slide taken using optical microscope.....	84
Figure 33: Glass flakes length are determined by measuring two longest separated points on the glass flakes perimeter	85
Figure 34: Dot plot for 350nm milled glass flakes measured length	86

Figure 35: Fit test analysis using Minitab to determine adequate statistic applicable to process measured length distribution	87
Figure 36: Log-normal distribution of 350nm milled glass flakes	87
Figure 37: Balled milled aspect ratio with respect to time - 100nm milled glass flakes.....	90
Figure 38: Balled milled aspect ratio with respect to time - 350nm milled glass flakes.....	91
Figure 39: Balled milled aspect ratio with respect to time - 350nm unmilled glass flakes	92
Figure 40: Balled milled aspect ratio with respect to time - 850nm milled glass flakes.....	93
Figure 41: Balled milled aspect ratio with respect to time - 850nm unmilled glass flakes	94
Figure 42: Balled milled aspect ratio with respect to time - 0.8 - 1.3 μ m glass flakes	95
Figure 43: Schematic illustration of representative volume element of composite material. Adapted from Ref [260].....	96
Figure 44: Application of Rule of Mixture model for analysing composite material system	96
Figure 45: Illustration of composite material failure depending on reinforcement filler aspect ratio whether it is higher or lower than the composite material system critical aspect ratio. Adapted from Ref [26].....	98
Figure 46 Influence of glass flakes thickness on critical aspect ratio for Epoxy at different interfacial shear strength.....	103
Figure 47: Influence of glass flakes thickness on critical aspect ratio for Polypropylene at different interfacial shear strength.....	103
Figure 48: Influence of glass flakes thickness on critical aspect ratio for Nylon 6 at different interfacial shear strength.....	104
Figure 49: Influence of glass flakes thickness on critical aspect ratio for Polyethylene at different interfacial shear strength.....	104
Figure 50: Effect of varied glass flakes thickness on composite strength at 60% wt. for Epoxy matrix	107

Figure 51: Effect of varied glass flakes thickness on composite strength at 60% wt. for Polypropylene matrix.....	107
Figure 52: Effect of varied glass flakes thickness on composite strength at 60% wt. for Nylon 6 matrix	108
Figure 53: Effect of varied glass flakes thickness on composite strength at 60% wt. for Polyethylene matrix.....	108
Figure 54: Effect of varied glass flakes thickness on composite modulus at 60% wt. for Epoxy matrix	109
Figure 55: Effect of varied glass flakes thickness on composite modulus at 60% wt. for Polypropylene matrix.....	110
Figure 56: Effect of varied glass flakes thickness on composite modulus at 60% wt. for nylon 6 matrix	110
Figure 57: Effect of varied glass flakes thickness on composite modulus at 60% wt. for Polyethylene matrix.....	111
Figure 58: Effect of varied aspect ratio on composite strength of glass flakes / Nylon 6 - GF 0.8 - 1.3 μ m at 60% wt.	112
Figure 59: Effect of varied aspect ratio on composite modulus of glass flakes / Nylon 6 - GF 0.8 - 1.3 μ m at 60% wt.	113
Figure 60: Effect of varied aspect ratio on composite strength of glass flakes / Nylon 6 - GF 850nm M at 60% wt.	113
Figure 61: Effect of varied aspect ratio on composite modulus of glass flakes / Nylon 6 - GF 850nm M at 60% wt.	114
Figure 62: Effect of varied aspect ratio on composite strength of glass flakes / Nylon 6 - GF 850nm UM at 60% wt.	114
Figure 63: Effect of varied aspect ratio on composite modulus of glass flakes / Nylon 6 - GF 850nm UM at 60% wt.	115

Figure 64: Effect of varied aspect ratio on composite strength of glass flakes / Nylon 6 - GF 350nm M at 60% wt.	115
Figure 65: Effect of varied aspect ratio on composite modulus of glass flakes / Nylon 6 - GF 350nm M at 60% wt.	116
Figure 66: Effect of varied aspect ratio on composite strength of glass flakes / Nylon 6 - GF 350nm UM at 60% wt.	116
Figure 67: Effect of varied aspect ratio on composite modulus of glass flakes / Nylon 6 - GF 350nm UM at 60% wt.	117
Figure 68: Effect of varied aspect ratio on composite strength of glass flakes / Nylon 6 - GF 100nm M at 60% wt.	117
Figure 69: Effect of varied aspect ratio on composite modulus of glass flakes / Nylon 6 - GF 100nm M at 60% wt.	118
Figure 70: Effect of varied aspect ratio on composite strength of glass flakes / Polypropylene - GF 0.8 - 1.3 μ m at 60% wt.	118
Figure 71: Effect of varied aspect ratio on composite modulus of glass flakes / Polypropylene - GF 0.8 - 1.3 μ m at 60% wt.	119
Figure 72: Effect of varied aspect ratio on composite strength of glass flakes / Polypropylene - GF 850nm M at 60% wt.	119
Figure 73: Effect of varied aspect ratio on composite modulus of glass flakes / Polypropylene - GF 850nm M at 60% wt.	120
Figure 74: Effect of varied aspect ratio on composite strength of glass flakes / Polypropylene - GF 850nm UM at 60% wt.	120
Figure 75: Effect of varied aspect ratio on composite modulus of glass flakes / Polypropylene - GF 850nm UM at 60% wt.	121
Figure 76: Effect of varied aspect ratio on composite strength of glass flakes / Polypropylene - GF 350nm M at 60% wt.	121

Figure 77: Effect of varied aspect ratio on composite modulus of glass flakes / Polypropylene - GF 350nm M at 60% wt.	122
Figure 78: Effect of varied aspect ratio on composite strength of glass flakes / Polypropylene - GF 350nm UM at 60% wt.	122
Figure 79: Effect of varied aspect ratio on composite modulus of glass flakes / Polypropylene - GF 350nm UM at 60% wt.	123
Figure 80: Effect of varied aspect ratio on composite strength of glass flakes / Polypropylene - GF 100nm M at 60% wt.	123
Figure 81: Effect of varied aspect ratio on composite modulus of glass flakes / Polypropylene - GF 100nm M at 60% wt.	124
Figure 82: Effect of varied aspect ratio via ball milling on composite strength for glass flakes / Epoxy - GF 0.8 - 1.3 μ m at 60% wt.	124
Figure 83: Effect of varied aspect ratio via ball milling on composite modulus for glass flakes / Epoxy - GF 0.8 - 1.3 μ m at 60% wt.	125
Figure 84: Effect of varied aspect ratio via ball milling on composite strength for glass flakes / Epoxy - GF 850nm M at 60% wt.	125
Figure 85: Effect of varied aspect ratio via ball milling on composite modulus for glass flakes / Epoxy - GF 850nm M at 60% wt.	126
Figure 86: Effect of varied aspect ratio via ball milling on composite strength for glass flakes / Epoxy - GF 850nm UM at 60% wt.	126
Figure 87: Effect of varied aspect ratio via ball milling on composite modulus for glass flakes / Epoxy - GF 850nm UM at 60% wt.	127
Figure 88: Effect of varied aspect ratio via ball milling on composite strength for glass flakes / Epoxy - GF 350nm M at 60% wt.	127
Figure 89: Effect of varied aspect ratio via ball milling on composite modulus for glass flakes / Epoxy - GF 350nm M at 60% wt.	128

Figure 90: Effect of varied aspect ratio via ball milling on composite strength for glass flakes / Epoxy - GF 350nm UM at 60% wt.	128
Figure 91: Effect of varied aspect ratio via ball milling on composite modulus for glass flakes / Epoxy - GF 350nm UM at 60% wt.	129
Figure 92: Effect of varied aspect ratio via ball milling on composite strength for glass flakes / Epoxy - GF 100nm M at 60% wt.....	129
Figure 93: Effect of varied aspect ratio via ball milling on composite modulus for glass flakes / Epoxy - GF 100nm M at 60% wt.....	130
Figure 94: Effect of varied aspect ratio on composite strength of glass flakes / Polyethylene - GF 0.8 - 1.3 μ m at 60% wt.	130
Figure 95: Effect of varied aspect ratio on composite modulus of glass flakes / Polyethylene - GF 0.8 - 1.3 μ m at 60% wt.	131
Figure 96: Effect of varied aspect ratio on composite strength of glass flakes / Polyethylene - GF 850nm M at 60% wt.	131
Figure 97: Effect of varied aspect ratio on composite modulus of glass flakes / Polyethylene - 850nm M at 60% wt.	132
Figure 98: Effect of varied aspect ratio on composite strength of glass flakes / Polyethylene - GF 850nm UM at 60% wt.	132
Figure 99: Effect of varied aspect ratio on composite modulus of glass flakes / Polyethylene - 850nm UM at 60% wt.	133
Figure 100: Effect of varied aspect ratio on composite strength of glass flakes / Polyethylene - GF 350nm UM at 60% wt.	133
Figure 101: Effect of varied aspect ratio on composite modulus of glass flakes / Polyethylene - 350nm UM at 60% wt.	134
Figure 102: Effect of varied aspect ratio on composite strength of glass flakes / Polyethylene - GF 350nm M at 60% wt.....	134

Figure 103: Effect of varied aspect ratio on composite modulus of glass flakes / Polyethylene - 350nm M at 60% wt.	135
Figure 104: Effect of varied aspect ratio on composite strength of glass flakes / Polyethylene - GF 100nm M at 60% wt.	135
Figure 105: Effect of varied aspect ratio on composite modulus of glass flakes / Polyethylene - 100nm M at 60% wt.	136
Figure 106: Composite strength at critical aspect ratio for different thickness of glass flakes at 60% wt. for Epoxy matrix.....	138
Figure 107: Composite modulus at critical aspect ratio for different thickness of glass flakes at 60% wt. for Epoxy matrix.....	138
Figure 108: Composite strength at critical aspect ratio for different thickness of glass flakes at 60% wt. for Polypropylene matrix	139
Figure 109: Composite modulus at critical aspect ratio for different thickness of glass flakes at 60% wt. for Polypropylene matrix	139
Figure 110: Composite strength at critical aspect ratio for different thickness of glass flakes at 60% wt. for Nylon 6 matrix	140
Figure 111: Composite modulus at critical aspect ratio for different thickness of glass flakes at 60% wt. for Nylon 6 matrix	140
Figure 112: Composite strength at critical aspect ratio for different thickness of glass flakes at 60% wt. for Polyethylene matrix	141
Figure 113: Composite modulus at critical aspect ratio for different thickness of glass flakes at 60% wt. for Polyethylene matrix	141
Figure 114: Equivalent volume fraction plotted against percentage weight load for different reinforcement - Epoxy	156

List of Tables

Table 1: Polyethylene mechanical properties, adapted from ref [88].....	17
Table 2: Compositions by percentage weight for typical glass fibres, extracted and adapted from ref [111].....	27
Table 3: Using layer-by-layer to increase nanofiller (Montmorillonite) in poly(vinyl alcohol). Adapted from Ref [42].....	52
Table 4: Mechanical properties of carbon fibre. Adapted from Ref [54]	71
Table 5: Nanofillers mechanical and physical properties	73
Table 6: Matrix mechanical properties used in computing modelling of composite material system mechanical properties (for epoxy and polypropylene data given in range, therefore mean value used. * indicate average value).....	73
Table 7: Interfacial shear strength (IFSS) value range for different matrix systems with E-glass	74
Table 8: Interfacial shear strength (IFSS) value range for different matrix systems with carbon fibre.	75
Table 9 Thickness measurement of each glass flakes investigated	83
Table 10: Average length measured for each glass flakes investigated before ball milling	88
Table 11: Average aspect ratio determined for each glass flakes investigated before ball milling	88
Table 12: Average aspect ratio determined for 100nm milled glass flakes at different milling time duration.....	89
Table 13: Average aspect ratio determined for 350nm milled glass flakes at different milling time duration.....	90
Table 14: Average aspect ratio determined for 350nm unmilled glass flakes at different milling time duration.....	91
Table 15: Average aspect ratio determined for 850nm milled glass flakes at different milling time duration.....	92
Table 16: Average aspect ratio determined for 850nm unmilled glass flakes at different milling time duration.....	93

Table 17: Average aspect ratio determined for 0.8 - 1.3 μ m glass flakes at different milling time duration	94
Table 18: Mechanical properties of glass flakes at their known thickness.....	101
Table 19: Required critical aspect ratio on glass flakes for various matrix systems at different interfacial shear strength.....	102
Table 20: Comparison of average aspect ratio measured ((S) in yellow column) with critical aspect ratio (Sc) for different matrices to determine applicable fraction term (α).....	105
Table 21: Comparison of composite strength and modulus at average aspect ratio to critical aspect ratio for Epoxy matrix system	142
Table 22: Comparison of composite strength and modulus at average aspect ratio to critical aspect ratio for Polypropylene matrix system	143
Table 23: Comparison of composite strength and modulus at average aspect ratio to critical aspect ratio for Nylon 6 matrix system	143
Table 24: Comparison of composite strength and modulus at average aspect ratio to critical aspect ratio for Polyethylene matrix system.....	144
Table 25: Comparison of composite material mechanical properties for glass fibre to glass flakes under tough fracture for Epoxy matrix.....	145
Table 26: Comparison of composite material mechanical properties for glass fibre to glass flakes under tough fracture for Polypropylene matrix.....	146
Table 27: Comparison of composite material mechanical properties for glass fibre to glass flakes under tough fracture for Nylon 6 matrix.....	146
Table 28: Comparison of composite material mechanical properties for glass fibre to glass flakes under tough fracture for polyethylene matrix	146
Table 29: Comparison of composite material mechanical properties for carbon fibre to glass flakes under tough fracture for Epoxy matrix.....	148

Table 30: Comparison of composite material mechanical properties for carbon fibre to glass flakes under tough fracture for Polypropylene matrix	148
Table 31: Comparison of composite material mechanical properties for carbon fibre to glass flakes under tough fracture for Nylon 6 matrix	148
Table 32: Comparison of composite material mechanical properties for carbon fibre to glass flakes under tough fracture for Polyethylene matrix.....	149
Table 33: Mechanical properties reported for some fibre reinforced composite materials.....	151
Table 34: Composite material mechanical properties of Epoxy with different nanofillers.....	152
Table 35: Composite material mechanical properties of Polypropylene with different nanofillers ..	153
Table 36: Composite material mechanical properties of Nylon 6 with different nanofillers	153
Table 37: Composite material mechanical properties of Polyethylene with different nanofillers	153
Table 38: Mechanical properties of some reported nanocomposites.....	160

1.0 Introduction

Strength, stiffness, and toughness are mechanical properties highly desired in most materials for diverse applications. This research explores the feasibility of producing composite materials with high strength and stiffness, while the toughness is maintained through modelling.

1.1 Background of the research

The need for lightweight materials that are strong, stiff, and tough continues to be driven by the desire to improve performance and efficiency, which provides socio-economic benefits. For most engineering and technological applications, materials are to have high strength, stiffness, and toughness. While the trio mechanical properties (strength, stiffness, and toughness) are often desired in a material, advancements in technology and engineering have also shown the importance of such materials to have low density. In essence, a material that is lightweight yet possesses high tensile strength, stiffness, and toughness. For instance, in modern aircraft, weight reduction has been the main driving force of innovation in the aerospace industry to improve fuel efficiency, performance, and range without compromising safety, [1]. The socio-economic benefits of having aircraft with less weight include the ability to make nonstop flights while carrying more passengers which in return make the cost of air travel cheaper. Also, aircraft with lesser weight yields better fuel efficiency and reduce pollution due to emission, which is better for the environment [1], [2], [3].

Similarly, transportation is crucial to present-day development; meanwhile, the transportation industry is regarded as one of the top four contributors causing global warming and climate change due to greenhouse gas release through emission [4]. In the effort to

mitigate the effect of global warming and climate change, the automotive industry particularly car manufacturers are required to reduce car emission and by so doing also helps to combat poor air quality and generally improve public health [5], [6], [7]. Considering that the energy required to power a car depends on the car weight, car manufacturers need to make the car lighter by reducing bodyweight without compromising the structural integrity of cars. Hence the need for a lightweight material that is sufficiently strong, stiff, and tough to save car buyers money as more distance can be covered. Also, energy provides fundamental socio-significance to present-day development while the future also depends on it. Considerably, energy penetrates all facets of life directly or indirectly. Almost day-to-day activities and critical features of social structures are driven by energy availability and the technical know-how to convert the energy available into the usable form [8]. Whilst electricity is one of the main forms of energy consumed, which is generated from various sources but largely from combustible fuels, i.e. fossil fuels which is detrimental to the environment due to greenhouse gas emissions [9], [10]. Hence the need for an alternative electricity generation source through renewable energy sources such as wind power which use turbine blades manufactured from strong, stiff, tough, and lightweight material designed to meet required aerodynamic performance and structural challenges [11], [12]. Sporting activities like bicycle racing tournaments often take advantage of high power to weight ratio considering that lap-time is of importance by using lightweight materials. Nevertheless, such advantage is irrelevant if the material used for fabrication experience unwanted or excessive deformation, hence impeding aerodynamical performance and efficiency but could be overcome provided that the material is sufficiently stiff and maintain good strength and toughness [13]. Also, strong, stiff and tough, lightweight materials such as biocomposite materials are used for various applications, including dental, maxillofacial, skeleton / orthopaedic applications [14],

[15]. For example, in addition to biocompatibility requirements for biocomposites materials such as the orthopaedic application, material mechanical properties (strength, stiffness, and fracture toughness) are of importance to ensure that the biocomposites material is capable of providing the needed support. In bone replacement, it is expected that the biocomposites material would have strength and stiffness like bone or higher while maintaining good fracture toughness, considering that exerted load on skeletal structures can be enormous. Typically, load on a hip joint is 3.5 times the bodyweight for slow walking, which could increase to about nine times body weight when stumbled, while for the knee is about 2 to 2.5 times bodyweight during normal activities [14].

Briefly discussed above is the need for materials to possess adequate strength, stiffness, and toughness with low density for some highlighted applications. While the use of metallic materials, i.e. engineering alloys shows that such materials meet mechanical properties requirements. However, heavyweight characterised with such metallic materials is becoming prohibitive when compared to composite materials, considering that composite materials possess high specific strength and specific stiffness [1], [2], [16]. However, the ability to develop a composite material that possesses the trio mechanical properties (strength, stiffness, and toughness) within a single material system has remained to be a challenge to material scientists and researchers. Meanwhile, natural materials like nacre and bone have been able to circumvent the challenge of retaining the trio mechanical properties [17]. But for synthesised materials such as polymer composite materials which use high strength and high modulus filler (i.e. fibres, whiskers, and platelets) to reinforce weak and tough polymer matrix [16], [18], [19]. Results obtained from these materials often show improvement of some but not all of these properties with the current state-of-the-art technologies, i.e. fibre composite [20], [21] and nanocomposite [22], [23], [24], [25], [26]. Considering that stiffness

and strength often come together, but strength and toughness are properties that are generally mutually exclusive of each other [27]. Therefore, resulting in the enhancement of composite material strength and stiffness, while toughness is often compromised and vice versa [17].

Considering the need for lightweight material to be strong, stiff, and tough, material scientists and researchers continue to intensify effort by trying out various approaches and material systems developed over time. Consequently, fibre reinforcement technology has been developed and applied for the fabrication of composite materials. Most fibres employed in fabricating composite materials are often synthetic fibres, i.e. glass, carbon, aramid, polyethylene, etc. [28], [29]. Ordinarily, fibres in bulk form are weak and do not have high strength and stiffness for applications that require such mechanical properties for reinforcement. However, having the bulk form transformed into fibre form reduces defects and invariably increases strength and stiffness [30]. Nevertheless, for some fibres, comparing their strength and stiffness to their theoretical values, the fibres' strength and stiffness are still well below their theoretical values. For instance, graphene is reported to have an in-plane theoretical tensile strength of 100 GPa and tensile modulus (stiffness) of 1 TPa [31]. Though high strength carbon fibre has a microstructural arrangement as graphene, carbon fibres still exhibit tensile strength less than 10% of the theoretical value. Considering that carbon fibre available with the highest tensile strength, i.e. poly-acrylonitrile (PAN) carbon fibre has about 7 GPa tensile strength and tensile modulus of about 30%. While available high modulus carbon fibre could reach 90% theoretical value of the tensile modulus but have a tensile strength of about 2%, i.e. pitch carbon fibre. Thus, carbon fibres are produced in either high strength or high modulus [31], [32]. While these fibres possess high strength and stiffness along the fibre direction but are lacking in failure strain and are prone to breakage, therefore

are not sufficient to be used on their own for most engineering and technological applications. However, embedding the fibres within matrix systems known to have high failure strain but low strength and stiffness such as seen with fibre reinforced composite material. Therefore, with such a combination of fibre and matrix, composite materials are developed with improved properties [16], [30].

Fibre-reinforced composite materials are anisotropic in their design and can fully utilise the mechanical properties the fibre possesses when tensile stress is applied to the composite material along the fibre length direction. The material failure occurs at the fibre's failure strain, provided the composite material has a fibre volume fraction that is sufficiently high [30], considering that for a composite material with fibres embedded in a matrix system, when fibre breaks, redistribution of stress is controlled by the matrix. The load is transferred from the broken fibre to the next fibre within the broken fibre's vicinity via the fibre/matrix interface. Accumulation of these fibre failures increases stress concentration, thereby causes the composite material to fail at the fibre strain, therefore resulting in a brittle failure [33] [34]. In the effort to maintain toughness within a fibre reinforced composite system, different approaches have been taken including the use of elastomers like nitrile rubber as part of the composite system, but this has not been effective as the strength and stiffness of the composite material is compromised [35], [36]. Likewise, fibre composites are often produced as multi-direction materials, i.e. laminates. However, such materials are susceptible to interlaminar damage such as delamination which affects the composite materials' mechanical properties adversely, with fibres aligned in the laminate plane and not reinforcing the laminate thickness. Laminated composite ply could fail due to matrix cracks and delamination linking together to produce a fracture surface without the need for fibre breakage [37]. Several techniques have been developed particularly reinforcement of the through-thickness

of laminated composite materials, including stitching to improve damage tolerance to enhance fracture toughness and improve mechanical properties in the through-thickness direction of multi-direction laminated composite materials [38]. Stitching involves the use of high-tensile strength sewing yarn like carbon, glass, or Kevlar to reinforce the composite in the through-thickness direction using an industrial sewing machine [39], [40]. However, while stitching apparently could reinforce the through-thickness direction, there are concerns on in-plane mechanical properties reducing as a result of such technique due to fibre damage caused by stitch needle and fracture due to stitching fibre friction [39], [41].

Though fibre reinforced composites are widely used for various engineering and technological applications, but considering all indications, it is plausible to consider that fibre, and fibre reinforcement technology is limited in achieving composite material that is strong, stiff, and tough concurrently and this has contributed to the development of nanocomposite. However, composite reinforcement is a function of reinforcement filler volume fraction. Fibre-reinforced composite materials are reported at low volume fraction to have poor reinforcement efficiency. On the contrary, nanocomposite materials have been reported to exhibit improved mechanical performance at low volume fraction with nanofiller, i.e. exfoliated nanoclay used as reinforcement filler with less than 10% wt. [23]. Nanocomposite materials provide better reinforcement efficiency at low volume fraction compared to fibre reinforced composite material. Then again, since reinforcement efficiency is dependent on reinforcement filler volume fraction, fibre reinforced composite material provides better reinforcement efficiency at high volume fraction compared to nanocomposite with a low volume fraction of reinforcement filler [23]. Fabrication of high filler volume nanocomposite without adopting adequate fabrication process yield composites with the fillers agglomerating, resulting in nanocomposite with low mechanical properties. However,

adopting an adequate fabrication process to increase the reinforcement filler volume fraction in the nanocomposite, i.e. using a bottom-up method like layer by layer approach, the nanocomposite strength and stiffness enhances due to increase in volume fraction and high aspect ratio of the nano-filler, but the toughness is significantly reduced thereby causing the material to fail in a brittle manner [23], [42].

Whilst nature could harness the trio mechanical properties in a single material system such as gastropod, bone, and nacre with about 95%wt. CaCO_3 reinforcement filler and 5%wt. organic matrix. Material scientist and researcher have tried to replicate structural arrangement in natural materials that can maintain the trio mechanical properties within a material system, i.e. nacre inspired composites but are yet to have a breakthrough [43], [44] [45]. Different methods of composite fabrication have been developed, including the use of elastomers [46], reinforcement of composite through-thickness [38] and incorporation of nano-filler in fibre reinforcement [47], but the challenge remains which is the ability to have a composite material system with sufficient high strength, stiffness and toughness maintained the same time.

1.2 Research aims

To mitigate the limitations associated with fibre reinforcement and nanocomposites technologies. This research is to design reinforcement technology that will overcome shortcomings associated with both fibre reinforced composites and nanocomposites to achieve comprehensive improvement of strength, stiffness, and toughness at the same time. The aim is to design new reinforcement material with a rational analysis of its potential in reinforcement with commodity polymers. This involves investigating suitable reinforcing fillers for the new composite system by considering glass flakes as model fillers to explore the

potential properties that can be achieved in the new composite design with polypropylene, polyethylene, nylon 6, and epoxy using existing models. Thus, providing rational analysis in comparison with other types of available reinforcement fillers to establish the deficiency of current technologies of fibres and nanofillers in achieving strong, stiff, and tough nanocomposites.

The thesis is written in chapters of six, which includes the 'Introduction' as Chapter one. Chapter two provides a detailed study of literatures, and Chapter three is on methodology relating to the research work and the adopted process undertaken for modelling work. Chapter 4 provides results and discussions of research work carried out and modelling work analysis; Chapter 5 provides general conclusions and Chapter 6 provides recommendation of areas that would require further research work to be done as future work.

2.0 Literature survey

This chapter reviews the fundamental knowledge and advancement on composite materials to improve composite materials strength, stiffness, and toughness. The review includes polymer and its composite system with an evaluation of advantages and disadvantages of types of polymer composite systems, fibres and fillers for composite materials reinforcement, factors influencing reinforcement of composite systems and current progress on toughness enhancement mechanism to develop strong, stiff, and tough materials and challenges associated with existing technologies. The review also includes composite modelling to predict the strength and stiffness of composite materials by exploring existing models, while also reviewing strong, stiff and tough materials inspired through a biomimetic approach such as nacre. Section 2.1 is about polymer and its composite system which focuses on polymers considered within the scope of the research (epoxy, polypropylene, polyethylene, and nylon 6) discussing their structure, strength, modulus, failure strain and interfacial adhesion with reinforcement fillers. Section 2.2 focus on various fibres and fillers considered within the research work which includes carbon fibre, glass fibre, glass flakes, montmorillonite nanoclay (MMT), graphene and single-wall carbon nanotube (SWCNT) with discussion relating to their structure, strength, modulus, failure strain and mechanical properties achieved in their composite form. Section 2.3 focuses on reinforcing composite systems and limitations associated with current technologies regarding improving composite system strength, stiffness, and toughness while reviewing existing toughness mechanisms to develop strong, stiff, and tough materials. Section 2.4 is on bio-inspired composite with focus on mechanical properties improvement achieved. Section 2.5 explore existing models often used in

composite modelling to predict composite materials properties, such models include Rule of Mixture, Shear -Lag and Halpin-Tsai.

2.1 Polymer and its composite system

A polymer is described as a large molecule alternatively referred to as macromolecule, consisting of chains of linked subunits called monomers in a repeating pattern forming a one, two, or three-dimensional network. Polymers are categorised into natural and synthetic polymers. Natural polymers are polymers known to widely exist in nature such as commonly found in plants and animals. Typical examples of natural polymers include deoxyribonucleic acid (DNA), ribonucleic acid (RNA), starch, collagen, silk, rubber, wool and cellulose to mention few. Unlike natural polymers, synthetic polymers are produced artificially and are often referred to as man-made polymers. Examples include polyethylene, nylon, polyvinylchloride, polystyrene, polyesters, polycarbonates, etc. Polymer could be either organic or inorganic depending on the atom forming the backbone structure of the polymer. Organic polymers have carbon atoms that constitute their backbone while inorganic polymers have the carbon atoms replaced with other atoms within their backbone structure [48], [49], [50]. Polymer research predates far back as 19th century with development and research contributions from many whose work precedes the likes of Jons Jacob Berzelius, Wallace Carothers and Herman Mark and Hermann Staudinger who developed the modern understanding of polymer as macromolecules in contrast to initial knowledge that considered polymer as an aggregation of small molecules also known as micellar [48], [51].

The evolutionary development of polymer continues and has transited into present-day material that now has applications across many facets of human lives, making a positive influence. This has made the polymer industry grow over time with polymer production to

the tune of 359 million metric tons [52]. Though polymer in its bulk form is characterised with relatively low strength and stiffness, it is interesting to note that polymer has found applications in technology and engineering for various purposes. This is possible due to making polymer stronger by transforming bulk polymer into a fibre used for reinforcement. Secondly, is the ability to reinforce polymer as a matrix system to make composite materials [30], [53].

2.1.1 Polymer matrices

Fabrication of polymer composite materials involves the reinforcement of polymer matrix with reinforcement fillers. The polymer matrix is divided into two types which are thermoset and thermoplastic polymer matrices.

2.1.1.1 Thermoset polymer matrix

A typical example of thermoset polymers, alternatively referred to as thermosetting resins include epoxy, cyanate ester, phenolic, vinyl ester, etc. Thermoset polymers are produced through the process known as curing, which involves applying heat at elevated temperature and pressure to thermosetting resin over time for polymerisation to complete and polymer molecules to form cross-link of three-dimensional networks as the resin solidifies. While the curing process of thermosetting resin happens gradually for it to finish and when this happens, the thermoset resin hardens and solidifies into infusible high molecular weight solid. It becomes unpliant it is unable to be reformed or re-melted. An effort to reshape cured thermosetting resin with the application of heat even at higher temperature results in polymer disintegration and decomposition before it melts due to the chemical bond between its molecules which are irreversible. Thermoset polymer mechanical properties are dependent on factors like the degree of polymerisation, the density of cross-linking, curing

conditions and composition of the thermosetting resin [54], [55], [56], [57]. Thermoset polymer has been widely used in composite material fabrication due to its advantages of good strength and modulus, high dimensional and thermal stability, ability to withstand high temperature, possess good resistance to solvent and corrosion and it is relatively inexpensive to produce. Likewise, there are disadvantages associated with thermoset polymers which include; relatively high fabrication time, low ductility, brittle behaviour, inability to reshape or remould thermoset polymer once it is cured therefore recycling is not feasible [54], [55], [58].

Epoxy

Epoxy is used for various applications including adhesives, printing of circuit boards, boats building, aerospace as composite matrices. Epoxy is produced by combining resin with a curing agent, i.e. hardener which reacts together chemically to produce cured thermoset epoxy resin. The epoxy resin consists of long-chain molecular structure with the reactive epoxy groups often at the end. Figure 1a shows a typical reactive epoxy group composed of two carbon atoms bonding to an oxygen atom and Figure 1b an idealised epoxy resin chemical structure with the epoxy reactive group attached at the end of the epoxy resin that are already bonded in some way with other atoms, i.e. hydrogen atoms. The epoxy resin reaction occurs with the curing agent due to the resin's reactivity during curing to form a cross-linking of a three-dimensional network [59], [60], [61].

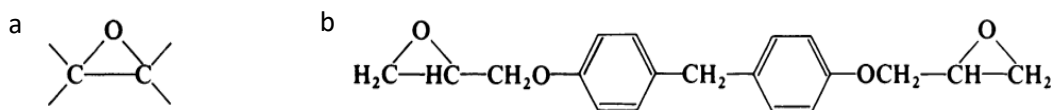


Figure 1: (a) Typical reactive epoxy group, (b) an idealised epoxy resin chemical structure. Adapted from ref [59]

The epoxy resin molecule also consists of ring groups capable of withstanding thermal and mechanical stresses better than linear group members of the epoxy structural molecule, thereby providing epoxy resin with good stiffness, strength, and heat resistant properties [60], [61]. While the epoxy resin needs to react with the curing agent, the mix ratio must be correct, i.e. mix ratio measured out by weight or volume between resin and curing agent to ensure a complete curing process. Considering that each resin molecule has a reactive group at the terminals that constitute the three-dimensional network formed and in the instance the mix ratio is incorrect, unreacted resin or curing agent remains within the matrix which affects the final properties of the epoxy after curing [59], [60], [61]. The reactivity possessed by the epoxy resin molecules allows for composite material fabrication with different reinforcement fillers, i.e. nanofillers, glass and carbon fibres, and with the possibility of improving the interfacial adhesion bond that exists between the epoxy resin and the reinforcement fillers through interfacial modification [62], [63], [64]. Research shows interfacial properties influence composite material mechanical properties. Therefore, various approaches towards enhancement of epoxy interfacial properties with reinforcement fillers have been reported, i.e. improving carbon fibre/epoxy interfacial shear strength through electrochemical oxidation and epoxy sizing [65]. Likewise, glass fibre/epoxy interfacial shear strength enhanced using γ -aminopropyl-triethoxysilane (γ -APS) [66]. Epoxy possesses tensile strength of about 35 – 100 MPa and tensile modulus 3 – 6 GPa [16]. However, the epoxy's high cross-linked molecular structures also provide shortcomings such as having low failure strain, i.e. 1 – 6 % [16]. This, coupled with a very strong interface, could cause the epoxy to fail in a brittle manner due to poor resistance to fracture and low fracture toughness [67], [68].

2.1.1.2 Thermoplastic polymer matrix

A typical example of thermoplastic polymers includes polyethylene, nylon, polystyrene, polypropylene, polyvinyl chloride, Polyether-ether-ketone, etc. Unlike thermoset polymers that are produced through a reactional process facilitated with the application of heat and pressure for curing to occur, thermoplastic polymer is produced through processing at a temperature above the melting temperature with the application of heat energy. Most thermoplastics at room temperatures maintain a solid state and, in such state, their molecular chains possess limited energy, hence, with the application of heat, the molecular chains gain energy and can move farther than initially possible. As the molecular chains continue to gain energy through heating, a temperature also known as melt temperature is reached when sufficient energy is gained causing the thermoplastic molecules to move freely having the form of a viscous fluid often referred to as melt. With the thermoplastic polymer melted makes it easy for shape forming and on cooling solidifies into a solid with molecules forming a linear or branched network. Thermoplastic polymers are divided into amorphous (i.e. polystyrene), and semicrystalline (i.e. high-density polyethylene - HDPE) which depends on the molecular chain arrangement of the polymer and affects the behaviour of the polymer when subjected to heat. The semicrystalline polymer is characterised by molecular chains that are organised and tightly packed, having some degree of crystallinity referred to as spherulites of various shapes and sizes while having an amorphous that exists within the crystalline region. Semicrystalline thermoplastics tend to have good strength, likewise good wear and chemical resistance. Amorphous thermoplastic polymer chains are not organised and tightly packed as a semicrystalline polymer; rather, the molecules are randomly oriented in their arrangement. Thus the molecules move relatively to each other without having the bonds that held the molecules together broken and as such contributes to the polymer's high

strain to failure, toughness, and damage tolerance [50], [54], [69] [70]. In general, thermoplastic polymers are increasingly used due to its advantages, such as high recyclability, environmentally friendly, good resistance to high Impact and chemicals, and easy to reshape/reform. Also, there are disadvantages identified with thermoplastic polymers which include poor resistance to high temperature, particularly above the glass transition temperature as this decreases the polymer strength and stiffness (modulus), requires high processing temperature, and relatively high production cost compared to thermoset polymers [54], [58].

Nylon-6

Nylon-6 alternatively called polyamide 6, is a semicrystalline polymer used for a wide range of engineering applications including tissue engineering and composite material fabrication due to its attractive combination of good mechanical properties and processability [71], [72]. Nylon-6 is produced through ring-opening polymerisation of caprolactam which is a molecule having six carbon atoms (Figure 2), that constitute the nylon-6 molecular chain which is characterised by amide groups held together by strong hydrogen bonding that provides nylon-6 with unique mechanical properties [73], [74], [75], [76], [77]. However, nylon-6 is hydrophilic, therefore susceptible to absorb moisture which causes a decrease in strength and stiffness but increases the ability to elongate [78], [79]. Nylon-6 tensile strength measures at about 88 MPa, tensile modulus 1.75 GPa, and strain at break more than 50% [80]. Like most composite matrix systems, nylon-6 composite is fabricated through reinforcement of nylon-6 matrix with reinforcement fillers for improved performance, i.e. reinforcement of nylon-6 with clay as demonstrated by Toyota [81]. The reinforcement fillers are mostly treated with a coupling agent to enhance adequate interfacial adhesion, using silane to promote bond

adhesion between nylon-6 and carbon fibre for better mechanical properties [82], similarly with glass fibre/nylon-6 [83].

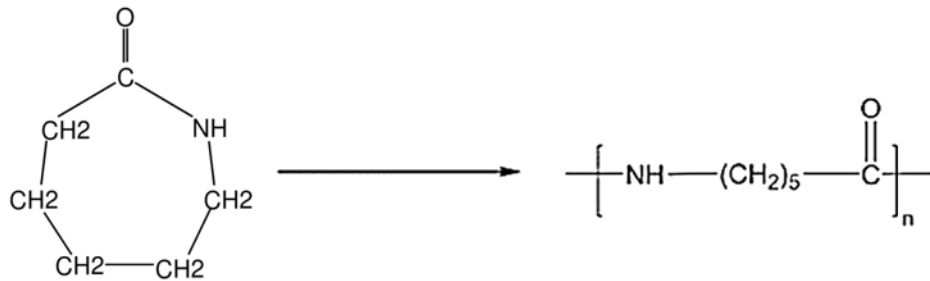


Figure 2: Nylon 6 chemical structure illustrates ring opening of caprolactam. Adapted from Ref [73]

Polyethylene

Polyethylene is a semicrystalline polymer produced through polymer polymerisation of ethylene monomers, having a molecular chain characterised with hydrogen atoms bonded to carbon backbone in a repeating pattern (Figure 3) and has wide use including packaging film, agricultural purpose i.e. mulch, housewares, electrical cable insulation, oil spill clean-up, etc [84], [85], [86].

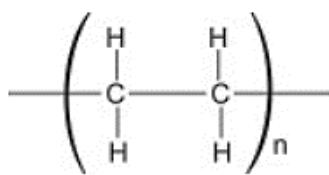


Figure 3: Chemical structure illustration for polyethylene. Adapted from Ref [86]

The polymerisation of ethylene at varying conditions of temperature, process time, pressure, and catalyst allows for a wide range of polyethylene to be produced with a differing degree of chain branching, crystallinity, molecular weight, entanglements, and cross-linking, i.e. low-density polyethylene (LDPE), linear low-density polyethylene (LLDPE), high-density polyethylene (HDPE) and ultrahigh-molecular-weight polyethylene (UHMWPE) [84], [85],

[86], [87]. While polyethylene could be produced at varying conditions, this affects the morphological structure of the polyethylene which influences their mechanical properties (Table 1 [88]), i.e. crystallinity for LDPE and LLDPE are less closely packed compared to HDPE, therefore LDPE and LLDPE possess less stiffness compared to HDPE [84], [85], [86], [87], [89], [90]. Additional use of polyethylene is as reinforced material for automotive application, hence; reinforcement of polyethylene with various reinforcement fillers including carbon and glass fibres has developed over time to produce composite materials. Different mechanisms used to ensure adequate interfacial bond adhesion to promote efficient load transfer, i.e. use of beam irradiation to enhance interfacial adhesion between carbon fibre and HDPE [91], likewise, application of sizing on glass fibre to improve bonding with polyethylene matrix [92].

Table 1: Polyethylene mechanical properties, adapted from ref [88]

	Density (g/cm³)	Tensile Strength (MPa)	Modulus of Elasticity (GPa)	Elongation at Break (%)
LDPE	0.917 - 0.940	10 - 20	0.130 - 0.300	200 - 600
LLDPE	0.915 - 0.950	25 - 45	0.266 - 525	300 - 900
HDPE	0.940 - 0.970	30 - 40	0.500 - 1.100	500 - 700

Polypropylene

Polypropylene is a semicrystalline thermoplastic polymer produced through a polymerisation reaction of propylene monomers involving the use of catalyst, i.e. Ziegler–Natta or metallocene with careful control of heat and pressure [93], [94]. Like other commodity polymer required for commercial needs, polypropylene is used for fabrics, fibre, films, automotive, etc [95]. Polypropylene molecular chain structure consists of hydrogen atoms bonded to the carbon atom in a repeating pattern with methyl groups arranged along the

polymer chain. Thus, different polypropylene types are produced, i.e. isotactic, syndiotactic, or atactic, which depends on the polymer chain's methyl groups' position. Isotactic polypropylene methyl groups are positioned on the same side of the polymer chain. In contrast, in syndiotactic polypropylene, the methyl groups are alternated, and in atactic polypropylene, the methyl groups have a random arrangement along the polymer chain (Figure 4) [94]. Compared to isotactic and syndiotactic polypropylenes which are semicrystalline, atactic polypropylene is amorphous and does not have less practical applications due to its low stiffness. However, it possesses good stretchability, reflecting its polymer chain's low crystallinity structure and has some niche area of applications, i.e. hot-melt adhesives. Isotactic and syndiotactic polypropylenes are both semicrystalline polymers with better mechanical properties than atactic polypropylene. Isotactic polypropylene is widely used for most applications and considered the most common commercially available polypropylene. Isotactic polypropylene is easily produced using Ziegler–Natta or metallocene catalysts, unlike syndiotactic polypropylenes produced with only some metallocene catalysts [93] [94]. Also, isotactic polypropylene exhibits better mechanical properties than syndiotactic polypropylene, i.e. high tensile strength and stiffness which is due to the high degree of crystallinity of the regular repeating structure of the polymer chain [94]. Polypropylene has a tensile modulus of about 1.0-1.4 GPa, tensile strength 25-38 MPa and failure strain more than 300% [16]. Reinforced polypropylene composite material interfacial adhesion is commonly enhanced for efficient load transfer to overcome poor interfacial adhesion exhibited due to chemically inert surface and low surface energy using techniques such as plasma and silane treatment of carbon fibre [96] and graft copolymerisation of glass fibres for reinforcement [97].

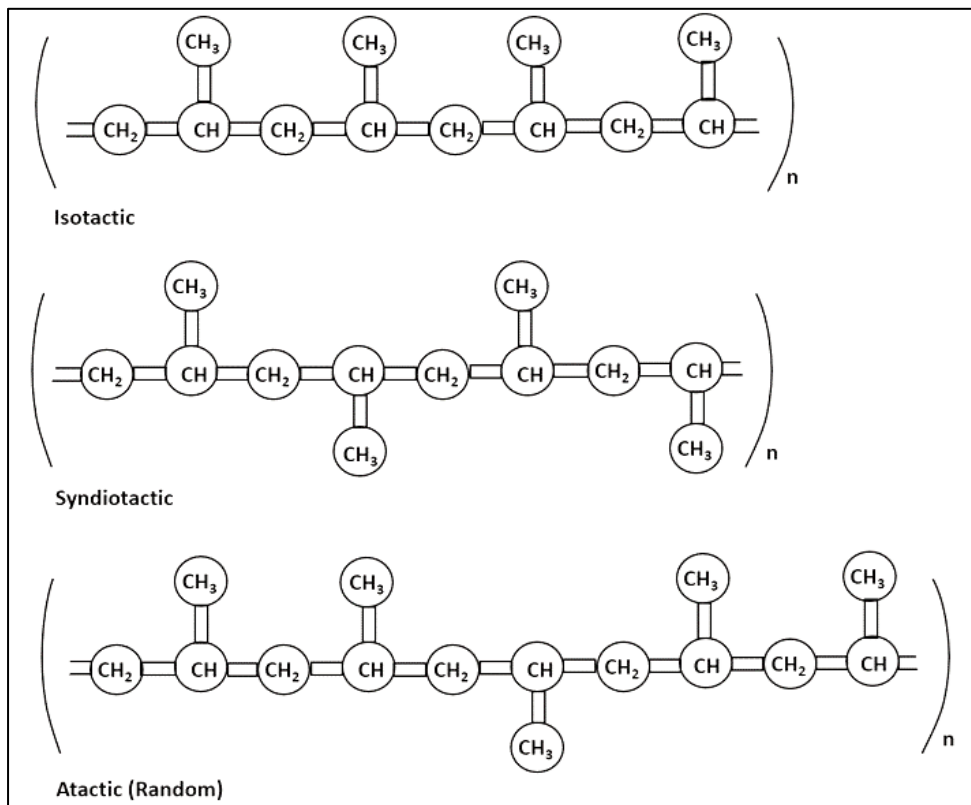


Figure 4: Illustration of polymer chain structure for different types of polypropylene, adapted from ref [94]

2.2 Reinforcement fibres and fillers

Over the years, material scientist and researchers have been able to gain insight into performance optimisation of fibres and fillers for reinforcement. These fibres and fillers are known to have high strength and stiffness compared to their matrices which serve as host and are often characterised with lower strength and stiffness but on the other hand, do have high strain which is often lacking in most fibres and fillers [30], [98].

2.2.1 Carbon fibre

A type of carbon fibre was first produced around 1879 when Thomas Alva Edison invented the first incandescent light bulb, by using electricity to heat-up a thin strip of cotton material filament to high temperature till it begins to glow after several attempts with different materials, thereby causing the cotton filament to carbonise. The filaments produced by

Edison has poor mechanical properties; hence, research intensifies to make carbon fibre with better-improved properties. The importance of having such carbon fibre is to support the dawn of space program in the USA, and by 1959 carbon fibre is produced from carbonised rayon a cellulosic base polymer like cotton. The carbonised rayon has improved properties and was used in high-temperature insulation applications replacing fibreglass used in rocket nozzle exit cones and re-entry heat shields. Improved carbon fibres satisfactorily considered fit for purpose within respective niches, but generally, the carbon fibre still has poor mechanical properties and therefore considered not suitable for structural usage. With the need for carbon fibre with better mechanical properties, research continued relentlessly with contributions made in USA, Japan and Royal Aircraft Establishment (RAE) Farnborough UK which has caused carbon fibre to evolve into a material used for a wide range of structural applications. Meanwhile, the trend continues with novel research, particularly in carbon fibre production, to reduce production cost [99], [100].

With further improvement in the fabrication process, the cellulosic rayon precursor is carefully controlled under the heating process to carbonise, thereby producing carbon fibre with improved mechanical properties [99]. These fibres were made available commercially, making rayon-based carbon fibre first available commercial carbon fibre [100]. Subsequently, other precursors like poly-acrylonitrile (PAN) and pitch were identified and are used to produce carbon fibres which are also available commercially [54], [99], [100]. Though rayon based carbon fibre is the first commercially available carbon fibre, overtime PAN-based carbon fibre has become dominant with 90% of commercially produced carbon fibres being PAN carbon fibre, while pitch and rayon carbon fibres make up the remaining 10% [54], [101]. This is due to reasons which include a good combination of mechanical properties exhibited

by PAN fibre predominantly tensile strength and reasonable production cost. On the contrary, highly graphitised pitch-based carbon fibre is expensive, with low tensile strength but high tensile modulus [54], [100].

The inherent properties of carbon fibre are influenced by the precursor used for their fabrication [100], [101]. Carbon fibre fabrication begins with polymer feedstock, often referred to as a precursor with long chains of molecules held together by backbone carbon atoms [102]. Precursors are usually held with secrecy as it is often considered as trade secret considering that individual carbon fibre producer determines their precursor composition and does vary from one producer to another [99], [101], [102]. Nevertheless, PAN carbon fibre is produced from precursor composition of acrylonitrile while rayon carbon fibre is produced from a cellulosic precursor with cellulose composition and pitch carbon fibre is produced from either isotropic pitch or anisotropic pitch precursors which can be processed into meso-pitch to produce high-performance carbon fibre [99], [103]. However, making each precursor into fibrous material varies using various spinning process, i.e. wet, dry and melt. However, the subsequent process of making the precursors into carbon fibre is quite similar. Considering that most commercially available carbon fibres are produced as either PAN or pitch-based carbon fibres, details of the process involved in fabricating the fibre is described (Figure 5).

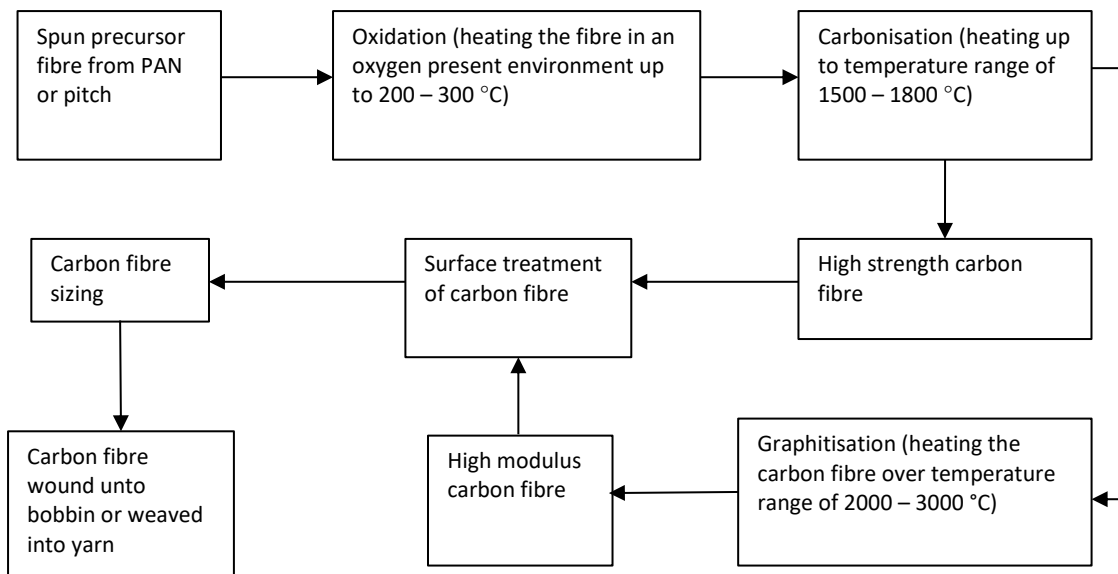


Figure 5: Illustration of process involved in fabrication of carbon fibre

Once the precursor is spun into fibre, the conversion process to make carbon fibre is started by making the fibre thermally stable, a process known as stabilisation for PAN fibre and infusibilisation for pitch fibre [54]. It involves heating the fibre in an environment with sufficient oxygen, i.e. atmospheric air, at a temperature range of 200 – 300°C to undergo oxidation which is done by passing the fibre through controlled heating chambers or hot rollers. Allowing the fibre to capture oxygen molecules and have their atomic bonding pattern rearranged to become thermally stable [99], [102]. Following the stabilisation/infusibilisation process is a pyrolysis process known as carbonisation. The carbonisation process involves heating the fibre in an inert environment, hence lacking oxygen. This prevents the fibres from burning when heated to high temperatures while keeping the gas pressure within the carbonisation furnace higher than the surrounding pressure and having the furnace's inlet and outlet sealed to prevent oxygen from entering. Heating the fibre to a temperature of about 1000°C causes the fibre to lose and expel non-carbon atoms and few atoms of carbon in the form of gases, leaving behind crystals of tightly bonded carbon atoms aligned along the fibre axis. With further heating to a temperature range of 1500 - 1800°C, high strength carbon

fibre is produced and further heating above this temperature range to over 2500°C the fibre lose strength (Figure 3) as it becomes more graphitised by undergoing graphitisation yielding high modulus carbon fibre [99], [102], [103], [104].

Upon completing the carbonisation process, the carbon fibre surface has a low bond affinity to adhere to matrix systems to fabricate composite material. Therefore, to enhance the carbon fibre bonding properties, the fibre surface is given an oxidative treatment using different methods, i.e. electrolytic or electrochemical bath or immersion in various gases such as ozone. The oxidative treatment allows for oxygen atoms to be added to the fibre surface to promote bond adhesion and also through slight etching to enhance bonding properties mechanically. The surface treatment needs to be carefully controlled, avoiding the formation of surface defects such as pits that could affect the fibre mechanical properties to decrease [99] [102]. Following the carbon fibre surface treatment is fibre sizing, whereby the carbon fibre is coated with sizing material. Selection of sizing material is often determined to be compatible and to provide adhesion with the intended matrix system while protecting the fibre from damaging when handled or weaved [54], [102].

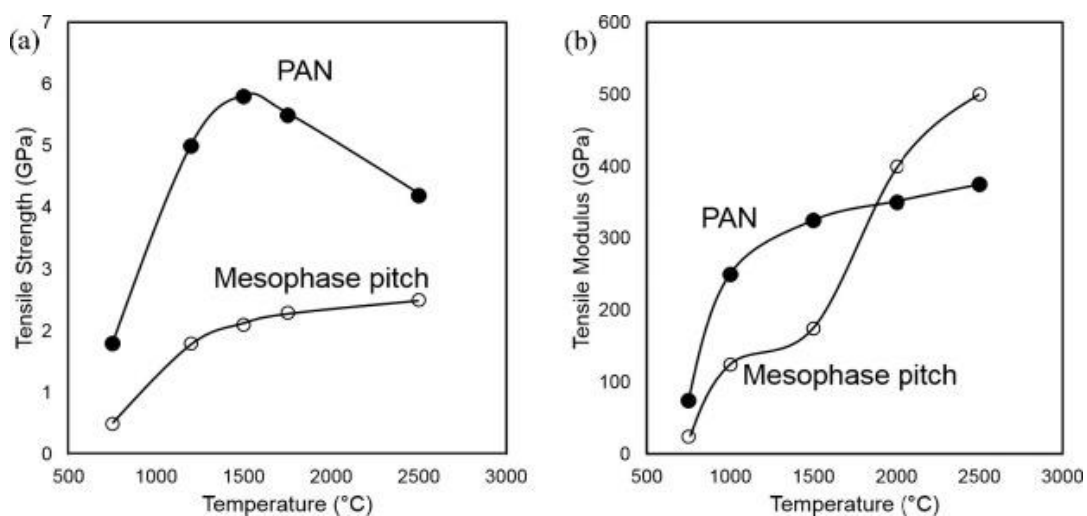


Figure 6: (a) Tensile strength and (b) tensile modulus as a function of heat treatment temperature of PAN and pitch carbon fibre during carbonisation and graphitisation processes. Adapted from Ref [104]

Carbon fibre properties are ultimately dependent on the fibre structure. Meanwhile, the fibre structure is influenced by the fibre fabrication process. Therefore, due diligence is given to heat treatment temperature applied to manufacture the fibre and ease graphitising the carbon fibre precursor. For instance, PAN-based carbon fibres exhibit turbostratic structure even at a high heat treatment temperature of 2000°C, thus makes graphitisation challenging [54]. Figure 6 shows that heat treatment temperature of carbon fibre above 2000°C causes the carbon fibre strength to decrease particularly for PAN-based carbon fibre but the modulus is not. According to Marsh-Griffith diagram (Figure 7) [105], the carbon fibre aromatic sheets are formed as temperature increases. The stretching applied during melt spin and high-temperature treatment, causing the carbon fibre graphite sheets to orientate in the fibre direction. As graphitisation ensued at a temperature above 2000°C, the carbon fibre aromatic sheets formed are stacked in a graphitic layered type of structure but are not infinitely large. Therefore, interconnection is lacking between the aromatic sheets, which is a contributing factor for relatively low strength in high modulus carbon fibres and therefore does not have high strength. Meanwhile, to achieve high strength, the carbon fibre aromatic sheets need to be interlinked. Carbon fibre processed at heating treatment temperature below 2000°C, preferably between 1500°C - 1800°C is often characterised with high strength as the carbon fibre structure is turbostratically crosslinked due to interlinks that exist between the fibre aromatic sheets. However, at this temperature, the aromatic sheets are not fully developed and cannot be well aligned in the direction of the carbon fibre, thereby yielding carbon fibre with low modulus though characterised with high strength [30], [104].

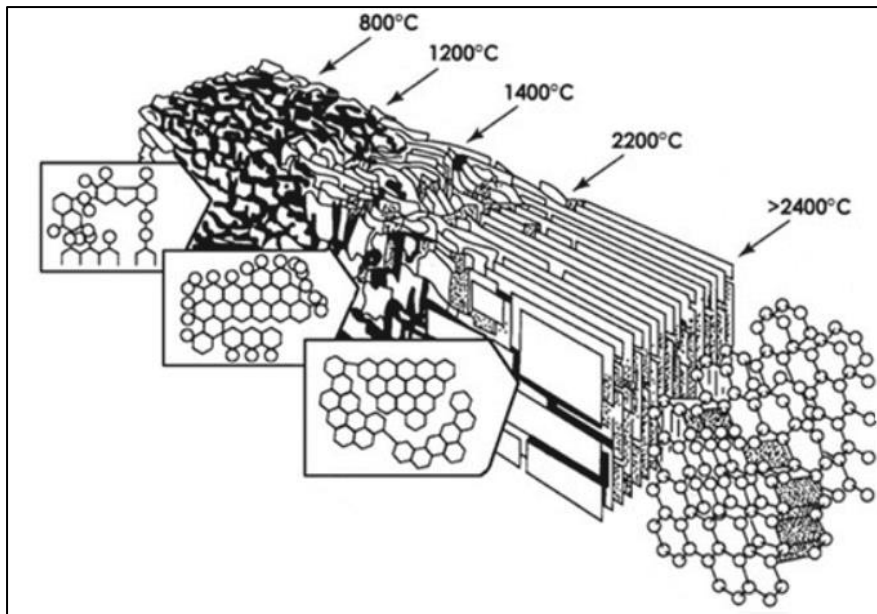


Figure 7: Progressive development of aromatic sheets during carbonisation/graphitisation with increase in heating treatment temperature for carbon fibre fabrication. Adapted from Ref [100]

PAN-based carbon fibres are grouped according to their carbonisation temperature, i.e. PAN-based carbon fibre carbonised at a temperature above 2000°C, 1500°C, or 1000°C are referred to as Type I, Type II, or Type III, respectively [104]. Type I, II and III carbon fibres are regarded as high modulus carbon fibre (i.e. tensile strength 1.9 GPa and tensile modulus 517 GPa), high strength carbon fibre (i.e. tensile strength 3.7 GPa and tensile modulus 240 GPa) and general-purpose carbon fibre (i.e. tensile strength 720 MPa and tensile modulus 32 GPa) respectively [54], [104]. While flaws, i.e. surface and internal flaws tend to influence the carbon fibre mechanical properties, most carbon fibres are characterised with low failure strain, i.e. about 2%, carbon fibres are used either as a long continuous or short fibre for reinforcement of matrix system [54], [104]. For example, Zhang et al. [106] reported unidirectional carbon fibre/epoxy with a fibre volume fraction of 45-50% reinforcement without interface modification with graphene-oxide having a composite tensile strength of about 1.45 GPa and modulus 45 GPa, and with interfacial modification with graphene-oxide having a composite tensile strength of 1.95 GPa and modulus 50 GPa. Likewise, Capela, Oliveira and Ferreira [107]

reported epoxy reinforced with short carbon fibre with 5-20% fibre volume fraction having a composite tensile strength of 67.2 – 101.7 MPa and modulus 3.6 – 18.5 GPa depending on fibre volume fraction. Similarly, Karsli and Aytac [108] investigate the influence of fibre length and the fibre content (weight fraction 2-20%) of short carbon fibre reinforced polyamide 6 with tensile strength 42 – 90 MPa and modulus 450 – 1600 MPa.

2.2.2 Glass fibre

Glass usage predates back to the ancient time during the Egyptians, Greeks, and Phoenicians era using glass for adornment, i.e. jewellery making and used in the decoration of vases and vessels for drinking [109], [110]. The ability to understand and transform melted glass into thin fibres to make specialised gowns was exhibited by the Venetians in the early seventeenth century [109]. While the use of glass exists historically, however, the development of the engineering and science was until recent around the 1930s, has made it possible for glass to be produced in fibre form for structural reinforcement in composites. In 1938, the merger of Owens-Illinois and Corning Glass Works forming Owens-Corning Fiberglas Corp which in the same year awarded patents that brought about the development of commercially practical production process of glass fibre [109], [110], [111]. Hence making glass fibre commercially available has undoubtedly created a market that has grown to 2.5 billion pounds as of 2018 to support modern reinforcement composites production [110].

Glass an amorphous material having three-dimensional network atomic arrangements of silicon atom bonded covalently to oxygen atoms in a coordinated tetrahedral pattern [111]. Glass fibre is one of the end products of the glass production process, therefore having similar molecular structure arrangement as glass [109]. Different glass types exist, and the end-use of the individual glass determines such glass raw material composition. Therefore, the glass

composition is an important factor determining the glass fibre properties, adapted to numerous and diverse applications based on individual glass fibres' inherent unique properties [109]. The main base material composition for glass production is silica which makes up between 50 – 75% of the entire batch composition, while other materials such as aluminium oxide, magnesium oxide, calcium oxide, etc. to mention few makes up the remaining composition at required percent proportion depending on the type of glass fibre to be produced, i.e. E-glass, ECR-glass, A-glass, C-glass, D-glass, R-glass and S-glass (Table 2) [109], [110], [111].

Table 2: Compositions by percentage weight for typical glass fibres, extracted and adapted from ref [111]

Constituent	E	ECR	C	A	S-2	R	AR1	AR2	D
SiO ₂	55.2	58.4	65	71.8	65	60	60.7	61	75.5
Al ₂ O ₃	14.8	11	4	1	25	25	-	0.5	0.5
B ₂ O ₃	7.3	0.09	5	-	-	-	-	-	20
ZrO ₂	-	-	-	-	-	-	21.5	13	-
MgO	3.3	2.2	3	3.8	10	6	-	0.05	0.5
CaO	18.7	22	14	8.8	-	9	-	5	0.5
ZnO	-	3	-	-	-	-	-	-	-
TiO ₂	-	2.1	-	-	-	-	-	5.5	-
Na ₂ O	0.3	-	8.5	13.6	-	-	14.5	-	3
K ₂ O	0.2	0.9	-	0.6	-	-	2	14	
Li ₂ O	-	-	-	-	-	-	1.3	-	-
Fe ₂ O ₃	0.3	0.26	0.3	0.5	trace	-	trace	-	-
F ₂	0.3	-	-	-	-	-	-	-	-

Silica is the main base composition for glass fibre production, which consist of silicon and oxygen atoms. Meanwhile, silicon is known to have high liquefaction temperature; therefore, the addition of other composition materials helps to lower the melt temperature to produce molten glass with viscosity that would allow easy drawing of the molten glass into fibres [109]. Figure 8 describes the manufacturing process of glass fibre. Glass is produced by having a batch which is a process of dry mixing the constituent materials based on the type of glass fibre to be produced. After proper mixing of the batch, the next glass fibre production process is to feed the batch into a high-refractory furnace for melting. The melt temperature of the batch depends on the glass composition and could be up to 1400°C. While the batch melts, an effort is made to ensure uniformity and bubbles removed to eliminate fibre discontinuities, affecting the fibre properties. Typical glass furnace is divided into sections with the end section of the furnace to be the fibre drawing furnace where the molten glass directly flows to during the melting process. From the fibre drawing furnace, the molten glass can be made into glass marble using a marble making machine, and the glass marbles can later be re-melted and processed into a drawn fibre. Alternatively, the molten glass undergoes a process of fiberisation, which is direct processing into fibres [109], [110], [111].

With fiberisation process, continuous glass fibre is formed from the molten glass through extrusion and glass fibre attenuation. From the glass drawing furnace, the molten glass is extruded through a bushing plate made of a material that is erosion resistant, i.e. platinum/rhodium alloy. The bushing plate has many fine orifices that could range from 200 to 8000, allowing for the passage of extruded molten glass. For the glass to maintain constant viscosity, the bushing plate temperature is controlled through heating electronically. On exiting the bushing plate, the glass extrudes are cooled by lightly applying a jet spray of water.

This is followed by applying attenuation, which is drawing extruded molten glass into fibres with the diameter determined mechanically. The attenuation process requires high-speed winder to catch the extruded molten glass. The winder revolves at a much faster circumferential speed than the molten glass exiting the bushing plate, i.e. at an approximated circumferential speed of 2 miles/3 kilometres per minute. This, therefore, causes tension stress to be exerted on the molten glass extrude resulting in the glass extrude being drawn into thin glass fibres. The thin glass fibres are coated with size, which consists of lubricants and coupling agents. The lubricant protects the thin glass fibres from abrading and breakage when handled or weaved while coupling agents enhance the fibre affinity to strengthen the bond adhesion at the interface with matrix systems. The glass fibre dries from the sizing applied and collected together into a bundle to be wound onto spool for continuous fibre filament or chopped into short-staple fibres packaged for end-use applications [109], [110], [111].

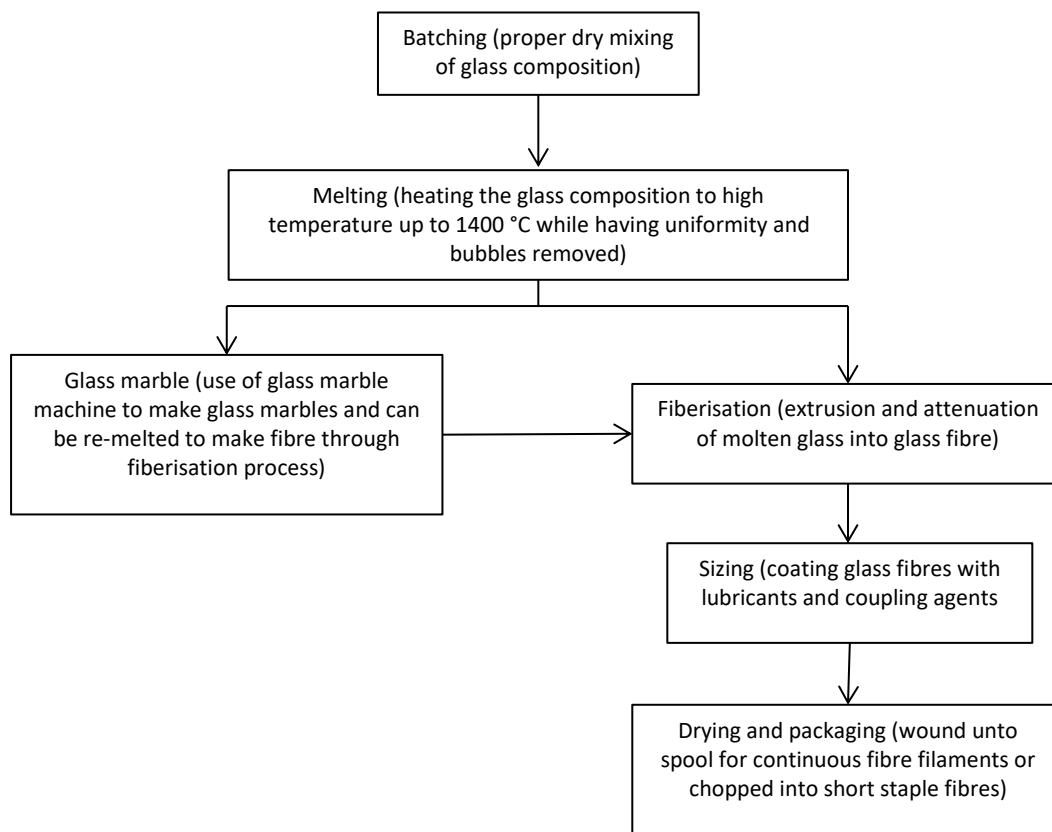


Figure 8: Melt process of producing glass fibre

Considering that glass fibre is produced via the formulation of glass composition requiring different raw materials to be dry-mixed, invariably the glass composition influences the amorphous three-dimensional network structure formed, which affects the glass fibre mechanical properties due to the chemical forces that are operational within the amorphous network. For instance, the use of network modifiers like alkali and alkaline earth oxide tend to cause a decrease in the number and strength of the chemical bonds that exist within the three-dimensional network, thereby causing a decrease in mechanical properties, i.e. pure silica glass without alkali network modifier could exhibit a tensile strength of about 7 GPa which reduces to about 2.5-3 GPa with network modifiers [111]. Thus, a typical E-glass tensile strength is about 3.5 GPa, the tensile modulus 70-80 GPa and failure strain 1.8-3.2%.

However, glass composition does not absolutely determine glass fibre tensile strength and modulus rather flaws such as internal defects also contributes. When the glass fibre is drawn into a smaller diameter, internal defects are regarded to decrease thereby causing glass fibres with smaller diameter exhibit high tensile strength and modulus than glass fibre with a large diameter [16], [111]. Glass fibre has been used widely for reinforcement of various matrix systems and a common practice for efficient load transfer often requires the fibre/matrix surface modified. Rijdsdijk, Contant and Peijs investigate the use of maleic-anhydride-modified polypropylene to improve glass fibre/polypropylene interfacial adhesion and determine the influence it has on mechanical properties at a fibre volume fraction of 58%. The investigation shows that the tensile modulus did not change significantly as the tensile modulus is 43.4 GPa without modification and 43.6 GPa for the modified interface. However, the tensile strength without modification and 720 MPa and 890 MPa for the modified interface [112]. Also, Mohan and Kanny investigate the effect of nanoclay on glass fibre/high-density polyethylene (HDPE) mechanical properties at 20% fibre volume fraction with neat HDPE/glass fibre having tensile strength 77 MPa and tensile modulus 17.3 GPa while nanoclay modified HDPE/glass fibre tensile strength is about 78-86 MPa and tensile modulus 17.7-23.1 GPa [113].

2.2.3 Glass flakes

The existence of glass flakes originated from the effort to resolve difficulty associated with reinforcement of roof-light panels. A technology developed around 1959 after inadequacy was identified using glass fibre to reinforce polyester resin used in producing the roof-light panels. Unreinforced roof-light panels experienced distortion when exposed to strong sunlight, a shortfall with the material stiffness. To mitigate the shortfall, the polyester resin was reinforced with glass fibre. In a way, the glass fibre enhanced the polyester resin stiffness

at required volume; this resulted in light transmission through the roof-light panels to be severely reduced, thereby negating the purpose the roof-light meant to serve. Therefore, to resolve both challenge of reinforcement and maintaining good light transmission through the roof-light panel, a better substitute of reinforcement filler needs to be applied. Hence the development of glass flakes which was able to provide substantial modulus improvement to the polyester resin and simultaneously maintain good light transmission through the roof-light panel thereby solving both challenges of distortion and light transmission [114].

While the roof-light panel is one of the early applications of glass flakes, other industrial applications have been able to adapt and adopt glass flakes for use, i.e. coatings industry [114]. Glass flakes as the name connotes is a type of filler produced using glass composition as highlighted in section 2.2.2 (Table 2), therefore having similar properties to glass with regards to the raw material composition used to produce the glass flake but produced using a different production process [114], [115]. Compared to glass fibres that provide anisotropic reinforcement, glass flake is a typical example of planar reinforcement platelet fillers capable of providing reinforcement in the platelet two principal planes. With such reinforcement arrangement parallel to the principal planes of a composite material system and harnessing the isotropic reinforcement capability of such platelet, filler tends to achieve high performance compared to fibre reinforcements for loading condition that is two dimensional [116], [117].

Amidst various qualities that could affect the performance of glass flakes, the thickness is of high importance. While glass flakes thickness varies, due diligence needs to be given to the glass flakes' production process to produce glass flakes with consistent thickness and narrow distribution [114], [118]. Therefore, to produce glass flakes, several methods can be applied,

which include the bubble, spun and liquid phase deposition (LPD) methods [114], [119]. The bubble method is considered much more cost-effective as it allows for high production throughput [114]. With the bubble method of producing glass flakes, molten glass is inflated with gas through a nozzle to the required thickness of the glass bubble by controlling the gas volume. Inflated glass bubble is then smashed and milled into various sizes. Glass flakes thickness produced using the bubble method tends to range from 1-18 μm on average. While the bubble method might be cost-effective economically, the technique also has limitation such as producing curved glass flake which is dependent on glass bubble size [114], [120]. Producing glass flakes via spun glass method has the advantage of producing glass flakes with no curved flakes and tighter product control to produce glass flakes that have a thickness less than 1 μm from molten glass using centrifugal force. Molten glass is fed downward into a rotary cup that spins the molten glass around the rotating cup thereby forming a film of glass round the cup when cooled and the glass film formed is crushed into glass flakes [114], [121], [122]. Unlike bubble and spun methods for producing glass flakes from molten glass, LPD method uses a sol-gel technique to produce ultra-thin glass flakes by coating stainless steel substrate with silica sol solution at near room temperature of 50 – 60°C after the silica sol solution has reached desired viscosity. Applied silica sol solution dries at 120 – 150°C to form film gel which is peeled off from the substrate to be sintered at 900 – 1200°C to form glass then processed into glass flakes with an average thickness of 0.588 μm [119]. Considering that glass flake is relatively similar to glass fibre; therefore, theoretical tensile strength and modulus are the same as ideal glass molecular tensile strength and modulus. However, like glass fibre, glass flakes tensile strength and modulus depend on the glass flakes' thickness with thinner glass flakes exhibiting higher tensile strength and modulus than thicker flakes [116], [123]. Though the reinforcement of composite materials with glass flakes is not as

popular as glass fibre, research has shown improvement in composite material mechanical properties using glass flakes as the reinforcement filler [116]. Li [124] investigate the enhancement of polymer composite of glass flakes/nylon-6 using 25% weight fraction of glass flakes with a sub-micron thickness of 350nm glass flakes, with the composite material without surface modification having a tensile strength of about 74.1 MPa and tensile modulus 4.13 GPa and with surface modification with an amino-silane tensile strength of 68.32 MPa and tensile modulus of 6.11 GPa. Broughton, Lodeiro and Pilkington investigate coupling agents' influence on glass flakes reinforced polypropylene behaviour using glass flakes with an average thickness of 7 μ m and average volume fraction of 13%. Untreated glass flakes/polypropylene exhibited a tensile strength of about 24.4 MPa and tensile modulus of 4.2 GPa, while treated composite material with amino-silane and titanate exhibit an average tensile strength 28.9-29.4 MPa and 23.4-24.3 MPa respectively and tensile modulus 4.77-4.91 and 4.05-4.67 GPa respectively [125].

2.2.4 Graphene

Graphene is a single layer of two-dimensional lattice array of carbon atoms covalently bonded together, forming a honeycomb-like structure [126], [127]. Graphene is described to be the lightest, strongest and thinnest material discovered with many hypothesised superlative potentials that can be harnessed for various applications ranging from energy, sensors, electronics, coatings and composites to mention few [128], [129], [130]. However, graphene is a monolayer material but regarded as the parent form of many carbon materials i.e. graphite and carbon nanotubes [126]. Regarding composite application and considering that graphene is a relatively flat material with high surface area to volume ratio. Also, with the graphene atoms at the surface, therefore, have accessibility from both sides to surrounding

molecules to interact with. This coupled with the strength of the covalent bonds that exist between the carbon atoms along the plane provides graphene with high tensile strength of about 130 GPa, a tensile modulus of 1 TPa and elastic tensile strain up to 25% making it appealing and possibly ideal filler for use in composite material applications [126], [130], [131].

While graphene predates back to the nineteenth century with Benjamin Collins Brodie's knowledge contributions recognising the highly layered nature of thermally reduced graphite oxide and determining the graphite atomic weight in 1859 [127]. Likewise, in 1947 Phil Wallace was the first to calculate graphene band structure, providing a starting point to help understand bulk graphite electronic properties, which is a stacked layer of graphene sheets held together by weak Van der Waal's forces [129], [132]. Similarly, several other contributions have been made towards graphene with reports published before 2004 with the inclusion of synthesising monolayer of graphene which was achieved through the use of silicon carbide substrates in 1975 [129], [132]. With many reports published about graphene before 2005, none of the reports identifies the unique properties of graphene until the work of Geim and Novoselov which received physics Nobel Prized award in 2010 for their pioneering contribution of simple exfoliation technique to isolate pristine graphene using scotch tape and effort made to identify the unique properties of graphene [127], [129], [132]. Through Geim and Novoselov contributions towards development and identifying graphene's unique properties has led to an increase in research on graphene application and further exploration of graphene properties. As well as developing a reliable process of producing graphene at large scale to support graphene required applications considering that method of scotch tape to isolate graphene is limited to laboratory applications [129].

Graphene is produced using several methods; liquid-phase exfoliation of graphite, reduction of graphite oxide, chemical vapour deposition (CVD), and synthesis on silicon carbide (SiC) substrate, etc. Concerning graphene unique properties, some of these properties have been achieved solely with highest quality samples of graphene such as pristine graphene mechanically exfoliated using scotch tape and graphene deposited on special substrates like hexagonal boron nitride. However, the equivalent of some properties trends is yet to be witnessed with some of these techniques used to produce graphene. Improvement of these techniques to produce graphene with the same outstanding performance as graphene produced in laboratories pose an advantage for industrial application on large scale production and hence the need for development of such production process [129], [130]. Taking advantage of graphene awesome mechanical properties to reinforce matrix system, Rafiee et al. investigate comparative studies of different nanocomposite mechanical properties with epoxy reinforced at 0.1% weight fraction, epoxy/graphene sheets exhibit a tensile strength of about 78 MPa and 3.74 GPa compared to neat epoxy which exhibits a tensile strength about 55 Mpa and modulus of about 2.85 GPa [133]. Also, Huang et al. report polypropylene performance reinforced with different weight fraction of graphene sheets (1-20 wt.%) exhibiting tensile strength 33.74 to 22.28 MPa and tensile modulus 1.621-4.037 GPa respectively with an increase in weight fraction [134].

2.2.5 Carbon nanotubes

While graphene is a relatively flat material, carbon nanotubes could be considered the rolled form of a graphene sheet in single-wall carbon nanotube and rolled stacks of graphene sheets for multiwall carbon nanotube [135]. Carbon nanotube exists as either single-walled carbon nanotube having single well or multi-walled carbon nanotubes that has more than one well

and can range from two walls of carbon nanotube often referred to as double-walled carbon nanotube, triple-walled carbon nanotube that has three walls of carbon nanotube and multiple walls of carbon nanotube ranging from four upwards up to about fifty [136], [137], [138]. Depending on the carbon nanotube roll-up into a cylindrical one-dimensional structure, single-walled carbon nanotube takes a structural form of either armchair, chiral or zigzag which affects the nanotubes electrical properties (Figure 9) [135], [136], [139]. The multi-walled carbon nanotubes have two types of structural models which are the Russian Doll and Parchment. A multi-walled carbon nanotube characterised such that thinner nanotube is contained within another nanotube with greater diameter is referred to as Russian Doll model, and the Parchment model looks like a single graphene sheet rolled up into a scroll form having manifold round itself (Figure 10) [136], [140].

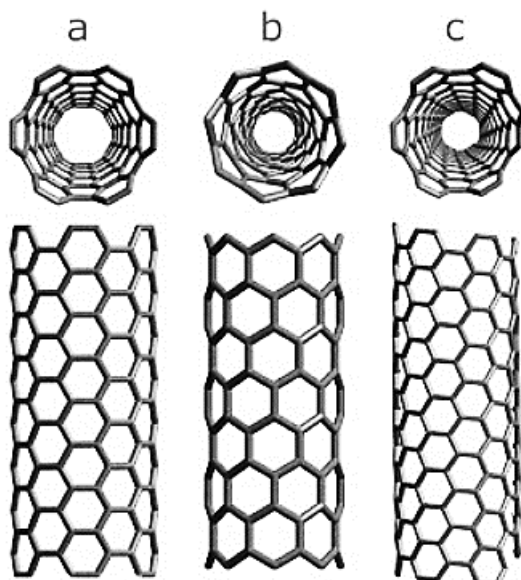


Figure 9: Schematic illustration of (a) an armchair nanotube, (b) a zig-zag nanotube, and (c) a chiral nanotube. Adapted from Ref [135]

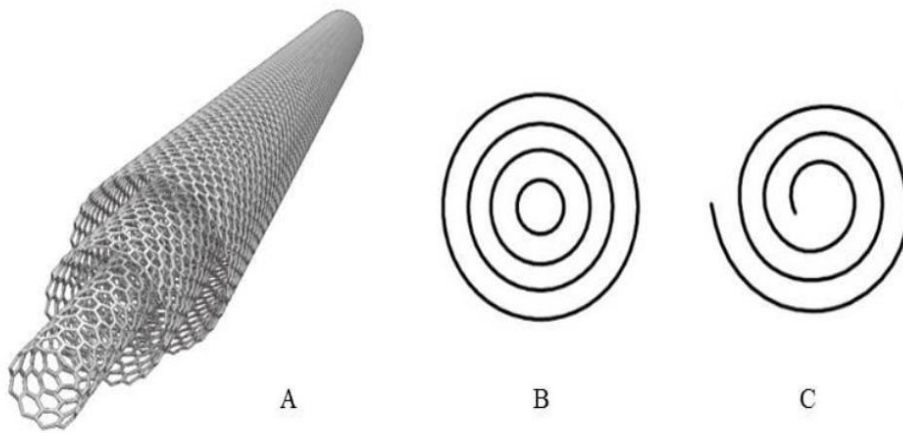


Figure 10: Schematic model illustration of (A) Russian doll multi-walled carbon nanotube (B) sketch of Russian doll layer arrangement and (C) Parchment model layer arrangement of multi-walled carbon nanotube. Adapted from Ref [140]

Multi-walled carbon nanotube was discovered and reported by Iijima in 1991 [137]; later in 1993, single-walled was reported by Iijima and Ichihashi [138]. Most of the carbon nanotube physical properties are relatively similar to graphene and realisation of their properties including mechanical, thermal, and electrical has encouraged many researchers to explore the potentials of carbon nanotubes particularly in the area of composite material fabrication due to the high aspect ratio carbon nanotube possess together with remarkable Young's modulus of about 1 TPa, tensile strengths up to 63 GPa and failure strain of about 12% [141], [142]. The carbon nanotube is produced using either chemical vapour deposition technique, laser ablation technique or carbon arc discharge technique. Syntheses of carbon nanotube were usually through laser ablation or arc discharge however chemical vapour deposition has become an alternative as the high temperature required for laser ablation, and arc discharge fabrication process contributes to the high cost of production. Though carbon nanotubes produced using arc discharge and laser ablation often have fewer defects than the chemical

vapour deposition technique, which affects the nanotube properties. However, chemical vapour deposition allows for fine-tuning the nanotube, unlike arc discharge and laser ablation techniques [136], [141]. Like graphene, carbon nanotubes have been employed as reinforcement filler to enhance polymers mechanical properties, i.e. 0.5% weight fraction surface-modified single-wall carbon nanotube/polyethylene composite with tensile strength 33.3 MPa and tensile modulus 800 MPa [143], and 0.1% weight fraction of SWCNT/epoxy exhibit a tensile strength of about 65 MPa and tensile modulus about 3 GPa [133].

2.2.6 Clay – montmorillonite (MMT)

Clay alternatively referred to as nanoclays are a type of nanoparticles made of layered mineral silicates having layered structural units that form complex clay crystallites through the stacking of the mineral silicate layers [144]. A unit layer consists of an array of octahedral and tetrahedral sheets arrangement. The octahedral sheet has aluminium or magnesium bonded in six-fold coordination with oxygen atom that forms a bond attachment with a tetrahedral sheet and hydroxyl. The Tetrahedral sheets are composed of silicon-oxygen tetrahedral which links together with neighbouring tetrahedral such that the three corners of the tetrahedra are shared while the fourth corner of each tetrahedron within the tetrahedral sheet connects with adjacent octahedral sheet through a covalent bond (Figure 11) [144], [145]. Depending on these sheets' arrangements, which impact various defining and distinguishing aspects of the nanoclays and their mineralogical composition. There exist different types of nanoclays which are used for various applications depending on the nanoclay properties. The nanoclay properties are characterised by the nanoclays' chemical composition and particle morphology used in organising the nanoclays into several classes such as kaolinite, smectite, illite and chlorite [145]. There are three common noticeable sheet arrangements with nanoclays,

having structural array identified as 1:1, 2:1 and 2:1:1 sheet arrangements. Nanoclays with 1:1 sheets arrangement has individual tetrahedral sheet linked to one octahedral sheet, 2:1 sheets arrangement has individual octahedral sheet attached to two tetrahedral sheets with one sheet linked on each side, while a 2:1:1 sheets arrangement has individual octahedral sheet adjacent to another octahedral sheet that is attached to two tetrahedral sheets [144], [145].

Montmorillonite is a layered plate-like nanoclay that belongs to the smectite clay class and has 2:1 octahedral and tetrahedral sheets arrangement (Figure 11). Each layer is about 1nm thick, consisting of alumina-silicate with layers surface having metal cations stacked in multilayer of about 10nm approximately [144], [145]. Montmorillonite is commonly used in polymer applications by having the nanoclay staked layers dispersed in the polymer matrix as either fillers or additives to enhance polymer/nanoclay composites performance. With such applications, having the montmorillonite nanoclay, which can allow the interlayer space to expand due to high cation exchange capability, allows for polymer monomers or chains to intercalate within the clay structure. Thereby enabling the fabrication of nano polymer composites by allowing the individual nanoclay layer in-plane tensile strength about 3GPa and tensile modulus 160 GPa to be harnessed for reinforcement of polymer matrix systems [144], [145], [146], [147], [148]. This attributes provides smectite clay like montmorillonite to be used in polymer nanocomposite reinforcement, i.e. modified montmorillonite clay/nylon-6 at 2.7-4.5 % weight fraction exhibits a tensile strength 79.5-87.7 MPa and tensile modulus 3.49-4.32 GPa [149]. Likewise, epoxy/exfoliated clay at varied weight fraction 0-5% exhibits tensile modulus 2-2.75 GPa with an increase in weight fraction while tensile strength decreases exhibiting 70-55 MPa correspondently [150].

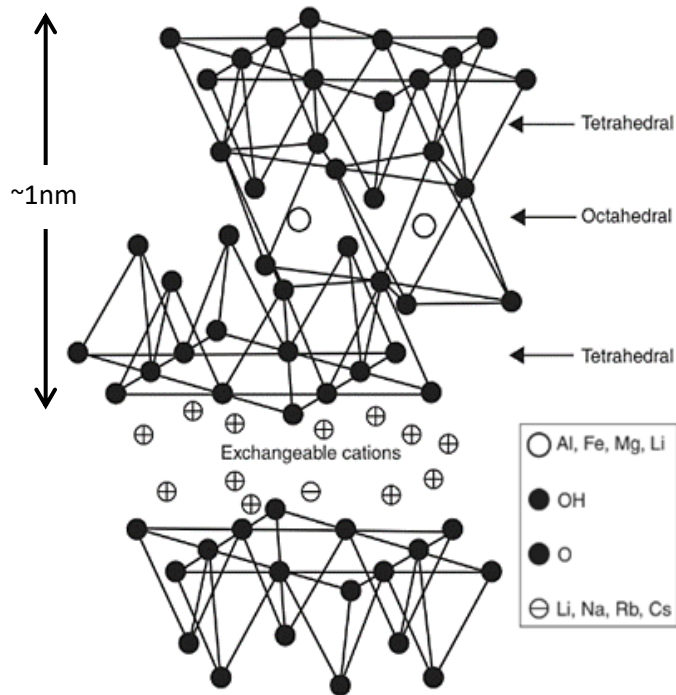


Figure 11: Schematic illustration of octahedral and tetrahedral sheets arrangement of montmorillonite nanoclay layer. Adapted and modified from Ref [147]

2.3 Reinforcement of composite systems and limitations associated with current technologies

With the understanding that composite material is described as the combination of two or more constituent materials to produce a new type of material that has property characteristics that supersede its constituent materials. It is indicative that the constituent materials are optimum components that determine the composite material's mechanical properties [151], together with the knowledge to fine-tune through manoeuvring various parameters of the composite material system, i.e. volumetric content, filler size, orientation, aspect ratio and filler/matrix interfacial interaction [27], [152]. The knowledge in tuning these parameters for optimum performance is important and presents an exciting and significant challenge in materials science. Nevertheless, despite the vast number of possibilities, i.e.

composite reinforcement with fibres, particles, flakes and fillers; there are mainly few designs that currently dominate the engineering world which can be categorised into, fibre reinforced composites which mostly dominates micro-scale composite reinforcement and nanocomposite technologies but yet to fabricate composite material that is strong, stiff and tough remains a challenge [152], [153].

2.3.1 Limitation of fibre reinforcement technology to develop strong, stiff and tough composite material

Fibre reinforcement technology has evolved and has been used widely for various applications with different fibres used to reinforce composite material systems with polymer matrices. While it is evident that these fibres have higher strength and stiffness than their host matrices which are characterised with low strength and stiffness but possess high strain which is often lacking in most fibres. Thus, knowing that these fibres' properties invariably influence the properties of their composite material system [98]. High-performance fibres are mostly of interest for high-tech engineering applications, although the definition of high-performance fibre is not discrete [154]. However high-performance fibres are expected to possess high strength, high stiffness (modulus), toughness, durability, resistance to chemical, flame resistance, etc., but unfortunately, most fibres used for composite reinforcement do not ultimately possess multiple properties as expected [154], [155].

For example, carbon fibre is manufactured in either high strength or high modulus fibre [31], [155] which is dependent on the precursor used for the production of the carbon fibre [31], [154]. Carbon fibres are manufactured through the extrusion of their precursor materials, stabilisation and carbonisation processes to make the precursor filaments into carbon fibres. Thus, based on the precursor of the carbon fibre and processing conditions, the end product

of the carbon fibre tends to have a different microstructure and also different properties [154]. With the structure of carbon fibres influencing their properties, PAN-based carbon fibres have microstructural arrangement reported to be disordered in its arrangement. It is turbostratic and is considered the reason for its high tensile strengths. Considering the difference in the structural property, this has led to carbon fibre selection to be on the merit of desired properties for the intended application, to utilise the benefit of each type of carbon fibre optimally. Thus, most PAN-based Type II carbon fibres are used for applications where strength is essential, and pitch-based carbon fibres are used for applications that require a high stiffness material. Meanwhile, rayon-based carbon fibres have witnessed a decrease in its use compared to PAN or pitch-based carbon fibre. It has a comparatively low tensile strength, and the cost of production is high compared to other precursors type of carbon fibres [154], [155].

The effect of fibre mechanical properties been dependent on its morphological structure has led researchers and material scientist to explore a different mechanism to enhance fibre mechanical properties [156], [157]. Research shows that most fibres strength and stiffness are below their theoretical strength, hence the possibilities to further improve the fibres' strength and modulus through optimisation of their production process [31]. Mikhailova et al. [158] reported that PAN carbon fibre could be produced with a high tensile strength of about 3 - 3.5 GPa and high tensile modulus higher than 700 GPa through fabrication process that involves heat treatment at a temperature range of 2700 - 2900°C together with boronation process. The boronation process allows for the integration of boron into the microstructure of PAN carbon fibre compared to carbon fibre that would ordinarily be spun from PAN carbon fibre precursor at such high graphitisation temperature which often is

characterised with low strength around 2 GPa or less and about 650 GPa tensile modulus [156]. Also, Chae et al. [31] reported a different approach to accustom gel spinning technique for PAN precursor carbon fibre which usually undergoes carbonisation in batches. A different approach was taken in their work with carbonisation process done as a continuous process using poly(acrylonitrile-co-methacrylic acid) (PAN-co-MAA) copolymer to fabricate high strength, high modulus PAN carbon fibre with a tensile strength of 5.5 - 5.8 GPa and tensile modulus of 354 - 375 GPa as average mechanical properties.

Carbon fibre has been reported with various mechanical properties (Mikhailova et al. and Chae et al.), particularly for PAN carbon fibre, as research shows that other PAN carbon fibre have been reported with values reported for both tensile strength and tensile modulus, i.e. IM7 carbon fibre produced by Hexcel widely used for the aerospace application having a tensile strength of 5.6 GPa and tensile modulus of 276 GPa and T1100G carbon fibre manufactured by Toray has a tensile strength of 6.6 GPa and tensile modulus of 324 GPa [31]. While pitch precursor carbon fibre is reported to have a tensile strength of about 3.1 - 3.3 GPa and tensile modulus as high as 820 - 965 GPa [31], [159]. Therefore, it is evident that carbon fibre is fabricated with a wide spectrum of mechanical properties values (tensile strength and tensile modulus). Hence the need for carbon fibres to be classified for easy referencing. International Union of Pure and Applied Chemistry (IUPAC) cited criteria that has put the classification in perspective by providing detailed criteria for fibres classification as follows [54], [159];

- *“Ultra-high modulus type: carbon fibres with modulus greater than 500 GPa*
- *High modulus type: carbon fibres with modulus greater than 300 GPa and strength-to-modulus ratio less than 1%*

- *Intermediate modulus type: carbon fibres with modulus up to 300 GPa and strength-to-modulus ratio above 1×10^{-2}*
- *Low modulus type: carbon fibres with modulus as low as 100 GPa and low strength. They have an isotropic structure*
- *High strength type: carbon fibres with strength greater than 3 GPa and strength-to-modulus ratio between 1.5 and 2×10^{-2} "*

With the improvement made so far, carbon fibres indicate that obtainable mechanical properties like strength and stiffness (modulus) are still remarkably below theoretically predicted values. Considering that carbon fibre is known to have at least about 92 % wt., the composition of carbon atoms which are arranged within in-plane layer having honeycomb-like structures and held together via covalent bond that exist within the atoms thereby having similar crystal structure to graphene which has an in-plane tensile strength of 100 GPa and tensile modulus of about 1TPa theoretically [54]. Despite the improvement in tensile strength and tensile modulus over the years, PAN carbon fibre which is widely used due to its strength measures at about 7 GPa approximately for tensile strength, a value less than 10% its theoretical carbon-carbon bond strength and 324 GPa for modulus which is about 30% its theoretical value [31], [54]. Although tensile modulus over 600 GPa has been reported for PAN carbon fibre, this is achieved at the expense of the tensile strength [158]. Meanwhile, carbon fibre produced from pitch precursor could have a high modulus of about 965 GPa which is above 90% the theoretical value, but the fibre is accompanied with low strength [31], [32], [160].

Similarly, theoretical value for melt-spun polyethylene (PE) fibre is estimated to have 300 GPa modulus and about 30 GPa strength, but so far obtainable values reported is 60 GPa for

modulus and 1.3 - 3 GPa for strength via a melt-spun process. Although 100 GPa has been reported for modulus for fibre produced using gel spinning, which is still less than 50%, the theoretically predicted value [161]. Likewise, fibres like Kevlar, Spectra, M5 poly(hydroquinone-diimidazopyridine) (PIPD) and Poly-p-phenylenebenzobisoxazole (PBO) has also been reported with tensile modulus below their theoretical values, and tensile strengths of about 40-50% of their theoretical values have been achieved so far [154]. This indicates that there might be possibilities to optimise the fibre properties, but the effort to improve these mechanical properties in a single type of fibre often result in property trade-off and more, so improvement seen is still below theoretically predicted values [31], [155]. Research shows that most fibres do not ultimately possess multiple properties as desired especially properties like strength, stiffness and toughness in a fibre. While to some extent, there have been possibilities to improve these mechanical properties in fibre, as research shows, fibre fabrication processes influence fibre mechanical properties.

Smith and Lemstra [162] investigate fabrication process of ultra-high-strength polyethylene fibre using solution spinning and hot drawing technique to improve polyethylene fibre, which exhibits a tensile strength at break of about 3 GPa and tensile modulus (stiffness) 90 GPa, compared to solid-state extruded polyethylene fibre which has a modulus of about 70 GPa and strength below 1 GPa. Also, use of the gel-spinning process by Chae et al. to improve mechanical properties of poly(acrylonitrile-co-methacrylic acid) (PAN-co-MAA) copolymer carbon fibre carbonised subsequently in a continuous process to produce fibres with a high level of structural orientation and crystallinity, thereby improving fibre mechanical properties [31], [163]. Kitagawa et al. [164] investigate the fabrication of Poly-p-phenylenebenzobisoxazole (PBO) fibre using non-aqueous coagulation and conventional heat

treatment which is different to the usual process that involves fabrication of PBO fibre through aqueous coagulation process. The resulting fibre from non-aqueous coagulation method is reported to have its modulus enhanced by approximately 27% compared to aqueous coagulation method. The non-aqueous coagulation method influences the PBO fibre molecular orientation causing it to be more orientated in the fibre axis direction.

Research shows that fibre fabrication process development or modification could improve mechanical properties like fibres' strength and stiffness. Otto [165] expressed a similar view investigating the relationship of the tensile strength of glass fibre to diameter, hence having a varied stance to Griffith [123] which has been given credence by other researchers tensile strength of glass fibre increases with reduction in fibre diameter. In Otto's work, the improvement of fibre strength is influenced by careful control of conditions at which the fibre is formed, i.e. temperature and pulling speed (drawability) rather than diameter-pendent [165]. While it is indicative that fibre fabrication process influences the mechanical properties of fibres as the process appears to enhance desired mechanical properties like strength and modulus, but there exist some shortcomings associated with some of these processes. For example, high-performance polymer fibres processed via gel spun often use solvent as part of the process that is considered to be hazardous to health and environment, i.e. gel spun ultra-high molecular weight polyethylene (UHMWPE) fibre [154], [166]. Other non-hazardous solvents have been investigated as an alternative solvent for fabricating such fibres by various researchers. However, significant success is yet to be reached as results reported were not definite whether or not the newly aimed solvents are a factor in enhancing mechanical properties but could help achieve higher drawability [167]. Regarding fibre forming process, while Otto indicated that conditions at which fibres are formed influences there strength

rather than general acceptance of Griffith's work, Anderegg [168] cited similar views to Otto but buttressed the position of Griffith. Anderegg's work involving glass fibres cited that fibres solidify from melt process often contain impurities, i.e. collected dissolved and undissolved gas present within the fibre, thereby causing discontinuities within the fibre giving rise to defects [168].

Thus, to ensure homogeneity and eliminate defect with attention given to the fibre forming process by maintaining purity and uniform dispersion, together with adequate measures to ensure as far as practicable to eliminate gas bubbles. While such a process is considered an ideal approach, it undoubtedly remains a daunting technical process [168]. Meanwhile, when the fibres are drawn into a smaller diameter, the tendency of defect present such as gas bubbles reduces and reported strength and modulus of fibres is noted to increase as the fibre diameter decreases as Griffith reported [123], [168]. Most conventional fibres, i.e. carbon fibres, glass fibres, ceramic fibres, aramid fibre, etc. have been reported to increase in strength and modulus with the decrease in diameter [123], [168], [169], [170]. However, fibres used in fibre reinforcement technology are still few microns thick without the absolute certainty of being defect-free regardless of the fabrication process used, thus affecting the composite material system mechanical properties. Studies show that ultrafine fibre, which is less than a micron in diameter size compared to conventional fibres possess mechanical properties that surpass conventional fibres [154], [171], [172] but are lacking in strain like conventional fibre due to high draw ratio [173].

Nevertheless, that most available fibres mechanical properties are below their theoretical predicted values; however, based on their available mechanical properties like strength and stiffness, these fibres have been adequately employed to fabricate composite materials. Due

to stretching fibres undergoes during the fibre production process, their ability to elongate like the host matrix poses toughness challenges. Therefore, to fabricate composite material that is strong, stiff and tough with fibre reinforcement technology is limited as there is often a trade-off in properties. While fibre reinforced composite material system could be processed in either short or long continuous fibre reinforcement within a matrix system, i.e. thermoplastic and thermosetting polymers [174]. To complement the inherent properties of the reinforcement fibre, the interplay of various parameters such as fibre/matrix interfacial adhesion, the aspect ratio of fibre, orientation of fibre, fibre volume fraction, and fibre distribution to allow for efficient transfer of stress load from the matrix to the fibre requires consideration to ensure the optimum design of a composite material system with best mechanical properties is important [16], [175], [176]. While interfacial adhesion is necessary to be adequate for transfer of stress from the matrix to the fibre, the fibre volume fraction is required to be sufficiently high for the composite material strength and stiffness to be maintained, but the composite material toughness is often sacrificed [17], [177]. Considering that the fibre cannot withstand significant elongation like the matrix and when stressed to the point of fracture, the applied stress is redistributed to nearby fibre through the fibre/matrix interface causing a high-stress concentration thereby causing successive fibre breakage which leads to the composite material to experience fibre dominated failure as a result of failure at fibre strain which is often characterised with a brittle failure [33], [34].

2.3.2 Shortfall of nanocomposite technology in developing strong, stiff, and tough composite material

Whilst filler reinforcement volume fraction is one of the parameters that influence composite system reinforcement, and fibre reinforced technology been reported of the inefficiency to

provide adequate reinforcement at low volume fraction [23]. Meanwhile, nanocomposite technology has taken advantage of inherent filler properties to reinforce matrices at low volume fraction with better performance than fibre technology [22], [23]. For example, the reinforcement of nylon 6 with exfoliated clay yields improved mechanical properties (strength and stiffness) of the matrix systems with <10 wt. % volume fraction of clay [23], [178]. The nanofillers are regarded as close to ideal defect-free material and therefore possess high strength and stiffness compared to their counterpart reinforcement fillers in the micron size range [42]. Taking advantage of their large surface area to volume ratio and high aspect ratio to utilise their inherent mechanical properties (high strength and stiffness) in reinforcing matrix systems [19]. Meanwhile, with the understanding that increasing the volume fraction of reinforcement filler within a composite system should ideally result in the corresponding improvement of the composite system mechanical properties. This is not the reality with nanocomposite materials at high volume fraction due to various difficulties, i.e. agglomeration formation. Though, nanofillers could improve composite material mechanical properties at low volume fraction, nevertheless, when compared to fibre reinforced composite materials at high volume fraction; fibre reinforcement provides better reinforcement efficiency with regards to improved mechanical properties [23], [42], [179].

Nanocomposite systems modelled through continuum mechanics considers fillers form and volume fraction loading within a matrix system as required parameters to predict the composite system properties [178], [180]. The improvement of nanocomposites mechanical properties at low volume fraction with nanofillers was considered astonishing as it was not initially expected [178]. This has propelled researchers' interest to explore further nanofillers potentials which have been adapted to other applications such as flame resistance,

biomedical, thermal, electrical and barrier properties to mention few [178], [181], [182], [183]. Nanocomposites' underperformance at high volume fraction has been investigated to gain insight into such unimpressive performance, and some factors are identified and considered to influence the nanocomposites materials' mechanical properties. This includes morphology of the nanofillers and composite material, method of processing and matrix/filler interactions [184].

Morphology reflects the size and structural array of nanofillers embedded within the matrix to provide reinforcement. Nanocomposite matrices are reinforced with nanofillers having at least one of the nanometer scale's geometry sizes below 100 nm while ensuring uniform distribution of nanofillers within the nanocomposite, the process used in fabricating the nanocomposites contributes to the fillers' effectiveness to provide reinforcement [147]. Different techniques have been used to fabricate nanocomposites, i.e. in-situ polymerisation, solution induced intercalation, melt intercalation, etc. [19], [23], [147]; however, fabrication process needs to be adequate to ensure composite material with improved properties can be produced. For example, layered fillers such as clays show different interaction between the filler and the polymer in Figure 12. Figure 12c illustrates the exfoliated clay nanocomposites fillers can effectively use their inherent mechanical properties compared to Figure 12a, which is phase-separated with the fillers stacked, and invariably the reinforcing element cannot effectively provide reinforcement [19]. More so, with the clay exfoliated increases the filler aspect ratio, a parameter that influences composite mechanical properties [147].

So far with these processes, research shows that effective reinforcement is mainly obtainable at a low weight fraction of about <5%wt [23], [185]; meanwhile, composite material tensile strength and modulus achieved is incomparable to fibre reinforced technology at high volume

fraction [23]. Podsiadlo, P. et al., [42] showed a possible approach to increase weight fraction of nanofillers in a composite system using a bottom-up assembly approach known as layer-by-layer fabricate composite material with high filler volume fraction using Montmorillonite (MTM) clay as reinforcement filler in poly(vinyl alcohol) up to about 70% wt (≈ 50 volume %) which yield improvement in strength and stiffness of about 100% and 62% respectively compared to neat poly(vinyl alcohol), but unfortunately, the challenge to maintain toughness persist as the material's toughness is significantly reduced (Table 3).

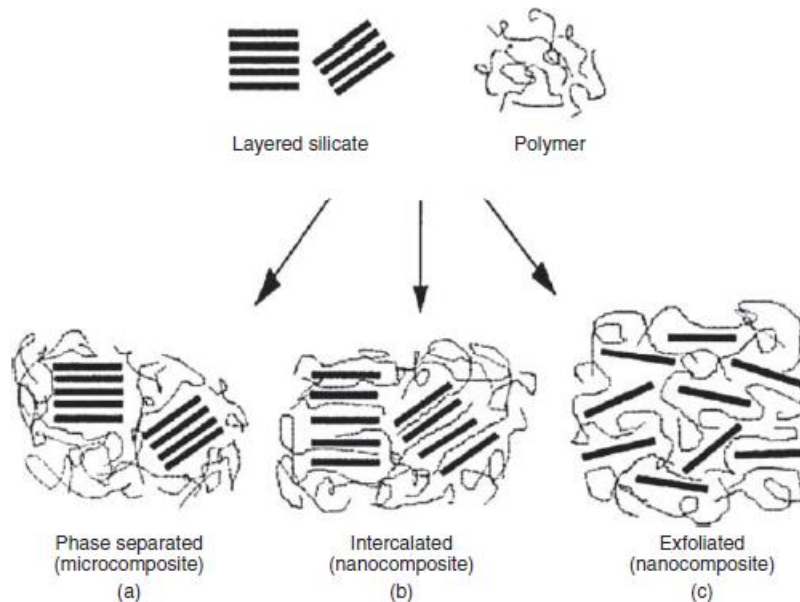


Figure 12: Illustration of embedded silicate clay layers for polymer reinforcement. Adapted from Ref [147]

Table 3: Using layer-by-layer to increase nanofiller (Montmorillonite) in poly(vinyl alcohol). Adapted from Ref [42]

Sample type (N)	Tensile strength σ_{UTS} (MPa)	Modulus E' (GPa)	Ultimate strain ϵ (%)
PVA (5)	40 ± 4	1.7 ± 0.2	35 ± 4
PVA with GA (5)	40 ± 10	2.0 ± 0.5	3.3 ± 1.3
PDDA (5)	12 ± 4	0.2 ± 0.03	48 ± 9
PDDA-MTM (*)	100 ± 10	11 ± 2	10 ± 2
PVA/MTM (5)	150 ± 40	13 ± 2	0.7 ± 0.2
PVA/MTM with GA (5)	400 ± 40	106 ± 11	0.33 ± 0.04

2.3.3 Current progress on toughness enhancement mechanism to develop strong, stiff, and tough materials

The ability to maintain toughness in either fibre reinforced composite and nanocomposite has kept researchers and material scientists to continue to intensify effort to make a breakthrough with the intention to design composite material that is strong, stiff and tough. Considering that both technologies could have synthesised composite material achieve improved strength and stiffness compared to the neat polymer matrix but often challenging to maintain toughness and vice-versa [186], [187]. While the reinforcement filler could be similar or dissimilar to the matrix in nature, thereby having an interface between the matrix and reinforcement filler [188]. Despite this and through research, both technologies have been adapted such that the interface can transfer stress subjected to the matrix unto the reinforcement filler. Hence, there must exist good bond adhesion at the interface between the matrix and the reinforcement filler without toughness being compromised [16], [188].

The existence of good interfacial bond adhesion has a synergistic effect of the interfacial region together with the composite material fillers size, volume fraction, aspect ratio, state of dispersion and alignment in affecting the material fracture toughness and correspondingly other composite material mechanical properties [16], [188], [189]. The interfacial bond adhesion is influenced through various mechanisms which include, i.e. wetting, adsorption, chemical bonding, electrostatic attraction and mechanical. However, optimisation of conditions at the interfacial region is often achieved through modification mechanically, i.e. fibre etching to introduce surface roughness that interlocks with the matrix and chemically, i.e. through the use of coupling agents like silane [189]. Thus, a process achieved through

approaches involving reinforcement filler modification such as surface treatment using silanes, plasma, alkalis, etc.; matrix modification such as the introduction of specific functional group in a matrix structure, i.e. maleic anhydride grafted polypropylene (PP-g-MA) or both [97], [190]. While it is important to have adequate interfacial bond adhesion for efficient stress transfer, to maintain toughness the prime importance is to have composite materials absorb as much fracture energy as possible before failure, thus exhibiting different fracture mechanisms such as crack bridging, crack deflection, pull-out, etc. [191], [192]. Therefore, to increase composite material toughness, various techniques have been developed, such as introducing rubber, i.e. nitrile liquid rubber, to the matrix system [35]. While this approach has shown to be efficient to improve composite material toughness, it is at the expense of other properties such as the decrease in either tensile strength or tensile modulus and possibly both [187], [193]. For example, Laura et al. [194] investigate rubber toughened nylon-6 composite material reinforced with glass fibre surface-treated with different modifiers, while the effect of the rubber yield significant improvement, no considerable changes with tensile modulus, however, the tensile strength for each composite material drastically reduces and several other research has reported similar trend considering that rubber possesses relatively low tensile strength and tensile modulus and composite material properties depend on its constituents materials [35], [195], [196].

Likewise, research has also shown the use of nanomaterials like graphene, nanoclay, and carbon nanotubes as second phase reinforcement filler to optimise composite material mechanical properties with the inclusion of maintaining toughness in reinforced polymer composites [187], [197], [198]. The nanomaterial is either dispersed within the matrix system or grown on fibres to impede crack growth and increase toughness, thereby exhibiting various

toughness enhancement mechanism such as crack pinning, crack deflection, debonding, pull-out, etc. [199]. While some reports show an increase in composite toughness, others reported contrary results. Also, the tensile strength and tensile modulus often exhibit no significant improvement and decrease in value than composite material reinforced without nanomaterial, thereby providing less reinforcement efficiency [199], [200], [201]. Meanwhile, delamination is recognised to undermine composite material fracture toughness and other mechanical properties, particularly in laminated composite materials. Various techniques have been applied to maintain toughness; this includes reinforcement in the through-thickness direction of the composite material using techniques such as stitching and z-pinning. Stitching uses high tensile strength yarn, i.e. glass, carbon or Kevlar sewn through the thickness of the composite material, while z-pinning uses high stiffness, high strength thin metal or fibrous pins, i.e. titanium alloy, steel or fibrous carbon. Reinforcement in the through-thickness direction has been reported to enhance composite material elastic properties while delamination toughness is improved. However, the composite material's in-plane properties decrease due to defect caused by reinforcement of the composite through-thickness such as fibre breakage and waviness [38], [39], [40], [41]. Similarly, to maintain toughness, interleaving technique has been applied by integrating a thin, tough, flexible material between composite layers to improve the composite material damage tolerance. The interleaving material could be incorporated in the form of particles, film or fibre material between the plies to promote interlaminar toughness and decrease delamination. While improvement is achieved regarding toughness, this is accompanied by a decrease in composite material in-plane strength and stiffness [202], [203].

2.4 Bio-inspired composite in developing strong, stiff and tough materials such as nacre

Nature has been able to circumvent the challenge of maintaining the trio mechanical properties, unlike synthesised materials. Naturally developed composite materials like nacre and bone are typical examples of materials scientists have tried to replicate to design composite materials with strength, stiffness and toughness. Biological material like nacre is part of the hierarchical structure of shell anatomies of mollusc and gastropods located at their shell's inner layer (Figure 13). Nacre is composed of polygonal aragonite and organic materials. The aragonite is a nanometer-sized crystallographic form of calcium carbonate (CaCO_3) having a width of about $5\mu\text{m}$ and thickness 500nm that constitutes about 95wt.% of the nacre structure and reinforces the 5wt.% organic material consisting of proteins and polysaccharides which act as the matrix system [45], [204]. Considering such percentage of reinforcement phase (aragonite) of material with the organic matrix which plays a significant role in spatial and chemical control of crystal nucleation and growth of aragonites, forming a brick-and-mortar like microstructure with aragonite to provide toughness via dissipation of fracture energy, by enhancing crack deflection and slip resistance, which has led to extensive studies of nacre [204], [205], [206].

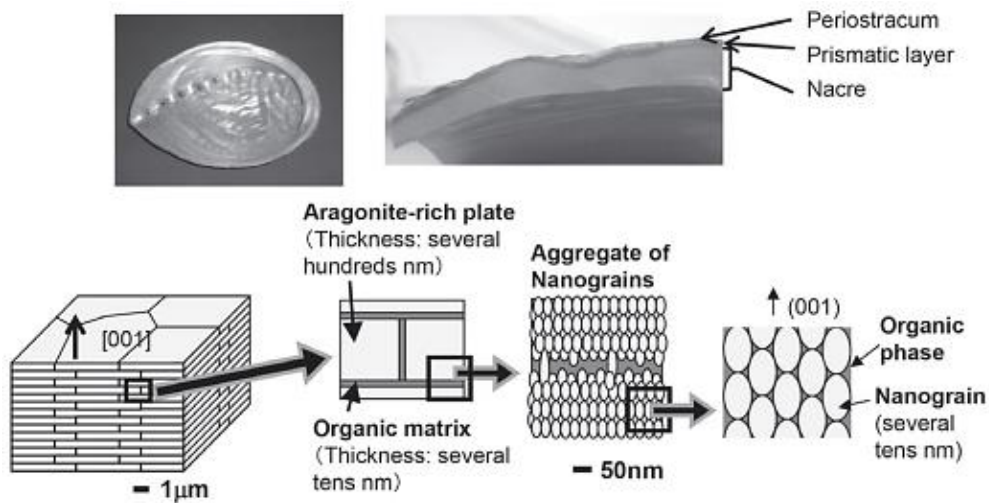


Figure 13: Schematic structure of nacre showing its brick and mortar arrangement aragonite platelets in organic matrix. Adapted from Ref [206]

Research shows that nacre excellent mechanical properties is influenced by its architecture structural array [204], [205], [206]. The aragonite platelets show firmly interlocked structural arrangement within the organic matrix and depending on nacre's hydration condition exhibits different mechanical response (Figure 14). Under tensile stress, hydrated nacre deforms elastically and afterwards exhibit work-hardening behaviour due to further deformation (Figure 14a). The interlocked platelets deform linearly and after yielding point reached begins to slide along the interface between the platelets. Exerted stress beyond the yield point causes work hardening to ensue through debonding of the platelets at the boundaries (Figure 14b) for sliding to proceed resulting in the macroscopic elongation of the nacre leading to successive accumulation of pull-out of the platelets entirely to cause a failure (Figure 14c). Meanwhile, dried nacre exhibits a brittle failure showing linear deformation up to the yielding point and fractures catastrophically. However, though the failure is catastrophic yet indicates that the platelets get pulled out [206]. Hydrated nacre shows higher toughness than dried nacre, though the interface's morphology cannot solely explain the dependence of the nacre's

mechanical response on its hydrated condition. However, it is considered that the organic matrix between the platelets plays a crucial role to control the interface sliding behaviour of hydrated nacre. With the organic matrix sensitive to water, the nacre interfacial properties are altered due to hydration, thereby influencing the nacre's macroscopic mechanical response. The hydrated organic matrix functions as a lubricant to control the interface shear sliding, unlike dried nacre, which has the organic matrix dehydrated and stiffened as flexibility and fluidity lost [206].

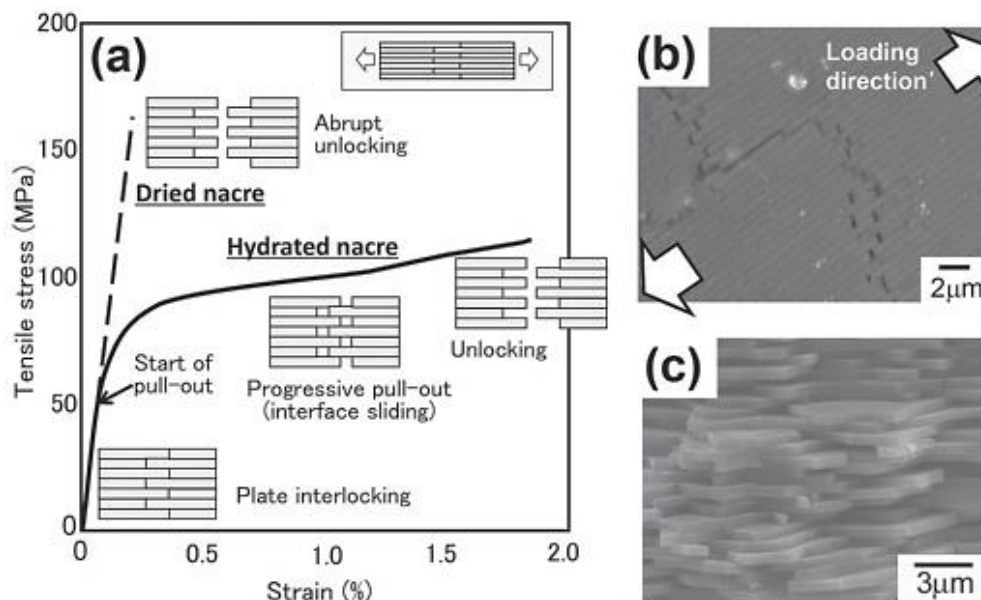


Figure 14: (a) Stress-strain curve of fractured hydrated and dried nacre, (b) debonding of polygonal aragonite platelet at the boundary with the organic matrix without platelet fracture and (c) pulled out platelets. Adapted from Ref [206]

Furthermore, in addition to the interface influence of nacre exhibiting adhesion and viscoelastic of the organic interface, the toughening effect of nacre has been attributed to several other toughening mechanisms, i.e. fracturing and delamination to create new fracture surface, crack deflection, pull-out of the platelets, crack bridging etc.; while different factors such as nanoasperity on platelets, mineral bridging and platelet waviness are considered components influencing the toughening mechanism exhibited. However, the interlocking of

the platelets and their accumulative pull-out to fracture has been the dominant influence on nacre toughness while maintaining strength and stiffness as cumulative stress is required for successive accumulation of platelets pull-out to occur during work hardening [206], [207]. Mimicking structural array of nacre to fabricate bio-inspired synthesised composite material has been explored by several researchers using various fabrication methods such as; layer-by-layer, electrophoretic deposition, sputtering, spin coating and ice templating [206]. Research shows that improved strength and stiffness achievable with toughness maintained; however, this is achieved at a relatively low volume fraction of about 20% [26], [45]. Meanwhile, increasing the volume fraction to higher percentage result in increased strength and stiffness with sufficiently high fracture toughness but fails without indication of plastic deformation, which is often catastrophic and brittle [42], [45].

2.5 Composite modelling

Modelling of the composite system has been used as an accessible tool to predict material behaviour through computational (i.e. numerical and analytical) evaluation to understand the physical mechanisms that govern a material's behaviour. Hence, it provides the knowledge that can be used to design, improve, and effectively tailor material properties such that components and morphology structures of composite materials can be investigated in depth [208]. With various developed models used in composite material system modelling, it is essential that when adopting a model for composite system analysis, the model adequately considered closely representing problem been investigated with underlying assumptions [208], [209]. Some of the commonly used modulus and strength prediction models include the Rule of Mixtures, Shear Lag, dilute Eshelby, Halpin-Tsai, and Mori-Tanaka. Accordingly, these models are modified to suit the modelling analysis to adequately represent the problem

investigated [124], [210]. Most of the model micro-mechanical analysis often involves the concept of representative volume element (RVE) [211], [212]. Rule of Mixture is the simplistic model to predict composite material system mechanical properties; however, Shear Lag model is used within the scope of this research to predict composite strength and Halpin-Tsai model composite modulus under tough fracture.

Cox developed the shear-lag model in 1952 on the basis that the force balance between the matrix and fibre is due to the matrix being able to transfer exerted stress unto the fibre via shear stresses at the interface [213]. The model is widely used for theoretical prediction of strength and damage failure of both long and short fibre reinforced composites and nanocomposites [211], [214], [215], [216], [217], [218]. Comparing the Shear Lag model with Rule of Mixture accordingly, it is credible to consider that with the introduction of fracture term (α) the Shear Lag model could be regarded as modified Rule of Mixture model [218]. The Rule of Mixtures model is a relatively simple model used to predict mechanical properties of composite material systems, particularly the bi-component material system like long fibres aligned parallel in the same direction within a matrix [124]. When the loading condition is in the direction of the reinforcement filler, i.e. parallel to fibre length, Rule of Mixture model assumed that both the matrix and fibre experience same strain (isostrain) when subjected to external load stress exerted in the fibre longitudinal direction. Though the Poisson contraction of the fibre differs from that of the matrix, resulting in additional stress unaccounted for, this is regarded to be about 2% of an error compared to experimental verification and could be considered as inconsequential. However, Rule of Mixture does not consider other parameters that influence composite material mechanical properties, i.e. aspect ratio, the interfacial property, etc. which are accounted for in modified Rule of Mixture [16], [218].

Furthermore, according to the Rule of Mixture, when the composite system is loaded in the transverse direction (perpendicular direction to the longitudinal direction). It is assumed that both the fibre and matrix experience the same exerted stress (isostress). However, the composite material experiences non-uniform strain distribution, resulting in strain magnification within the composite system. Meanwhile, Hapin-Tsai simplified the solution by making more realistic assumptions that consider the various composite system characteristics, i.e. aspect ratio, packing geometry, and loading condition, in making better estimations unlike Rule of Mixture model [16].

Hence, using Shear Lag and Hapin-Tsai models for modelling different reinforcement fillers to investigate the feasibility to produce composite materials material with strength, stiffness, and toughness through an approach based on data-driven material characterisation methodology [219], [220], [221]. Four types of polymer matrices (epoxy, nylon, polypropylene and polyethylene) are modelled with different reinforcement fillers (glass fibre, carbon fibre, glass flakes, montmorillonite clay, graphene and single-wall carbon nanotube). Theoretical analysis of these fillers having different thickness sizes is assessed to determine obtainable mechanical properties within their size range to identify ideal filler in developing a novel composite material system under tough fracture with modelling data extracted from published literature.

3.0 Methodology

The chapter provides details of experimental procedures carried out and modelling work conducted regarding the research aims. The experimental procedure describes materials used and techniques applied for material characterisation to support modelling work performed on various reinforcement fillers. The modelling work focuses on providing details involved in gathering data for different reinforcement fillers to compute modelling for comparable analysis using existing composites models to determine composite material mechanical properties. Section 3.1 describes the material characterisation of size and distribution to establish the average aspect ratio of each glass flakes investigated. This involves identifying the type of glass flakes to be examined, details of procedures used to determine the size and distribution of individual glass flakes investigated, and the inclusion of statistical analysis used. Section 3.2 focuses on the modelling work and details how values used in composite models have been generated to determine obtainable mechanical performance of a typical composite system of different fillers investigated to reinforce commonly used matrices.

3.1 Material characterisation – Glass flakes

The glass flakes used in this study were supplied by Glass Flakes Ltd in various thickness namely 100nm milled, 350nm milled, 350nm unmilled, 850nm milled, 850nm unmilled, 0.8 - 1.3 μm and 2.3 - 3.3 μm . The glass flakes were labelled as untreated E-glass type. This was confirmed and identified as untreated E glass type via FT-IR analysis using Perkin-Elmer Universal ATR Sampling Accessory (Spectrum 100 FT-TR) spectrometer at 2 cm^{-1} spectra resolution with FTIR spectra scanning in the range of 4000 - 650 cm^{-1} . To determine the average aspect ratio of each glass flake which is the ratio of the glass flakes length to

thickness, thickness size and length distribution characterisation of the glass flakes are required, hence details of the characterisation procedures are given in subsequent sections.

3.1.1 Size Characterisation – Thickness Measurement

Though the supplier specified the glass flakes thickness, the importance of filler's aspect ratio to support the modelling work requires that the glass flakes thickness be ascertained. Each of the glass flakes thickness was measured using a scanning electron microscope (SEM). Samples were prepared for each glass flakes by having 2-3mg of the glass flakes dispersed on a carbon tape affixed to the angular face of an angled etched SEM stud. The stud's dispersed glass flakes were given a 10nm gold coating using Quorum (Q150R ES) gold coater before the stud been placed in JEOL Field Emission Scanning Electron Microscope (JSM-7100F) and operated at 1kV acceleration voltages for thickness examination. An angular etched SEM stud was preferred as it helps with effective positioning, i.e. tilt of dispersed glass flake for easy view analysis. Sample images were taken and analysed using Image-J, which is an image processing software.

3.1.2 Size Distribution – Length Measurement

To determine individual glass flakes aspect ratio; the average length of the glass flakes was measured with Celestron LCD Digital optical microscope using objective lens 4x. The camera sensor provides 10x the objective lens to yield 40x object magnification. For each glass flakes, 3-5mg is placed on a microscope slide and spread out using a spatula. The micrographs of the dispersed glass flakes were taken under the optical microscope. Micrograph of a graticule was also taken to enable length measurement of the micrographs taken for the dispersed glass flakes using Image-J¹ for each glass flakes investigated. Similarly, the same procedure was

¹ ImageJ; National Institutes of Health (NIH) version 1.52

repeated to determine the aspect ratio after manoeuvring each glass flakes via ball milling. Individual glass flakes aspect ratio was altered via ball milling by filling 50ml centrifuge tubes for each glass flakes and 11 milling balls which are 13mm in diameter to breakdown the glass flakes aspect ratio over time through handshaking. Each centrifuge tube was filled as follows; 0.5g for 100nm, 1g for 350nm milled, 1g for 350nm unmilled, 1.5g for 850nm milled, 1.5g for 850nm unmilled and 1.5g for 0.8 - 1.3 μ m respectively.

Manual shaking the centrifuge tubes through a handshake to breakdown the glass flakes at times duration of 2.5mins, 5mins and 7.5mins, except for 100nm milled glass flakes at times duration of 1.5mins, 3mins and 4.5mins. While 2.3 - 3.3 μ m glass flakes were excluded from aspect ratio breakdown, its aspect ratio without breakdown is very small and does not require further chopping down. Data of length measurement obtained from micrographs processed with Image-J for glass flakes without size breakdown and those with size breakdown was analysed statistically using Minitab².

3.2 Modelling Work

The modelling analysis is computed for different reinforcement fillers investigated through a data-driven approach with commodity polymers. Reinforcement fillers investigated include glass flakes, glass fibre, carbon fibre, montmorillonite clay, graphene, and single-wall carbon nanotube (SWCNT). Each filler is modelled with polypropylene, polyethylene, nylon 6, and epoxy matrix systems using shear-lag and Hapin-Tsai models. Based on these models, reinforcement filler and matrix system tensile strength and tensile modulus were obtained through a literature search of published data; likewise, the interfacial shear strength (IFSS) for individual filler/matrix system used in computing the modelling analysis. For glass and carbon

² Minitab; Minitab, LLC version Minitab 19

fibres, considering that the fibre diameter correlates to the fibre tensile strength and tensile modulus. The data obtained is processed through the application of logarithm to have a linear equation. The linear equation's anti-logarithm provides an equation used to determine the fibre mechanical properties at specified diameter, i.e. 3 μm and 7 μm for glass fibre and carbon fibre respectively. Furthermore, glass flakes' mechanical properties are determined using the equation obtained for glass fibre at each glass flakes determined thickness, in-view that the glass flakes are identified to be the same type of glass material considered for glass fibre. Whilst tensile strength and tensile modulus of graphene, clay and SWCNT are applied directly for modelling analysis. IFSS for each matrix system is determined at maximum and minimum values for glass fibre and carbon fibre. However, IFSS values for glass flakes is taken to be same for glass fibre as it is the same glass material. Also, the IFSS value of montmorillonite clay is as well taken as that of glass fibre on the assumption that their morphology composition is relatively similar for modelling purposes. Likewise, for graphene and SWCNT, IFSS value for carbon fibre is applied on the assumptions that the fillers are carbonaceous.

3.2.1 Glass fibre/glass flakes tensile strength and tensile modulus

Identifying the type of glass, the glass flakes are manufactured from through Fourier Transform Infra-Red (FT-IR) analysis helps minimise error and likewise serve as a guide in searching for publications related to the type of glass flakes identified. Figure 15 shows the FT-IR analysis plotted for 350nm milled glass flakes, while all studied glass flakes exhibited the same trend. Comparing the FT-IR result with reported article FT-IR on E-glass fibre (Figure 16) [222], shows that the FT-IR profile is similar to untreated E-glass fibre as the peaks tend to exhibit the stretching of the Si-O vibration which is around approximately 1000 cm^{-1} [222], [223]. Therefore, ascertains that the glass flakes are also surface untreated. On this basis, investigated glass flakes are considered to be E-glass type without surface treatment.

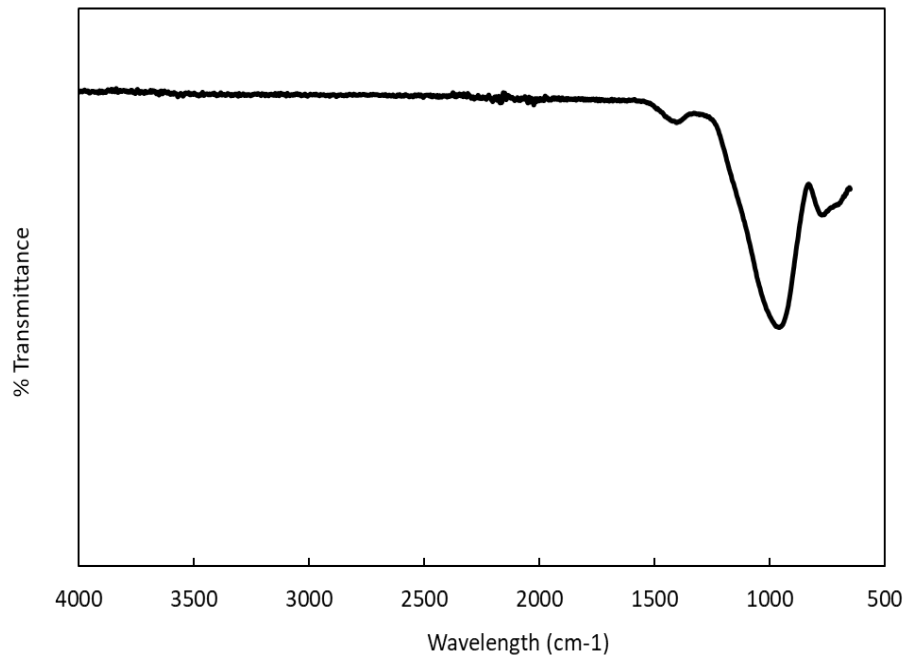


Figure 15: FT-IR profile for investigated glass flakes (350nm milled)

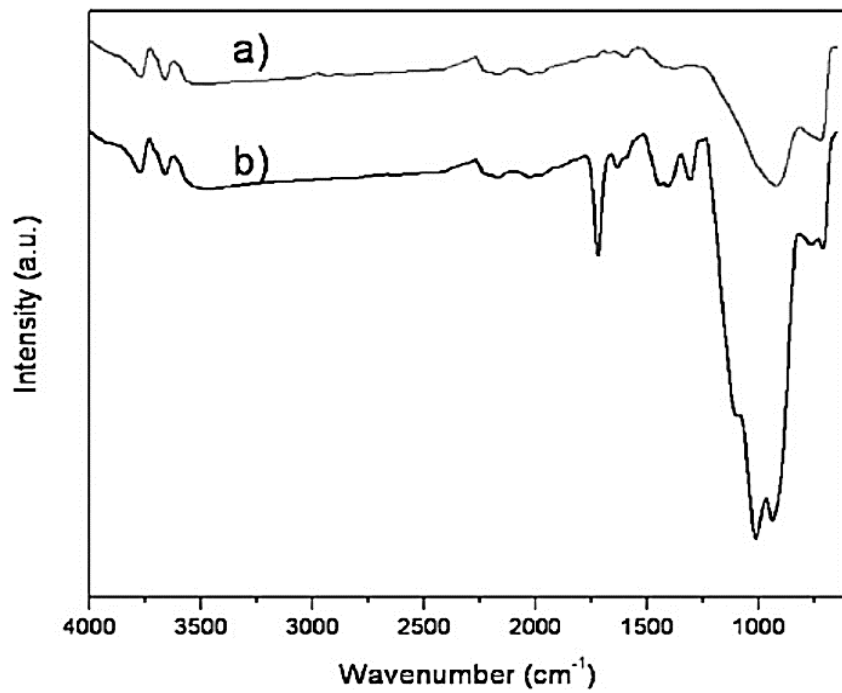


Figure 16: FT-IR analysis of E glass (a) nonsilanised (surface untreated) and (b) silane treated. Adapted from Ref [222]

The glass flakes identified as E-glass type, tensile strength and tensile modulus for E-glass extracted from published literature Ref [224] and [225] respectively. Using Web-plot Digitizer [226], Figures 17 and 18 shows the extracted tensile strength and tensile modulus data plotted against fibre diameter for E-glass, respectively. Extracted data translated into log-plot by taking the logarithm value of data points from which a linear equation is obtained for tensile strength (Figure 19) and tensile modulus (Figure 20). Determining the anti-log for the linear equation; a general equation is obtained. Hence, for glass fibre and glass flakes, Equation 1 and 2 are the general equations for tensile strength and tensile modulus, respectively. Therefore, tensile strength and tensile modulus for investigated glass flakes determined at their known thickness. Though the mechanical properties are fibre related and studied glass flakes are irregularly flat/non-spherical shape. However, research shows that dependency of material mechanical properties on shape decreases as the material increase in size, (i.e. > 50nm) [227], [228]. Meanwhile, the thinnest glass flakes investigated has an average thickness of 100nm. Likewise, the tensile strength and tensile modulus for glass fibre analysed at 3 μ m diameter are determined using Equation 1 and 2.

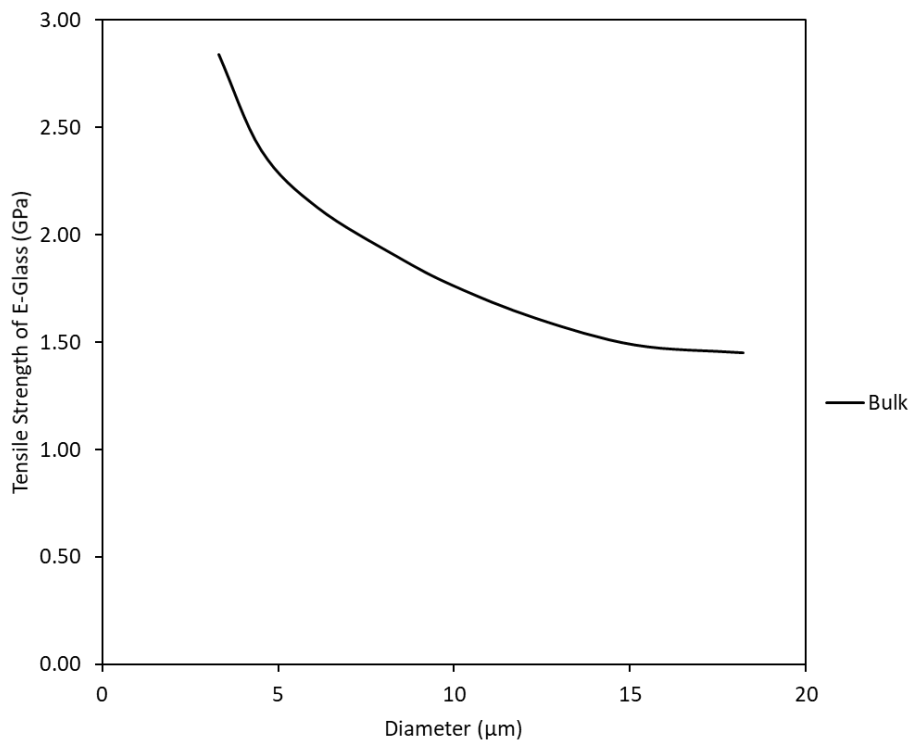


Figure 17: E-glass strength plotted against fibre diameter. Adapted from Ref [224]

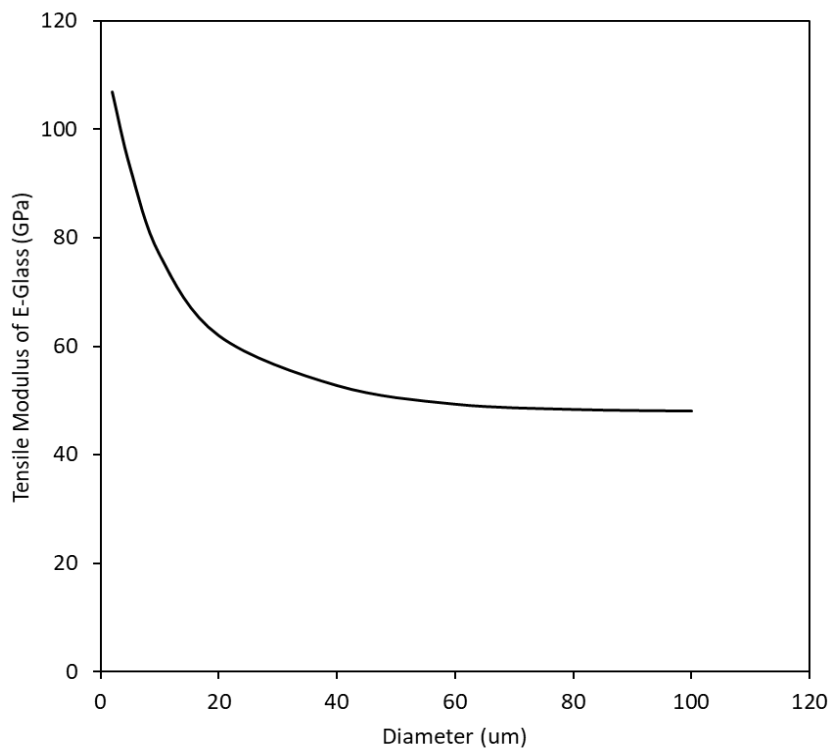


Figure 18: E-glass modulus plotted against fibre diameter. Adapted from Ref [225]

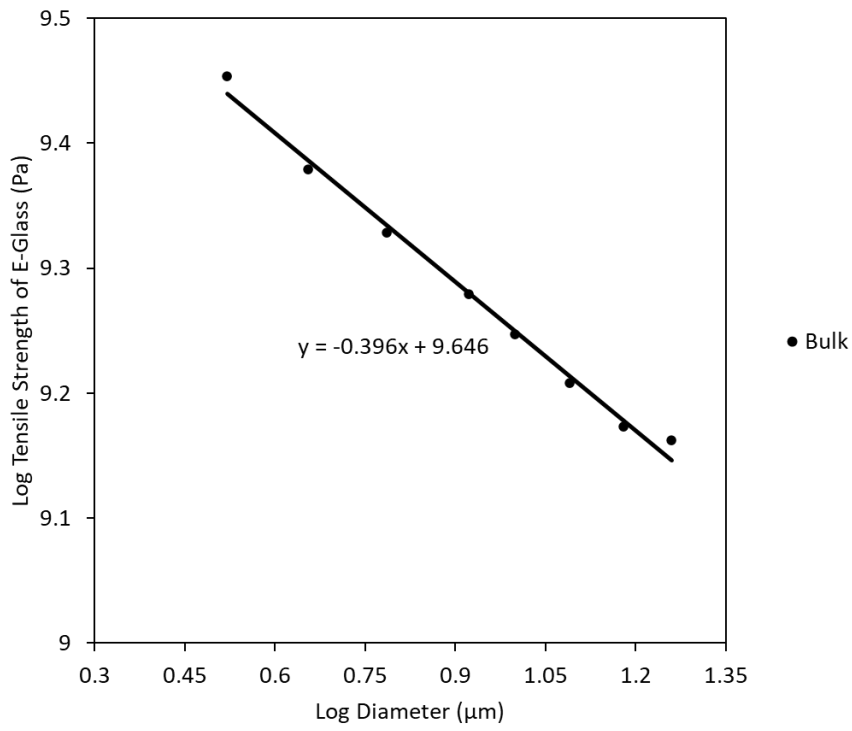


Figure 19: Log-plot for E-glass strength plotted against fibre diameter

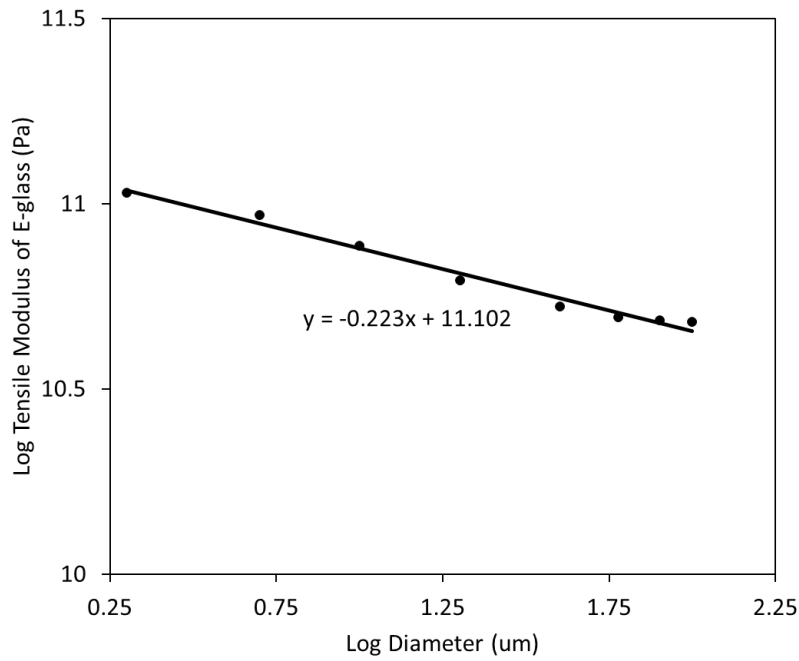


Figure 20: Log-plot for E-glass modulus plotted against fibre diameter

$$\text{Equation 1: } \sigma_f = \frac{10^{9.646} \times t^{-0.396}}{10^9}$$

$$\text{Equation 2: } E_f = \frac{10^{11.102} \times t^{-0.223}}{10^9}$$

Where σ_f and E_f represent glass flakes ultimate tensile strength and modulus respectively, and t represents glass flakes thickness.

3.2.2 Carbon fibre tensile strength and modulus

Tensile strength and tensile modulus for carbon fibre extracted from published literature Ref [54], which involve considering classification criteria for high-strength type carbon fibres. According to IUPAC classification criteria, high-strength types carbon fibres are considered to have strength greater than 3 GPa and the strength-to-modulus ratio between 1.5 and 2 x 10⁻². Table 4 shows mechanical properties for high-strength type carbon fibres. Thus, taking the logarithm value for both tensile strength and tensile modulus (Table 4), the logarithm values are plotted in Figure 21 and 22 for tensile strength and tensile modulus respectively with their corresponding linear equations shown. Finding the linear equation's anti-log is used as a general equation to determine the carbon fibre tensile strength (Equation 3) and tensile modulus (Equation 4) at known fibre diameter.

Table 4: Mechanical properties of carbon fibre. Adapted from Ref [54]

Diameter (um)	Ultimate Tensile strength (MPa)	Tensile modulus (GPa)	Strength to Modulus ratio (10^{-2})
5	5490	294	1.87
5	4382	276	1.59
5	4140	242	1.71
5.2	5590	294	1.90
6	5490	323	1.70
7	4410	250	1.76
7	3530	230	1.53
8	3795	235	1.61

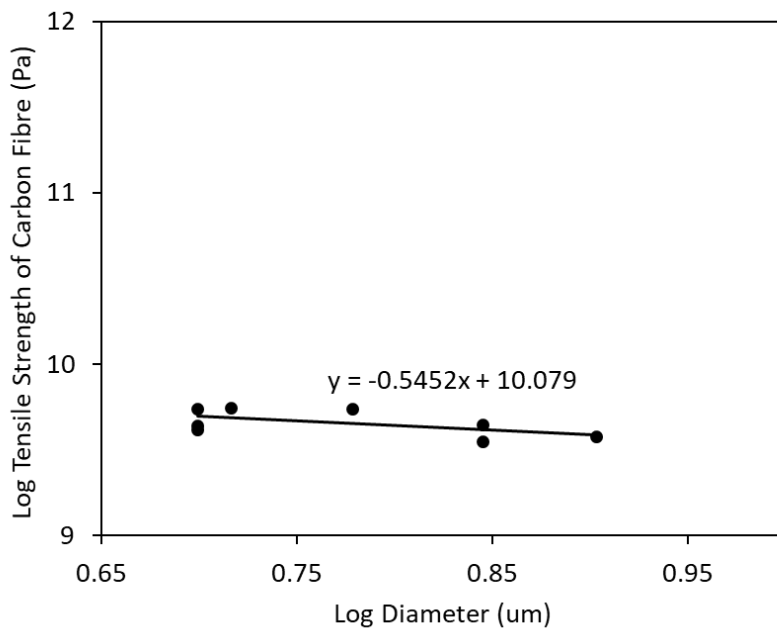


Figure 21: Log-plot for carbon fibre strength plotted against fibre diameter

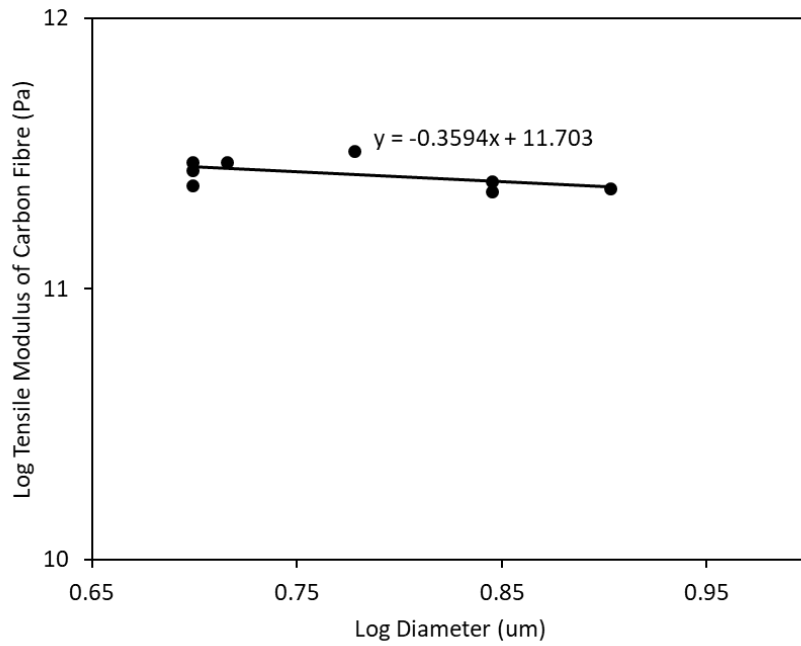


Figure 22: Log-plot for carbon fibre modulus plotted against fibre diameter

$$\text{Equation 3: } \sigma_f = \frac{10^{10.079} \times d^{-0.5452}}{10^9}$$

$$\text{Equation 4: } E_f = \frac{10^{11.703} \times d^{-0.3594}}{10^9}$$

Where σ_f and E_f represent carbon fibre ultimate tensile strength and modulus respectively, and d represents carbon fibre diameter.

3.2.3 Investigated nanofillers tensile strength and tensile modulus

For various nanofillers investigated, tensile strength and modulus obtained for each filler detailed in Table 5.

Table 5: Nanofillers mechanical and physical properties

Type of Nanofiller	Strength (GPa)	Modulus (GPa)
Graphene [229]	130	1000
SWCNT [230]	30	1000
MMT [148]	3	160

3.2.4 Polymer tensile strength and tensile modulus

Similar to reinforcement fillers, polymer matrix system tensile strength and tensile modulus obtained detailed in Table 6.

Table 6: Matrix mechanical properties used in computing modelling of composite material system mechanical properties (for epoxy and polypropylene data given in range, therefore mean value used. * indicate average value)

Matrix system	Ultimate Tensile Strength (GPa)	Elastic Modulus (GPa)	Density (g/cm³)
Epoxy* [16]	0.068	4.5	1.25
Polypropylene* [16]	0.032	1.2	0.905
Nylon 6 [80]	0.088	1.75	1.15
Polyethylene (HDPE) [231]	0.035	1.15	0.95

3.2.5 Interfacial shear strength (IFSS)

Glass fibre

The modelling analysis requires the interfacial property of reinforcement/matrix system known. Table 7 details the IFSS values obtained for glass fibre with specified polymer matrix systems and plotted in Figure 23. As stated above, the IFSS values would also be applied for glass flakes and MMT nanoclay composite systems.

Table 7: Interfacial shear strength (IFSS) value range for different matrix systems with E-glass

Interfacial Shear Strength (IFSS) – τ (Mpa)		
	Min	Max
Epoxy [66], [232], [233], [234]	30	73
Polypropylene [97], [235], [236], [237]	3.2	19.4
Nylon 6 [238], [239], [240], [241]	24	88
Polyethylene [240], [242], [243]	4.6	15.1

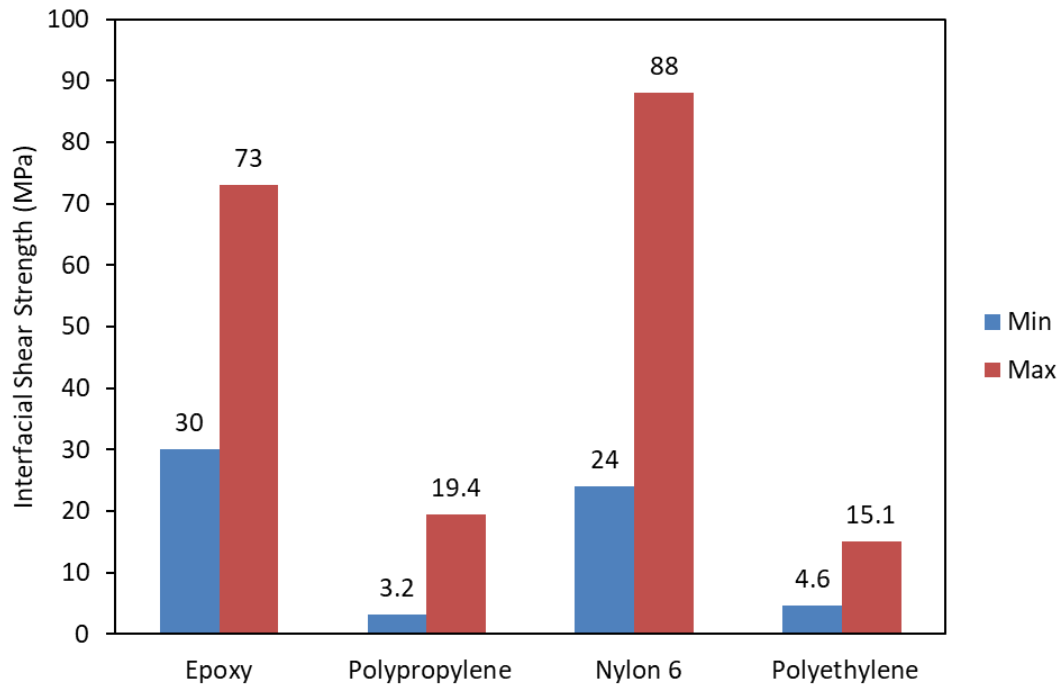


Figure 23: Interfacial shear strength value for specified matrix systems with E-glass

Carbon fibre

Listed in Table 8 is the IFSS values for carbon fibre with specified polymer matrix systems plotted in Figure 24, which will also be used for composite system relating to other carbonaceous fillers, i.e. graphene and SWCNT to compute the modelling analysis.

Table 8: Interfacial shear strength (IFSS) value range for different matrix systems with carbon fibre

Interfacial Shear Strength (IFSS) – τ (Mpa)		
	Min	Max
Epoxy [65], [244], [245], [246]	11.8	80
Polypropylene [247], [248], [249], [250]	7.5	35.4
Nylon 6 [251], [252], [253], [254]	35	68
Polyethylene [91], [255], [256]	21	61

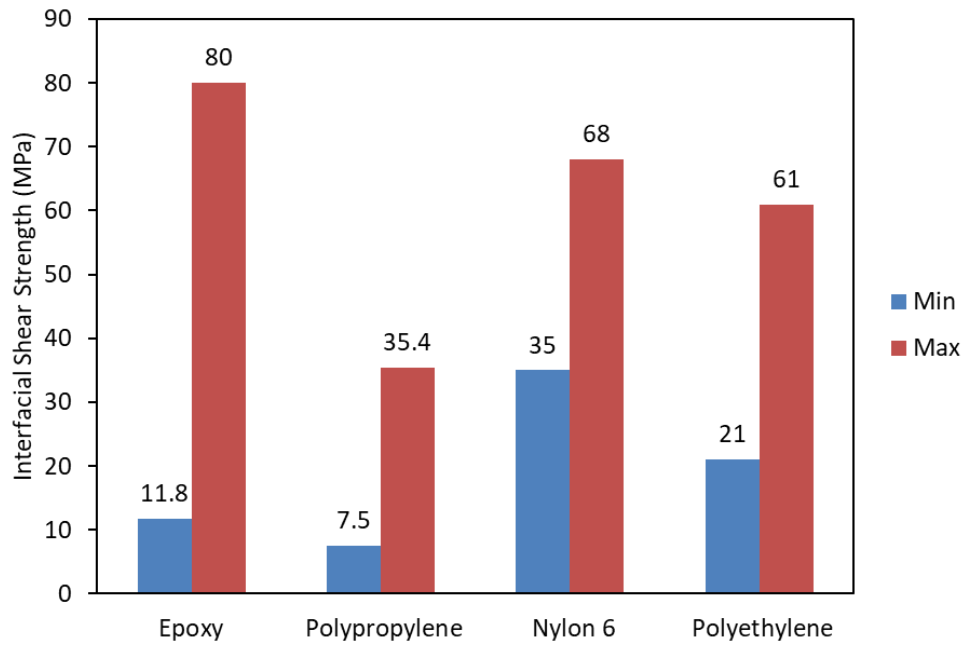


Figure 24: Interfacial shear strength value for specified matrix systems with carbon fibre

4.0 Result and Discussion

Whilst there are various parameters to consider that influence composite material mechanical properties. The reinforcement fillers' aspect ratio has been reported to influence composite material mechanical properties [257]. Composite material systems reinforced with reinforcement filler having high aspect ratio are reported to provide good reinforcement efficiency and better mechanical performance than the reinforcement filler with low aspect ratio [257], [258]. However, for a composite material system to achieve adequate strength, stiffness, and toughness; the reinforcement filler aspect ratio needs to complement the interfacial property between the reinforcement filler and the matrix [232]. Thus, while high aspect ratio is important for composite material to have good strength and stiffness, the interfacial adhesion bond between the reinforcement filler and the matrix system is also important to harness the reinforcement filler's inherent strength and stiffness [189], [259]. Most reinforcement fillers have a limited strain range, unlike their host matrix. When the reinforcement filler aspect ratio is very high, the interfacial shear strength at the interface is also high, coupled with the composite material having a high volume fraction. Thus, such composite material's strength and stiffness improve but adversely affect the composite material toughness, as the reinforcement filler dominates the composite failure. Consequently, causing the composite material to fail at the reinforcement filler strain, which is often characterised by a brittle failure such as seen with fibre reinforcement and nanocomposite technologies [42].

Meanwhile, suppose the aspect ratio is reduced, i.e. by decreasing the reinforcement filler length or increasing the diameter/thickness. In that case, this causes the composite material strength and stiffness to decrease though toughness is enhanced while maintaining good

interfacial adhesion [258]. The contrary is not to reduce the aspect ratio of the filler but compromise on the interfacial adhesion; this would undermine the reinforcement efficiency of the composite material mechanical properties as the reinforcement filler's inherent strength, and stiffness cannot be harnessed. This, therefore, requires a balance to be achieved between the interfacial adhesion and the reinforcement filler aspect ratio by determining the threshold where toughness is not sacrificed at the expense of strength or stiffness and vice versa. While this threshold varies based on composite systems, hence, fibre reinforcement technology achieving such balance is challenging. As an adequate interfacial adhesion is desired and to maintain toughness, this would therefore require the aspect ratio decreased which invariably would have strength and stiffness compromised. Meanwhile, for composite materials reinforced with nanofillers known to have a very high aspect ratio, which exceeds the threshold, hence often achieving high strength and stiffness but toughness compromised.

Understanding the shortcomings of existing technologies in achieving comprehensive strength, stiffness, and toughness concurrently is why the research investigates suitable reinforcing fillers with rationale on their potential and feasibility to reinforce commodity polymers with the trio mechanical properties maintained through modelling analysis. Glass flakes is investigated as a model reinforcing filler in comparable analysis with other existing reinforcing fillers. The chapter provides details of results obtained for experimental work conducted and computational modelling analysis. Section 4.1 includes thickness measurement, size characterisation, and glass flakes distribution for both non-chopped and chopped-down glass flakes aspect ratios. Statistical process employed to determine individual glass flakes average length to determine their average aspect ratios is also stated. Section 4.2 focuses on modelling work computed using Shear-Lag and Hapin-Tsai models to determine

composite material systems strength and modulus with toughness maintained, respectively, by computing modelling analysis of composite material system failure under tough fracture.

4.1 Investigation of suitable fillers for the new composite in practical application

Due to the project's time restriction, fabrication technology to produce samples for validation became a constrain. Instead, the project is designed to exploit if a filler system could be available and tailorable to fit into the new composite design. If successful, the ideal reinforcement filler's size range would need to be determined, i.e., micron, submicron or nano-composites. For this purpose, glass flakes is selected since it is possible to be made in different size range and available commercially. This section will present the experimental study of these commercially available glass flakes and how to change these materials' aspect ratio in a manufacturing process.

Considering that reinforcement filler's aspect ratio has been a contributing factor influencing the composite material system mechanical properties [257]. Hence the reason for ensuring adequate characterisation of each glass flakes investigated to determine their average aspect ratio. Reinforcement filler aspect ratio (l/d or l/t) is the length (l) of the filler divided by its diameter (d) for fibrous fillers, while the thickness (t) substitutes for diameter if the filler is a plate-like material (platelet) like glass flakes.

4.1.1 Glass flakes thickness measurement

Figure 25 - 31 shows a typical image illustration of each glass flakes thickness. Individual glass flakes thickness was measured using Image-J to process images taken for each glass flakes from the SEM analysis. Thickness measurement obtained from Image-J for each glass flakes is statistically analysed using basic statistics (mean and standard deviation), and this is reported in Table 9.

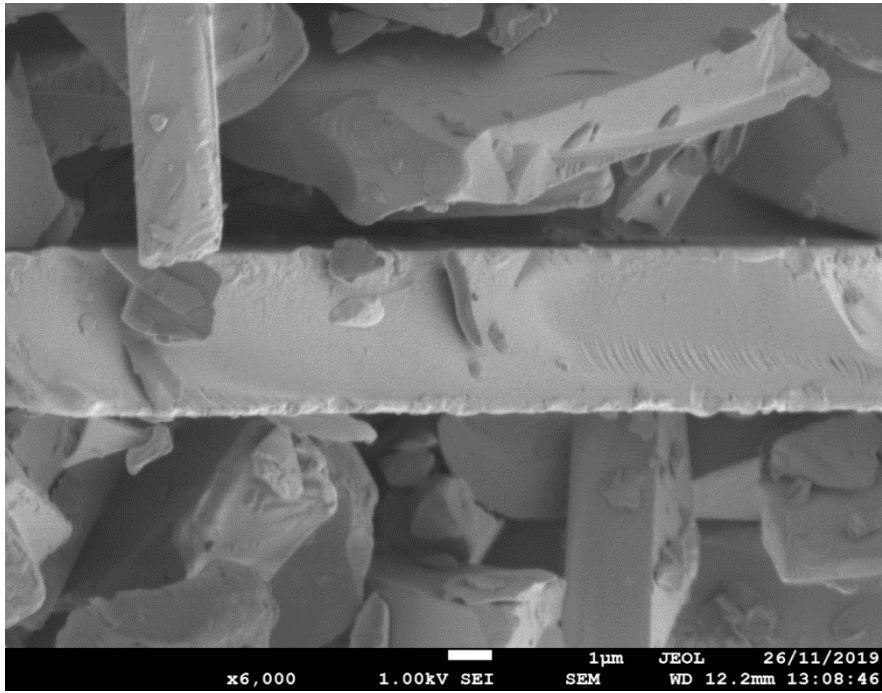


Figure 25: SEM image illustration of 2.3 - 3.3µm glass flakes

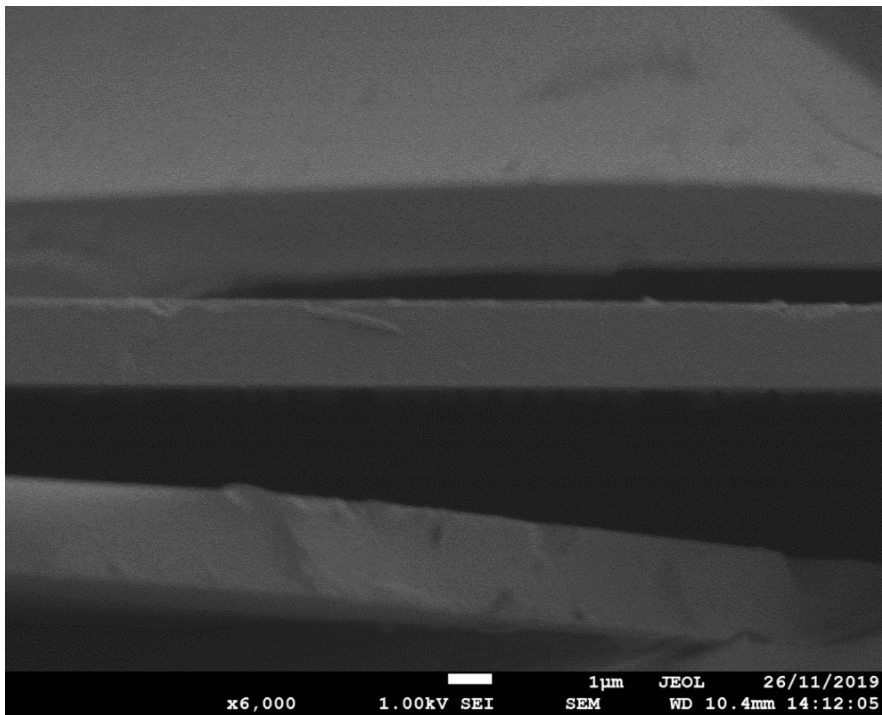


Figure 26: SEM image illustration of 0.8-1.3µm glass flakes

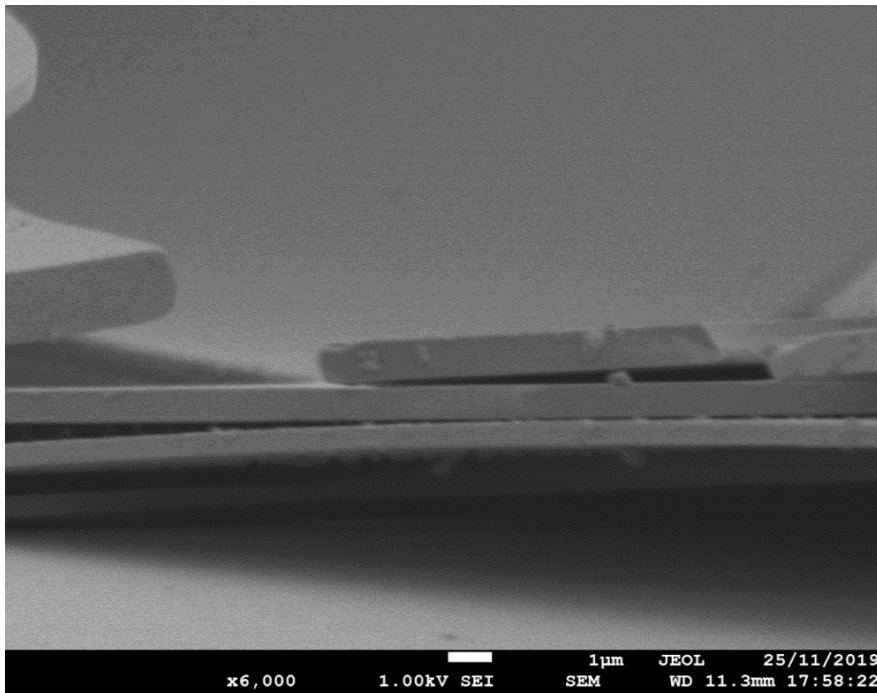


Figure 27: SEM image illustration of 850nm unmilled glass flakes

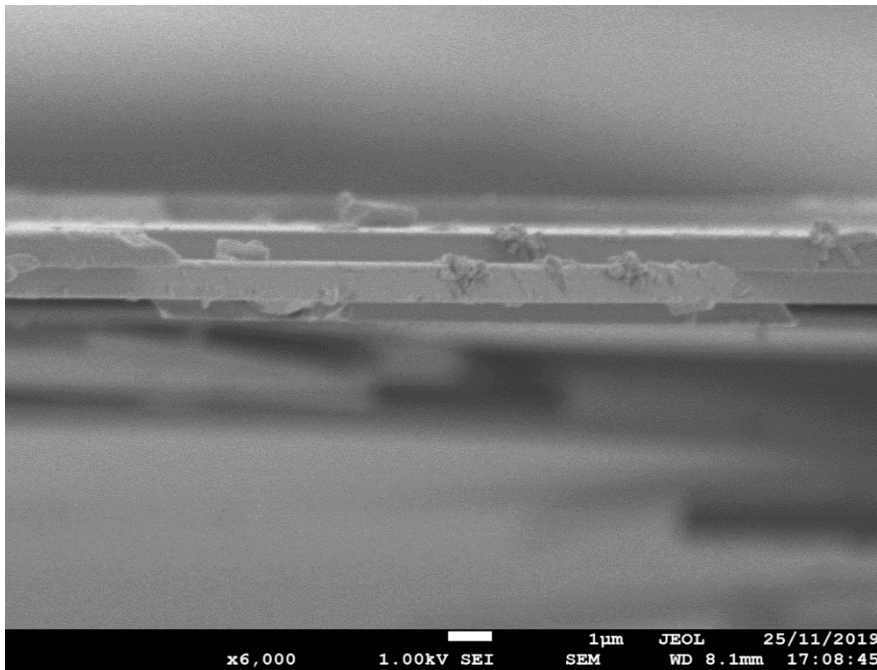


Figure 28: SEM image illustration of 850nm milled glass flakes

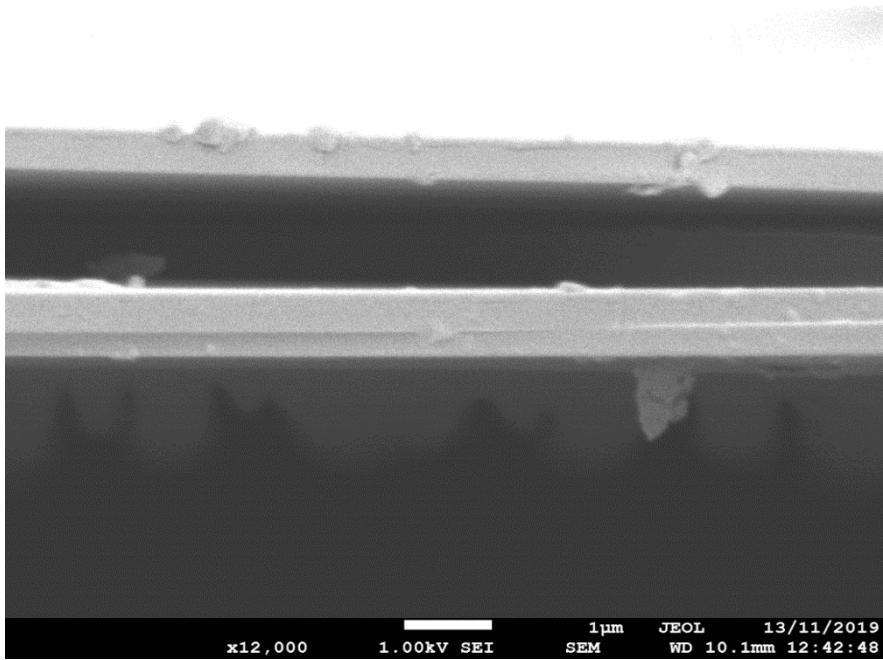


Figure 29: SEM image illustration of 350nm unmilled glass flakes

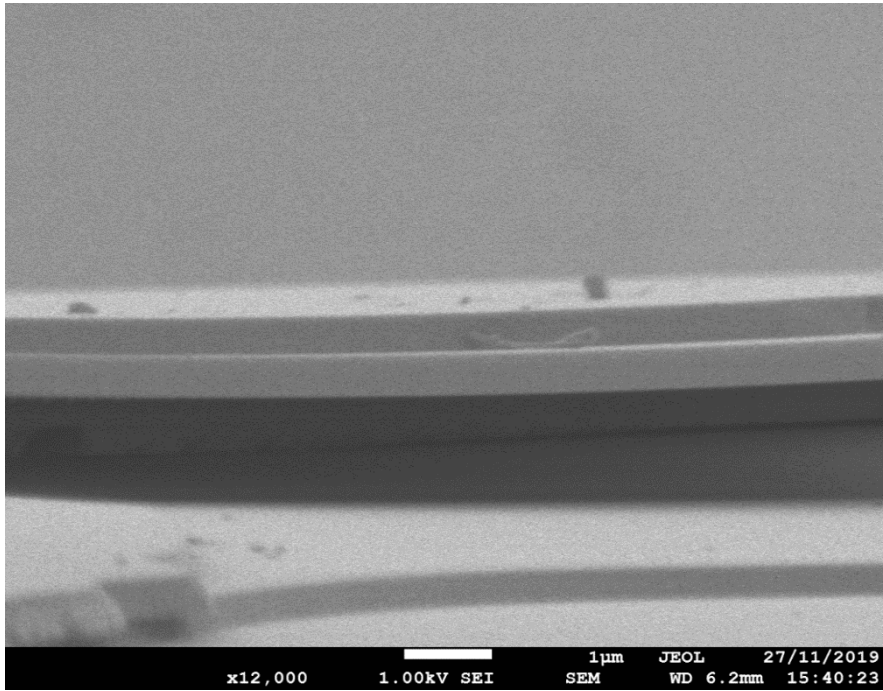


Figure 30: SEM image illustration of 350nm milled glass flakes

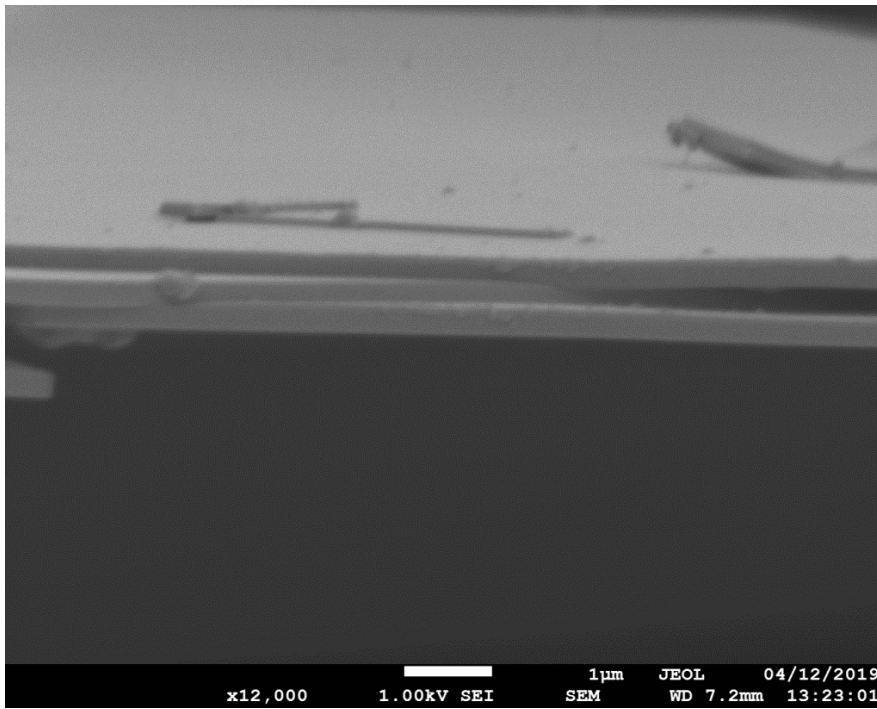


Figure 31: SEM image illustration of 100nm milled glass flakes

Table 9 Thickness measurement of each glass flakes investigated

Glass flakes thickness size	No of sample measurement	Mean	Standard deviation
2.3 - 3.3µm	106	2.75µm	0.55
0.8 - 1.3µm	118	1.87µm	0.16
850nm Milled	115	830nm	41
850nm Unmilled	110	746nm	49
350 Unmilled	108	362nm	30
350nm Milled	110	363nm	28
100nm Milled	112	120nm	15

While Table 9 shows that most of the glass flakes average thickness measurements are within proximity to specified thickness size by the supplier, 850nm unmilled is not, and 0.8 – 1.3 μm is out of specified range. This further buttresses the need for size characterisation to determine the glass flakes' average thickness, considering that the glass flakes aspect ratio changes when the thickness changes.

4.1.2 Glass flakes Length measurement

In determining each glass flakes aspect ratio, their average length is determined by having images taken using an optical microscope for each glass flakes and processed in Image-J. Figure 32 shows a typical dispersion of each glass flakes on a microscopic glass slide. Figure 33 shows how the length is measured, considering that the glass flakes have irregular shapes. For every glass flake, the longest length is measured, as shown in Figure 33.

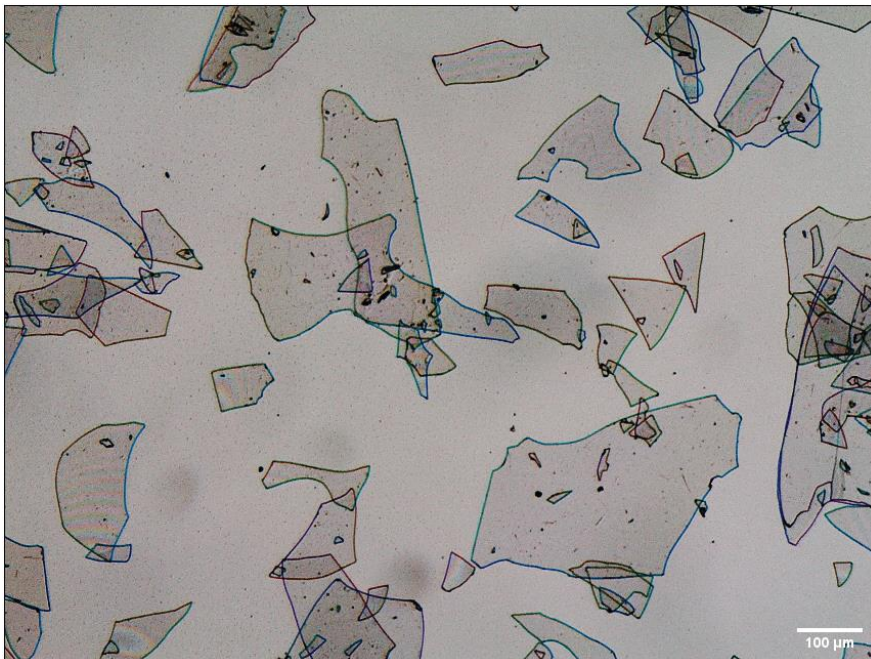


Figure 32: Image illustration of dispersed glass flakes on microscope slide taken using optical microscope

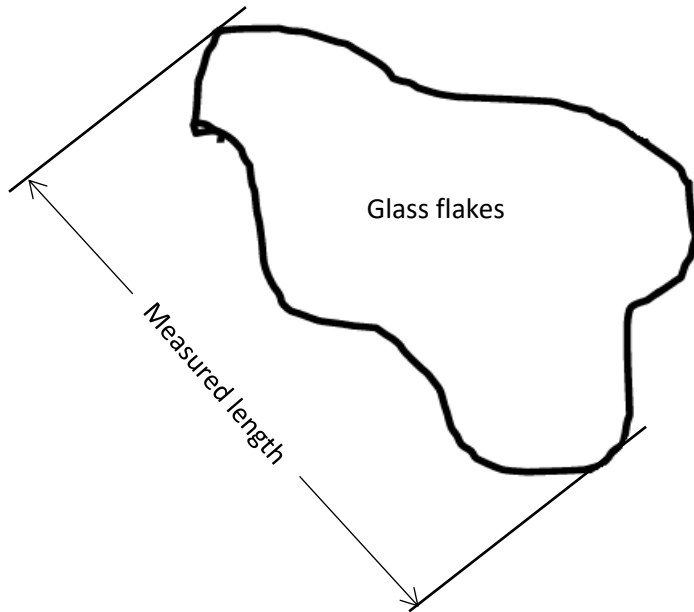


Figure 33: Glass flakes length are determined by measuring two longest separated points on the glass flakes perimeter

The length measurement obtained from Image-J is used to determine the mean length for each glass flakes. Using Minitab to compute dot plot for length measured for each glass flakes (Figure 34). The plot obtained for each glass flakes exhibited a similar asymmetric tendency of skewness to the right, as seen in Figure 34 for 350nm milled glass flakes. In order to make the distribution more representative of a normal distribution, a probability distribution fit-test was done on measured length data obtained using Minitab. The fit-test from Minitab (Figure 35) shows that lognormal has a better fit and good representation of the glass flakes distribution, considering that the glass flakes measured length is continuously random. Therefore, the measured length for each glass flakes is processed by using Minitab to take log value of each entry (measured length) of glass flakes to produce lognormal distribution. Figure 36 shows a histogram of log-length with lognormal distribution for 350nm milled glass flakes, indicating a better fit of the distribution, giving mean value and standard deviation in log form.

These values are converted using anti-log to determine the mean length in microns used to estimate the glass flakes aspect ratio. While N is the total number of glass flakes measured for each glass flakes with 546, 526, 499, 537, 536 and 517 for 2.3 - 3.3 μm , 0.8 - 1.3 μm , 850nm unmilled, 850nm milled, 350nm unmilled and 100nm milled glass flakes, respectively. Lognormal is used to determine the mean length of all glass flakes investigated and the mean lengths for each glass flakes shown in Table 10.

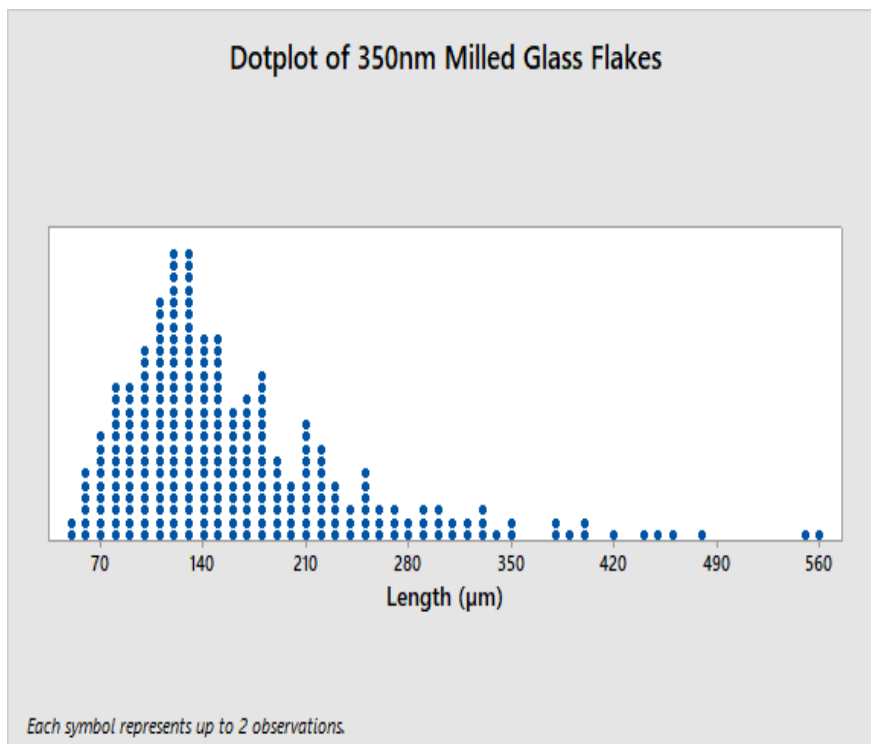


Figure 34: Dot plot for 350nm milled glass flakes measured length

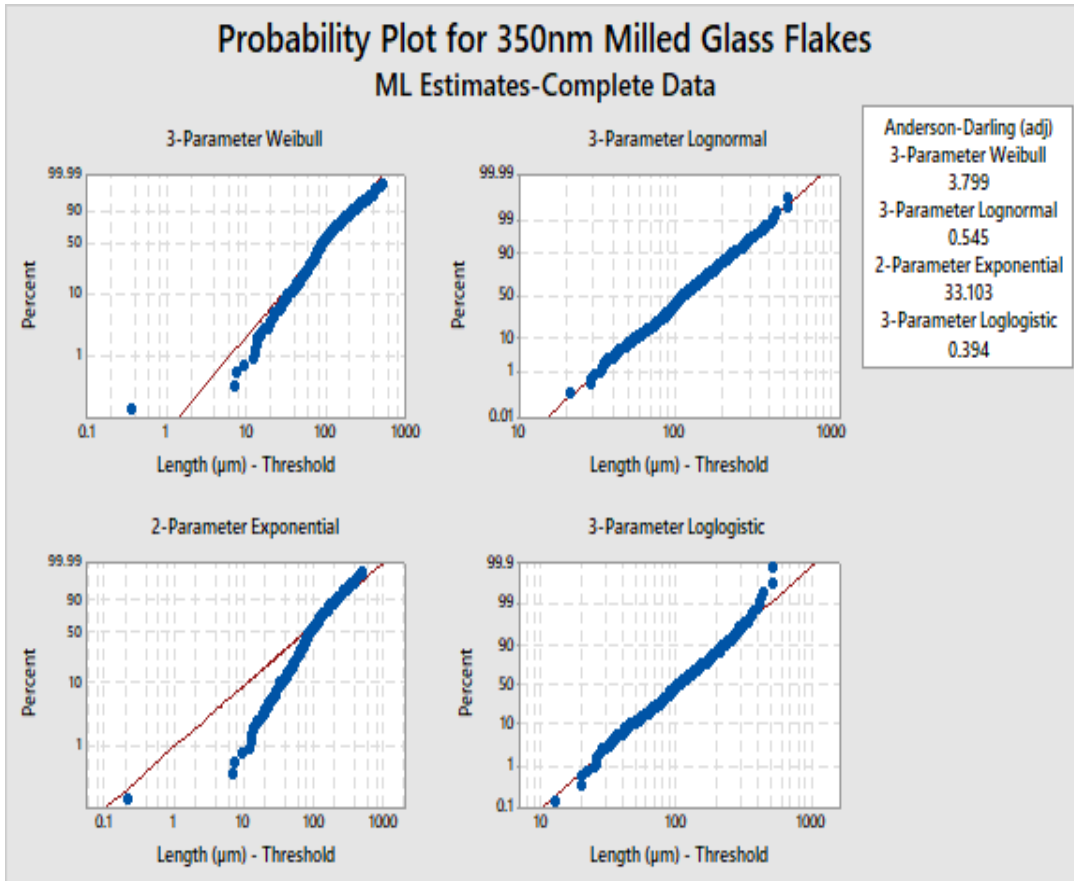


Figure 35: Fit test analysis using Minitab to determine adequate statistic applicable to process measured length distribution

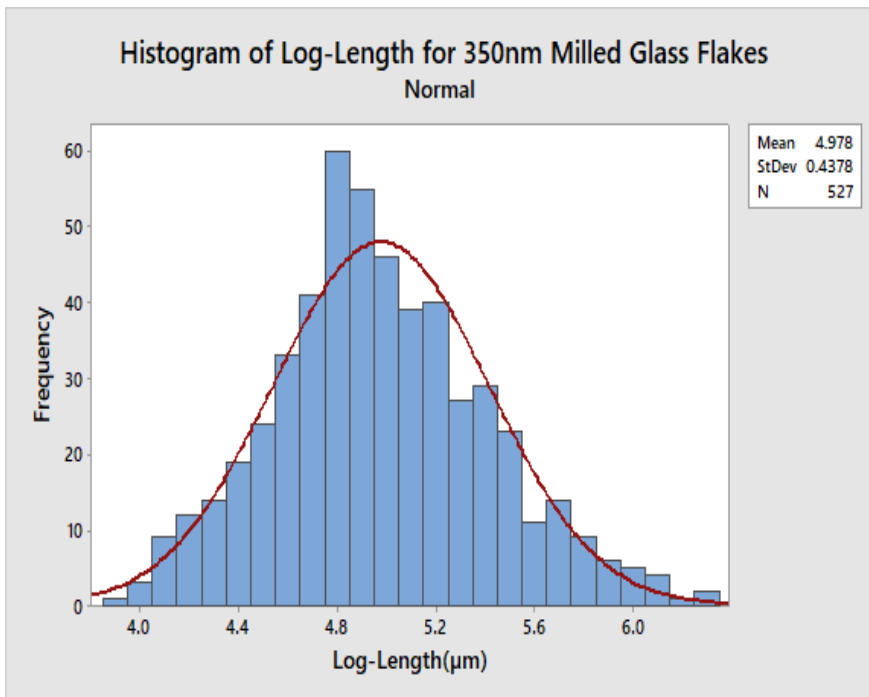


Figure 36: Log-normal distribution of 350nm milled glass flakes

Table 10: Average length measured for each glass flakes investigated before ball milling

	2.3 - 3.3μm	0.8 - 1.3μm	850nm Unmilled	850nm Milled	350nm Unmilled	350nm Milled	100nm Milled
No of Glass Flakes	546	526	499	537	536	527	517
Mean Log Length (μ m)	3.183	4.932	5.317	4.750	4.924	4.978	4.688
Log Length Standard Deviation (μ m)	0.2745	0.5272	0.3565	0.4722	0.5704	0.4378	0.4661
Mean Length (μ m)	24.12	138.66	203.77	115.58	137.55	145.18	108.64
Standard Deviation (μ m)	18.39 - 31.74	81.84 - 234.91	142.67 - 291.05	72.08 - 185.34	77.76 - 243.33	93.71 - 224.93	68.16 - 173.14

With the average thickness (Table 9) and length (Table 10) determined for each glass flakes, their aspect ratio before ball milling reported in Table 11.

Table 11: Average aspect ratio determined for each glass flakes investigated before ball milling

	2.3 - 3.3μm	0.8 - 1.3μm	850nm Milled	850nm UnMilled	350nm Unmilled	350nm Milled	100nm Milled
Average Thickness (μ m)	2.75	1.87	0.830	0.746	0.362	0.363	0.120
Mean Length (μ m)	24.12	138.66	115.58	203.77	137.55	145.18	108.64
Average Aspect Ratio	9	74	139	273	380	400	905

Similar characterisation procedure and statistics analysis employed for non-ball milled was applied to each glass flakes after ball milling to determine their average length. The length measurement is used to determine each glass flakes' aspect ratio after ball milling for each milling time to control the filler's aspect ratio. All glass flakes could have their aspect ratio reduced through ball milling except for 2.3 - 3.3 μm glass flakes with a relatively small aspect ratio (Table 11). Table 12 - 17 shows the length measured and the aspect ratio over time duration for milling. This is consequently plotted into graphs shown in Figure 37 – 42 for each glass flakes.

Table 12: Average aspect ratio determined for 100nm milled glass flakes at different milling time duration

100nm Milled	0 min	1.5 mins	3 mins	4.5 mins
Average Thickness (μm)	0.120	0.120	0.120	0.120
No of Glass Flakes	517	523	532	532
Mean Log Length (μm)	4.688	4.415	4.284	4.206
Log Length Standard Deviation (μm)	0.4661	0.4033	0.3206	0.2933
Mean Length (μm)	108.64	82.68	72.53	67.09
Standard Deviation (μm)	68.16 - 173.14	55.24 - 123.75	52.64 - 99.94	50.03 - 89.95
Average aspect Ratio	905	689	604	559

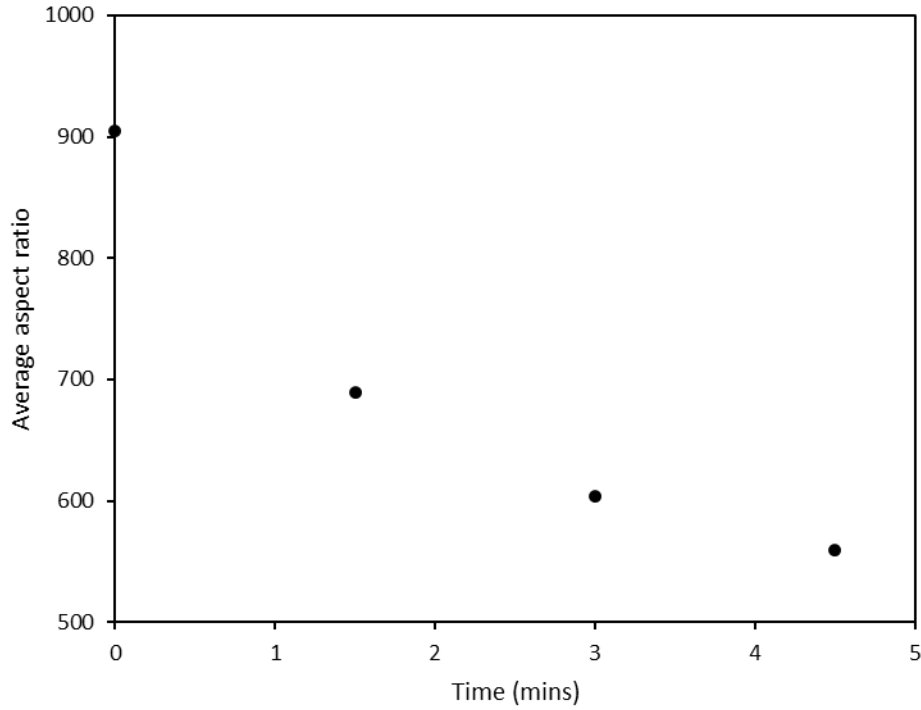


Figure 37: Balled milled aspect ratio with respect to time - 100nm milled glass flakes

Table 13: Average aspect ratio determined for 350nm milled glass flakes at different milling time duration

350nm Milled	0 min	2.5 mins	5 mins	7.5 mins
Average Thickness (μm)	0.363	0.363	0.363	0.363
No of Glass Flakes	527	535	541	534
Mean Log Length (μm)	4.978	4.613	4.197	4.074
Log Length Standard Deviation (μm)	0.4378	0.4634	0.3333	0.3016
Mean Length (μm)	145.18	100.79	66.49	58.79
Standard Deviation (μm)	93.71 - 224.93	63 - 160.2	47.64 - 92.79	43.48 - 79.49
Average Aspect Ratio	400	278	183	162

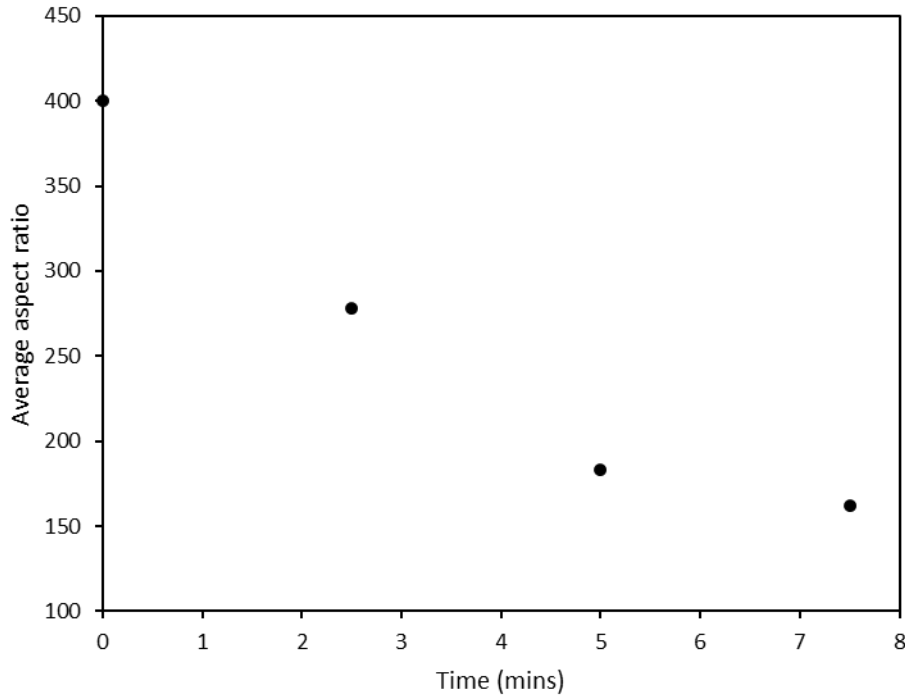


Figure 38: Balled milled aspect ratio with respect to time - 350nm milled glass flakes

Table 14: Average aspect ratio determined for 350nm unmilled glass flakes at different milling time duration

350nm Unmilled	0 min	2.5 mins	5 mins	7.5 mins
Average Thickness (μm)	0.362	0.362	0.362	0.362
No of Glass Flakes	536	556	572	544
Mean Log length (μm)	4.924	4.449	3.998	3.952
Log Length Standard Deviation (μm)	0.5704	0.4608	0.2836	0.2480
Mean Length (μm)	137.55	85.54	54.49	52.04
Standard Deviation (μm)	77.76 - 243.33	53.96 - 135.61	41.03 - 72.36	40.61 - 66.67
Average Aspect Ratio	380	236	151	144

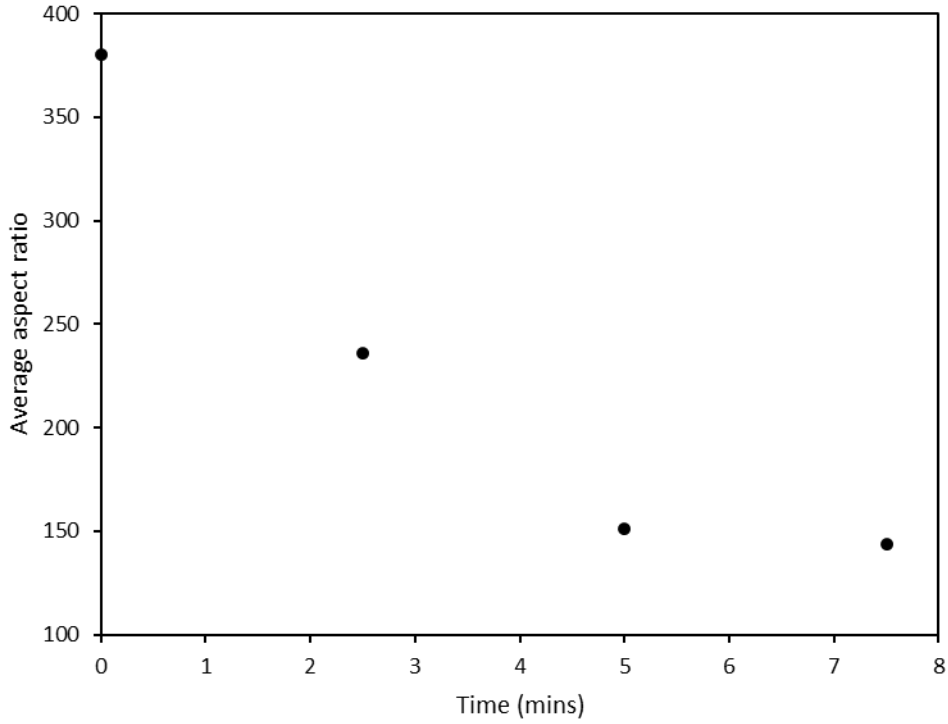


Figure 39: Balled milled aspect ratio with respect to time - 350nm unmilled glass flakes

Table 15: Average aspect ratio determined for 850nm milled glass flakes at different milling time duration

850nm Milled	0 min	2.5 mins	5 mins	7.5 mins
Average Thickness (μm)	0.830	0.830	0.830	0.830
No of Glass Flakes	537	531	537	532
Mean Log Length (μm)	4.750	4.071	3.831	3.367
Log Length Standard Deviation (μm)	0.4722	0.2564	0.2338	0.3100
Mean Length (μm)	115.58	58.62	46.11	28.99
Standard Deviation (μm)	72.08 - 185.34	45.36 - 75.75	36.5 - 58.25	21.26 - 39.53
Average Aspect Ratio	139	71	56	35

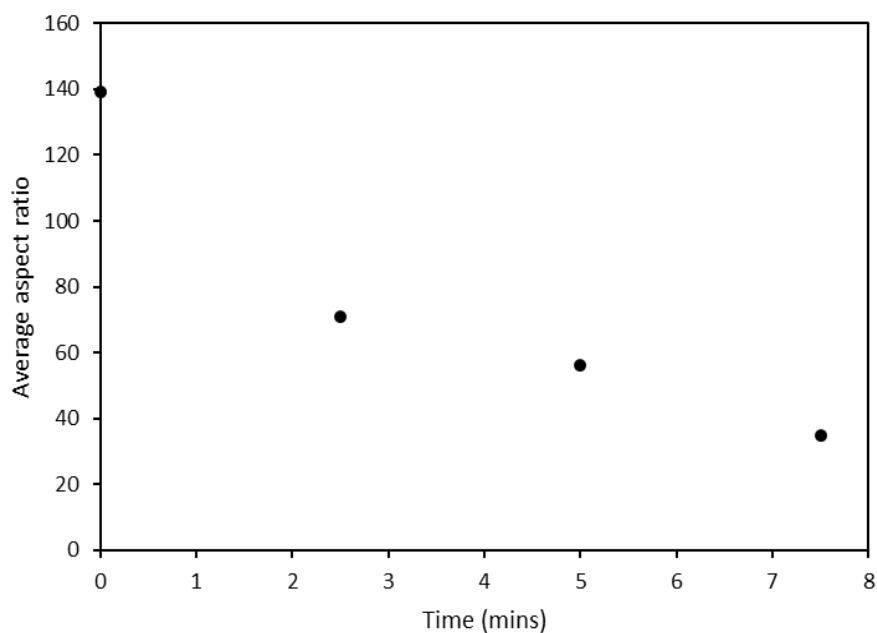


Figure 40: Balled milled aspect ratio with respect to time - 850nm milled glass flakes

Table 16: Average aspect ratio determined for 850nm unmilled glass flakes at different milling time duration

850nm Unmilled	0 min	2.5 mins	5 mins	7.5 mins
Average Thickness (μm)	0.746	0.746	0.746	0.746
No of Glass Flakes	499	526	541	540
Mean Log Length (μm)	5.317	4.194	3.861	3.326
Log Length Standard Deviation (μm)	0.3565	0.2929	0.2322	0.3046
Mean Length (μm)	203.77	66.29	47.51	27.83
Standard Deviation (μm)	142.67 - 291.05	49.46 - 88.85	37.67 - 59.93	20.52 - 37.74
Average Aspect Ratio	273	89	64	37

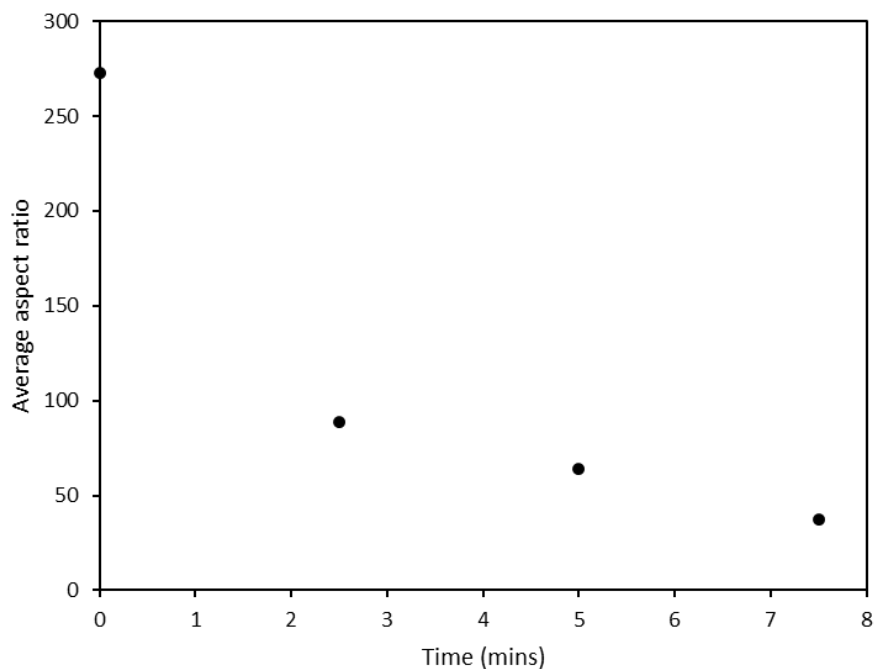


Figure 41: Balled milled aspect ratio with respect to time - 850nm unmilled glass flakes

Table 17: Average aspect ratio determined for 0.8 - 1.3 μ m glass flakes at different milling time duration

0.8 - 1.3 μ m	0 min	2.5 mins	5 mins	7.5 mins
Average Thickness (μ m)	1.87	1.87	1.87	1.87
No of Glass Flakes	526	544	556	567
Mean Log Length (μ m)	4.932	3.962	3.799	3.746
Log Length Standard Deviation (μ m)	0.5272	0.3667	0.2983	0.2877
Mean Length (μ m)	138.66	52.56	44.66	42.35
Standard Deviation (μ m)	81.84 - 234.91	36.43 - 75.85	33.14 - 60.18	31.76 - 56.47
Average Aspect Ratio	74	28	24	23

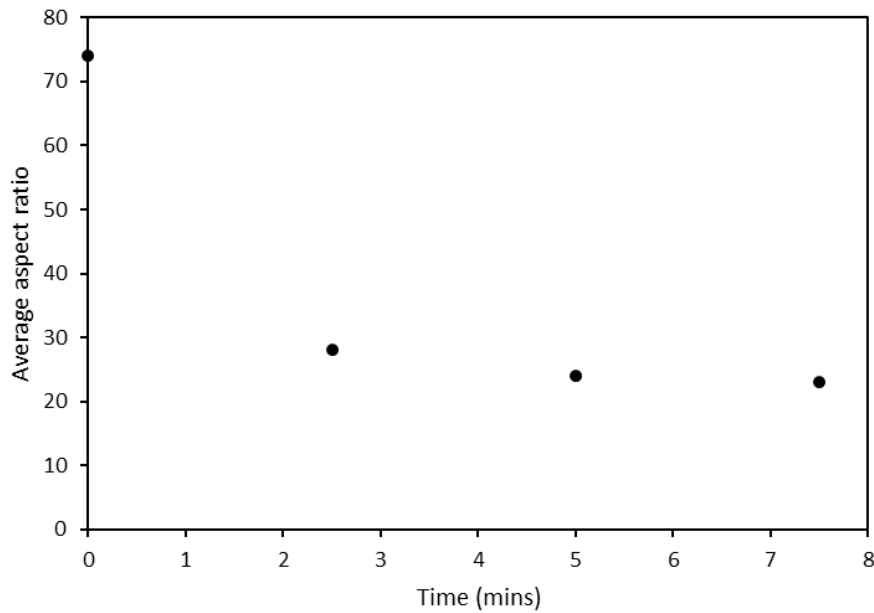


Figure 42: Balled milled aspect ratio with respect to time - 0.8 - 1.3µm glass flakes

4.2 Computation of modelling work and analysis

Figure 43 shows a relative volume element (RVE) representation of a typical composite material system. Assuming that stress is applied along the fibre's longitudinal length and both the fibre and matrix undergoes equal strain (isostrain) (Figure 44) [16] [260]. Rule of Mixture predicts the composite material mechanical properties using Equation 5 for strength and Equation 6 for elastic modulus. The equations show that predicted mechanical properties are only a function of fibre volume fraction and do not consider other composite system parameters, i.e. aspect ratio. Modulus is predicted using Equation 6 for the Rule of Mixture to predict the composite system elastic modulus along the fibre's longitudinal direction under isostrain assumption. It is regarded as the upper limit modulus, while Equation 7, also known as Inverse Rule of Mixture [261] predicts the composite material system modulus under isostress assumption when tensile load stress is applied in the transverse direction. Modulus

predicted in the transverse direction is lower than the modulus in the longitudinal direction, and it is regarded as the lower limit modulus of the composite material system [16].

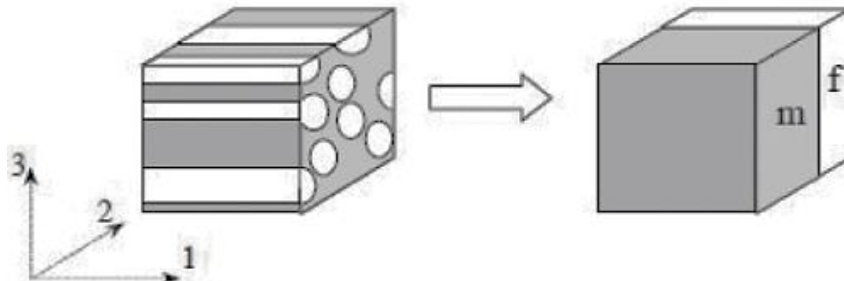


Figure 43: Schematic illustration of representative volume element of composite material. Adapted from Ref [260]

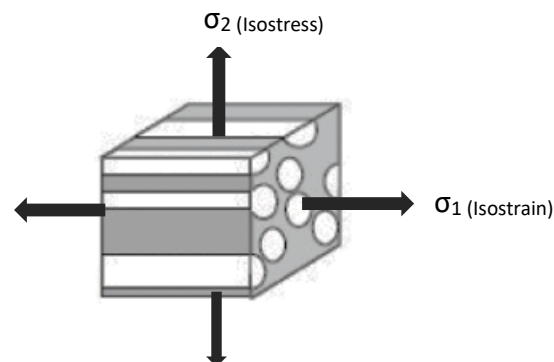


Figure 44: Application of Rule of Mixture model for analysing composite material system

$$\text{Equation 5: } \sigma_1 = \sigma_f V_f + \sigma_m (1 - V_f)$$

$$\text{Equation 6: } E_1 = E_f V_f + E_m (1 - V_f)$$

$$\text{Equation 7: } E_2 = \left[\frac{V_f}{E_f} + \frac{1 - V_f}{E_m} \right]^{-1}$$

Where σ , E and V represents ultimate tensile strength, modulus and volume fraction respectively, while subscripts f and m represent fibre and matrix respectively, 1 and 2 subscripts represent longitudinal and transverse directions respectively.

Halpin-Tsai model (Equation 8) compensates for the Inverse Rule of Mixture's inadequacy to predict composites material transverse modulus due to strain magnification. With the

introduction of the geometric factor (ξ) in Halpin-Tsai model, the assumption is that various values for ξ to determine the modulus of the composite is insensitive to Poisson ratio differences for fibre and matrix. Hence with the geometric factor (ξ), Halpin-Tsai model can be used to predict elastic modulus, transverse modulus and shear modulus [16], [124], [262].

$$\text{Equation 8: } \frac{E_c}{E_m} = \frac{1 + \eta \xi V_f}{1 - \eta V_f}$$

$$\text{Where Equation 9 is; } \eta = \frac{\frac{E_f}{E_m} - 1}{\frac{E_f}{E_m} + \xi}$$

$$\text{And Equation 10; } \xi = 2S$$

S is the aspect ratio (l/t) multiplied by two to give the geometric factor ξ . V_f is the volume fraction contribution by fibre, while E_f , E_m and E_c represent matrix modulus, reinforcement filler modulus and the composite material modulus respectively. Thus, the Halpin-Tsai model shows that composite material system modulus is influenced by fibre volume fraction and aspect ratio, unlike Rule of Mixture that is only affected by volume fraction of the reinforcement filler.

The modelling analysis for strength computed using the Shear-Lag model (Equation 11) based on Kelly and Tyson fibre fragmentation theory. According to Kelly and Tyson fibre fragmentation theory, single fibre embedded within a matrix subjected to external load stress under tension experience tensile stress due to shear stress, which is transferred from the matrix to the fibre through the fibre/matrix interface. The tensile strain experienced by the fibre due to the tensile stress increases correspondently with an increase in exerted load stress, such that when the failure strain of the fibre is reached the fibre fracture. The fracturing of the embedded fibre continues as the load stress increases until fragmented fibre

length is too short to undergo further fracturing. The fragmentation process is regarded to have reached saturation. Thus, the shortest fragment length on the application of stress is described as the fibre critical length [263], [264].

With reinforcement fillers' aspect ratio influencing the composite material system's mechanical properties and high reinforcement filler aspect ratio provide better reinforcement efficiency [257]. However, to maintain toughness in composite material, pull out mechanism is identified to enhance composite material toughness [265]. The pull-out mechanism requires the reinforcement filler aspect ratio not to exceed the critical aspect ratio (S_c) for the composite material system, which is the critical length (l_c) of the reinforcement filler divided by the filler diameter (d)/thickness (t) [264]. Therefore, according to Kelly and Tyson fragmentation theory and using Figure 45 for illustration. When the reinforcement filler aspect ratio (S) is below the critical aspect ratio (S_c), there is no reinforcement filler fracturing. Instead of fracture to occur, the reinforcement filler pulls out, but when the reinforcement filler aspect ratio is higher than the critical aspect ratio fracture occurs [26], [264], [266].

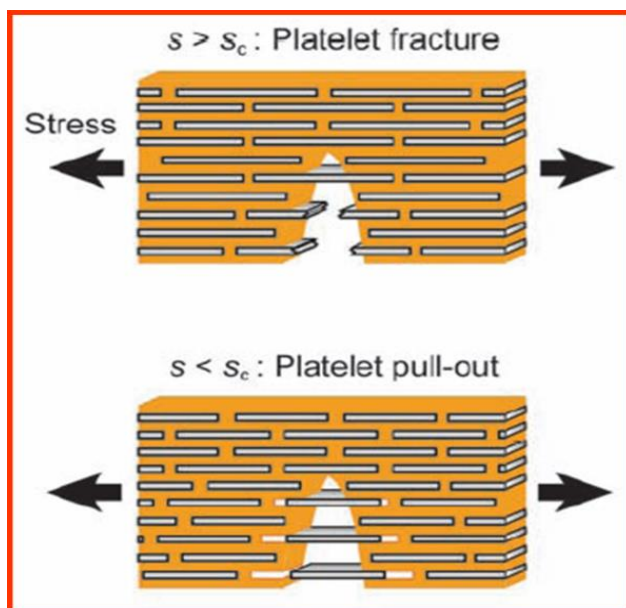


Figure 45: Illustration of composite material failure depending on reinforcement filler aspect ratio whether it is higher or lower than the composite material system critical aspect ratio. Adapted from Ref [26]

However, for toughness to be maintained, the reinforcement filler aspect ratio would also be affected, which would affect the composite material mechanical properties (strength and modulus). Considering that the reinforcement filler's aspect ratio will not exceed the critical aspect ratio required for the composite system threshold [257], the critical aspect ratio threshold depends on the interfacial bond that exist between the fibre and matrix [264]. Research shows that fillers strength and stiffness increase with decrease in reinforcement filler diameter/thickness [267]. Therefore, the modelling is computed to identify the filler type that is thin enough to provide sufficiently high strength and stiffness, but thick enough to reduce the filler aspect ratio. Thus, the reinforcement filler aspect ratio is not too high than the critical aspect ratio for the composite material system for toughness to be maintained, yet sufficiently high strength and stiffness achieved by manoeuvring the reinforcement fillers' aspect ratio. At the same time, an excellent interfacial adhesion bond exists between the reinforcement filler and the matrix.

To compute the modelling analysis, following assumptions are made.

- The reinforcement fillers within the matrix are oriented and aligned parallel in the direction of exerted load stress
- The reinforcement fillers are uniformly distributed and evenly dispersed throughout the matrix
- No defect, i.e. void present within the composite material system and as such not accounted for
- The reinforcement filler is subjected to tensile stress only through the shear stress transferred from the matrix via the interface

- Adhesion bond at the interface is sufficient enough to transfer stress from the matrix to the reinforcement filler
- The Poisson ratio effect is considered negligible

$$\text{Equation 11: } \sigma_c = \alpha \sigma_f V_f + \sigma_m (1 - V_f)$$

Where σ_f , σ_m and σ_c represent reinforcement filler strength, matrix strength and the composite material strength respectively, while V_f and $(1 - V_f)$ represent reinforcement filler and matrix volume fraction respectively. α is the fracture term dependent on whether the composite will fail in a brittle or tough manner.

Equation 12 is used to determine the composite material system critical aspect ratio (S_c) which is determined using the filler's strength and the interfacial shear strength of the filler with the matrix. Comparing the critical aspect ratio (S_c) to average measured aspect ratio (S) of the filler for the composite material system. If the reinforcement filler's average aspect ratio (S) is higher than the critical aspect ratio, the composite material will fail in a brittle manner (Figure 45) and Equation 13 is used to determine the fracture term (α) in Equation 11. However, suppose the reinforcement filler average aspect ratio (S) is lesser than the composite material system's critical aspect ratio (S_c). In that case, it will cause the composite material to fail in a tough manner and Equation 14 is used to determine the fracture term [26].

$$\text{Equation 12: } S_c = \frac{\sigma_f}{2 \tau}$$

$$\text{Equation 13: } \alpha_{F_b} = 1 - \frac{\sigma_f}{2 \tau S}$$

$$\text{Equation 14: } \alpha_{F_t} = \frac{\tau S}{2 \sigma_f}$$

Where S represents the reinforcement filler aspect ratio, and S_c represents the composite material system critical aspect ratio. σ_f represents the reinforcement filler ultimate tensile strength and τ represents the interfacial shear strength at the interface due to bond adhesion in response to exerted external load stress. α_{Fb} and α_{Ft} represent fracture term for brittle and tough failure, respectively.

4.2.1 Determination of critical aspect ratio for various glass flakes used as reinforcement filler for different composite material systems

To compute the modelling and identify the threshold for each composite system in developing a composite material system with strength, stiffness and toughness maintained concurrently, determination of critical aspect ratio (S_c) is important in order to know if investigated glass flakes would need to be chopped down or not. Thus, to determine the critical aspect ratio for each composite material system; using Equation 1 and 2, the glass flakes' mechanical properties (strength and stiffness) are obtained and listed in Table 18.

Table 18: Mechanical properties of glass flakes at their known thickness

Glass flakes	Mean thickness	Tensile strength (GPa)	Tensile modulus (GPa)
2.3 - 3.3 μ m	2.75 μ m	2.96	101
0.8 - 1.3 μ m	1.87 μ m	3.45	110
850nm Milled	830nm	4.76	132
850nm Unmilled	746nm	4.97	135
350 Unmilled	362nm	6.62	158
350nm Milled	363nm	6.61	158
100nm Milled	120nm	10.25	202

Using Equation 12 and values obtained for tensile strength for each glass flakes investigated at their known thickness (Table 18) and interfacial shear strength of various matrices with E-glass (Table 7). The critical aspect ratio (S_c) determined for each matrix system analysed and detailed in Table 19. Figure 46 - 49 shows the influence of change in glass flakes thickness on reinforcement filler's critical aspect ratio.

Table 19: Required critical aspect ratio on glass flakes for various matrix systems at different interfacial shear strength

Critical aspect ratio for various composite matrix systems at different interfacial values								
	Epoxy		Polypropylene		Nylon 6		Polyethylene	
	Min ($\tau - 30$ MPa)	Max ($\tau - 73$ MPa)	Min ($\tau - 3.2$ MPa)	Max ($\tau - 19.4$ MPa)	Min ($\tau - 24$ MPa)	Max ($\tau - 88$ MPa)	Min ($\tau - 4.6$ MPa)	Min ($\tau - 15.1$ MPa)
Glass Flakes 2.3 - 3.3 μ m	49	20	463	76	62	17	322	98
0.8 - 1.3 μ m	58	24	540	89	72	20	375	114
850nm Milled	79	33	744	123	99	27	518	158
850nm Unmilled	83	34	777	128	104	28	540	165
350nm UnMilled	110	45	1033	170	138	38	719	219
350nm Milled	110	45	1034	171	138	38	719	219
100nm Milled	171	70	1602	264	214	58	1114	339

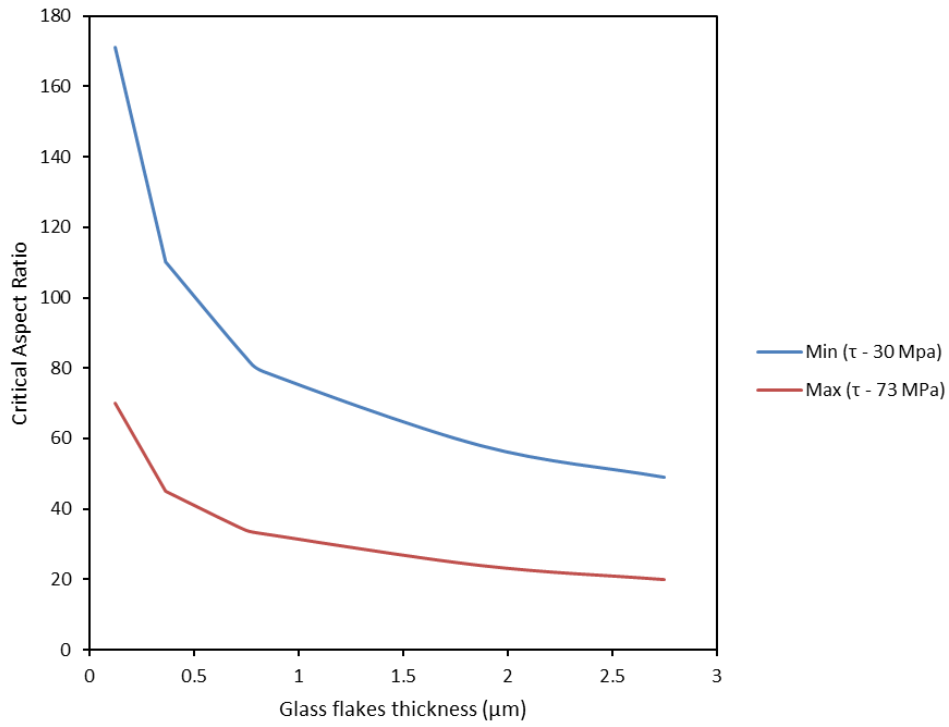


Figure 46 Influence of glass flakes thickness on critical aspect ratio for Epoxy at different interfacial shear strength

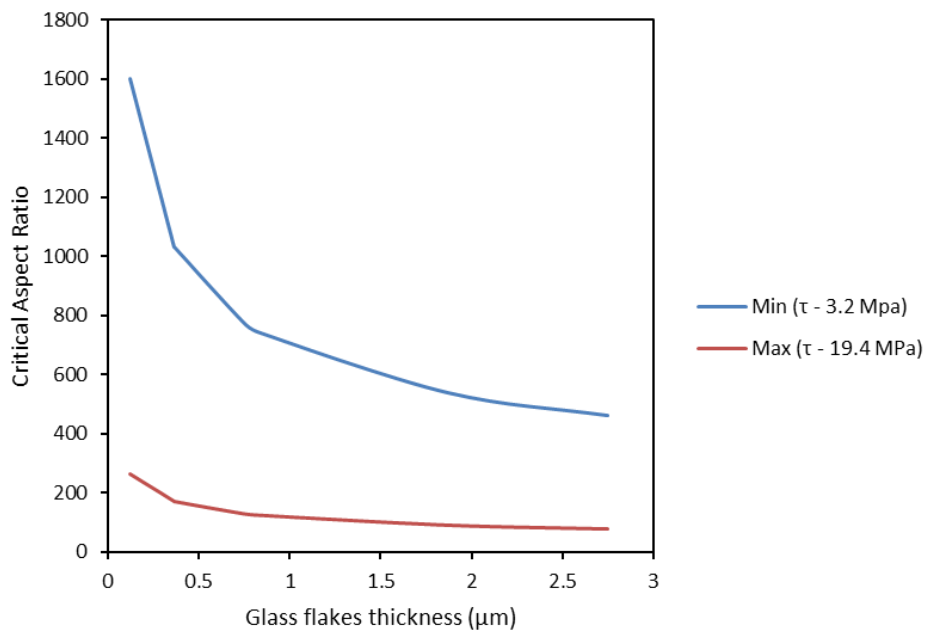


Figure 47: Influence of glass flakes thickness on critical aspect ratio for Polypropylene at different interfacial shear strength

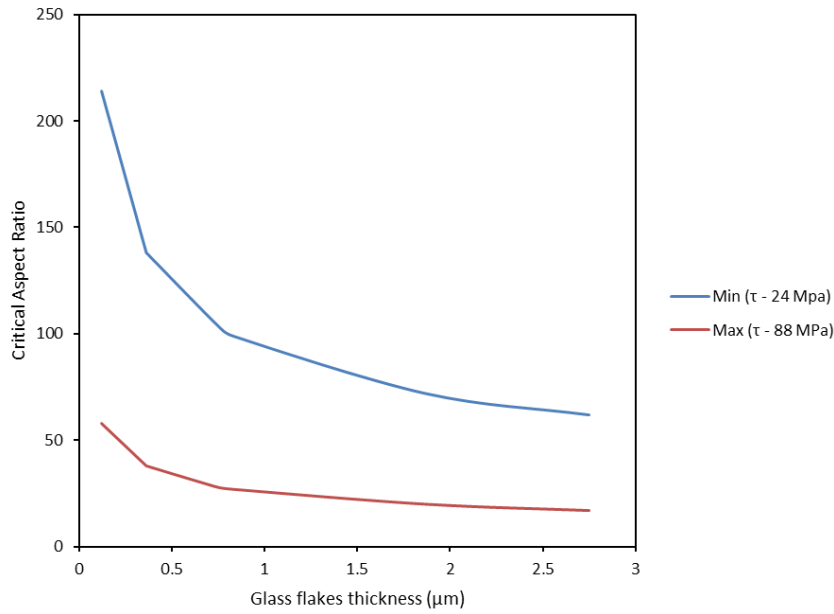


Figure 48: Influence of glass flakes thickness on critical aspect ratio for Nylon 6 at different interfacial shear strength

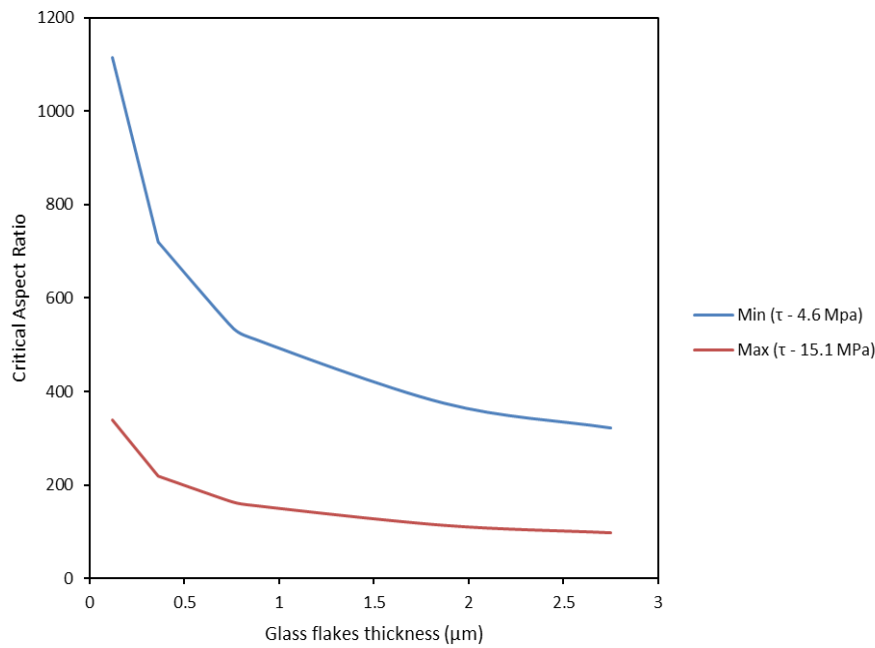


Figure 49: Influence of glass flakes thickness on critical aspect ratio for Polyethylene at different interfacial shear strength

Figure 46 – 49 exhibited similar trends for both minimum and maximum interfacial shear strength for the four matrix systems, which shows that the critical aspect ratio increases with a decrease in glass flakes thickness. However, the critical aspect ratio decreases for maximum

interfacial shear strength for the same glass flakes thickness compared to minimum interfacial shear strength. Meanwhile, research reported that high filler aspect ratio provides composite material with high strength and stiffness [257]. Though, interfacial shear strength depends on a good interfacial bond between the reinforcement filler and the matrix for the reinforcement filler to reinforce the matrix but has a reducing effect on the critical aspect ratio for the composite material systems.

4.2.2 Modelling of mechanical properties of glass flake reinforced polymer composites with tough fracture

4.2.2.1 Influence of glass flakes thickness on composite mechanical properties

Determining the change in composite material mechanical properties for various thickness of glass flakes at different interfacial shear strength is examined for the four matrices using Equation 8 and 11 for modulus and strength, respectively.

Table 20: Comparison of average aspect ratio measured (S) in yellow column) with critical aspect ratio (S_c) for different matrices to determine applicable fraction term (α)

Comparison of critical aspect ratio (S_c) for various composite matrix systems at different interfacial values with average measured aspect ratio (S) for investigated glass flakes									
	Epoxy		Polypropylene		Nylon 6		Polyethylene		Average aspect ratio (S)
	(S_c)		(S_c)		(S_c)		(S_c)		
Glass Flakes	Min ($\tau - 30$ MPa)	Max ($\tau - 73$ MPa)	Min ($\tau - 3.2$ MPa)	Max ($\tau - 19.4$ MPa)	Min ($\tau - 24$ MPa)	Max ($\tau - 88$ MPa)	Min ($\tau - 4.6$ MPa)	Min ($\tau - 15.1$ MPa)	
2.3 - 3.3 μ m	49	20	463	76	62	17	322	98	9
0.8 - 1.3 μ m	58	24	540	89	72	20	375	114	74
850nm Milled	79	33	744	123	99	27	518	158	139
850nm Unmilled	83	34	777	128	104	28	540	165	273
350nm Unmilled	110	45	1033	170	138	38	719	219	380
350nm Milled	110	45	1034	171	138	38	719	219	400
100nm Milled	171	70	1602	264	214	58	1114	339	905

The measured aspect ratio is higher than the critical aspect ratio, particularly at maximum interfacial shear strength for some matrix system. Thus, Table 20 provides comparison guide on fracture term (α) to apply for Equation 11 to determine if the average aspect ratio (S) for individual flakes investigated is higher (Equation 13) or lower (Equation 14) compared to the critical aspect ratio (S_c). Considering that the reinforcement filler aspect ratio below the critical aspect ratio yields tough failure of the composite material system through pull-out, the aspect ratio higher than the critical aspect ratio yields brittle failure. Hence, computing the modelling analysis at 60% weight filler loading through conversion into equivalent volume fraction using Equation 15. Table 6 provides details of mechanical properties for the four matrices studied. The glass flakes' mechanical properties detailed in Table 18, E-glass density value applied as 2.57 g/cm³ [268] to compute composite material mechanical properties. Plotted in Figure 50 - 53 are values obtained for tensile strength, and Figure 54 - 57 tensile modulus for the four matrices.

$$\text{Equation 15: } V_f = \frac{wt_f}{wt_f + \left[(1 - wt_f) \times \frac{\rho_f}{\rho_m} \right]}$$

V_f is the volume fraction for the reinforcement filler, wt_f is the weight fraction of the reinforcement filler, while ρ_f and ρ_m are densities for reinforcement filler and matrix respectively.

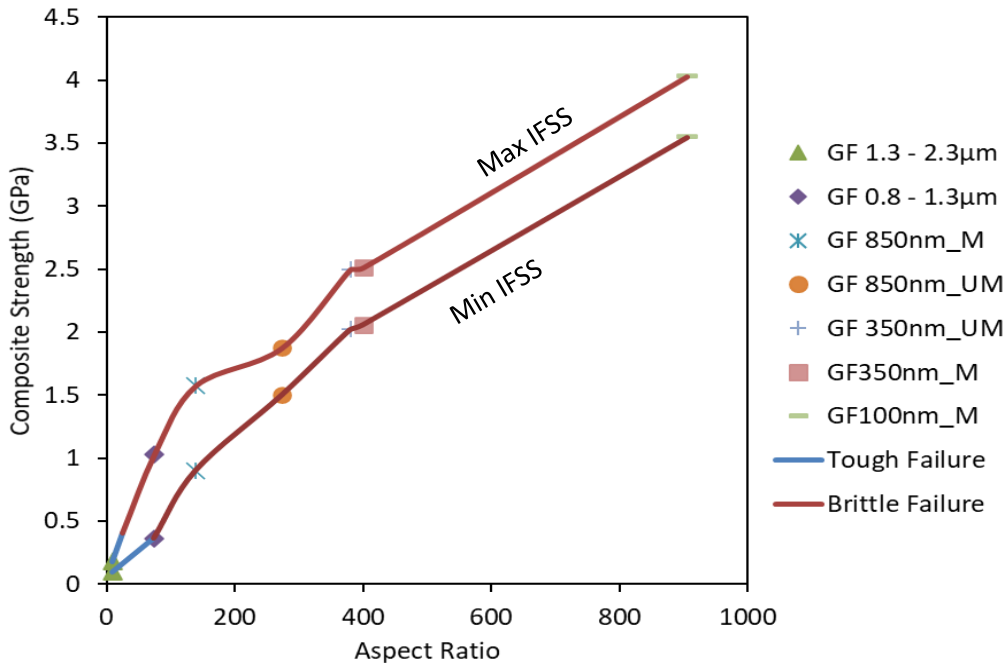


Figure 50: Effect of varied glass flakes thickness on composite strength at 60% wt. for Epoxy matrix

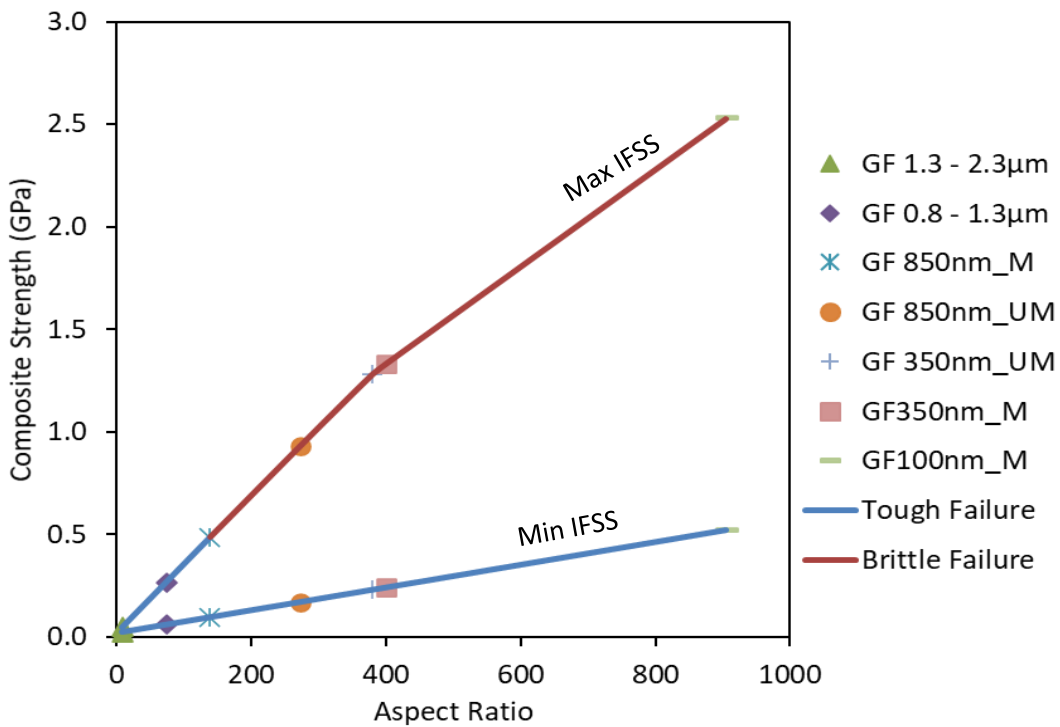


Figure 51: Effect of varied glass flakes thickness on composite strength at 60% wt. for Polypropylene matrix

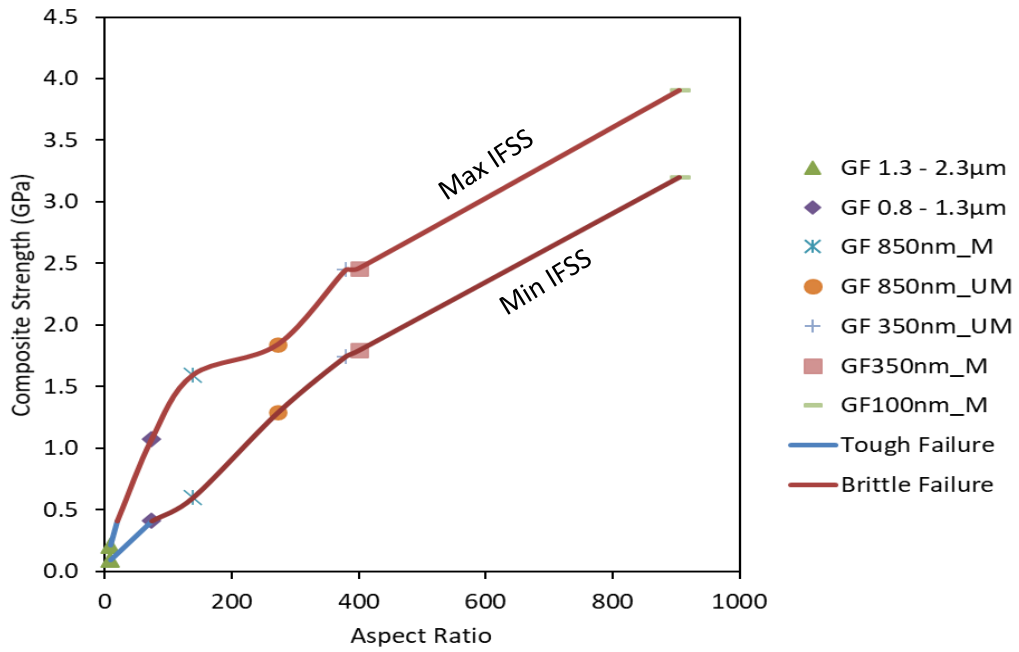


Figure 52: Effect of varied glass flakes thickness on composite strength at 60% wt. for Nylon 6 matrix

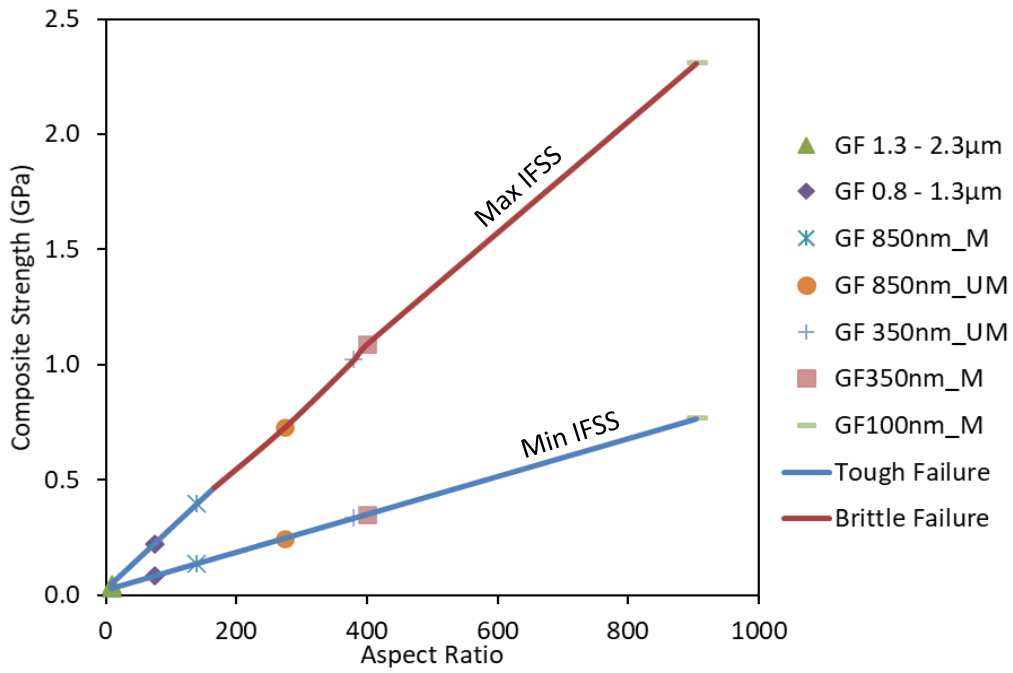


Figure 53: Effect of varied glass flakes thickness on composite strength at 60% wt. for Polyethylene matrix

Figure 50 – 53 shows the importance of thickness by investigating the change in composite strength concerning glass flakes interfacial shear strength (IFSS). While the measured aspect ratio for both maximum and minimum interfacial shear strength is the same for each glass flakes. Maximum interfacial shear strength provides better reinforcement, which is expected as inherent mechanical properties of the glass flakes is being harnessed due to good bond adhesion. This, coupled with the effect of glass flakes thickness, shows that thinner glass flakes provide better reinforcement efficiency, however, due to high aspect ratios associated with thinner glass flakes, the composite material yields brittle failure.

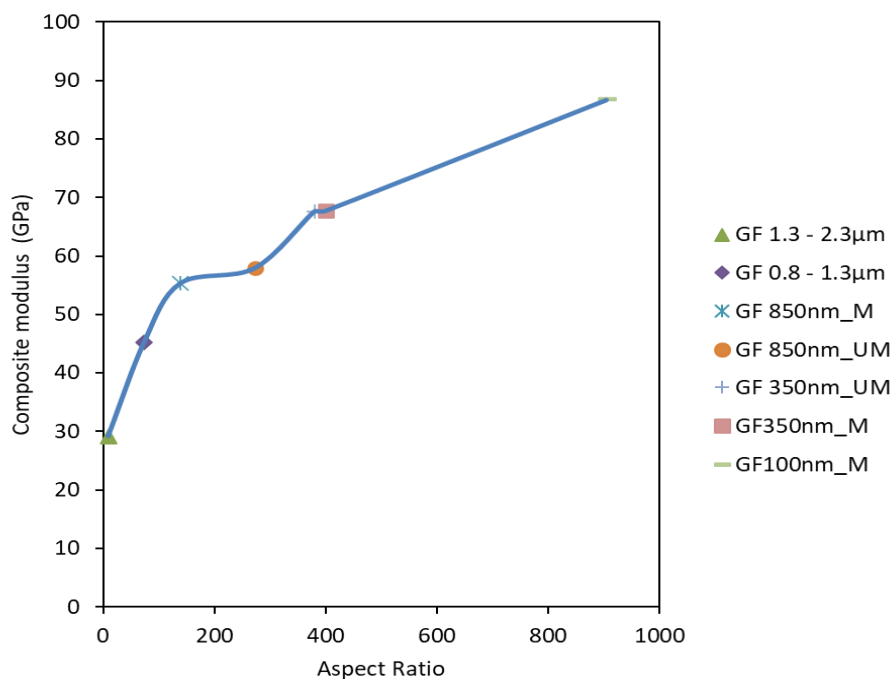


Figure 54: Effect of varied glass flakes thickness on composite modulus at 60% wt. for Epoxy matrix

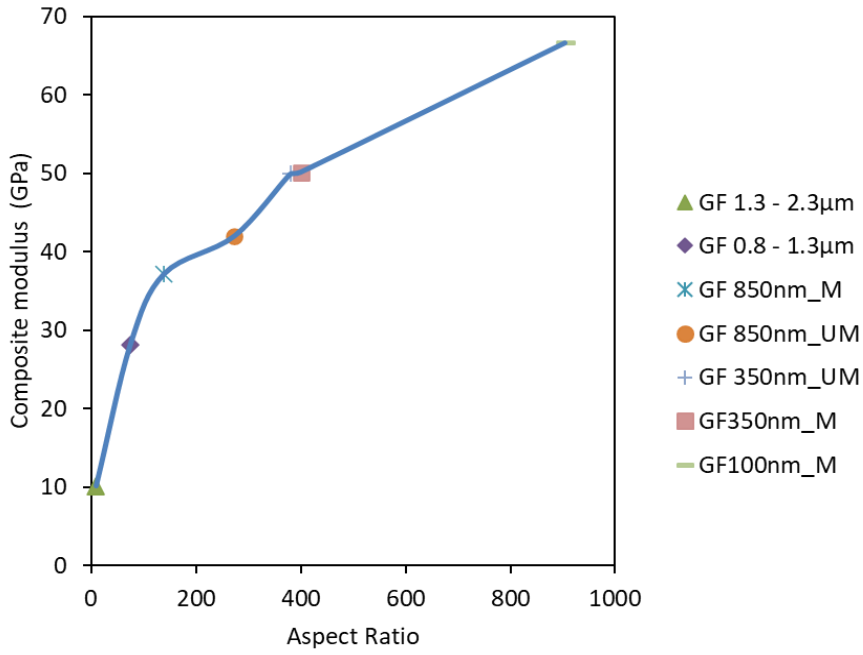


Figure 55: Effect of varied glass flakes thickness on composite modulus at 60% wt. for Polypropylene matrix

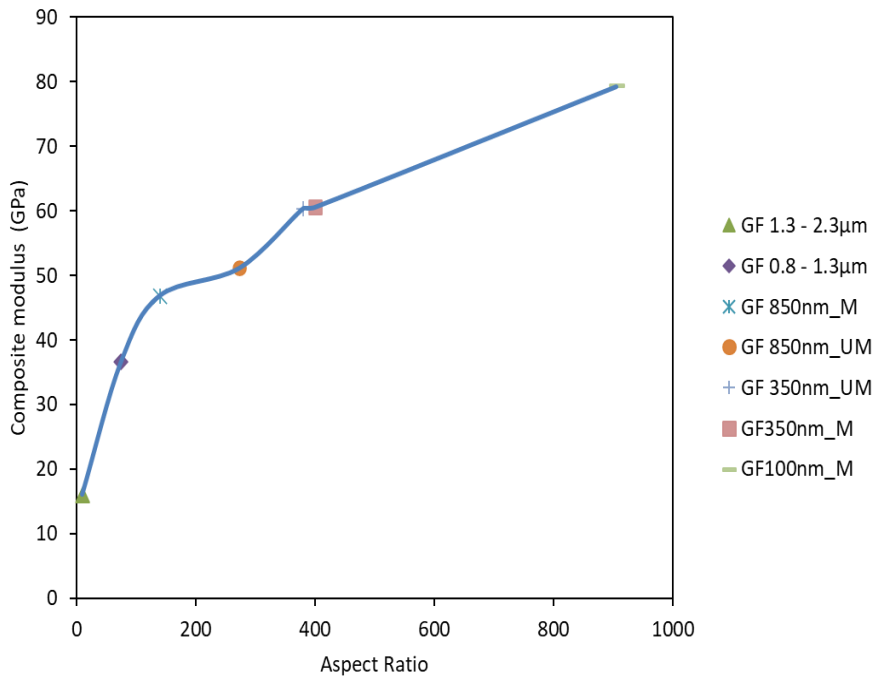


Figure 56: Effect of varied glass flakes thickness on composite modulus at 60% wt. for nylon 6 matrix

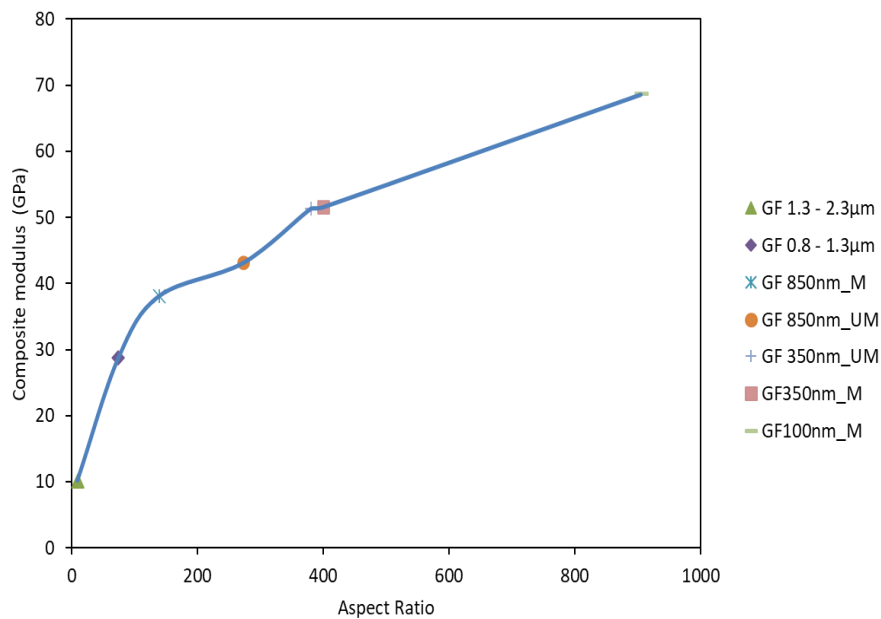


Figure 57: Effect of varied glass flakes thickness on composite modulus at 60% wt. for Polyethylene matrix

Figure 54 – 57 shows the composite modulus values obtained for each matrix system relating to individual glass flakes investigated. Correspondently, composite modulus for all matrix systems exhibited the same trend to composite strength, with thinner glass flakes providing better reinforcement.

4.2.2.2 Influence of glass flakes aspect ratio on composite mechanical properties

With Figure 50 – 53 showing plots for composite strength and Figure 54 – 57 composite modulus. All computed using the aspect ratio measured for each glass flakes and their corresponding strength and modulus at each glass flakes thickness. However, the effect of change in aspect ratio at a fixed thickness for each glass flakes investigated to determine the change in composite strength and modulus by having the glass flakes aspect ratio manoeuvred via ball milling. Using details in Table 12 – 17 for ball-milled glass flakes aspect

ratios and considering only maximum interfacial shear strength for each matrix system, being that good interfacial bond adhesion promotes effective stress transfer, which yields composite material with enhanced mechanical properties (Figure 50 – 53). Thus, the glass flakes strength and modulus remain unchanged as the glass flakes thickness is not changing for each matrix system, and also the interfacial shear strength remains unchanged. Results obtained for each matrix systems due to change in aspect ratio due to ball-milling for each glass flakes shown in Figure 58 - 69 for nylon-6 matrix composite strength and modulus. Figure 70 - 81 for polypropylene matrix composite strength and modulus. Figure 82 - 93 for epoxy matrix composite strength and modulus. Figure 94 - 105 for polyethylene matrix composite strength and modulus.

Nylon-6 matrix

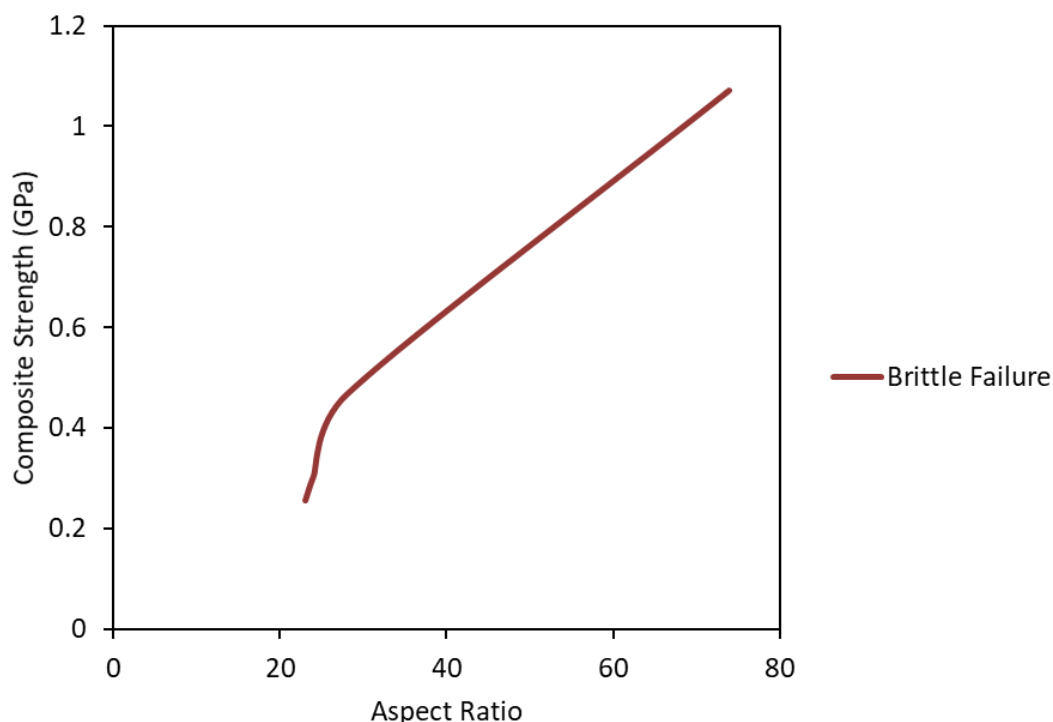


Figure 58: Effect of varied aspect ratio on composite strength of glass flakes / Nylon 6 - GF 0.8 - 1.3 μ m at 60% wt.

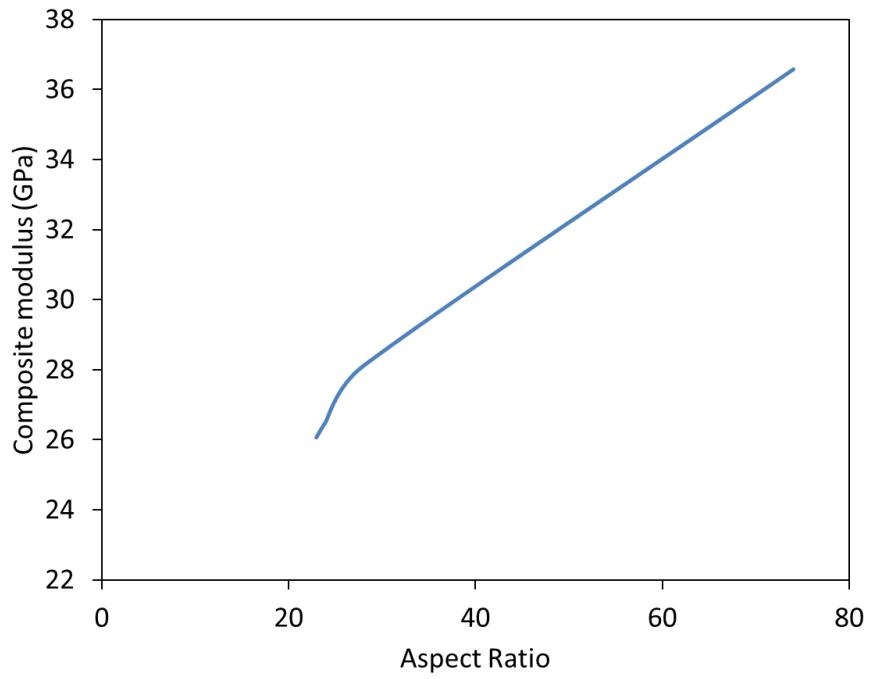


Figure 59: Effect of varied aspect ratio on composite modulus of glass flakes / Nylon 6 - GF 0.8 - 1.3µm at 60% wt.

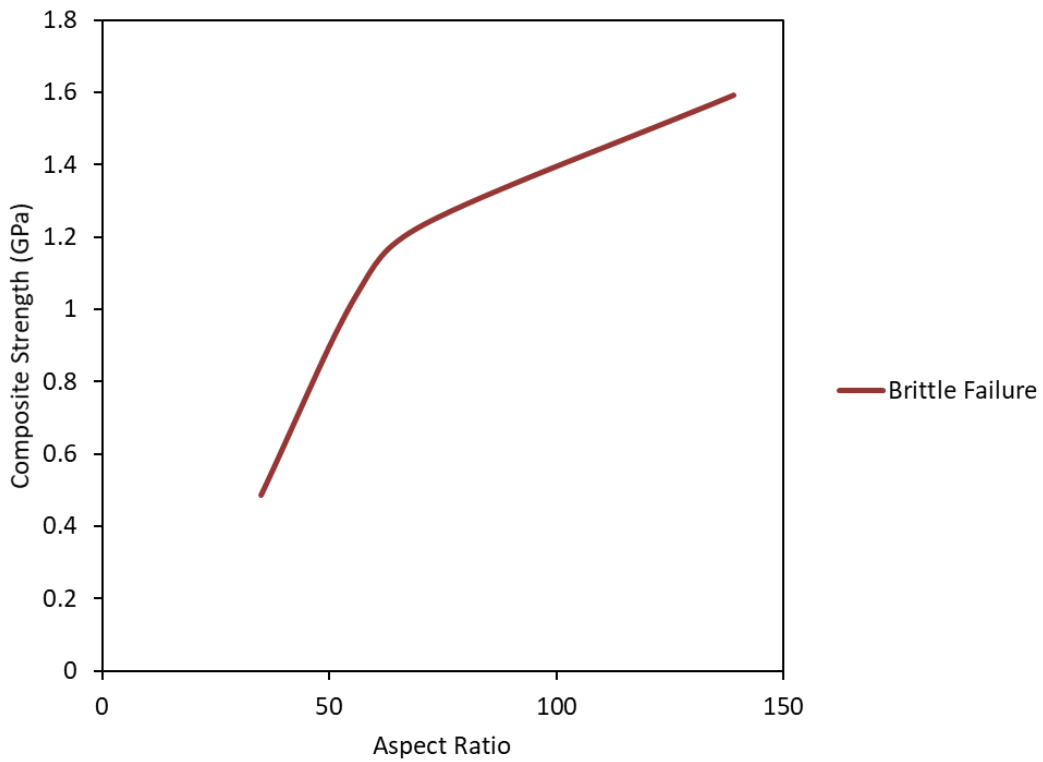


Figure 60: Effect of varied aspect ratio on composite strength of glass flakes / Nylon 6 - GF 850nm M at 60% wt.

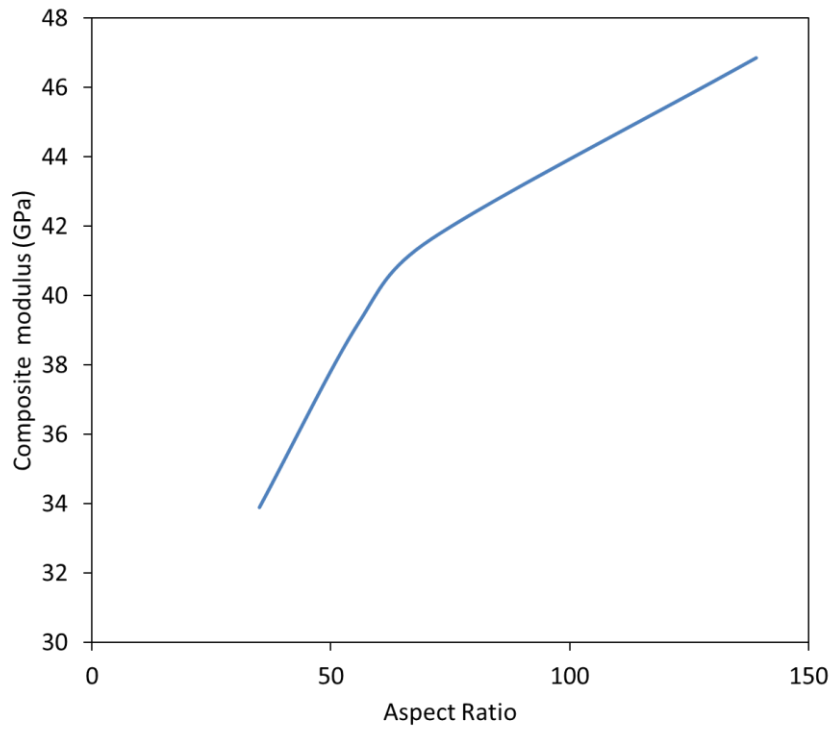


Figure 61: Effect of varied aspect ratio on composite modulus of glass flakes / Nylon 6 - GF 850nm M at 60% wt.

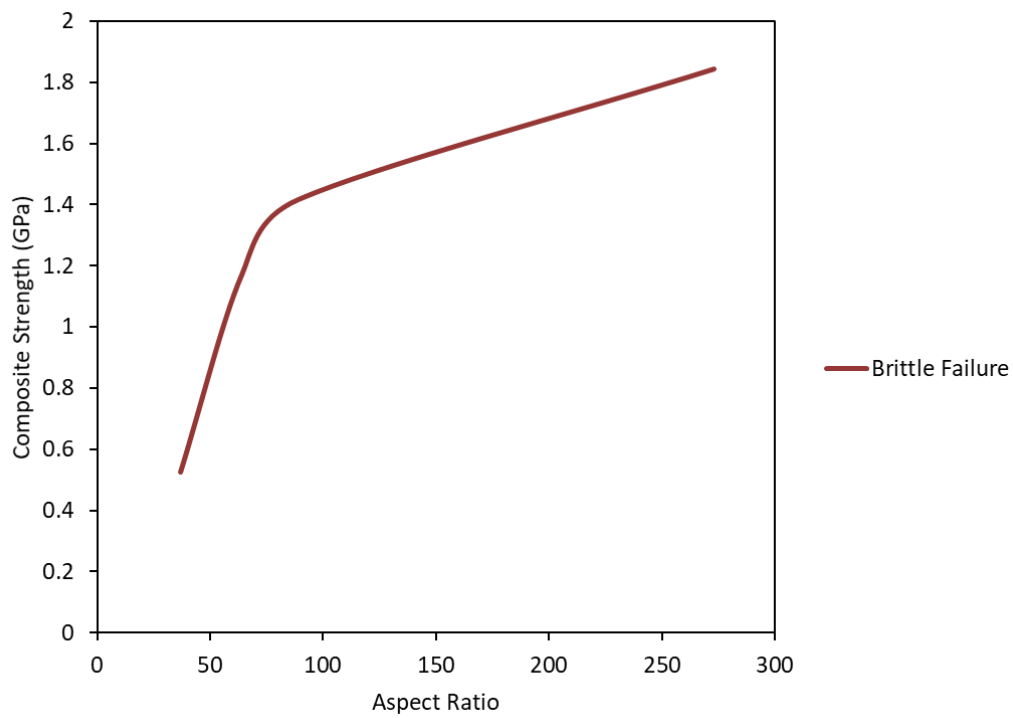


Figure 62: Effect of varied aspect ratio on composite strength of glass flakes / Nylon 6 - GF 850nm UM at 60% wt.

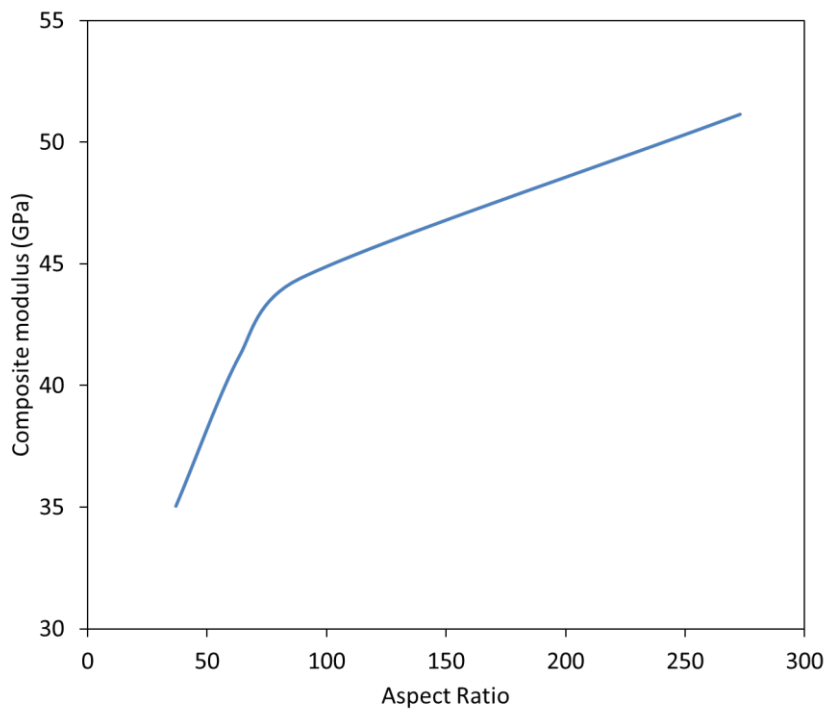


Figure 63: Effect of varied aspect ratio on composite modulus of glass flakes / Nylon 6 - GF 850nm UM at 60% wt.

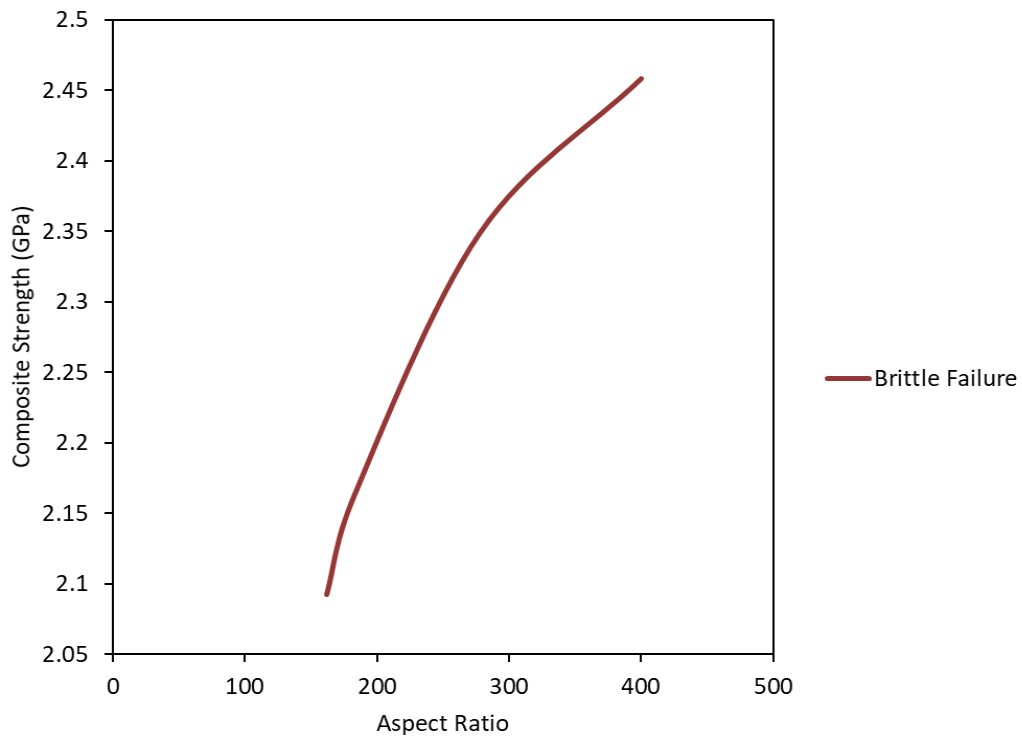


Figure 64: Effect of varied aspect ratio on composite strength of glass flakes / Nylon 6 - GF 350nm M at 60% wt.

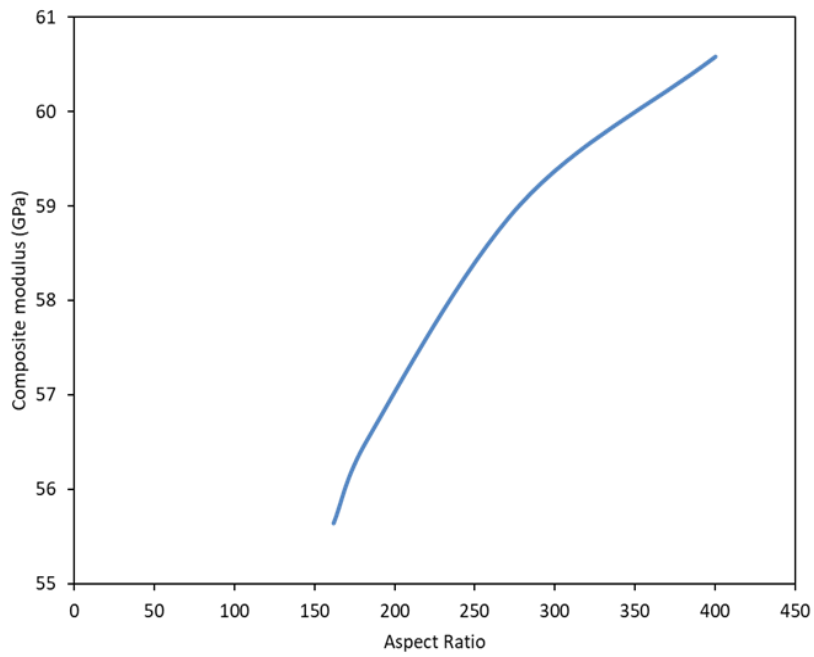


Figure 65: Effect of varied aspect ratio on composite modulus of glass flakes / Nylon 6 - GF 350nm M at 60% wt.

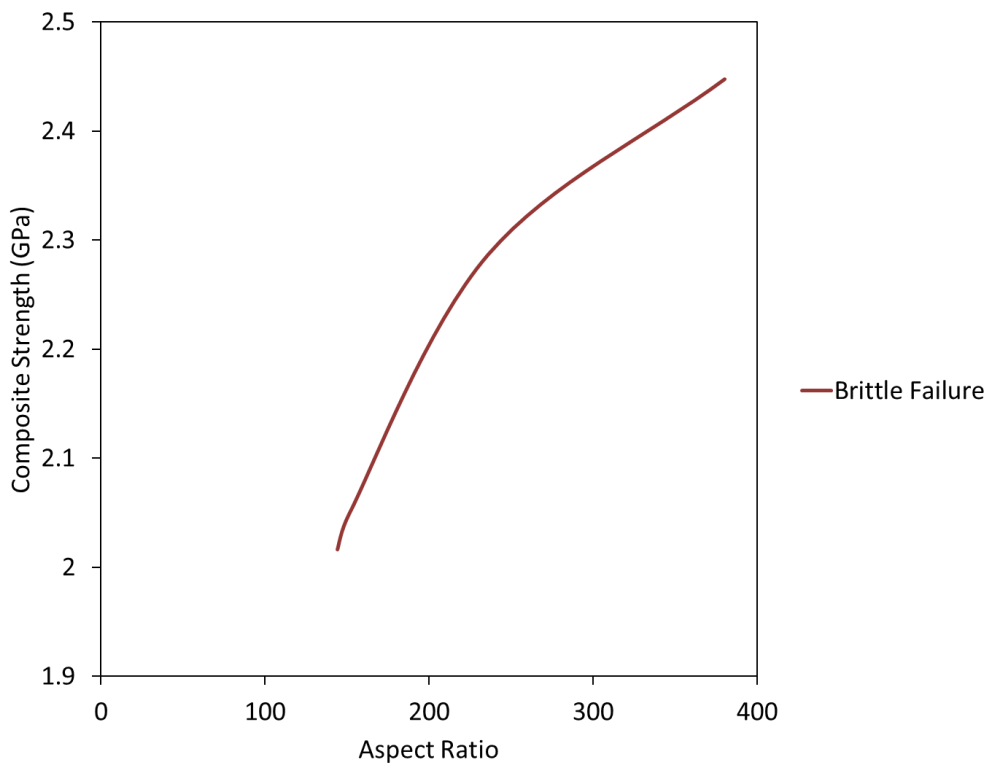


Figure 66: Effect of varied aspect ratio on composite strength of glass flakes / Nylon 6 - GF 350nm UM at 60% wt.

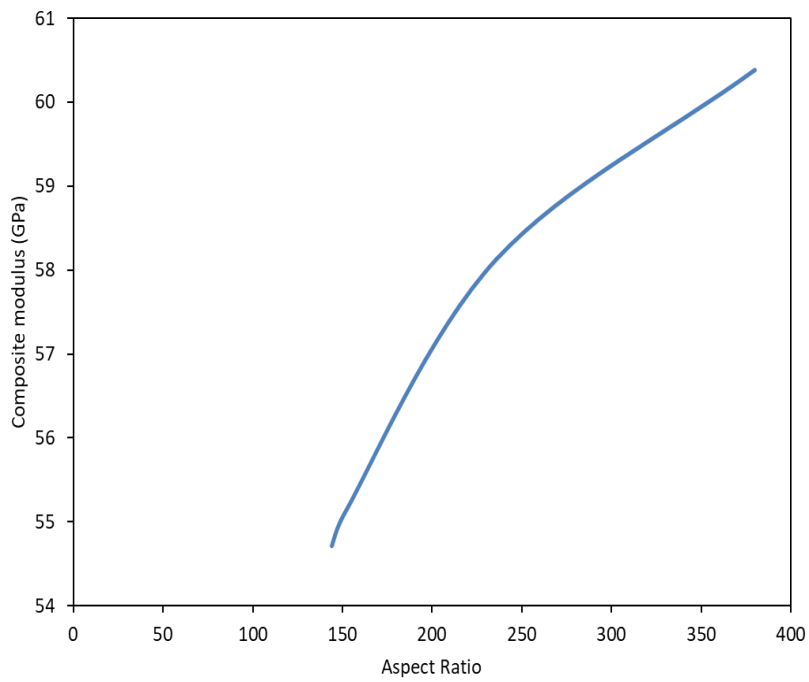


Figure 67: Effect of varied aspect ratio on composite modulus of glass flakes / Nylon 6 - GF 350nm UM at 60% wt.

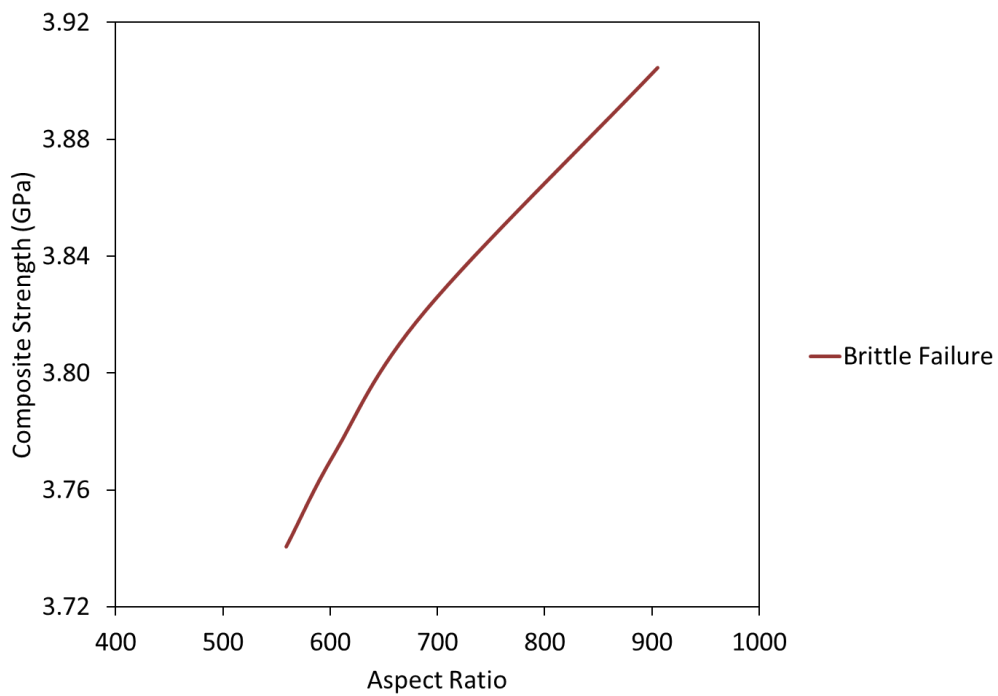


Figure 68: Effect of varied aspect ratio on composite strength of glass flakes / Nylon 6 - GF 100nm M at 60% wt.

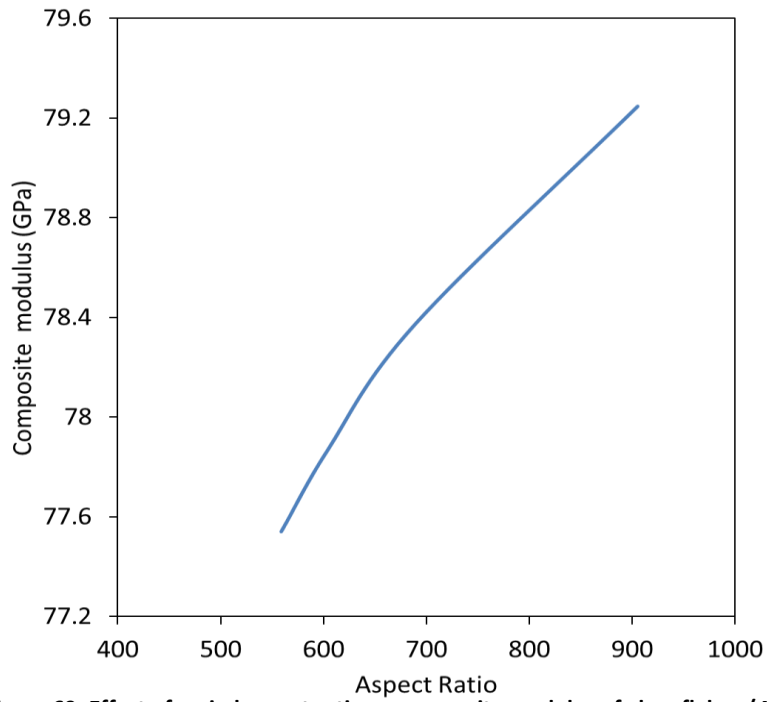


Figure 69: Effect of varied aspect ratio on composite modulus of glass flakes / Nylon 6 - GF 100nm M at 60% wt.

Polypropylene matrix

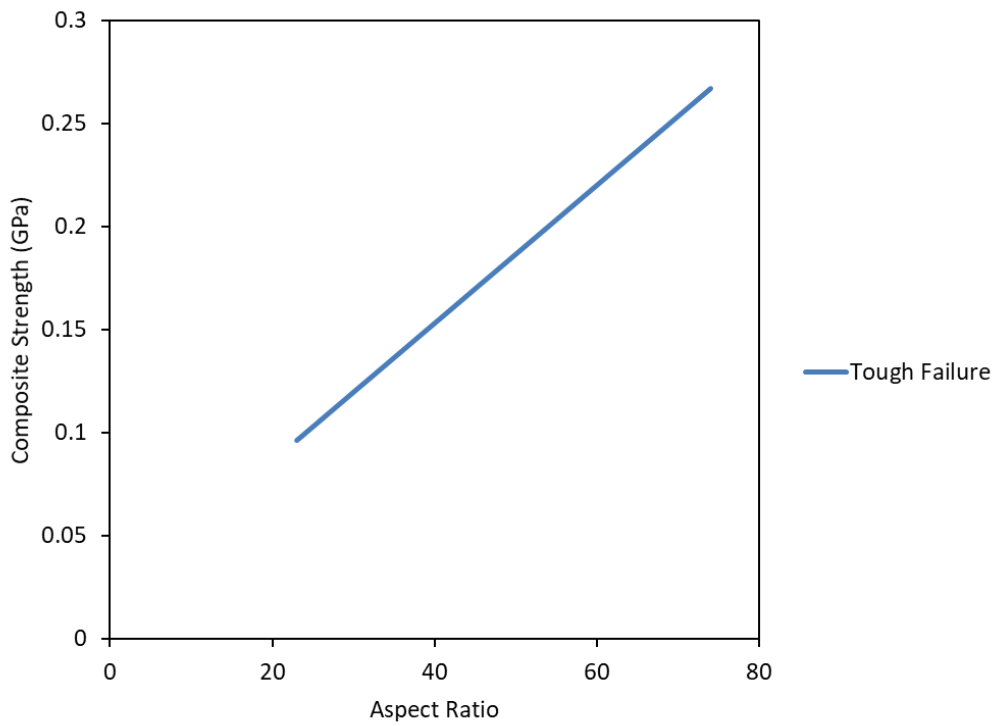


Figure 70: Effect of varied aspect ratio on composite strength of glass flakes / Polypropylene - GF 0.8 - 1.3µm at 60% wt.

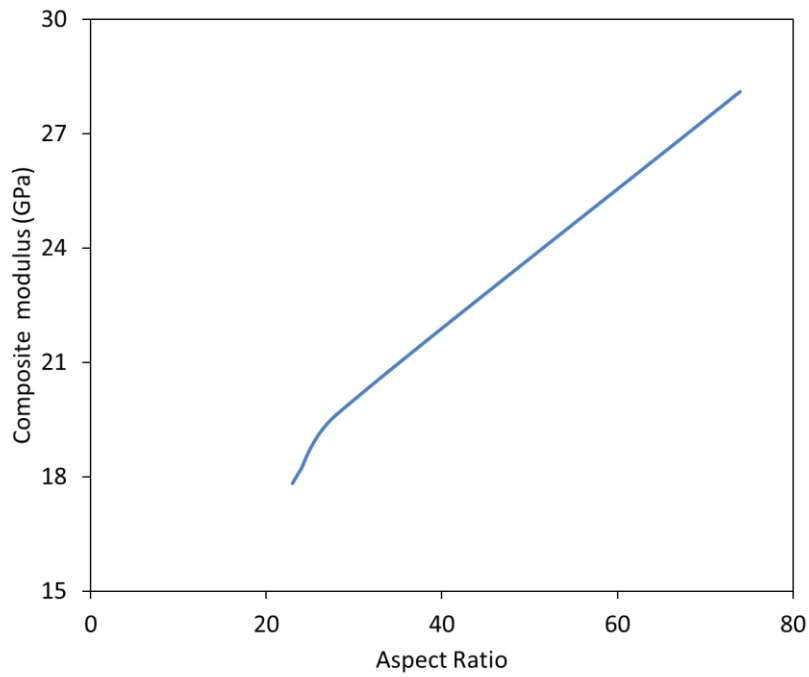


Figure 71: Effect of varied aspect ratio on composite modulus of glass flakes / Polypropylene - GF 0.8 - 1.3 μ m at 60% wt.

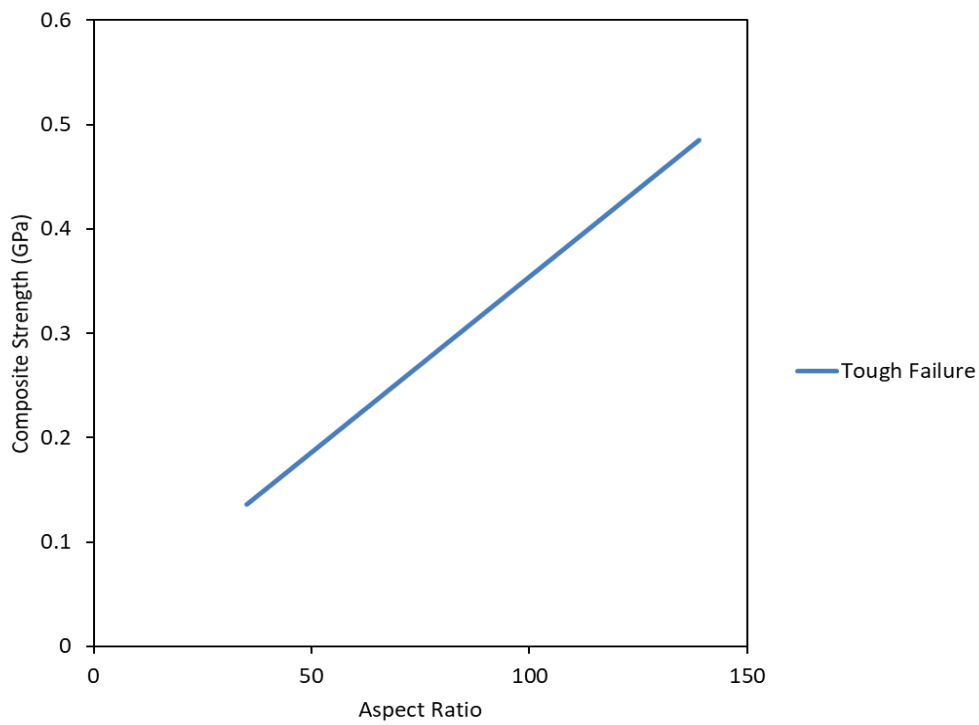


Figure 72: Effect of varied aspect ratio on composite strength of glass flakes / Polypropylene - GF 850nm M at 60% wt.

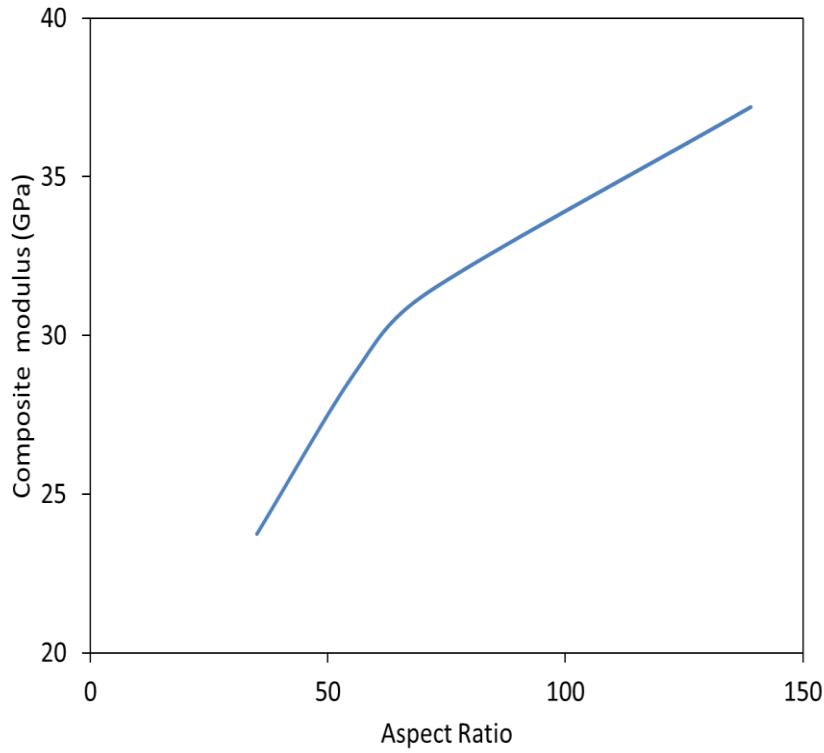


Figure 73: Effect of varied aspect ratio on composite modulus of glass flakes / Polypropylene - GF 850nm M at 60% wt.

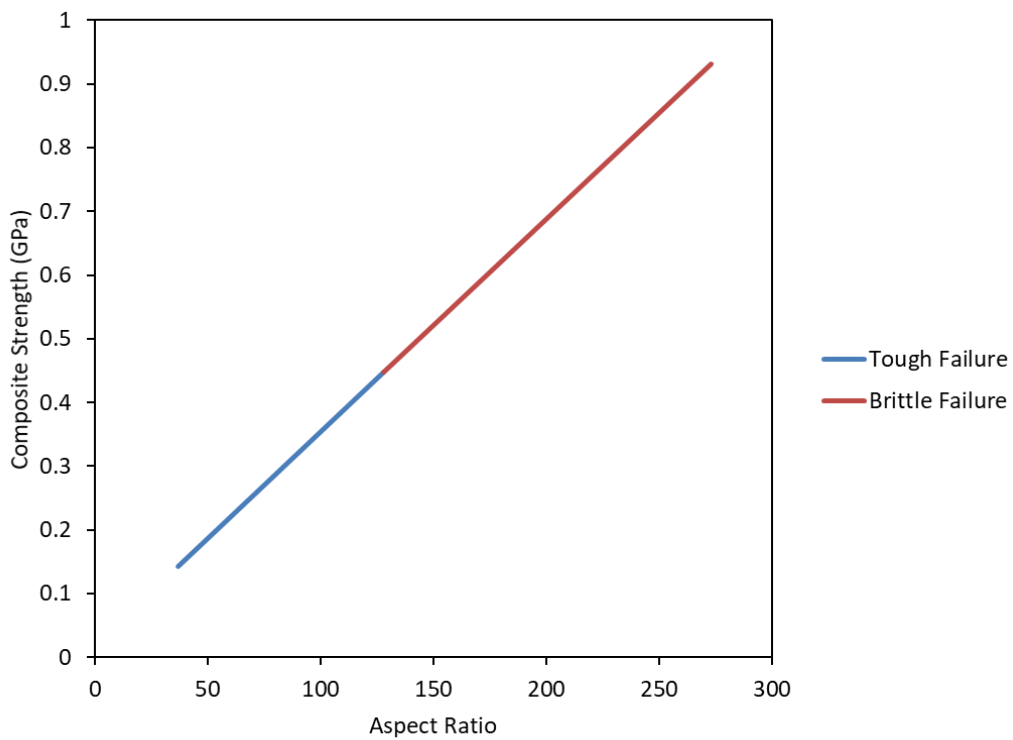


Figure 74: Effect of varied aspect ratio on composite strength of glass flakes / Polypropylene - GF 850nm UM at 60% wt.

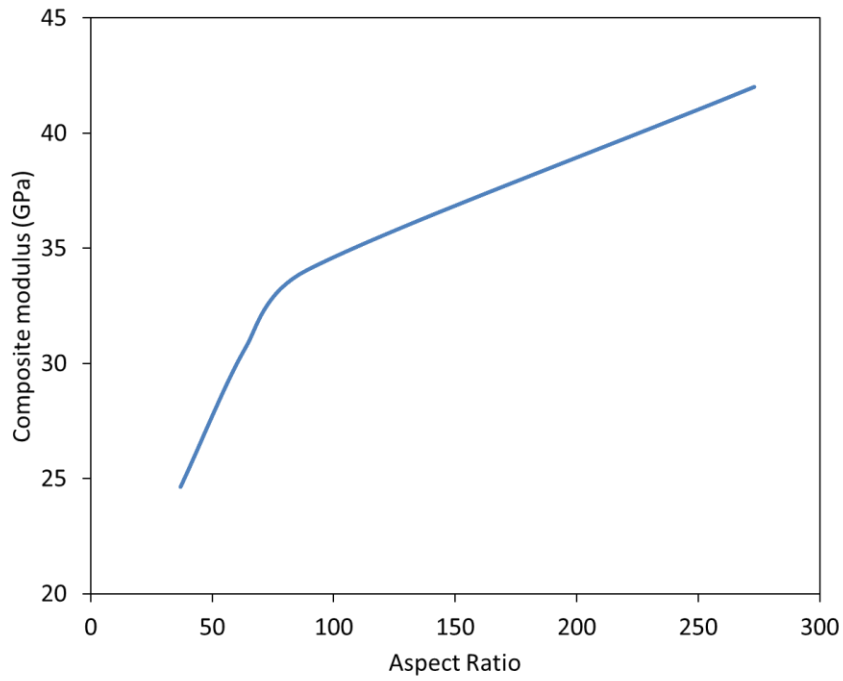


Figure 75: Effect of varied aspect ratio on composite modulus of glass flakes / Polypropylene - GF 850nm UM at 60% wt.

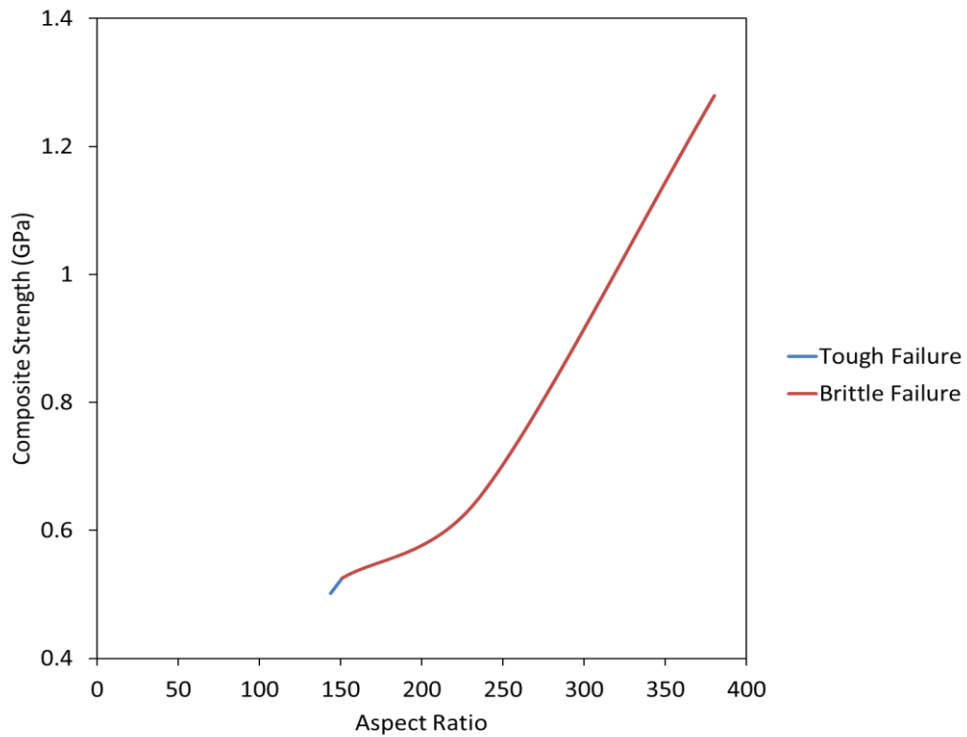


Figure 76: Effect of varied aspect ratio on composite strength of glass flakes / Polypropylene - GF 350nm M at 60% wt.

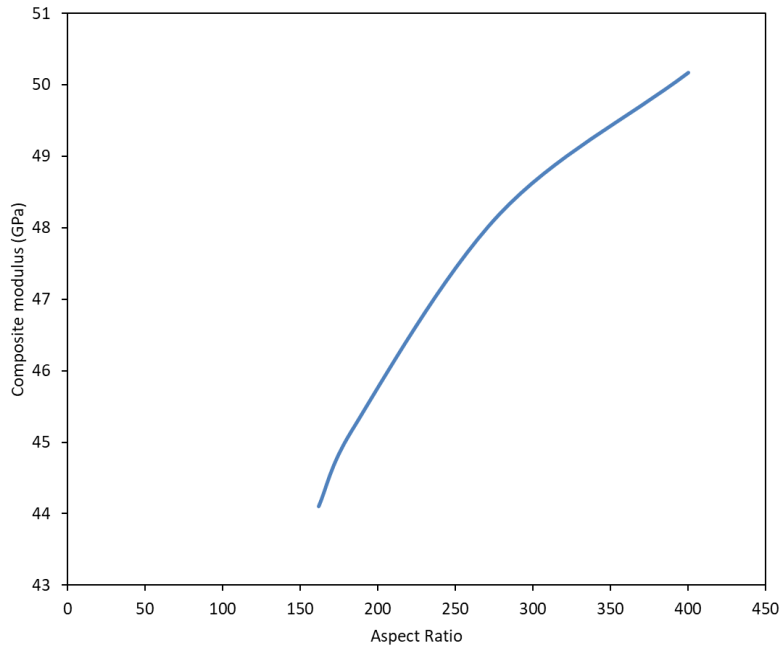


Figure 77: Effect of varied aspect ratio on composite modulus of glass flakes / Polypropylene - GF 350nm M at 60% wt.

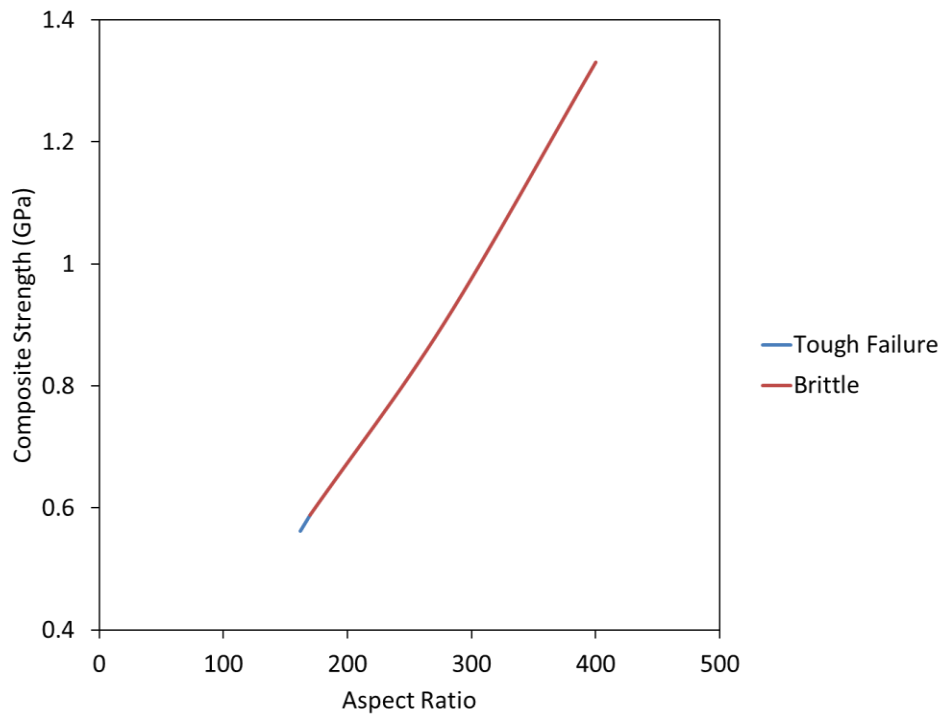


Figure 78: Effect of varied aspect ratio on composite strength of glass flakes / Polypropylene - GF 350nm UM at 60% wt.

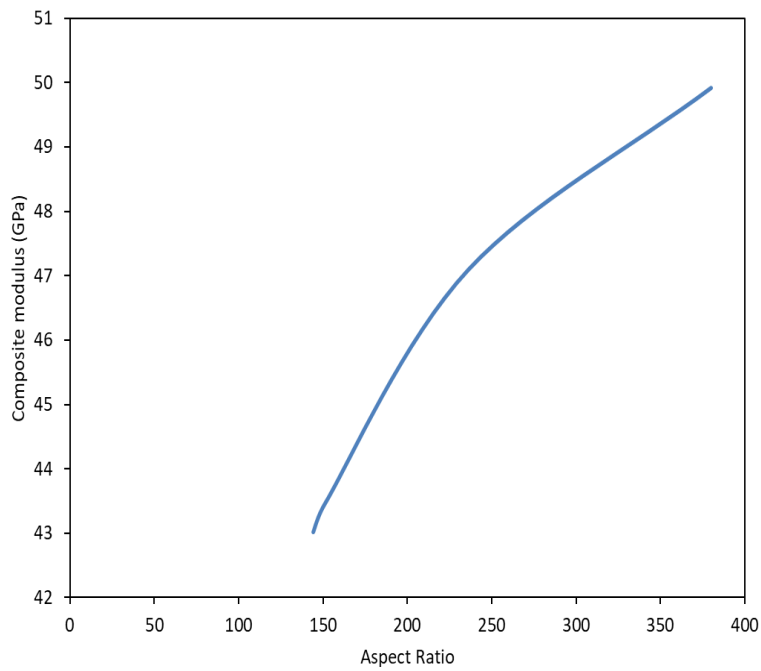


Figure 79: Effect of varied aspect ratio on composite modulus of glass flakes / Polypropylene - GF 350nm UM at 60% wt.

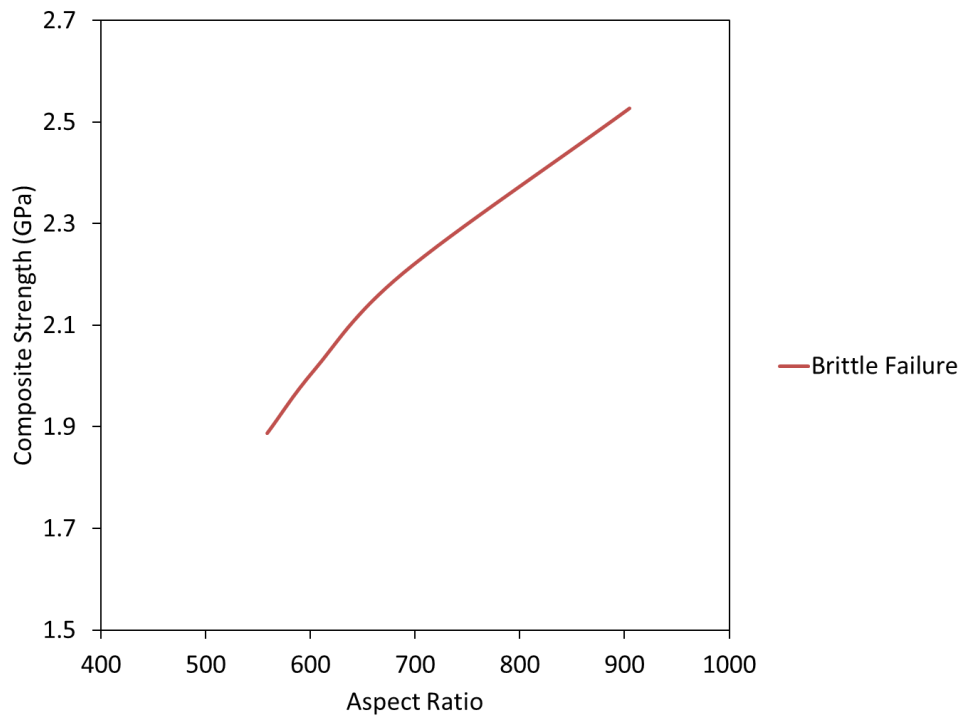


Figure 80: Effect of varied aspect ratio on composite strength of glass flakes / Polypropylene - GF 100nm M at 60% wt.

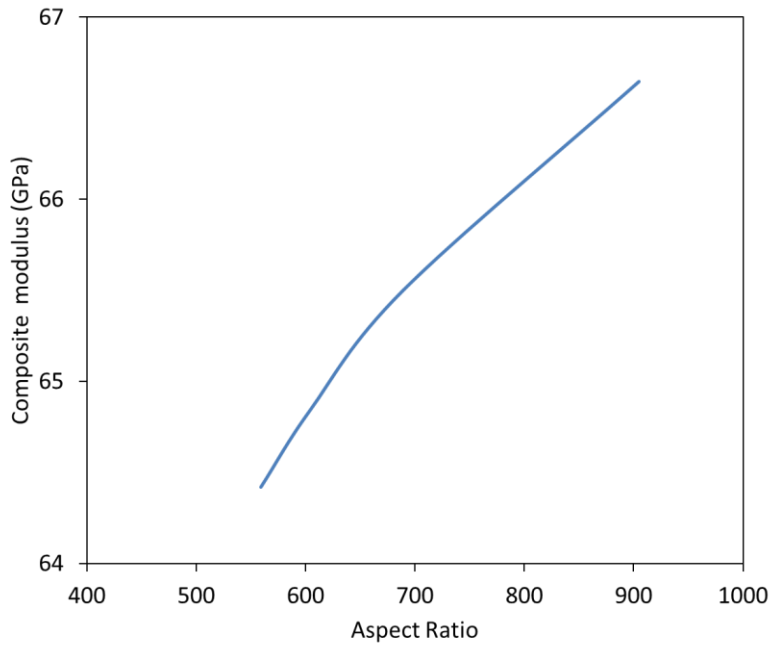


Figure 81: Effect of varied aspect ratio on composite modulus of glass flakes / Polypropylene - GF 100nm M at 60% wt.

Epoxy matrix

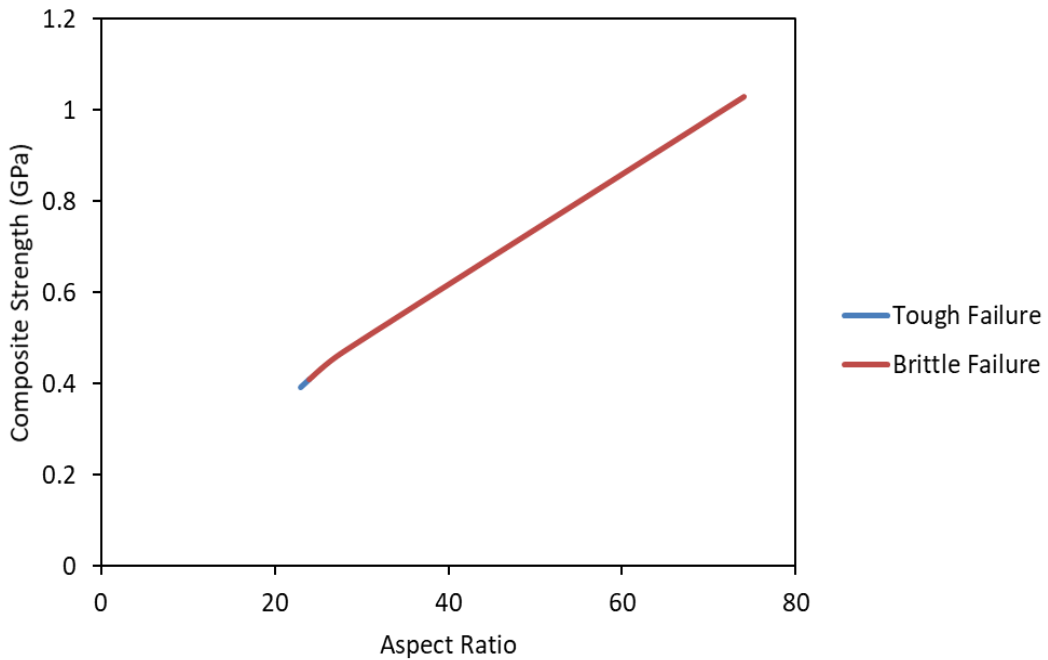


Figure 82: Effect of varied aspect ratio via ball milling on composite strength for glass flakes / Epoxy - GF 0.8 - 1.3 μ m at 60% wt.

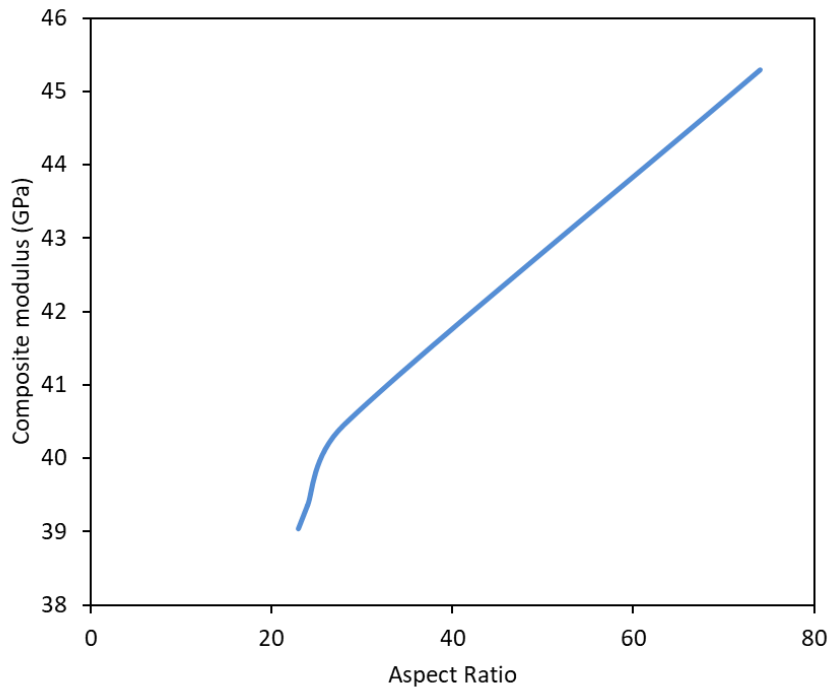


Figure 83: Effect of varied aspect ratio via ball milling on composite modulus for glass flakes / Epoxy - GF 0.8 - 1.3µm at 60% wt.

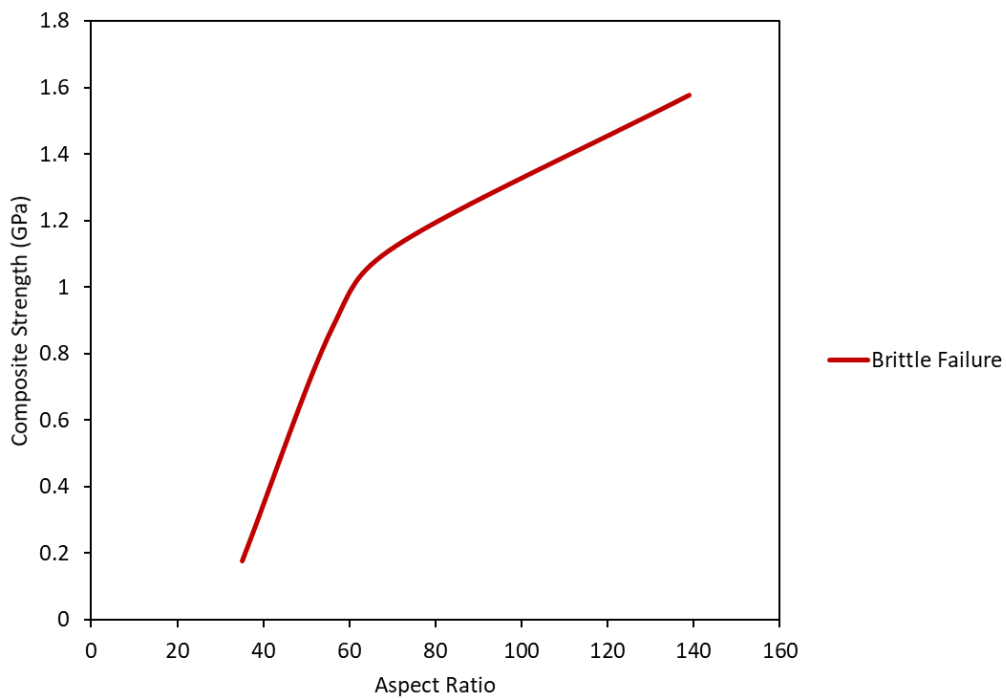


Figure 84: Effect of varied aspect ratio via ball milling on composite strength for glass flakes / Epoxy - GF 850nm M at 60% wt.

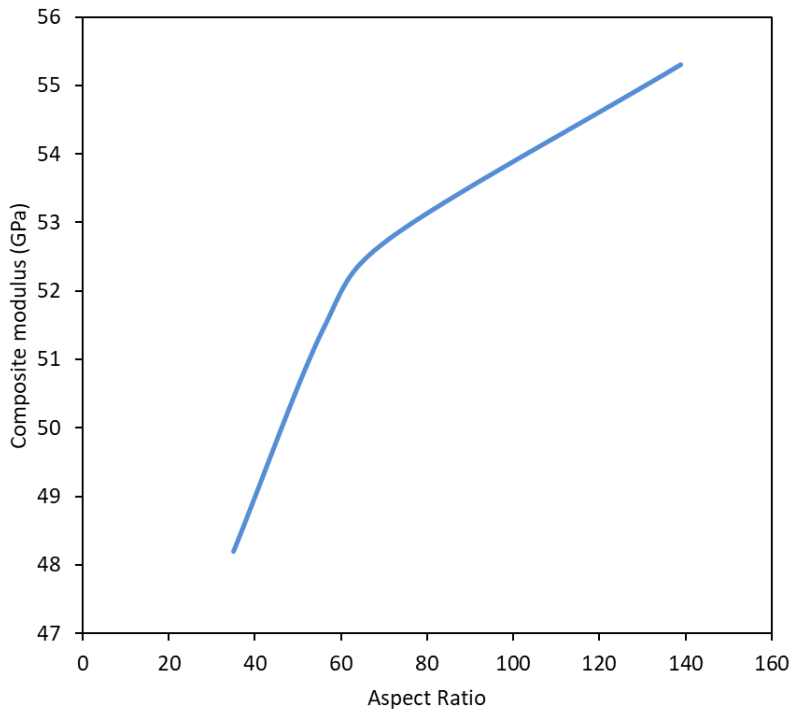


Figure 85: Effect of varied aspect ratio via ball milling on composite modulus for glass flakes / Epoxy - GF 850nm M at 60% wt.

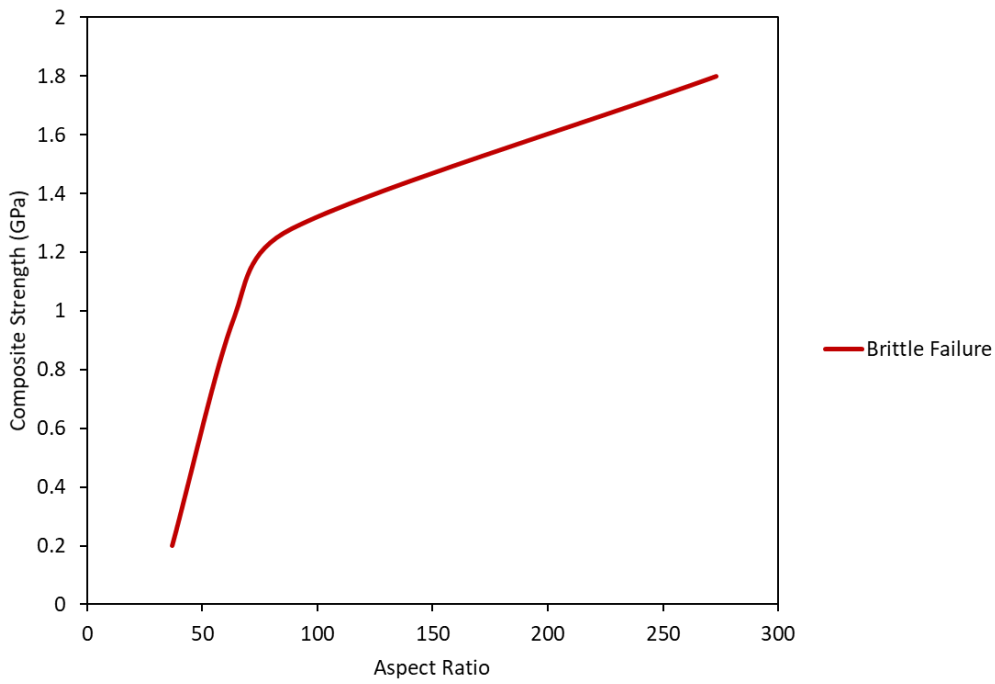


Figure 86: Effect of varied aspect ratio via ball milling on composite strength for glass flakes / Epoxy - GF 850nm UM at 60% wt.

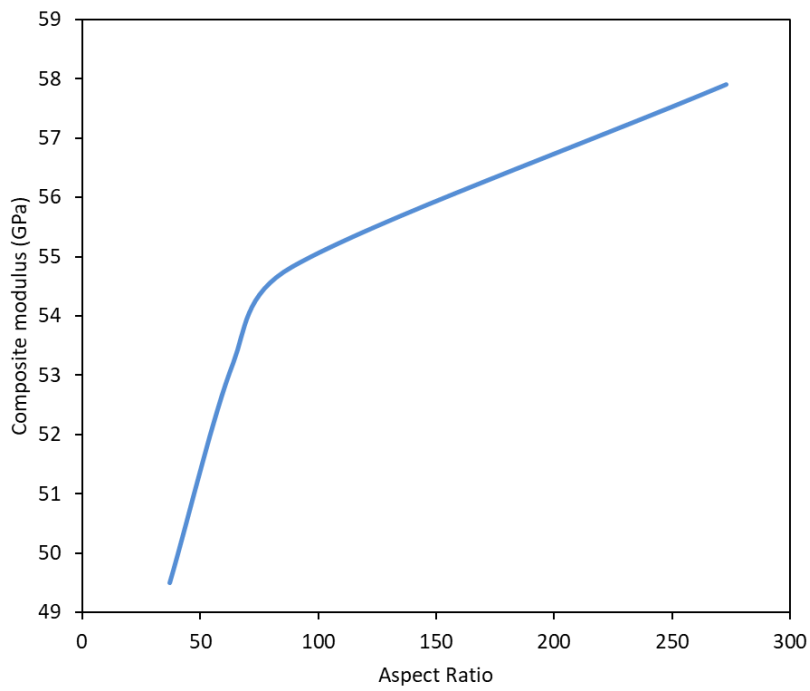


Figure 87: Effect of varied aspect ratio via ball milling on composite modulus for glass flakes / Epoxy - GF 850nm UM at 60% wt.

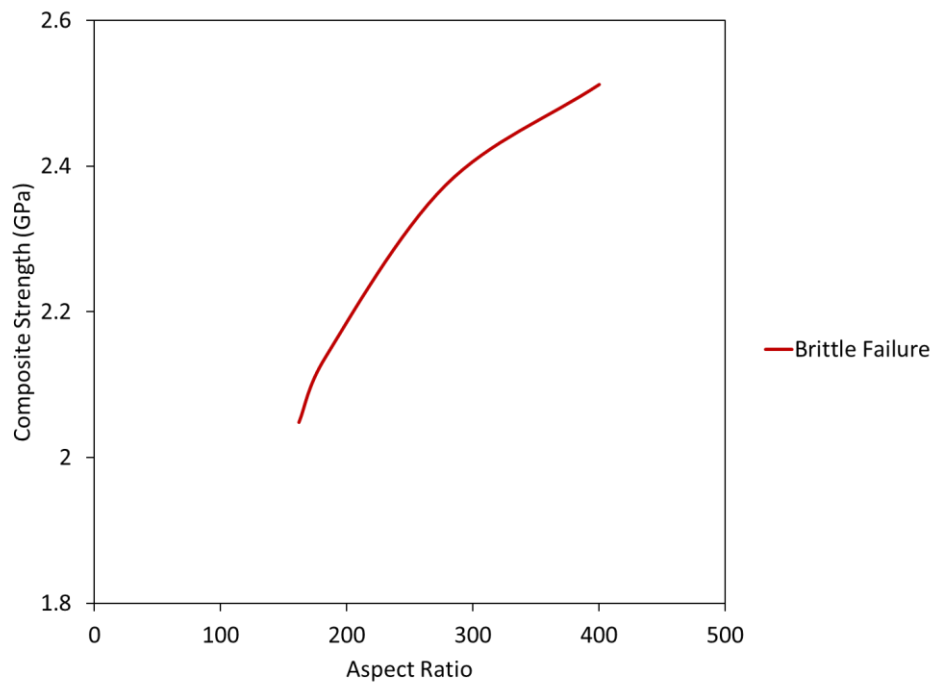


Figure 88: Effect of varied aspect ratio via ball milling on composite strength for glass flakes / Epoxy - GF 350nm M at 60% wt.

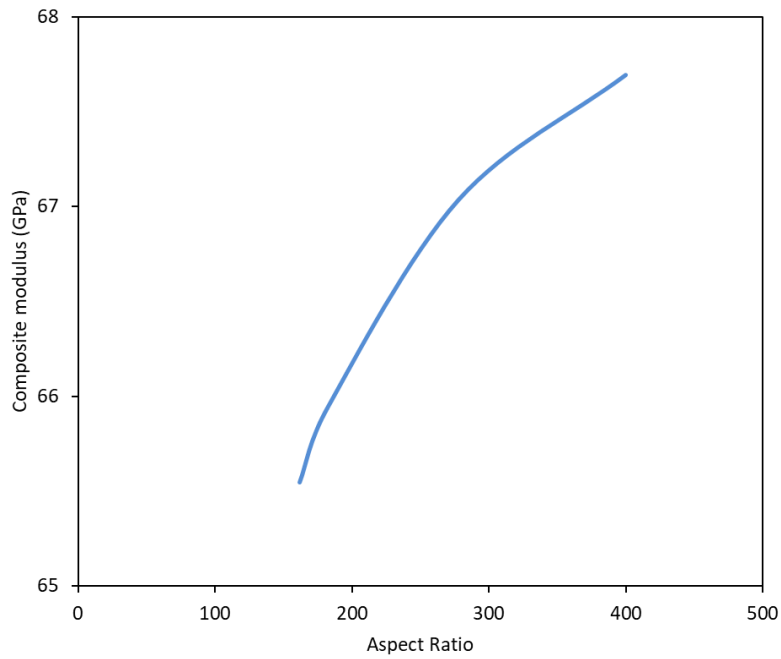


Figure 89: Effect of varied aspect ratio via ball milling on composite modulus for glass flakes / Epoxy - GF 350nm M at 60% wt.

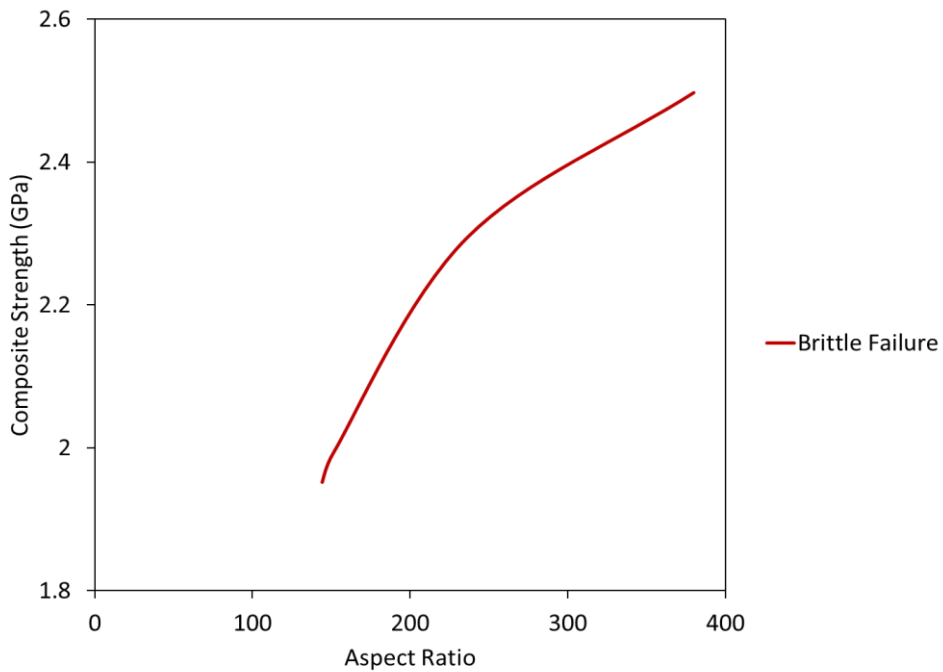


Figure 90: Effect of varied aspect ratio via ball milling on composite strength for glass flakes / Epoxy - GF 350nm UM at 60% wt.

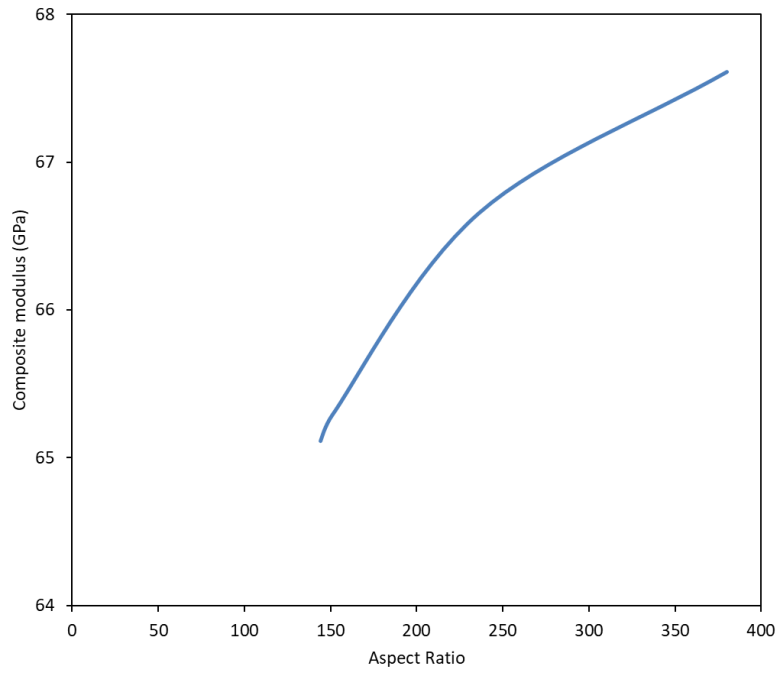


Figure 91: Effect of varied aspect ratio via ball milling on composite modulus for glass flakes / Epoxy - GF 350nm UM at 60% wt.

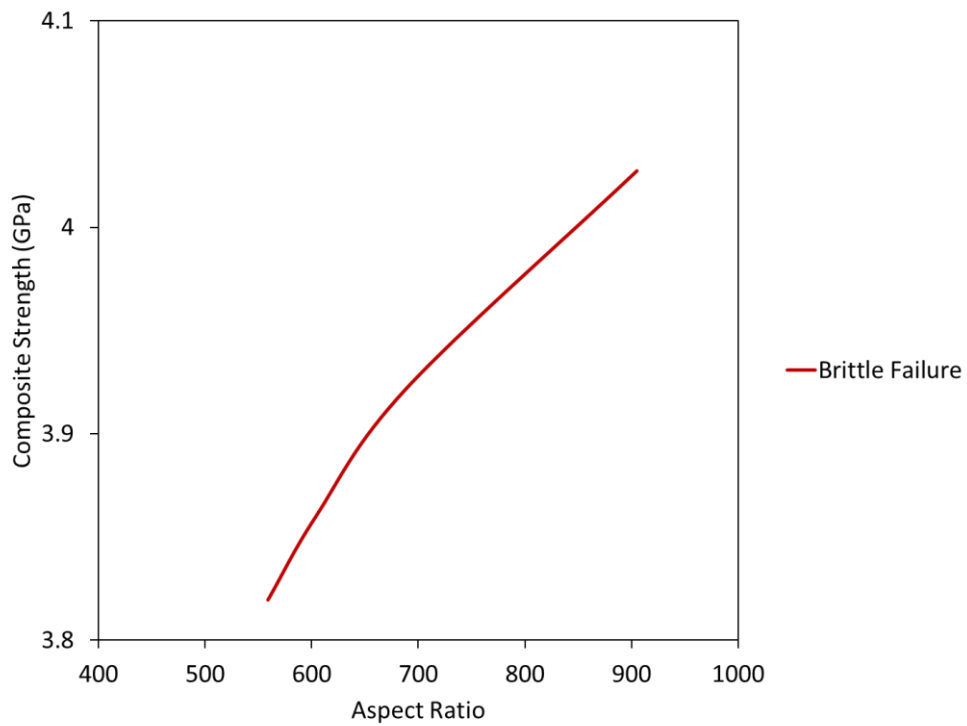


Figure 92: Effect of varied aspect ratio via ball milling on composite strength for glass flakes / Epoxy - GF 100nm M at 60% wt.

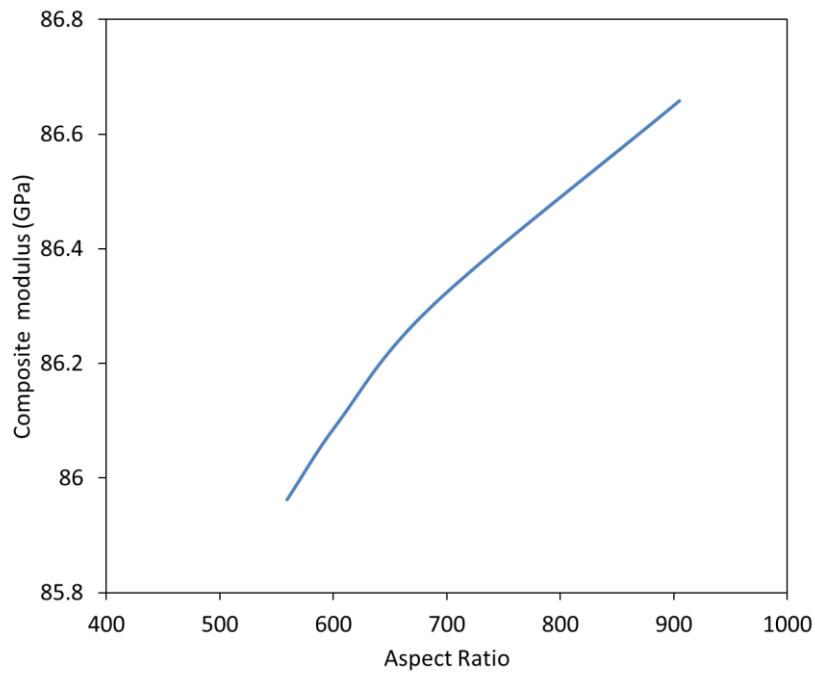


Figure 93: Effect of varied aspect ratio via ball milling on composite modulus for glass flakes / Epoxy - GF 100nm M at 60% wt.

Polyethylene matrix

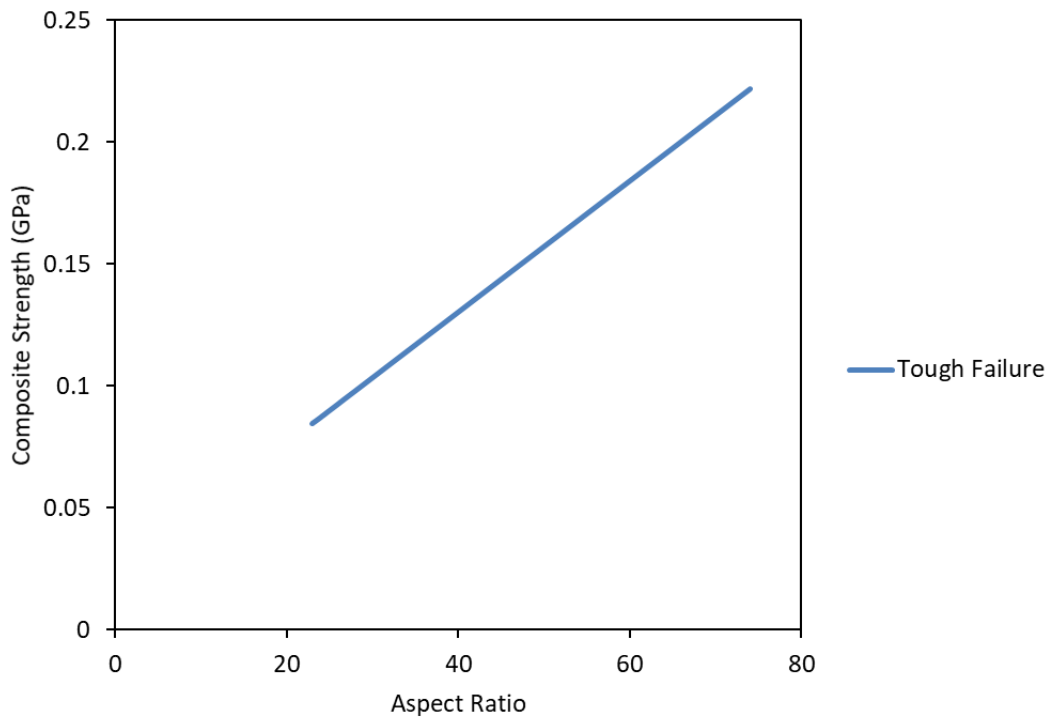


Figure 94: Effect of varied aspect ratio on composite strength of glass flakes / Polyethylene - GF 0.8 - 1.3 μ m at 60% wt.

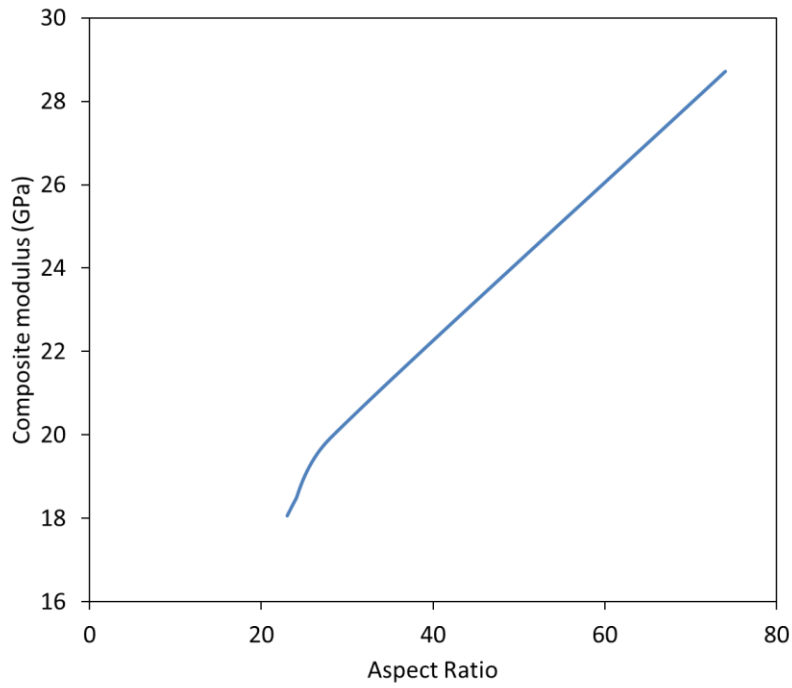


Figure 95: Effect of varied aspect ratio on composite modulus of glass flakes / Polyethylene - GF 0.8 - 1.3µm at 60% wt.

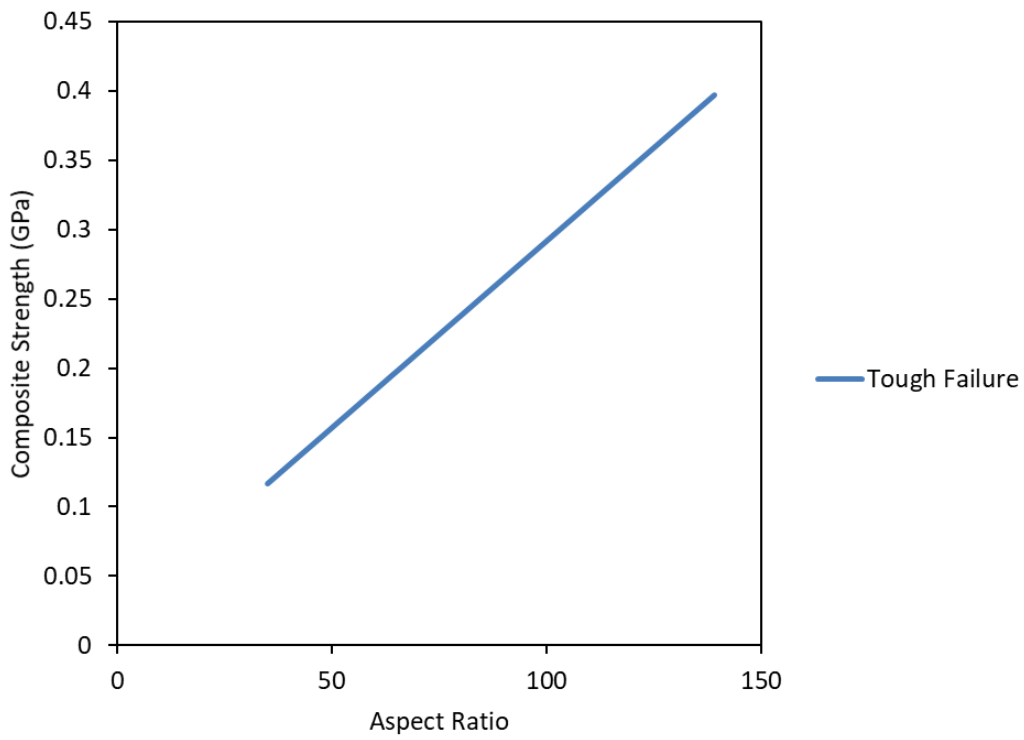


Figure 96: Effect of varied aspect ratio on composite strength of glass flakes / Polyethylene - GF 850nm M at 60% wt.

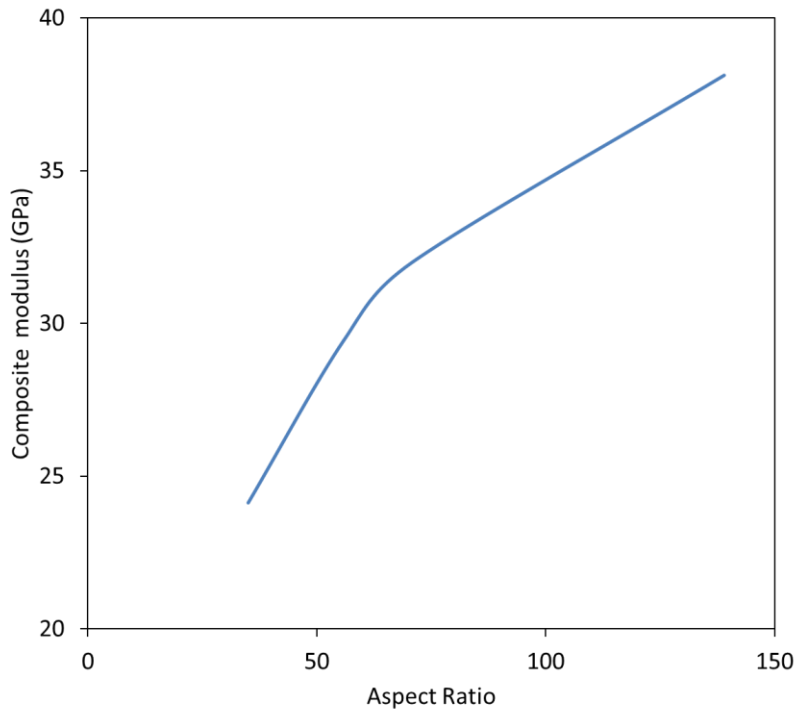


Figure 97: Effect of varied aspect ratio on composite modulus of glass flakes / Polyethylene - 850nm M at 60% wt.

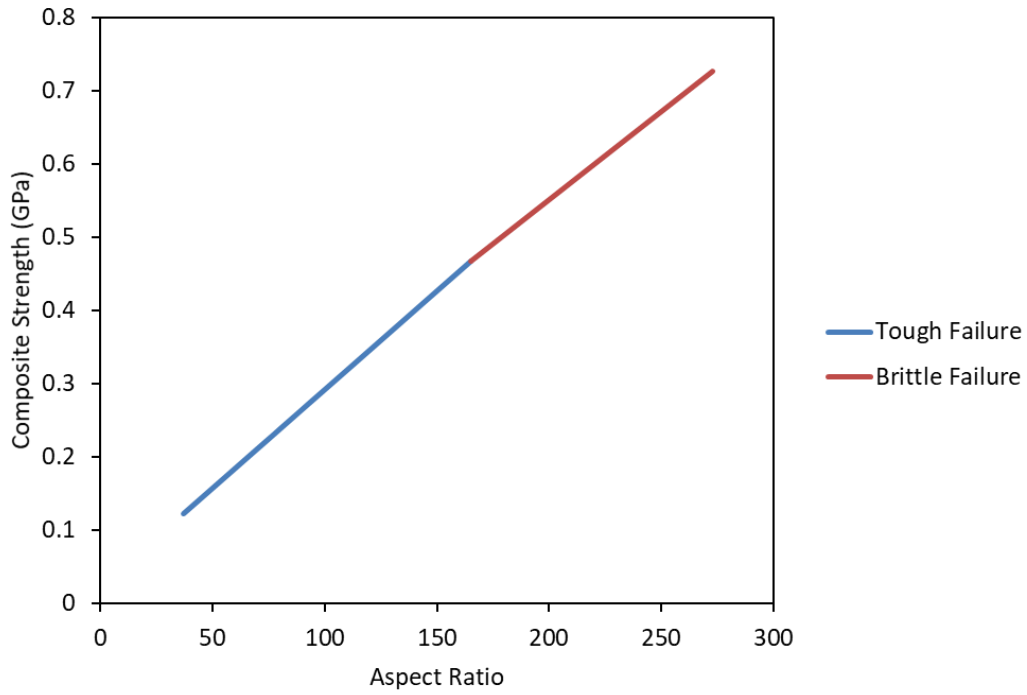


Figure 98: Effect of varied aspect ratio on composite strength of glass flakes / Polyethylene - GF 850nm UM at 60% wt.

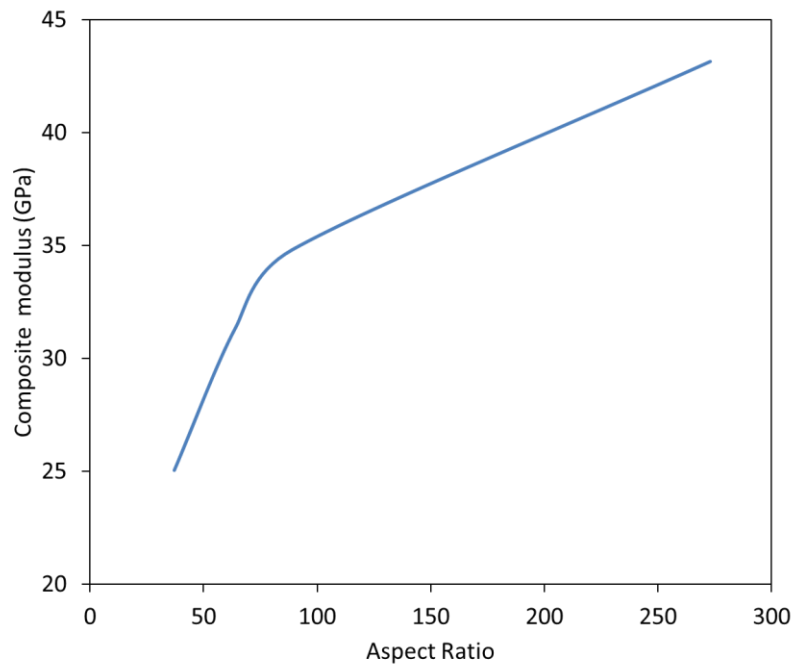


Figure 99: Effect of varied aspect ratio on composite modulus of glass flakes / Polyethylene - 850nm UM at 60% wt.

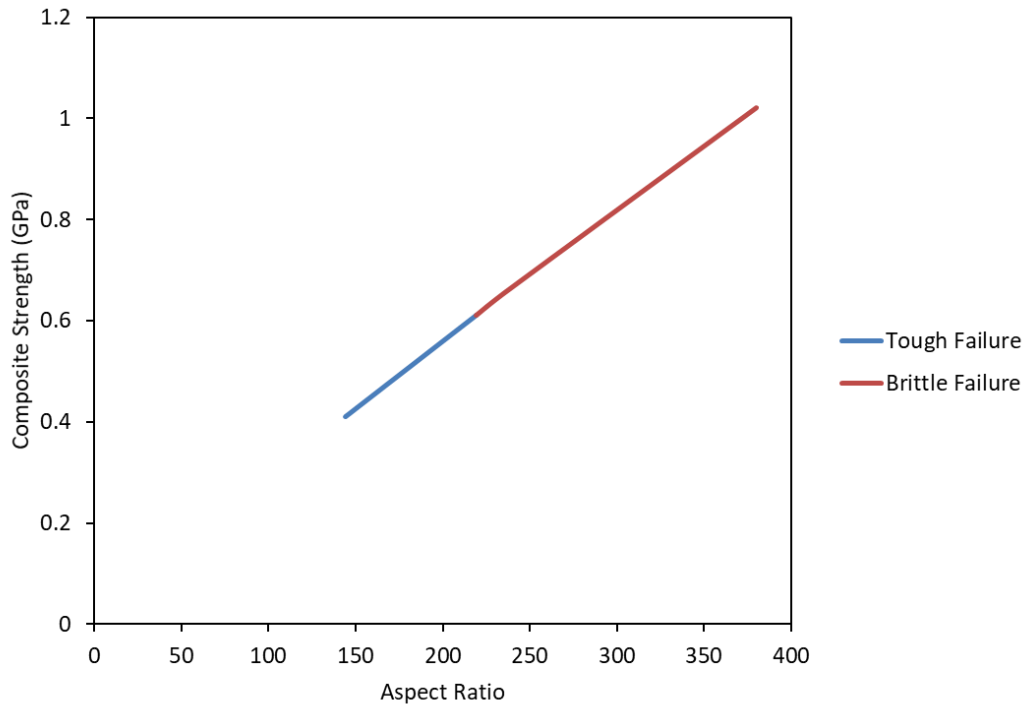


Figure 100: Effect of varied aspect ratio on composite strength of glass flakes / Polyethylene - GF 350nm UM at 60% wt.

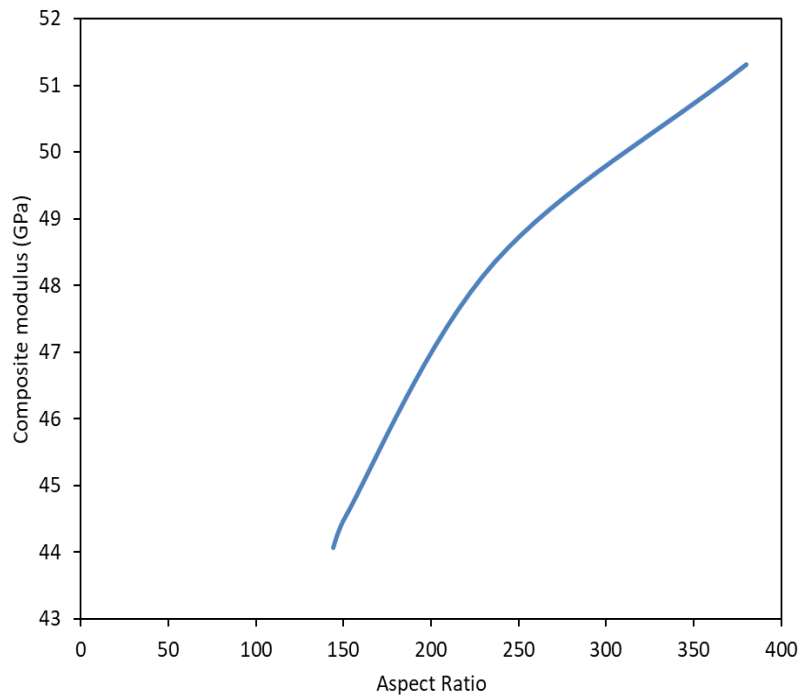


Figure 101: Effect of varied aspect ratio on composite modulus of glass flakes / Polyethylene - 350nm UM at 60% wt.

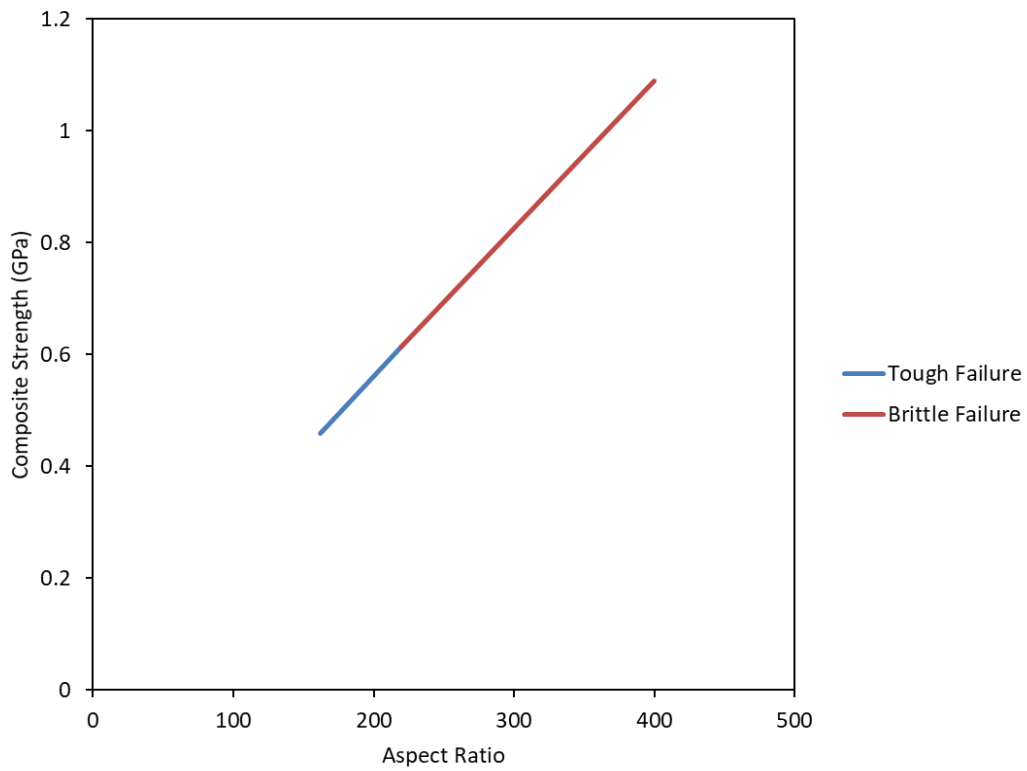


Figure 102: Effect of varied aspect ratio on composite strength of glass flakes / Polyethylene - GF 350nm M at 60% wt.

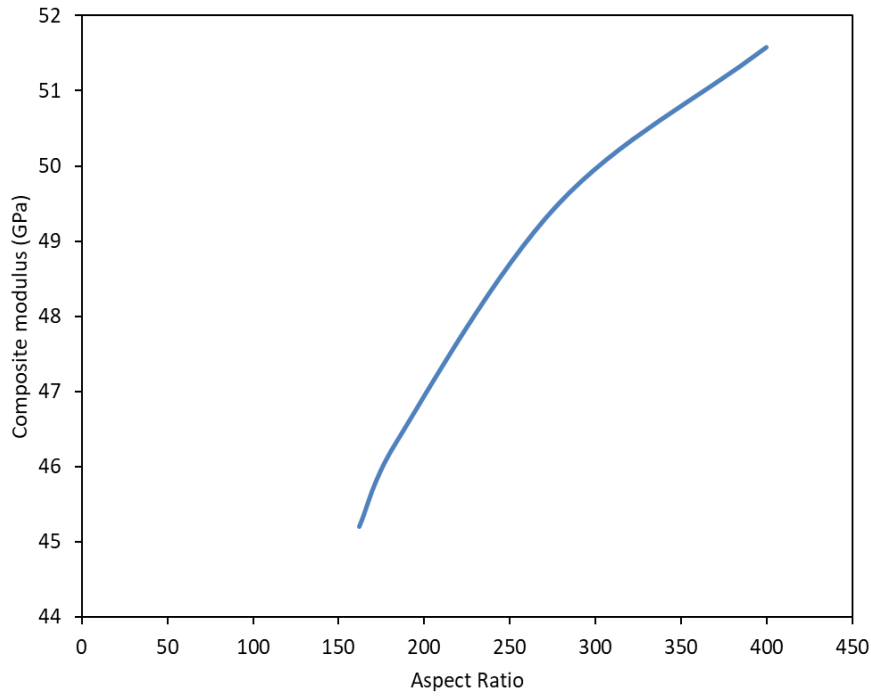


Figure 103: Effect of varied aspect ratio on composite modulus of glass flakes / Polyethylene - 350nm M at 60% wt.

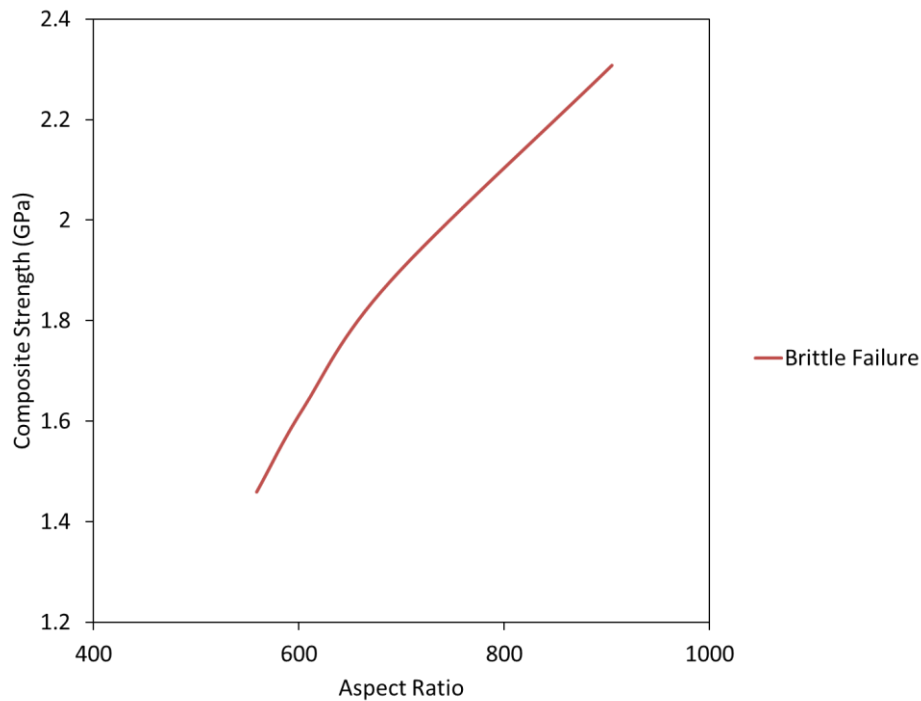


Figure 104: Effect of varied aspect ratio on composite strength of glass flakes / Polyethylene - GF 100nm M at 60% wt.

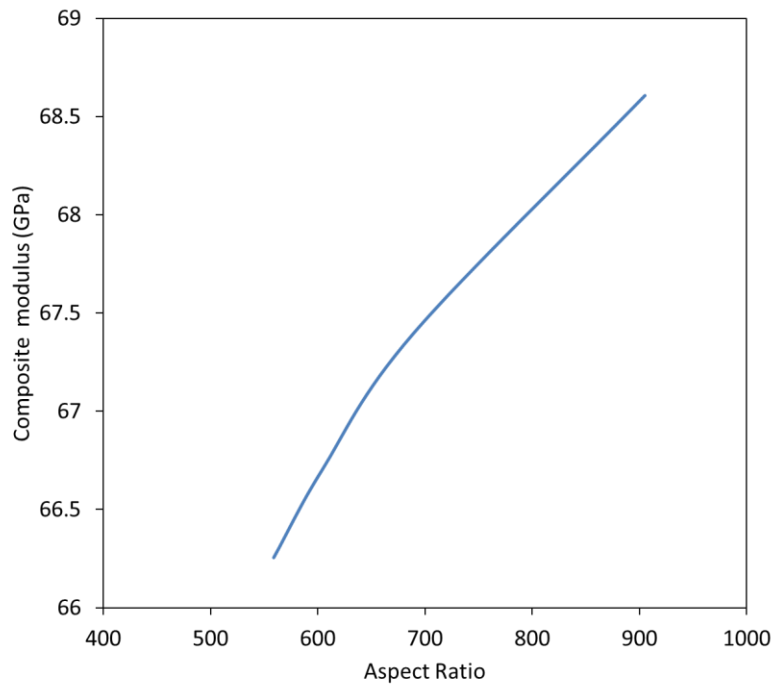


Figure 105: Effect of varied aspect ratio on composite modulus of glass flakes / Polyethylene - 100nm M at 60% wt.

While the interfacial shear strength is maintained for each matrix system as well as strength and modulus at each glass flakes determined thickness, the aspect ratio changes due to ball-milling. With individual glass flakes broken down, the smaller aspect ratio exhibits lower composite strength and modulus. However, the range of obtainable composite strength and modulus increases as the glass flakes gets thinner for all the matrices. Though, these thinner glass flakes exhibit a brittle failure with their matrix system, unlike the thick glass flakes. This is because the thinner glass flakes aspect ratios are still high, which also depend on the matrix system interfacial shear strength, hence further breakdown required.

4.2.2.3 Determination of composite strength and modulus at critical aspect ratio for each glass flakes with different matrix system

With the ball milling process used to manoeuvre the glass flakes aspect ratio, causing a decrease in the composite material mechanical properties. Meanwhile, some of the glass flakes chopped down could provide tough failure while other glass flakes still need to be further chopped down as their aspect ratio is still high, hence yields brittle failure. It is apparent that there needs to be a balance between interfacial shear strength and reinforcement filler's aspect ratio, which is characterised by the fillers average length and thickness for each matrix system. Therefore, to design a composite material system with the trio mechanical properties maintained, mechanical properties at the critical aspect ratio of each glass flakes are investigated with each of the matrix systems at maximum interfacial shear strength. Composite strength and modulus respectively for each matrix system at each glass flakes' critical aspect ratio under tough fracture shown in Figure 106 and 107 for epoxy, Figure 108 and 109 for polypropylene, Figure 110 and 111 for Nylon-6 and Figure 112 and 113 for polyethylene.

Composite strength at critical aspect ratio for each glass matrix system

Epoxy matrix

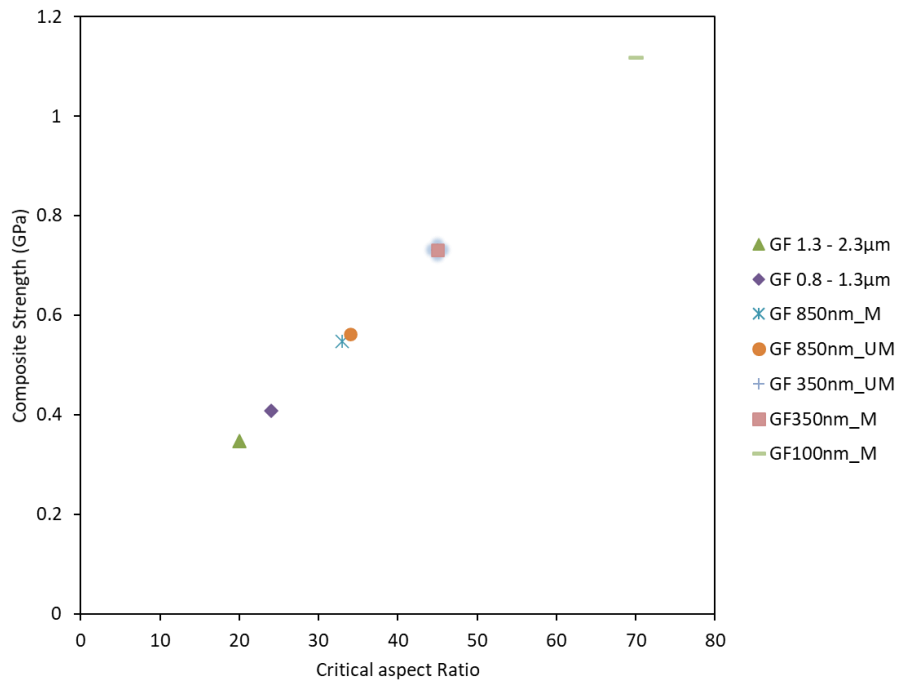


Figure 106: Composite strength at critical aspect ratio for different thickness of glass flakes at 60% wt. for Epoxy matrix

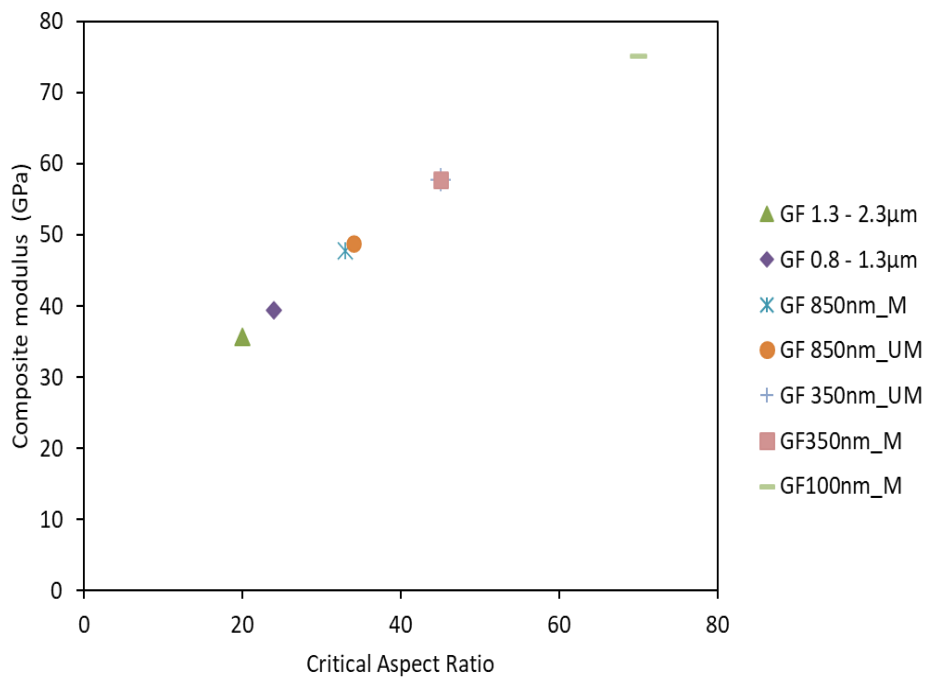


Figure 107: Composite modulus at critical aspect ratio for different thickness of glass flakes at 60% wt. for Epoxy matrix

Polypropylene matrix

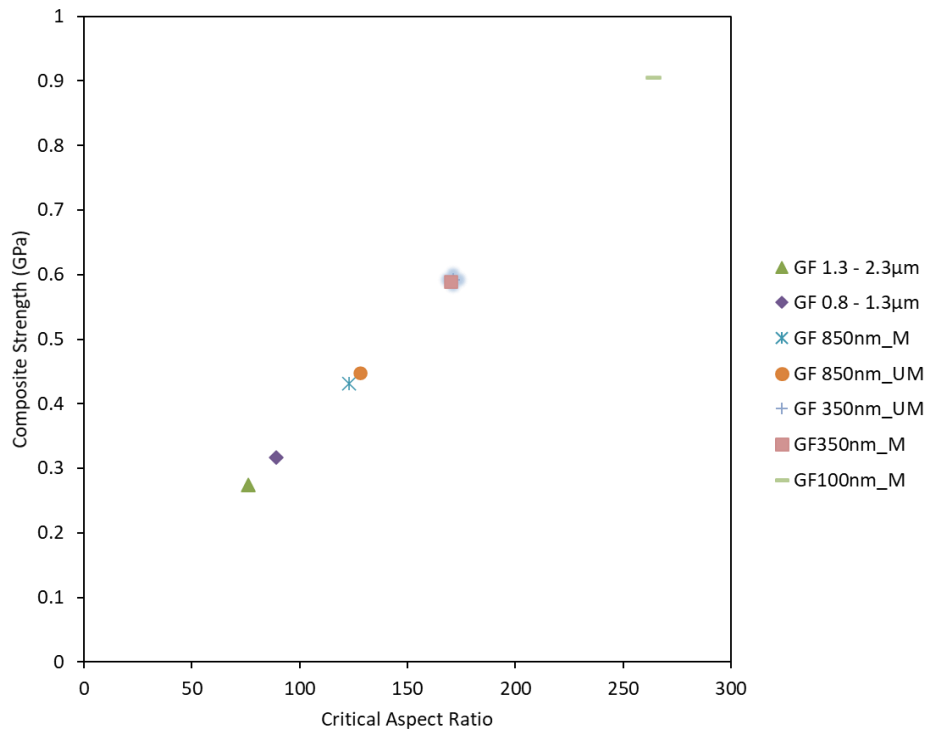


Figure 108: Composite strength at critical aspect ratio for different thickness of glass flakes at 60% wt. for Polypropylene matrix

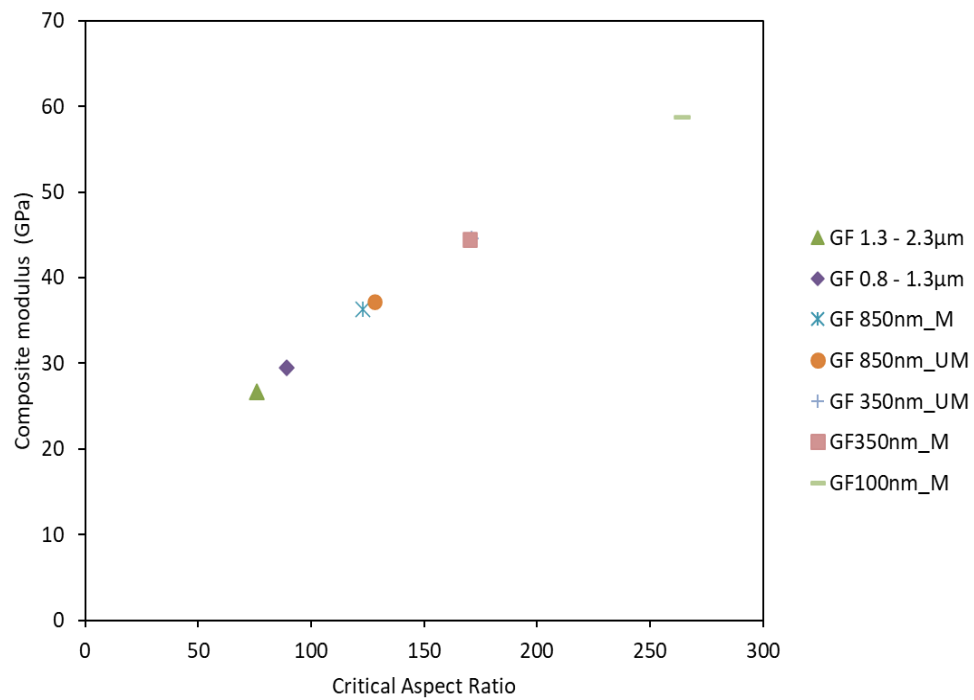


Figure 109: Composite modulus at critical aspect ratio for different thickness of glass flakes at 60% wt. for Polypropylene matrix

Nylon-6 matrix

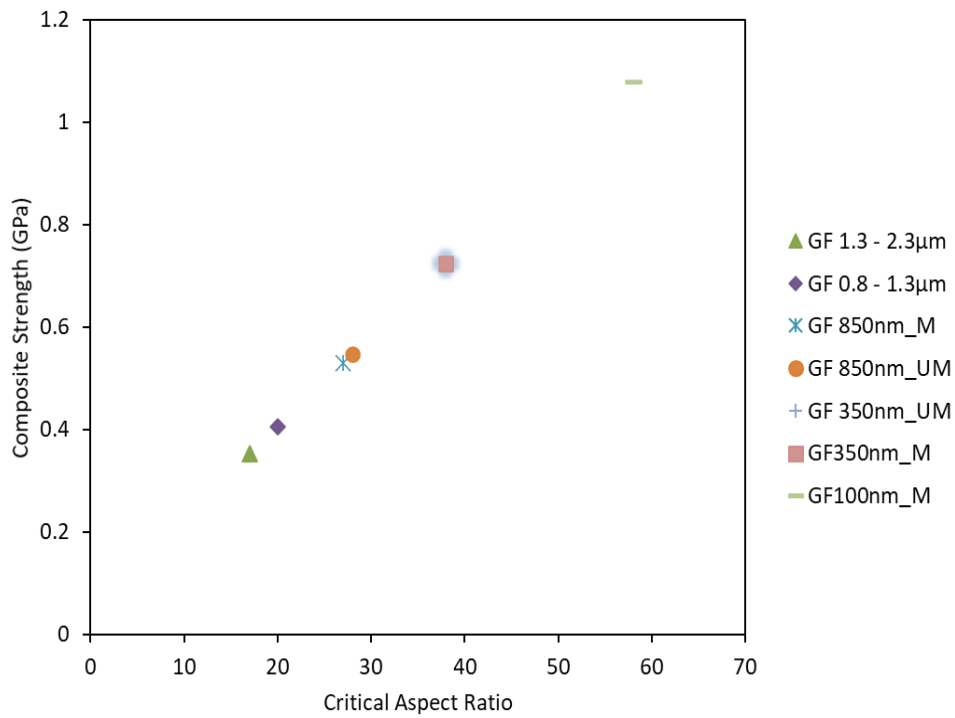


Figure 110: Composite strength at critical aspect ratio for different thickness of glass flakes at 60% wt. for Nylon 6 matrix

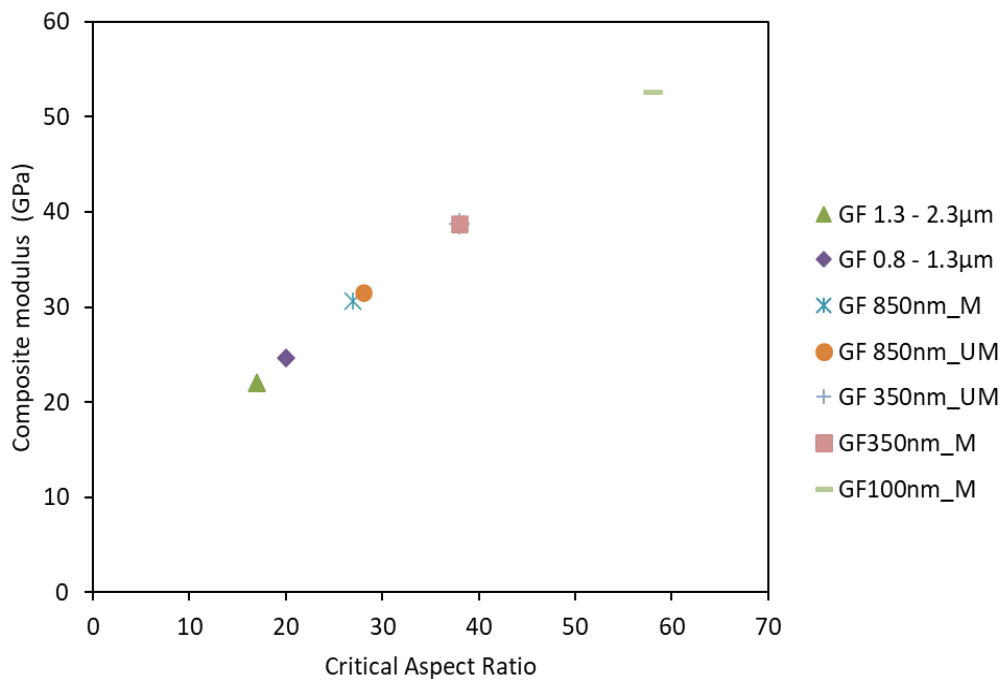


Figure 111: Composite modulus at critical aspect ratio for different thickness of glass flakes at 60% wt. for Nylon 6 matrix

Polyethylene matrix

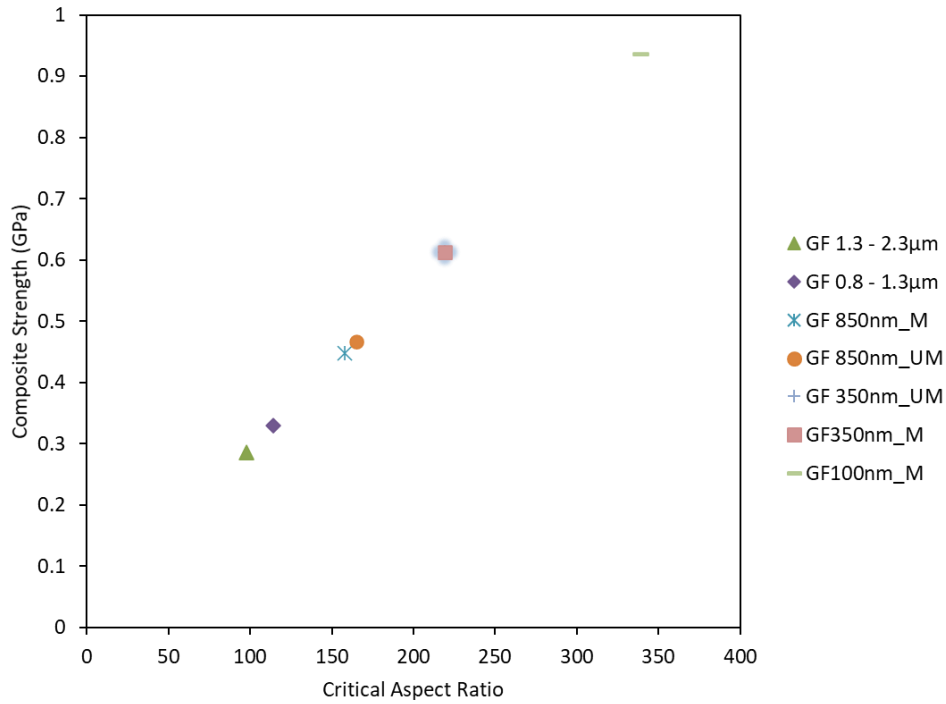


Figure 112: Composite strength at critical aspect ratio for different thickness of glass flakes at 60% wt. for Polyethylene matrix

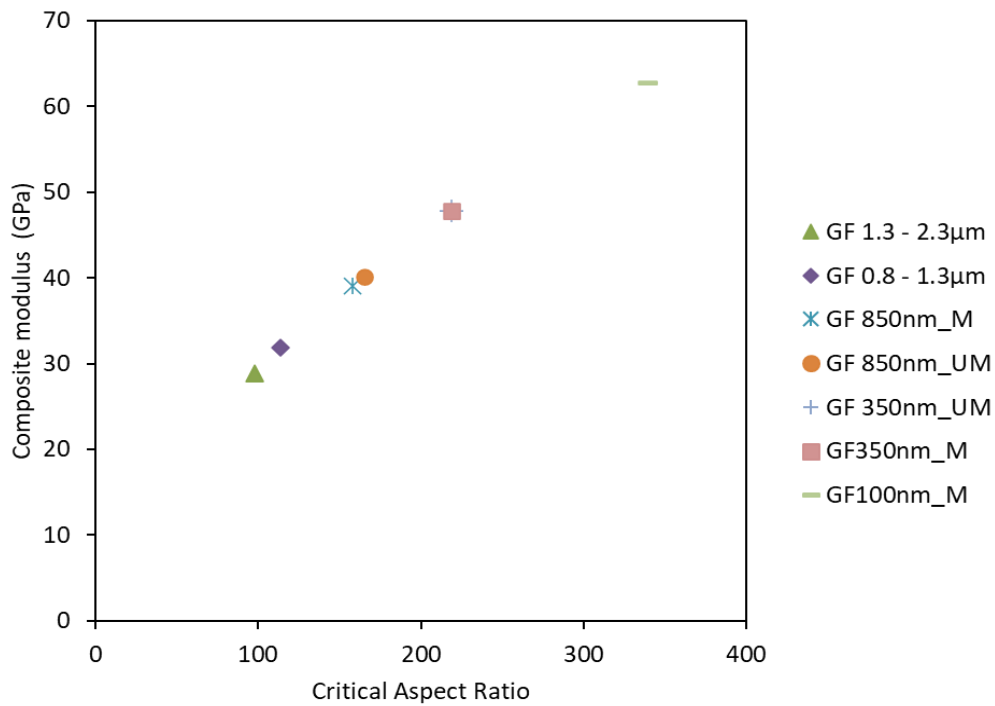


Figure 113: Composite modulus at critical aspect ratio for different thickness of glass flakes at 60% wt. for Polyethylene matrix

Composite strength and modulus plotted at each glass flakes critical aspect ratio for different matrices show that 100nm M glass flakes provide the best reinforcement at maximum interfacial shear strength for all the matrices. With composite material mechanical properties modelled at critical aspect ratio under tough fracture, Table 21 - 24 compares the composite mechanical properties for each glass flakes at their measured aspect ratio (S) for each matrix system to their critical aspect ratio (S_c).

Table 21: Comparison of composite strength and modulus at average aspect ratio to critical aspect ratio for Epoxy matrix system

Glass Flakes	(S _c) at τ - Max	(S)	Type of Failure	At Average Aspect Ratio (S) Composite:		At Critical Aspect Ratio (S _c) Composite:		% Comparison of Critical Aspect Ratio to Average Aspect Ratio:	
				Strength (GPa)	Modulus (GPa)	Strength (GPa)	Modulus (GPa)	Strength (GPa)	Modulus (GPa)
2.3 - 3.3μm	20	9	Tough	0.18	29.13	0.35	35.75	-49	-19
0.8 - 1.3μm	24	74	Brittle	1.03	45.29	0.41	39.36	60	13
850nm Milled	33	139	Brittle	1.58	55.30	0.55	47.72	65	14
850nm Unmilled	34	273	Brittle	1.87	57.91	0.56	48.79	70	16
350nm Unmilled	45	380	Brittle	2.50	67.61	0.73	57.72	71	15
350nm Milled	45	400	Brittle	2.51	67.69	0.73	57.72	71	15
100nm Milled	70	905	Brittle	4.03	86.66	1.12	75.10	72	13

Table 22: Comparison of composite strength and modulus at average aspect ratio to critical aspect ratio for Polypropylene matrix system

Glass Flakes	(S_c) at τ - Max	(S)	Type of Failure	At Average Aspect Ratio (S) Composite:		At Critical Aspect Ratio (S_c) Composite:		% Comparison of Critical Aspect Ratio to Average Aspect Ratio:	
				Strength (GPa)	Modulus (GPa)	Strength (GPa)	Modulus (GPa)	Strength (GPa)	Modulus (GPa)
2.3 - 3.3 μ m	76	9	Tough	0.05	10.13	0.27	26.64	-82	-62
0.8 - 1.3 μ m	89	74	Tough	0.27	28.10	0.32	29.44	-16	-5
850nm Milled	123	139	Brittle	0.49	37.21	0.43	36.28	11	2
850nm Unmilled	128	273	Brittle	0.93	42.00	0.45	37.22	52	11
350nm Unmilled	170	380	Brittle	1.28	49.92	0.59	44.58	54	11
350nm Milled	170	400	Brittle	1.33	50.17	0.59	44.53	56	11
100nm Milled	264	905	Brittle	2.53	66.65	0.90	58.70	64	12

Table 23: Comparison of composite strength and modulus at average aspect ratio to critical aspect ratio for Nylon 6 matrix system

Glass Flakes	(S_c) at τ - Max	(S)	Type of Failure	At Average Aspect Ratio (S) Composite:		At Critical Aspect Ratio (S_c) Composite:		% Comparison of Critical Aspect Ratio to Average Aspect Ratio:	
				Strength (GPa)	Modulus (GPa)	Strength (GPa)	Modulus (GPa)	Strength (GPa)	Modulus (GPa)
2.3 - 3.3 μ m	17	9	Tough	0.21	16.06	0.35	21.99	-40	-27
0.8 - 1.3 μ m	20	74	Brittle	1.07	36.58	0.41	24.60	62	33
850nm Milled	27	139	Brittle	1.59	46.86	0.53	30.66	67	35
850nm Unmilled	28	273	Brittle	1.84	51.15	0.55	31.49	70	38
350nm Unmilled	38	380	Brittle	2.45	60.39	0.72	38.80	70	36
350nm Milled	38	400	Brittle	2.46	60.58	0.72	38.80	71	36
100nm Milled	58	905	Brittle	3.90	79.25	1.08	52.49	72	34

Table 24: Comparison of composite strength and modulus at average aspect ratio to critical aspect ratio for Polyethylene matrix system

Glass Flakes	(S_c) at τ - Max	(S)	Type of Failure	At Average Aspect Ratio (S) Composite:		At Critical Aspect Ratio (S_c) Composite:		% Comparison of Critical Aspect Ratio to Average Aspect Ratio:	
				Strength (GPa)	Modulus (GPa)	Strength (GPa)	Modulus (GPa)	Strength (GPa)	Modulus (GPa)
2.3 - 3.3 μ m	98	9	Tough	0.05	10.19	0.29	28.90	-83	-65
0.8 - 1.3 μ m	114	74	Tough	0.22	28.71	0.33	31.82	-33	-10
850nm Milled	158	139	Tough	0.40	38.12	0.45	39.07	-11	-2
850nm Unmilled	165	273	Brittle	0.73	43.15	0.47	40.09	36	7
350nm Unmilled	219	380	Brittle	1.02	51.31	0.61	47.78	40	7
350nm Milled	219	400	Brittle	1.09	51.57	0.61	47.78	44	7
100nm Milled	339	905	Brittle	2.31	68.61	0.94	62.62	59	9

Table 21 – 24 exhibited a similar trend for each matrix and indicated how composite strength and modulus change due to reinforcement filler’s aspect ratio and the type of failure compared to the composite tensile strength and modulus at the critical aspect ratio under tough fracture. While toughness is maintained at critical aspect ratio, thinner glass flakes result in a high reinforcement efficiency of the composite tensile strength and modulus better than thicker glass flakes. However, there is a compromise on tensile strength and modulus compared to the glass flakes at their measured aspect ratios. Meanwhile, when the aspect ratio is too short, i.e. 2.3 - 3.3 μ m glass flakes, the reinforcement filler does not effectively reinforce the composite material. Therefore, it is ideal that the reinforcement filler aspect

ratio is in proximity to the critical aspect ratio for sufficient strength and stiffness to be maintained with toughness.

4.2.3 Modelling analysis of fibre reinforced composites

4.2.3.1 Glass fibre

Modelling glass fibre reinforced composite material mechanical properties by considering E-glass fibre with $3\mu\text{m}$ diameter, involving short and long fibres at 60% wt. loading respectively. The glass fibre mechanical properties are determined using Equation 1 and 2. The glass fibre properties determined at $3\mu\text{m}$ diameter with a tensile strength of 2.86 GPa and tensile modulus of 99 GPa. While maximum interfacial shear strength from Table 7 for each of the matrix systems is applied. Short fibres are regarded as fibres less than 1mm in length [269]; hence the modelling analysis considers 0.5mm fibre length for short fibre (SF) and 3mm for long fibre (LF). Using Equation 8 and 11, Table 25 - 28 shows composite mechanical properties for each matrix systems determined for long and short fibres at their determined aspect ratio and critical aspect ratio under tough fracture. Also, comparing 100nm milled glass flakes composite mechanical properties at the critical aspect ratio under tough fracture values with long and short glass fibres.

Table 25: Comparison of composite material mechanical properties for glass fibre to glass flakes under tough fracture for Epoxy matrix

Glass Fibre at $3\mu\text{m}$ Diameter	(S_c) at τ - Max	(S)	Type of Failure	At Average Aspect Ratio (S) Composite:		At Critical Aspect Ratio (S_c) Composite:		100nm Milled Glass Flakes at Critical Aspect Ratio ($S_c = 70$):	
				Strength (GPa)	Modulus (GPa)	Strength (GPa)	Modulus (GPa)	Strength (GPa)	Modulus (GPa)
SF: 0.5mm	20	167	Brittle	1.10	42.92	0.34	35.09	1.12	75.10
LF: 3mm		1000	Brittle	1.22	44.07				

Table 26: Comparison of composite material mechanical properties for glass fibre to glass flakes under tough fracture for Polypropylene matrix

Glass Fibre at 3µm Diameter	(S _c) at τ - Max	(S)	Type of Failure	At Average Aspect Ratio (S) Composite:		At Critical Aspect Ratio (S _c) Composite:		100nm Milled Glass Flakes at Critical Aspect Ratio (S _c = 264):	
				Strength (GPa)	Modulus (GPa)	Strength (GPa)	Modulus (GPa)	Strength (GPa)	Modulus (GPa)
SF: 0.5mm	74	167	Brittle	0.57	30.32	0.27	26.05	0.90	58.70
LF: 3mm		1000	Brittle	0.94	34.09				

Table 27: Comparison of composite material mechanical properties for glass fibre to glass flakes under tough fracture for Nylon 6 matrix

Glass Fibre at 3µm Diameter	(S _c) at τ - Max	(S)	Type of Failure	At Average Aspect Ratio (S) Composite:		At Critical Aspect Ratio (S _c) Composite:		100nm Milled Glass Flakes at Critical Aspect Ratio (S _c = 58):	
				Strength (GPa)	Modulus (GPa)	Strength (GPa)	Modulus (GPa)	Strength (GPa)	Modulus (GPa)
SF: 0.5mm	16	167	Brittle	1.09	37.24	0.34	21.35	1.08	52.49
LF: 3mm		1000	Brittle	1.18	40.12				

Table 28: Comparison of composite material mechanical properties for glass fibre to glass flakes under tough fracture for polyethylene matrix

Glass Fibre at 3µm Diameter	(S _c) at τ - Max	(S)	Type of Failure	At Average Aspect Ratio (S) Composite:		At Critical Aspect Ratio (S _c) Composite:		100nm Milled Glass Flakes at Critical Aspect Ratio (S _c = 339):	
				Strength (GPa)	Modulus (GPa)	Strength (GPa)	Modulus (GPa)	Strength (GPa)	Modulus (GPa)
SF: 0.5mm	95	167	Brittle	0.46	31.11	0.28	28.24	0.94	62.62
LF: 3mm		1000	Brittle	0.95	35.09				

For each matrix system, both the short and long fibre yields brittle failure considering that their aspect ratio is higher than the critical aspect ratio for each matrix system. However, comparing composite material strength and modulus to 100nm milled glass flakes at the critical aspect ratio for each matrix system. It is evident that 100nm milled glass flakes at critical aspect ratio is capable of yielding composite material with high strength and modulus with toughness maintained. The 100nm glass flakes compete with long glass fibre with higher aspect ratio in term of tensile strength and also has more than 50% improvement regarding stiffness for each matrix system, while toughness is maintained as the glass flakes mechanical properties are determined at critical aspect ratio for maximum interfacial shear strength.

4.2.3.2 Carbon fibre

Like glass fibre, carbon fibre modelled and compared with glass flakes for the four matrices. Mechanical properties for carbon fibre determined using Equation 3 and 4 at 7 μ m diameter carbon fibre with 4.15 GPa and 251 GPa for tensile strength and modulus, respectively. The modelling analysis considers short and long fibres with 0.5mm and 3mm lengths respectively at 60% wt. filler loading converted into equivalent volume fraction using Equation 15, density value taken as 1.8 g/cm³ [270]. Table 8 detailed the interfacial shear strength applied for each matrix system at maximum value, while Table 6 details the mechanical properties for various polymer applied for modelling analysis. Using Equation 8 and 11; composite mechanical properties for carbon fibre with each of the matrix system is detailed in Table 29 - 32 for long and short fibres at their determined aspect ratio and critical aspect ratio for tough fracture. Obtained values are compared with 100nm milled glass flakes composite mechanical properties at the critical aspect ratio under tough fracture with each matrix system.

Table 29: Comparison of composite material mechanical properties for carbon fibre to glass flakes under tough fracture for Epoxy matrix

Carbon Fibre at 7µm Diameter	(S _c) at τ - Max	(S)	Type of Failure	At Average Aspect Ratio (S) Composite:		At Critical Aspect Ratio (S _c) Composite:		100nm Milled Glass Flakes at Critical Aspect Ratio (S _c = 70):	
				Strength (GPa)	Modulus (GPa)	Strength (GPa)	Modulus (GPa)	Strength (GPa)	Modulus (GPa)
SF: 0.5mm	26	71	Brittle	1.38	110.41	0.56	87.90	1.12	75.10
LF: 3mm		429		2.02	126.34				

Table 30: Comparison of composite material mechanical properties for carbon fibre to glass flakes under tough fracture for Polypropylene matrix

Carbon Fibre at 7µm Diameter	(S _c) at τ - Max	(S)	Type of Failure	At Average Aspect Ratio (S) Composite:		At Critical Aspect Ratio (S _c) Composite:		100nm Milled Glass Flakes at Critical Aspect Ratio (S _c = 264):	
				Strength (GPa)	Modulus (GPa)	Strength (GPa)	Modulus (GPa)	Strength (GPa)	Modulus (GPa)
SF: 0.5mm	59	71	Brittle	0.34	60.02	0.463	54.80	0.90	58.70
LF: 3mm		429		1.56	95.47				

Table 31: Comparison of composite material mechanical properties for carbon fibre to glass flakes under tough fracture for Nylon 6 matrix

Carbon Fibre at 7µm Diameter	(S _c) at τ - Max	(S)	Type of Failure	At Average Aspect Ratio (S) Composite:		At Critical Aspect Ratio (S _c) Composite:		100nm Milled Glass Flakes at Critical Aspect Ratio (S _c = 58):	
				Strength (GPa)	Modulus (GPa)	Strength (GPa)	Modulus (GPa)	Strength (GPa)	Modulus (GPa)
SF: 0.5mm	31	71	Brittle	1.21	82.71	0.55	57.90	1.08	52.49
LF: 3mm		429		1.93	114.10				

Table 32: Comparison of composite material mechanical properties for carbon fibre to glass flakes under tough fracture for Polyethylene matrix

Carbon Fibre at 7µm Diameter	(S _c) at τ - Max	(S)	Type of Failure	At Average Aspect Ratio (S) Composite:		At Critical Aspect Ratio (S _c) Composite:		100nm Milled Glass Flakes at Critical Aspect Ratio (S _c = 339):	
				Strength (GPa)	Modulus (GPa)	Strength (GPa)	Modulus (GPa)	Strength (GPa)	Modulus (GPa)
SF: 0.5mm		71	Brittle	0.98	61.02				
	34					0.48	41.21	0.94	62.62
LF: 3mm		429	Brittle	1.71	97.80				

Table 29 – 32 shows that for each of the matrix systems reinforced with carbon fibre, both short and long fibres, the composite material would fail in a brittle manner because the fibres aspect ratio are higher than the critical aspect ratio. Compared with 100nm milled glass flakes at critical aspect ratio for all the matrix systems; long carbon fibre seems to perform slightly better particularly with strength but not so much with modulus. In comparison, short carbon fibre does not make much difference in terms of strength and modulus. However, for composite material with sufficient strength, stiffness and toughness, the 100nm milled glass flakes provide good strength and stiffness while toughness is maintained better than carbon fibre when compared at critical aspect ratio.

4.2.3.3 Analysis of mechanical properties of fibre reinforced composite systems

The modelling analysis shows that carbon fibre performs better than the glass fibre and similarly epoxy and nylon 6 matrices yield better performance compared to polypropylene and polyethylene. This is considered to be the cumulative attribute of the constituent materials mechanical properties that makes up the composite material system despite same filler aspect ratio is considered for different matrices, and also glass fibre composite material system having higher aspect ratio compared to carbon fibre composite material system.

Furthermore, reinforcement at critical filler's aspect ratio demonstrate the importance of good interfacial adhesion. Considering that matrices like polypropylene and polyethylene have high critical aspect ratio than epoxy and nylon 6 yet performs less when compared to these matrices, with both glass and carbon fibre composite reinforcement material systems respectively, being that epoxy and nylon 6 exhibit higher value of IFSS with carbon and glass fibres compared to polyethylene and polypropylene (Figure 23 and 24). Meanwhile, Table 33 shows mechanical properties of some composite material systems reported via literature. Almost similar trend reported for composite material systems reported in Table 33 with failure strain decreasing with increase in filler volume fraction which have compromising effect on toughness. Comparing composite materials mechanical properties in Table 33 with results obtained via modelling analysis for glass and carbon fibre reinforced composite systems respectively. It is evident that values predicted for carbon fibre reinforced composite systems are relatively high, however, glass fibre reinforced composite systems are relatable in values to composite systems reported in Table 33. Therefore, for glass flakes that is relatively close to glass fibre in characteristics, it is plausible to consider mechanical properties obtained for glass flakes to be in proximity to experimental values. Thus, considering 100nm milled glass flake at filler's critical aspect ratio which is predicted to fail under tough failure having better strength and stiffness (modulus) compared to both glass and carbon fibres. Thus, gives an indication of how feasible it is to have composite material with mechanical properties improved, compared to carbon and glass fibres which tends to fail in brittle manner due to their filler aspect ratio that is too high and when the filler aspect ratio is in proximity to critical aspect ratio strength and stiffness decreases. With reinforcement filler such as 100nm milled (M) glass flakes at critical aspect ratio, provide polymers like polyethylene and polypropylene which are commodity polymer readily available but having low strength and

stiffness to be put to use for composite material applications as improved mechanical properties are feasible to be obtained and also considering that these polymers are recyclable makes it more environmentally friendly unlike polymer like epoxy.

Table 33: Mechanical properties reported for some fibre reinforced composite materials

Reinforcement filler	Matrix	Composite strength (GPa)	Composite modulus (GPa)	Volume fraction (v_f)	Ref
Carbon fibre	Polypropylene	0.101	28.77	0.45	[271]
Carbon fibre	Epoxy	0.32	36	0.5	[272]
Glass fibre	Polypropylene	0.89	43.6	0.58	[112]
Glass fibre	Polypropylene	0.068	14	0.4	[273]
Glass fibre	Nylon 6	1.11	40.8	0.52	[274]
Carbon fibre	Polypropylene	0.35	22	0.35	[275]
Carbon fibre	Nylon 6	0.4	35	0.5	[276]
Carbon fibre	Nylon 6	0.41	50.2	0.6	[277]
Glass fibre	Nylon 6	0.68	37.9	0.53	[278]
Glass fibre	Epoxy	0.6	30	0.45	[279]
Glass fibre	Epoxy	0.85	37.5	0.5	[280]
Carbon fibre	Epoxy	0.7	40.53	0.6	[281]
Carbon fibre	Polyethylene	0.062	2.06	0.18	[282]
Glass fibre	Polyethylene	0.072	6.76	0.14	[283]
Carbon fibre	Polyethylene	0.054	17.1	0.26	[283]
Glass fibre	Polyethylene	0.065	8.87	0.2	[284]

4.2.4 Modelling analysis of composites reinforced with nanofillers

Reinforcement of specified matrices with different nanofillers modelled includes graphene, single-wall carbon nanotube (SWCNT) and montmorillonite (MMT) nanoclay. Modelling graphene and SWCNT; interfacial shear strength for carbon fibre (Table 8) applied, considering that the morphological structure of carbon fibre is similar to graphene and SWCNT [285]. Correspondingly, montmorillonite clays are composed of silicate, similar to glass [286]; therefore, interfacial shear strength for glass fibre (Table 7) used for modelling analysis. Mechanical properties for each nanofiller detailed in Table 5 and true density (g/cm^3) for graphene [287] [288], SWNT [289] [290] [291] and MMT [292] [293] [294] respectively taken as 2.3, 1.3, and 2.5. Using Equation 8 and 11; composite material mechanical properties determined at maximum interfacial shear strength and at critical aspect ratio for each matrix system reinforced with each nanofiller and compared with 100nm milled glass flakes. Table 34 – 37 shows mechanical properties for the nanofillers with various matrices modelled at 60% wt. filler loading converted to equivalent volume fraction (Equation 15).

Table 34: Composite material mechanical properties of Epoxy with different nanofillers

Type of Nano Filler	τ - Max	(S_c) at τ - Max	Type of Failure	At Critical Aspect Ratio (S_c) Composite:		100nm Milled Glass Flakes at Critical Aspect Ratio ($S_c = 70$):	
				Strength (GPa)	Modulus (GPa)	Strength (GPa)	Modulus (GPa)
MMT	73	21	Tough	0.36	49.86		
SWCNT	80	188	Tough	4.46	479.03	1.12	75.10
Graphene	80	813	Tough	14.63	420.41		

Table 35: Composite material mechanical properties of Polypropylene with different nanofillers

Type of Nano Filler	τ - Max	(S_c) at τ - Max	Type of Failure	At Critical Aspect Ratio (S_c) Composite:		100nm Milled Glass Flakes at Critical Aspect Ratio ($S_c = 264$):	
				Strength (GPa)	Modulus (GPa)	Strength (GPa)	Modulus (GPa)
MMT	19.4	77	Tough	0.28	37.23		
SWCNT	35.4	424	Tough	3.85	346.43	0.90	58.70
Graphene	35.4	1836	Tough	12.08	325.68		

Table 36: Composite material mechanical properties of Nylon 6 with different nanofillers

Type of Nano Filler	τ - Max	(S_c) at τ - Max	Type of Failure	At Critical Aspect Ratio (S_c) Composite:		100nm Milled Glass Flakes at Critical Aspect Ratio ($S_c = 58$):	
				Strength (GPa)	Modulus (GPa)	Strength (GPa)	Modulus (GPa)
MMT	88	17	Tough	0.36	27.34		
SWCNT	68	221	Tough	4.31	368.44	1.08	52.49
Graphene	68	956	Tough	13.98	367.28		

Table 37: Composite material mechanical properties of Polyethylene with different nanofillers

Type of Nano Filler	τ - Max	(S_c) at τ - Max	Type of Failure	At Critical Aspect Ratio (S_c) Composite:		100nm Milled Glass Flakes at Critical Aspect Ratio ($S_c = 339$):	
				Strength (GPa)	Modulus (GPa)	Strength (GPa)	Modulus (GPa)
MMT	15.1	99	Tough	0.29	41.18		
SWCNT	61	246	Tough	3.94	285.21	0.94	62.62
Graphene	61	1066	Tough	12.45	306.47		

Modelling shows that for each matrix system reinforced with nano reinforcement filler, similar trend is exhibited for fibre reinforcement with epoxy and nylon 6 yielding better mechanical properties compared to polypropylene and polyethylene which is due to the influence of the constituent materials mechanical properties. Composite material strength and modulus determined for each nanofiller with different matrices, MMT nanoclay provides least effective reinforcement. Composite material with graphene provides better strength reinforcement for all the matrices than SWCNT, while for modulus; SWCNT is slightly higher for all the matrices except for polyethylene matrix which is considered to be the effect of reduced aspect ratio when compared to matrix like polypropylene and having lower modulus value for the neat matrix compared to epoxy and nylon 6. Graphene strength is higher than SWCNT while modulus is the same for both nanofillers (Table 5) and likewise, the interfacial shear strength applied. Also, the aspect ratio is higher for graphene for all the matrices than SWCNT and the expectation is that graphene will yield higher modulus than SWCNT as shown by strength prediction, but the modelling shows otherwise. With detailed analysis, the rationale for such observation shows that the equivalent volume fraction at 60% wt. filler loading is higher for SWCNT than graphene, which is dependent on the nanofillers densities. Based on the conceptual idea of SWCNT regarded as folded graphene sheet, nanofiller density ascertained how it influences the composite material properties as a function of volume fraction. For instance, SWCNT with outer diameter 2.04nm and inner diameter 1.36nm [230] having length 2nm, compared with graphene of about the same length with a thickness of 0.335nm [229], thus having dimensions $(\pi \times 2.04\text{nm}) \times 2\text{nm} \times 0.335\text{nm}$. Also, for MMT nanoclay with a thickness 0.615nm [295] and similar dimensions, thus a platelet with dimensions $(\pi \times 2.04\text{nm}) \times 2\text{nm} \times 0.615\text{nm}$. Using Equation 16 and the true density value for

each nanofiller, each filler's volume is calculated to determine the corresponding mass as follows.

$$\text{Equation 16: } m = \rho \times V$$

Where m , ρ and V is the mass, true density and volume respectively.

$$\begin{aligned} \text{Graphene: } m &= 2.3 \frac{g}{cm^3} \times (\pi \times 2.04 \times 2 \times 0.335) nm^3 \times \left(\frac{1 cm}{10^7 nm} \right)^3 \\ &= 2.3 \frac{g}{cm^3} \times 4.29 nm^3 \times \frac{1 cm^3}{10^{21} nm^3} \\ &= 9.88 \times 10^{-21} g \end{aligned}$$

$$\begin{aligned} \text{SWCNT: } m &= 1.3 \frac{g}{cm^3} \times \left(\frac{\pi(2.04^2 - 1.36^2) nm^2}{4} \times 2 nm \right) \times \left(\frac{1 cm}{10^7 nm} \right)^3 \\ &= 1.3 \frac{g}{cm^3} \times 3.63 nm^3 \times \frac{cm^3}{10^{21} nm^3} \\ &= 4.72 \times 10^{-21} g \end{aligned}$$

$$\begin{aligned} \text{MMT nanoclay: } m &= 2.5 \frac{g}{cm^3} \times (\pi \times 2.04 \times 2 \times 0.615) nm^3 \times \left(\frac{1 cm}{10^7 nm} \right)^3 \\ &= 2.5 \frac{g}{cm^3} \times 7.88 nm^3 \times \frac{1 cm^3}{10^{21} nm^3} \\ &= 19.71 \times 10^{-21} g \end{aligned}$$

Above calculation shows that graphene and SWCNT mass differs with MMT being the most dense filler while SWCNT is the least dense. It therefore indicates that for 60% wt. more filler of SWCNT is required [296], [297]. Thus, resulting in SWCNT yielding higher equivalent volume fraction of 60% wt. loading compared to graphene and MMT. While composite material mechanical properties are a function of volume fraction, hence the reason SWCNT composite material for modulus higher than graphene. Meanwhile, unlike modulus, which is the same

for both SWCNT and graphene, graphene strength value is higher than SWCNT. Therefore, composite material strength modelled with graphene is higher than SWCNT despite that the equivalent volume fraction for graphene is lower than SWCNT.

The modelling analysis has been computed at an equivalent volume fraction of 60% wt. for all analysis to have equal filler loading. However, for nanofillers which has a relatively comparable density to their fibre counterparts. Figure 114 shows equivalent volume fraction plotted against percentage weight loading for each reinforcement filler for epoxy matrix using the epoxy matrix as an example as each matrix exhibited a similar trend. At 60% wt. loading, SWCNT exhibit the highest equivalent volume fraction followed by carbon fibre then graphene while MMT nanoclay and glass related fillers (glass fibre and flakes) are relatively equal. This therefore shows that composite materials reinforcement filler volume fraction is influenced by the filler’s density which have an effect on the ultimate composite material mechanical properties.

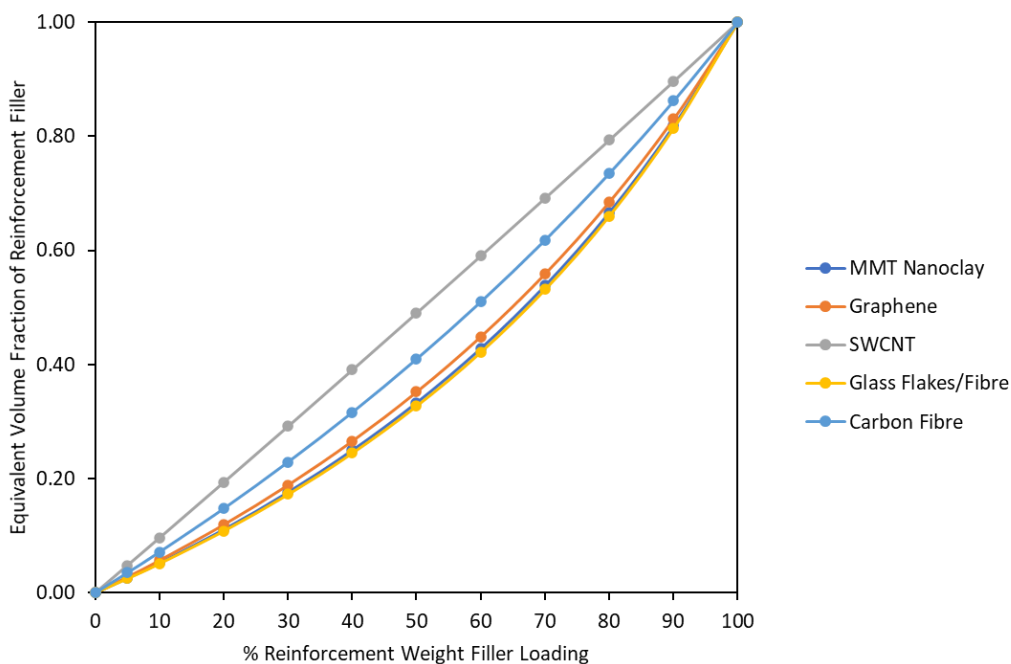


Figure 114: Equivalent volume fraction plotted against percentage weight load for different reinforcement - Epoxy

The modelling analysis for the nanofillers are computed at critical aspect ratio, meanwhile nano fillers aspect ratios are however higher than the critical aspect ratio considering that their lengths are often longer than critical length [145], [298], [299]. Therefore, fabrication of composite material with nanofiller at length above the critical length will often result in brittle failure. Thereby making it difficult to maintain toughness though strength and stiffness are enhanced with such nanofillers. While Figure 114 shows that for the same percentage filler loading for both nanofillers and fibres; the equivalent volume fraction could be fairly close. However, taking advantage of higher value of strength and modulus associated with nano sized filler provides greater potential to obtain a composite material with improved mechanical properties, which is a plausible reason for nanofiller composite having improved mechanical properties at low filler loading. Similarly, with adequate fabrication process for higher filler loading to achieve uniformly distributed filler within a composite material system, nanofillers have the potential to provide considerable improvement with regards to the composite material mechanical properties.

Whilst various research has investigated reinforcement of matrices with nano sized filler (Table 38) and have been able to establish that nano fillers provide better reinforcement efficiency at lower volume fraction compared to fibre reinforcement. However, reinforcement achieved is relatively low compared to fibre reinforcement at high volume fraction (Table 33), hence the need for nanocomposite to have high volume fraction [23]. Though better reinforcement often reported at these low volume fraction for nanocomposite, but reports has also shown that there could be a trade-off in terms of desired mechanical properties. For example, Zaman et al. [300] reported reinforcement of epoxy matrix with modified graphene platelet at 4% wt. which increases the neat matrix modulus from 2.69 to 3.27 GPa but the strength decreased from about 64 MPa to 54 MPa. Also, Salom et al. [301]

reported same observation as Zaman et al. for epoxy reinforced graphene platelet at 6% wt. with modulus increasing from 2.9 to 4 GPa but strength decreased from 65 to 48 MPa which is attributed to agglomeration effect within the composite system.

While comparative analysis shows that some of the reported nanocomposites in Table 38 have relatively low weight fraction compared to the modelling analysis, therefore, mechanical properties for the modelling analysis is expected to be higher. However, adopting adequate fabrication process of nanocomposites that allows for higher weight fraction to be achieved which replicates a typical nanocomposite system similar to the nanocomposite considered for the modelling analysis also examined, i.e. multi-walled nanocomposites. Bradford et al. [24] fabricated epoxy reinforced nanocomposite via their novel approach using aligned carbon nanotubes with length in millimetre range and weight fraction of 32% (equivalent volume fraction of 27%). While Bradford et al. reported nanocomposite with strength of about 400 MPa and modulus around 22 GPa, the nanocomposite exhibit decreases in strain not less than 50% with stress-strain curve replica of a brittle failure. Similarly, Cheng et al. [302] reported about fabricating bismaleimide resin reinforced with 60% wt. carbon nanotube having strength about 2.088 GPa and modulus 169 GPa. Also, Mora, Vilatela and Windle investigated reinforcement of epoxy with carbon nanotubes at 27% volume fraction to fabricate nanocomposite with strength 253 MPa and modulus 18.8 GPa, however, the strength and stiffness is accompanied with a decrease in failure strain [303]. Likewise, Wang et al. [304] reported fabrication of nylon nanocomposite with carbon nanotube at 15% volume fraction with strength of about 630 MPa and modulus 56 GPa. Nam et al. [305] reported fabrication of aligned multi-walled carbon nanotube/epoxy composite by stretching and pressing the carbon nanotubes. The nanocomposite which has about 63.4% volume fraction carbon nanotubes enhances the neat epoxy tensile strength at 780MPa and modulus 133.6GPa. Thus,

increasing the neat epoxy tensile strength and modulus at about 821% and 4042% respectively, however, the strain is significantly reduced by 88% which simply implies that high strength and modulus (stiffness) are achieved at the expense of toughness.

With cited research showing that having adequate improved process of fabricating carbon nanotube reinforced nanocomposite, by having the carbon nanotubes stretched, pressed, aligned with length 100,000 times the carbon nanotube diameter which are in mm range embedded within their matrix system [24] [303]. High strength and stiffness can be achieved yet toughness compromised considering that the aspect ratio is about 100,000, which is considerably high and above the critical aspect ratio predicted for the nanocomposite system considered for modelling analysis. However, with modelling for each of the nano fillers (graphene, SWCNT and MMT nanoclay), particularly 100nm milled glass flakes at critical aspect ratio shows that considerable high strength and modulus can be achieved while toughness is being maintained. Therefore, for the required critical aspect ratio for the nano fillers to be achieved remains a concern as these fillers are characterised with very high aspect ratio and would need to be controlled. Furthermore, IFSS applied for the nano fillers are relative values, meanwhile there has been research reporting higher IFSS value. For instance, Cooper et al. [306] reported interfacial shear strength value of 366MPa for SWCNT/epoxy composite, compared with 80MPa applied for modelling. It simply implies that the critical aspect ratio will be 4.5 times lesser than the value determined via the modelling. Therefore, higher interfacial shear strength will lower the critical aspect ratio of the matrix system. Hence, nanofillers aspect ratios will require to be manoeuvred such that it is in proximity to the matrix system critical aspect ratio for toughness to be maintained. Otherwise, the composite system will yield brittle failure for reinforcement filler having very high aspect ratio.

Table 38: Mechanical properties of some reported nanocomposites

Reinforcement filler	Matrix	Composite strength (GPa)	Composite modulus (GPa)	Volume fraction (%wt.)	Ref
SWCNT	Polyethylene	0.024	0.72	5	[307]
MMT Nano clay	Polypropylene	0.041	0.62	9	[308]
MMT Nano clay	Polyethylene	0.032	1.34	3	[309]
MMT Nano clay	Polypropylene	0.031	0.813	5	[310]
MMT Nano clay	Polyethylene	0.034	0.726	7.4	[311]
SWCNT	Polyethylene	0.024	0.648	1	[312]
MMT Nano clay	Nylon 6	0.076	2.43	5	[81]
MMT Nano clay	Nylon 6	0.091	4.71	4.6	[149]
MMT Nano clay	Epoxy	0.052	2.74	5	[150]
MMT Nano clay	Epoxy	0.058	3.44	10	[313]
SWCNT	Polypropylene	0.034	1.087	1	[314]
SWCNT	Polypropylene	0.084	1.059	10	[315]
SWCNT	Nylon 6	0.177	1.955	1	[316]
SWCNT	Nylon 6	0.089	1.47	0.5	[317]
SWCNT	Epoxy	0.095	2.632	1	[318]
SWCNT	Epoxy	0.081	4.6	5	[319]
Graphene	Epoxy	0.035	3.36	6	[320]
Graphene	Epoxy	0.075	3.7	0.1	[133]
Graphene	Polypropylene	0.025	2.9	20	[321]
Graphene	Polypropylene	0.031	2.5	0.5	[322]
Graphene	Polyethylene	0.032	1.2	1	[323]

Graphene	Polyethylene	0.031	2.3	30	[324]
Graphene	Nylon 6	0.082	4	3	[325]
Graphene	Nylon 6	0.068	2.569	0.31	[326]

5.0 Conclusion

The research investigates the feasibility to achieve composite materials with toughness maintained as well as sufficient strength and stiffness, thus identifying suitable reinforcement filler to reinforce polymer matrices. Through modelling analysis at 60% wt., the research considered composite reinforcement of commodity polymer matrices (epoxy, nylon 6, polypropylene and polyethylene) with reinforcement fillers which includes fibres (glass fibre and carbon fibre), nano sized fillers (graphene, SWCNT and MMT nanoclay) and sub-micron/nano sized glass flakes. The modelling analysis takes into consideration the interfacial shear strength (IFSS) for respective matrix system with each of the reinforcement fillers, thereby determines the critical aspect ratio required for the filler/matrix composite system in order for toughness to be maintained.

With critical aspect ratio determined at maximum IFSS for respective matrix system with individual reinforcement filler, the modelling shows that reinforcement with short and long reinforcement fibres of glass as well as carbon fibre with polymer matrices exceed the critical aspect ratio therefore unable for toughness to be maintained. Consequently, modelling the fibre fillers at critical aspect ratio show a considerable decrease in strength and modulus for toughness to be maintained. For glass flake reinforcement fillers, the research demonstrated ability to control the investigated glass flakes aspect ratios. Thus, with 100nm milled glass flake aspect ratio considered at critical aspect ratio for respective polymer matrices to ensure that toughness is maintained, obtainable strength and stiffness are higher compared to fibre reinforcement. Meanwhile, nanocomposite reinforcement with nano fillers shows that with adequate fabrication process, high strength and stiffness can be achieved but due to the high aspect ratio associated with the nano filler pose challenge for toughness to be maintained.

With due diligence given to the reinforcement fillers, the modelling shows that for composite material strength and modulus to be enhanced, it is ideal for the filler to be sufficiently thin in order for the filler itself to have considerable strength and stiffness (modulus). However, it is also important that the filler have considerable thickness for toughness to be maintained by having adequate aspect ratio in proximity to the composite system critical aspect ratio. Amidst all fillers investigated, 100nm milled glass flakes could be identified as typical example of such filler required to provide adequate strength and stiffness and sufficiently thick as with possibility of such fillers aspect ratio to be manoeuvred accordingly for toughness to be maintained.

6.0 Future work

The research has shown through modelling the feasibility to improve composite material strength, stiffness, and toughness. It shows that with such reinforcement filler as glass flakes within nanometre range and the ability to manoeuvre their aspect ratio, provide a considerable optimism of a composite material with strength, stiffness and toughness to be fabricated. The research investigates the approach towards producing such material; however, an adequate fabrication process is required. The fabrication process will be able to produce samples of reinforcement filler with polymers for mechanical validation, i.e. tensile testing having varied level of the aspect ratio altered. The fabrication process would need to be able to produce sample with sufficient high-volume fraction of reinforcement filler embedded and uniformly dispersed within polymer matrices with influence of interfacial properties investigated.

References

- [1] R. R. Boyer, J. D. Cotton, M. Mohaghegh and R. E. Schafrik, "Materials considerations for aerospace applications," *Materials & Engineering: Propelling Innovation*, vol. 40, no. 12, pp. 1055 - 1066, 2015.
- [2] B. Griffiths, "Boeing sets pace for composite usage in large civil aircraft," *Composites World*, [Online]. Available: <https://www.compositesworld.com/articles/boeing-sets-pace-for-composite-usage-in-large-civil-aircraft>. [Accessed 27 October 2020].
- [3] P. K. Sinha, *Composite Materials and Structures*, Kharagpur: Department of Aerospace Engineering, I. I. T., 1995.
- [4] United States Environmental Protection Agency, "Greenhouse Gas Emissions: Global Greenhouse Gas Emissions Data," 13 April 2017. [Online]. Available: <https://www.epa.gov/ghgemissions/global-greenhouse-gas-emissions-data>. [Accessed 13 June 2019].
- [5] Committee on Climate Change, "UK regulations: the Climate Change Act," [Online]. Available: <https://www.theccc.org.uk/tackling-climate-change/the-legal-landscape/the-climate-change-act/>. [Accessed 13 June 2019].
- [6] European Commission, "Reducing CO2 emissions from passenger cars - Policy," [Online]. Available: https://ec.europa.eu/clima/policies/transport/vehicles/cars_en. [Accessed 24 June 2019].
- [7] Asthana , Anushka ; Taylor, Matthew ;, "Britain to ban sale of all diesel and petrol cars and vans from 2040," *The Guardian*, 25 July 2017. [Online]. Available: <https://www.theguardian.com/politics/2017/jul/25/britain-to-ban-sale-of-all-diesel-and-petrol-cars-and-vans-from-2040>. [Accessed 24 June 2019].
- [8] . E. A. Rosa, G. E. Machlis and K. M. Keating, "Energy and Society," *Annual Review of Sociology*, vol. 14, pp. 149 - 172, 1988.
- [9] Editorial, "The role of society in energy transitions," *Nature Climate Change*, vol. 6, p. 539, 2016.
- [10] IEA, "Electricity Information: Overview," International Energy Agency, July 2020. [Online]. Available: <https://www.iea.org/reports/electricity-information-overview>. [Accessed 01 November 2020].
- [11] NewScientist, "Catch the breeze," New Scientist Ltd, 13 September 2013. [Online]. Available: <https://www.newscientist.com/article/dn24250-catch-the-breeze/#:~:text=There%20is%20only%20so%20much,makes%20them%20less%20aerodynamically%20efficient..> [Accessed 01 November 2020].

- [12] Matmatch, "Materials Used in Wind Turbines," Matmatch GmbH, 2020. [Online]. Available: <https://matmatch.com/learn/material/materials-used-in-wind-turbines>. [Accessed 02 November 2020].
- [13] "Why Bicycle Lightweighting Matters," AS Pro Engineering Ltd, [Online]. Available: https://www.asproengineering.com/lightweight-bicycles.html?gclid=CjwKCAiA_Kz-BRAJEiwAhJNY73xIlq8IWQkw6xJisXLqMAMAYTe-FaAcsUHTQLKKNAs6LSD91NfMGxoCBM4QAvD_BwE. [Accessed 05 December 2020].
- [14] K. E. Tanner, "Hard tissue applications of biocomposites," in *Biomedical Composites*, Duxford, Elsevier Ltd, 2017, pp. 37 - 58.
- [15] A. Iftexhar, "Biomedical Composites," in *Standard Handbook of Biomedical Engineering and Design*, London, The McGraw-Hill, 2004, pp. 1 - 17.
- [16] D. Hull, *An Introduction to Composite Materials*, Cambridge: Cambridge University Press, 1981.
- [17] F. Libonati, A. E. Vellwock, F. Ielmini, D. Abliz, G. Ziegmann and L. Vergani, "Bone-inspired enhanced fracture toughness of de novo fiber reinforced composites," *Scientific Reports*, vol. 9, no. 3142, pp. 1 - 12, 2019.
- [18] P. K. Mallick, *Composites Engineering Handbook*, New York: Marcel Dekker, Inc., 1997.
- [19] P. H. C. Camargo, K. G. Satyanarayana and F. Wypych, "Nanocomposites: synthesis, structure, properties and new application opportunities," *Materials Research*, vol. 12, no. 1, pp. 1 - 39, 2009.
- [20] J. D. H. Hughes, H. Morley and E. E. Jackson, "Aligned carbon fibre composite which approaches theoretical strength.," *Journal of Physics D: Applied Physics*, vol. 13, pp. 921 - 936, 1980.
- [21] D. U. Shah, P. J. Schubel, P. Licence and M. J. Clifford, "Determining the minimum, critical and maximum fibre content for twisted yarn reinforced plant fibre composites," *Composites Science and Technology*, vol. 72, no. 15, p. 1909 - 1917, 2012.
- [22] C. C. Okpala, "Nanocomposites - An Overview.," *International Journal of Engineering Research and Development*, vol. 8, no. 11, p. 17 - 23, 2013.
- [23] F. Gao, "Clay/polymer composites: the story.," *Materials today*, vol. 7, no. 11, p. 50 - 55, 2004.
- [24] P. D. Bradford, X. Wang, H. Zhao, J.-P. Maria, Q. Jia and Y. Zhu, "A novel approach to fabricate high volume fraction nanocomposites with long aligned carbon nanotubes," *Composites Science and Technology*, vol. 70, no. 13, pp. 1980 - 1985, 2010.

- [25] S. Rana, R. Alagirusamy and M. Joshi, "A Review on Carbon Epoxy Nanocomposites," *Journal of Reinforced Plastics and Composites*, vol. 25, no. 4, p. 461 – 487, 2009.
- [26] L. J. Bonderer, A. R. Studart and L. J. Gauckler, "Bioinspired Design and Assembly of Platelet Reinforced Polymer Films," *Science*, vol. 319, p. 1069 – 1073, 2008.
- [27] F. Barthelat and M. Mirkhalaf, "The quest for stiff, strong and tough hybrid materials: an exhaustive exploration," *Journal of the Royal Society Interface*, vol. 10, no. 89, pp. 1 - 8, 2013.
- [28] N. Saba and M. Jawaid, "Epoxy resin based hybrid polymer composites: Properties and Characterisation," in *Hybrid Polymer Composite Materials*, Duxford, Woodhead Publishing, 2017, pp. 57 - 82.
- [29] D. K. Rajak, D. D. Pagar, P. L. Menezes and E. Linul, "Fiber-Reinforced Polymer Composites: Manufacturing, Properties, and Applications," *polymers*, vol. 11, pp. 1 - 37, 2019.
- [30] F. Gao, "The future prospect of polymer nanocomposites in reinforcement application," *e-Polymers*, vol. no. T_004, pp. 1 - 7, 2002.
- [31] H. G. Chae, B. A. Newcomb, P. V. Gulgunje, Y. Liu, K. K. Gupta, M. G. Kamath, K. M. Lyons, S. Ghoshal, C. Pramanik, L. Giannuzzi, K. Şahin, S. Kumar and I. Chasiotis, "High strength and high modulus carbon fibers," *Carbon*, vol. 93, pp. 81 - 87, 2015.
- [32] C. Soutis, "Fibre reinforced composites in aircraft construction," *Progress in Aerospace Sciences*, vol. 41, no. 2, p. 143–151, 2005.
- [33] S. L. Ogin, P. Brøndsted and J. Zangenberg, "Composite materials: constituents, architecture, and generic damage," in *Modeling Damage, Fatigue and Failure of Composite Materials*, Cambridge, Woodhead Publishing, 2016, pp. 3 - 23.
- [34] V. Giurgiutiu, "Damage and Failure of Aerospace Composites," in *Structural Health Monitoring of Aerospace Composites*, Oxford, Academic Press, 2016, pp. 125 - 175.
- [35] M. R. Ricciardi, I. Papa, A. Langella, T. Langella, V. Lopresto and V. Antonucci, "Mechanical properties of glass fibre composites based on nitrile rubber toughened modified epoxy resin," *Composites Part B: Engineering*, vol. 139, pp. 259 - 267, 2018.
- [36] S. Sprenger, M. H. Kothmann and V. Altstaedt, "Carbon fiber reinforced composites using an epoxy resin matrix modified with reactive liquid rubber and silica nanoparticles," *Composites Science and Technology*, vol. 105, pp. 86 - 95, 2014.
- [37] M. R. Wisnom, "The role of delamination in failure of fibre-reinforced composites," *Phil. Trans. R. Soc. A*, vol. 370, no. 1965, pp. 1850 - 1870, 2012.
- [38] A. P. Mouritz, "Review of z-pinned composite laminates," *Composites Part A: Applied Science and Manufacturing*, vol. 38, no. 12, pp. 2383 - 2397, 2007.

- [39] A. Yudhanto, G. Lubineau, I. A. Ventura, N. Watanabe, Y. Iwahori and H. Hoshi, "Damage characteristics in 3D stitched composites with various stitch parameters under in-plane tension," *Composites Part A: Applied Science and Manufacturing*, vol. 71, pp. 17 - 31, 2015.
- [40] A. Aktas, P. Potluri and I. Porat, "Multi-needle stitched composites for improved damage tolerance," in *ICCM International Conferences on Composite Materials*, Manchester, 2009.
- [41] J.-q. Xuan, D.-s. Li and L. Jiang, "Fabrication, properties and failure of 3D stitched carbon/epoxy composites with no stitching fibers damage," *Composite Structures*, vol. 220, pp. 602 - 607, 2019.
- [42] P. Podsiadlo, A. K. Kaushik, E. M. Arruda, A. M. Waas, B. S. Shim, J. Xu, H. Nandivada, B. G. Pumphlin, J. Lahann, A. Ramamoorthy and N. A. Kotov, "Ultrastrong and Stiff Layered Polymer Nanocomposites," *Science*, vol. 318, no. 80, pp. 80-83, 2007.
- [43] A. R. Studart, "Towards High-Performance Bioinspired Composites," *Advanced Materials*, vol. 24, pp. 5024 - 5044, 2012.
- [44] G. Tan, J. Zhang, L. Zheng, D. Jiao, Z. Liu, Z. Zhang and R. O. Ritchie, "Nature-Inspired Nacre-Like Composites Combining Human Tooth-Matching Elasticity and Hardness with Exceptional Damage Tolerance," *Advanced Materials*, vol. 31, no. 1904603, pp. 1 - 9, 2019.
- [45] F. Bouville, E. Maire, S. Meille, B. Van de Moortèle, A. J. Stevenson and S. Deville, "Strong, tough and stiff bioinspired ceramics from brittle constituents," *Nature Materials*, vol. 13, pp. 508 - 514, 2014.
- [46] T. H. Hsieh, A. J. Kinloch, K. Masania, J. S. Lee and A. C. Taylor, "The toughness of epoxy polymers and fibre composites modified with rubber microparticles and silica nanoparticles," *Journal of Materials Science*, vol. 45, pp. 1193 - 1210, 2010.
- [47] H. Qian, E. S. Greenhalgh, M. S. P. Shaffer and A. Bismarck, "Carbon nanotube-based hierarchical composites: a review," *Journal of Materials Chemistry*, vol. 20, pp. 4751 - 4762, 2010.
- [48] A. M. Helmenstine, "What is a Polymer," ThoughtCo., 09 September 2019. [Online]. Available: <https://www.thoughtco.com/definition-of-polymer-605912>. [Accessed 21 May 2020].
- [49] The Editors of Encyclopaedia Britannica, "Polymer," Encyclopaedia Britannica, 26 February 2019. [Online]. Available: <https://www.britannica.com/science/polymer>. [Accessed 21 May 2020].
- [50] A. Shrivastava, "Introduction to Plastics Engineering," in *Introduction to Plastics Engineering*, Oxford, William Andrew, 2018, pp. 1 - 16.
- [51] P. J. Morris, *Polymer Pioneers: A Popular History of the Science and Technology of Large Molecules*, USA: American Institute of Chemical Engineers, 1986.

- [52] M. Garside, "Global plastic production statistics," Statista, 8 November 2019. [Online]. Available: <https://www.statista.com/statistics/282732/global-production-of-plastics-since-1950/>. [Accessed 21 May 2020].
- [53] K. Balani, V. Verma, A. Agarwal and R. Narayan, "Physical, Thermal and Mechanical Properties of Polymers," in *Biosurfaces: A Materials Science and Engineering Perspective*, New Jersey, John Wiley & Sons, Inc., 2015, pp. 329 - 344.
- [54] D. D. L. Chung, *Carbon Fiber Composites*, London: Butterworth-Heinemann, 1994.
- [55] M. R. Vengatesan, A. M. Varghese and V. Mittal, "Thermal Properties of Thermoset Polymers," in *Thermosets: Structure, Properties, and Applications*, Netherlands, Elsevier Ltd, 2018, pp. 69 - 102.
- [56] S. Lampman, *Characterization and Failure Analysis of Plastics*, USA: ASM International, 2003.
- [57] H. Madhav, N. Singh and G. Jaiswar, "Chapter 4 - Thermoset, bioactive, metal–polymer composites for medical applications," in *Materials for Biomedical Engineering: Thermoset and Thermoplastic Polymers.*, Oxford , Elsevier Inc., 2019, pp. 105 - 143.
- [58] Osborne Industries, "The Difference Between Thermoplastic and Thermosetting Plastic," Osborne Industries Inc., 15 May 2017. [Online]. Available: <https://www.osborneindustries.com/news/difference-between-thermoplastic-thermosetting-plastic/>. [Accessed 26 May 2020].
- [59] H. Kenn, "Epoxy Resins," in *Comprehensive Polymer Science and Supplements*, UK, Elsevier Ltd., 1989, pp. 667 - 699.
- [60] "Epoxy Resins," NetComposites, 24 January 2019. [Online]. Available: <https://netcomposites.com/guide/resin-systems/epoxy-resins/>. [Accessed 14 December 2020].
- [61] J. A. Brydson, "Epoxy Resins," in *Plastics Materials*, Oxford, Butterworth-Heinemann, 1999, pp. 744 - 777.
- [62] G. Gibson, "Epoxy Resins," in *Brydson's Plastics Materials* , Oxford, Butterworth-Heinemann, 2017, pp. 773 - 797.
- [63] H. Mahmood, M. Tripathi, N. Pugno and A. Pegoretti, "Enhancement of interfacial adhesion in glass fiber/epoxy composites by electrophoretic deposition of graphene oxide on glass fibers," *Composites Science and Technology*, vol. 126, pp. 149 - 157, 2016.
- [64] M. Li, Y. Gu, Y. Liu, Y. Li and Z. Zhang, "Interfacial improvement of carbon fiber/epoxy composites using a simple process for depositing commercially functionalized carbon nanotubes on the fibers," *Carbon*, vol. 52, pp. 109 - 121, 2013.

- [65] S. Deng, L. Ye and Y.-W. Mai, "Measurement of interfacial shear strength of carbon fibre/epoxy composites using a single fibre pull-out test," *Advanced Composite Materials*, vol. 7, no. 2, pp. 169-182, 1998.
- [66] X. F. Zhou, H. Wagner and S. Nutt, "Interfacial properties of polymer composites measured by push-out and fragmentation tests," *Composites Part A: Applied Science and Manufacturing*, vol. 32, no. 11, pp. 1543 - 1551, 2001.
- [67] M. M. Shokrieh, S. M. Ghoreishi and M. Esmkhani, "Toughening mechanisms of nanoparticle-reinforced polymers," in *Toughening Mechanisms in Composite Materials*, Cambridge, Woodhead Publishing, 2015, pp. 295 - 320.
- [68] J. Cha, G. H. Jun, J. K. Park, J. C. Kim, H. J. Ryu and S. H. Hong, "Improvement of modulus, strength and fracture toughness of CNT/Epoxy nanocomposites through the functionalization of carbon nanotubes," *Composites Part B: Engineering*, vol. 129, pp. 169 - 179, 2017.
- [69] S.-J. Park, *Carbon Fibers*, London: Springer, 2015.
- [70] N. K. MacVarish , "The Difference Between Amorphous & Semi-crystalline Polymers," *Impact Plastics*, 23 August 2017. [Online]. Available: <http://blog.impactplastics-ct.com/blog/the-difference-between-amorphous-semi-crystalline-polymers>. [Accessed 28 May 2020].
- [71] H. Unal, A. Mimaroglu and M. Alkan, "Mechanical properties and morphology of nylon-6 hybrid composites," *Polymer International*, vol. 53, pp. 56 - 60, 2004.
- [72] S. Das, S. Hollister, C. Flanagan, A. Adewunmi, K. Bark, C. Chen, K. Ramaswamy, D. Rose and E. Widjaja, "Freeform fabrication of Nylon-6 tissue engineering scaffolds," *Rapid Prototyping Journal*, vol. 9, no. 1, pp. 43 - 49, 2003.
- [73] J. Clark, "Polyamides," *Chemistry - LibreTexts*, 13 September 2020. [Online]. Available: [https://chem.libretexts.org/Bookshelves/Organic_Chemistry/Supplemental_Modules_\(Organic_Chemistry\)/Amides/Reactivity_of_Amides/Polyamides](https://chem.libretexts.org/Bookshelves/Organic_Chemistry/Supplemental_Modules_(Organic_Chemistry)/Amides/Reactivity_of_Amides/Polyamides). [Accessed 17 September 2021].
- [74] V. R. Sastri, "Engineering Thermoplastics: Acrylics, Polycarbonates, Polyurethanes, Polyacetals, Polyesters, and Polyamides," in *Plastics in Medical Devices: Properties, Requirements, and Applications*, Burlington, USA, William Andrew, 2010, pp. 121 - 173.
- [75] V. Moody and H. L. Needles, "Major Fibers and Their Properties," in *Tufted Carpet*, USA, William Andrew, Inc., 2004, pp. 35 - 59.
- [76] B. Rodgers and W. Waddle, "Tire Engineering," in *The Science and Technology of Rubber*, Oxford, Academic Press, 2013, pp. 653 - 695.
- [77] S. Dasgupta, W. B. Hammond and W. A. Goddard III, "Crystal Structures and Properties of Nylon Polymers from Theory," *Journal of American Chemical Society*, vol. 118, no. 49, pp. 12291 - 12301, 1996.

- [78] P. K. Vagholkar, "Nylon (Chemistry, Properties and Uses)," *International Journal of Science Research*, vol. 5, no. 9, pp. 349 - 351, 2016.
- [79] A. E. Campo, "Mechanical Properties of Polymeric Materials," in *Selection of Polymeric Materials*, USA, William Andrew Inc., 2008, pp. 41 - 101.
- [80] The Plastic Shop, "Product Data Sheet: ERTALON 6 PLA," 20 January 2011. [Online]. Available: https://www.theplasticshop.co.uk/plastic_technical_data_sheets/cast_nylon_6_technical_data_sheet.pdf. [Accessed 18 December 2020].
- [81] J. S. Shelley, P. T. Mather and K. L. DeVries, "Reinforcement and environmental degradation of nylon-6/clay nanocomposites," *Polymer*, vol. 42, no. 13, pp. 5849 - 5858, 2001.
- [82] Y. Guo, Y. Li, S. Wang, Z.-X. Liu, B. Cai and P.-C. Wang, "Effect of silane treatment on adhesion of adhesive-bonded carbon fiber reinforced nylon 6 composite," *International Journal of Adhesion and Adhesives*, vol. 91, pp. 102 - 115, 2019.
- [83] J. F. Collins, "The Strength and Failure Behaviour of Short Glass Fibre Reinforced Polyamide 6," June 1981. [Online]. Available: <http://epubs.surrey.ac.uk/847322/1/10798343.pdf>. [Accessed 22 December 2020].
- [84] The Editors of Encyclopaedia Britannica, "Polyethylene," *Encyclopædia Britannica*, 15 November 2019. [Online]. Available: <https://www.britannica.com/science/polyethylene>. [Accessed 22 December 2020].
- [85] L. A. Pruitt, "Structural Biomedical Polymers (Nondegradable)," *Comprehensive Biomaterials*, vol. 1, pp. 373 - 379, 2011.
- [86] I. M. Hutten, "Raw Materials for Nonwoven Filter Media," in *Handbook of Nonwoven Filter Media*, Oxford, Butterworth-Heinemann, 2016, pp. 158 - 275.
- [87] R. B. Richards, "Polyethylene - structure, crystallinity and properties," *Journal of Applied Chemistry*, vol. 1, no. 8, pp. 370 - 376, 1951.
- [88] M. Biron, "Transition of Plastics to Renewable Feedstock and Raw Materials: Bioplastics and Additives Derived From Natural Resources," in *A Practical Guide to Plastics Sustainability*, Cambridge, USA, William Andrew, 2020, pp. 469 - 555.
- [89] C. A. Sperati, W. A. Franta and H. W. Starkweather Jr, "The Molecular Structure of Polyethylene. V. The Effect of Chain Branching and Molecular Weight on Physical Properties," *Journal of the American Chemical Society*, vol. 75, no. 24, pp. 6127 - 6133, 1953.
- [90] J. L. Jordan, D. T. Casem, J. M. Bradley, A. K. Dwivedi, E. N. Brown and C. W. Jordan, "Mechanical Properties of Low Density Polyethylene," *Journal of Dynamic Behavior of Materials volume*, vol. 2, pp. 411 - 420, 2016.

- [91] S. Jung, S. K. Park, H.-d. Ghim, D. Y. Lee and S. H. Yoo, "Synergetic effect of cross-linking and interfacial interaction in carbon fiber reinforced thermoplastic to enhance its tensile strength by electron-beam irradiation," *Carbon Letters*, vol. 30, pp. 165 - 175, 2000.
- [92] J. L. Thomason, "Glass fibre sizing: A review," *Composites Part A: Applied Science and Manufacturing*, vol. 127, no. 105619, pp. 1 - 24, 2019.
- [93] M. Gahleitner and C. Paulik, "Polypropylene," in *Ullmann's Encyclopedia of Industrial Chemistry*, Weinheim, Wiley, 2014, pp. 1 - 44.
- [94] C. Maier and T. Calafut, "Chemistry," in *Polypropylene: The Definitive User's Guide and Databook*, USA, Plastics Design Library, 1998, pp. 3 - 9.
- [95] H. A. Maddah, "Polypropylene as a Promising Plastic: A Review," *American Journal of Polymer Science*, vol. 6, no. 1, pp. 1 - 11, 2016.
- [96] S. H. Han, H. J. Oh and S. S. Kim, "Evaluation of fiber surface treatment on the interfacial behavior of carbon fiber-reinforced polypropylene composites," *Composites Part B: Engineering*, vol. 60, pp. 98 - 105, 2014.
- [97] M. Etcheverry and S. E. Barbosa, "Glass Fiber Reinforced Polypropylene Mechanical Properties Enhancement by Adhesion Improvement," *Materials*, vol. 5, no. 6, pp. 1084 - 1113, 2012.
- [98] Composites World, "The Fibre," 17 March 2016. [Online]. Available: <https://www.compositesworld.com/articles/the-fiber>. [Accessed 5 April 2020].
- [99] P. Morgan, *Carbon Fibers and their Composites*, Boca Raton, Florida: Taylor & Francis Group, LLC, 2005.
- [100] American Chemical Society National Historic Chemical Landmarks, "High Performance Carbon Fibers," 17 September 2003. [Online]. Available: <https://www.acs.org/content/acs/en/education/whatischemistry/landmarks/carbonfibers.html>. [Accessed 08 June 2020].
- [101] V. McConnell, "The making of carbon fiber," *Composite World*, 12 December 2008. [Online]. Available: <https://www.compositesworld.com/articles/the-making-of-carbon-fiber>. [Accessed 15 June 2020].
- [102] Zoltek, "Carbon Fiber Education Center: How is Carbon Fiber Made," Toray Group, [Online]. Available: [https://zoltek.com/carbon-fiber/how-is-carbon-fiber-made/#:~:text=The%20raw%20material%20used%20to,made%20from%20polyacrylonitrile%20\(PAN\).&text=The%20precursor%20is%20drawn%20into,come%20in%20contact%20with%20Oxygen..](https://zoltek.com/carbon-fiber/how-is-carbon-fiber-made/#:~:text=The%20raw%20material%20used%20to,made%20from%20polyacrylonitrile%20(PAN).&text=The%20precursor%20is%20drawn%20into,come%20in%20contact%20with%20Oxygen..) [Accessed 17 June 2020].

- [103] S. J. Park and G. Y. Heo, "Precursors and Manufacturing of Carbon Fibers," in *Carbon Fibers*, Dordrecht, Springer, 2015, pp. 31 - 66.
- [104] B. A. Newcomb, "Processing, structure, and properties of carbon fibers," *Composites Part A: Applied Science and Manufacturing*, vol. 91, no. Part 1, pp. 262 - 282, 2016.
- [105] A. Celzard and V. Fierro, "Carbon, a Unique Model Material for Condensed Matter Physics and Engineering Science," in *Fundamental and Applied Nano-Electromagnetics*, Dordrecht, Springer, 2016, pp. 1 - 26.
- [106] X. Zhang, X. Fan, C. Yan, H. Li, Y. Zhu, X. Li and L. Yu, "Interfacial Microstructure and Properties of Carbon Fiber Composites Modified with Graphene Oxide," *Applied Materials and Interfaces*, vol. 4, pp. 1543 - 1552, 2012.
- [107] C. Capela, S. E. Oliveira and J. A. M. Ferreira, "Fatigue behavior of short carbon fiber reinforced epoxy composites," *Composites Part B: Engineering*, vol. 164, pp. 191 - 197, 2019.
- [108] N. G. Karsli and A. Aytac, "Tensile and thermomechanical properties of short carbon fiber reinforced polyamide 6 composites," *Composites Part B: Engineering*, vol. 51, pp. 270 - 275, 2013.
- [109] D. J. Vaughan, "Fiberglass reinforcement," in *Handbook of Composites*, London, Chapman & Hall, 1998, pp. 131 - 155.
- [110] G. Gardiner, "The making of glass fiber," *Composites World*, 01 June 2020. [Online]. Available: <https://www.compositesworld.com/articles/the-making-of-glass-fiber>. [Accessed 27 June 2020].
- [111] F. R. Jones and N. T. Huff, "The structure and properties of glass fibers," in *Handbook of Properties of Textile and Technical Fibres*, Kidlington, Elsevier Ltd, 2018, pp. 757 - 803.
- [112] H. A. Rijdsdijk, M. Contant and A. A. J. M. Peijs, "Continuous-glass-fibre-reinforced polypropylene composites: I. Influence of maleic-anhydride-modified polypropylene on mechanical properties," *Composites Science and Technology*, vol. 48, no. 1-4, pp. 161 - 172, 1993.
- [113] T. P. Mohan and K. Kanny, "Effect of nanoclay in HDPE-glass fiber composites on processing, structure, and properties," *Advanced Composite Materials*, vol. 21, no. 4, pp. 315 - 331, 2012.
- [114] S. J. Brigham and C. Watkinson, "Understanding and Use of Glass Flake," *Paint & Coatings Industry*, 02 March 2009. [Online]. Available: <https://www.pcimag.com/articles/85328-understanding-and-use-of-glass-flake>. [Accessed 06 July 2020].
- [115] Glassflake, "What is Glassflake," Glassflake Limited, 2020. [Online]. Available: <https://www.glassflake.com/what-is-glassflake/>. [Accessed 06 July 2020].

- [116] J. Rexer and E. Anderson, "Composites with Planar Reinforcements (Flakes, Ribbons) - A Review," *Polymer Engineering and Science*, vol. 19, no. 1, pp. 1 - 11, 1979.
- [117] Glassflakes, "Polymers," Glassflakes Limited, 2020. [Online]. Available: <https://www.glassflake.com/products/polymers/>. [Accessed 07 July 2020].
- [118] Glassflakes, "New Dimensions in Strength and Stability," Glassflakes Limited, [Online]. Available: https://chemie.worlee.de/uploads/chemistry/attachments/Standard%20Glassflake%20Brochure_5b7d33e1bea68.pdf. [Accessed 07 July 2020].
- [119] K. Takemura, K. Doushita, K. Yokoi and T. Mizuno, "Development of wet chemical processing in Nippon sheet glass," *Key Engineering Materials*, vol. 150, pp. 177 - 184, 1998.
- [120] N. Fujiura, T. Kida, K. Murata, N. Nakai and Y. Ogiya, "Method for producing glass flakes". Japan Patent JP2010229019A, 14 October 2010.
- [121] J. H. K. . Elvidge and C. J. Watkinson, "Method and apparatus for forming glass flakes". European Patent Office Patent EP0355104A1, 28 February 1990.
- [122] C. Watkinson, "Flakes made of materials such as glass". United States Patent US8796556B2, 05 August 2014.
- [123] A. A. Griffith, "The phenomena of rupture and flow in solids," *Philosophical Transactions of the Royal Society of London, Series A: Mathematical, Physical and Engineering Sciences*, vol. 221, p. 163 – 198, 1920.
- [124] Y. Li, *The development of sub-micro filler enhanced polymer composites*, Nottingham, UK: School of Science and Technology, Nottingham Trent University, 2007.
- [125] W. R. Broughton, M. J. Lodeiro and G. D. Pilkington, "Influence of coupling agents on material behaviour of glass flake reinforced polypropylene," *Composites Part A: Applied Science and Manufacturing*, vol. 41, no. 4, pp. 506 - 514, 2010.
- [126] Graphene-Info, "Graphene: structure and shape," Metalgrass LTD, 31 December 2018. [Online]. Available: <https://www.graphene-info.com/graphene-structure-and-shape#:~:text=It%20is%20composed%20of%20carbon,forms%20a%20single%20graphene%20sheet.&text=In%20graphene%2C%20each%20carbon%20atom,to%20three%20other%20carbon%20atoms..> [Accessed 14 July 2020].
- [127] D. Bradley, "A chemical history of graphene," *Materialstoday*, 10 June 2014. [Online]. Available: <https://www.materialstoday.com/carbon/comment/chemical-history-of-graphene/>. [Accessed 14 July 2020].
- [128] Graphene Flagship, "What is graphene?," Graphene Flagship, 02 March 2018. [Online]. Available: [https://graphene-flagship.eu/what-is-graphene-\(3\)](https://graphene-flagship.eu/what-is-graphene-(3)). [Accessed 14 July 2020].

- [129] E. P. Randviir, D. A. C. Brownson and C. E. Banks, "A decade of graphene research: production, applications and outlook," *Materialstoday*, vol. 17, no. 9, pp. 426 - 432, 2014.
- [130] K. S. Novoselov, V. I. Fal'ko, L. Colombo, P. R. Gellert, M. G. Schwab and K. Kim, "A roadmap for graphene," *Nature*, vol. 490, pp. 192 - 200, 2012.
- [131] C. Si, Z. Sun and F. Liu, "Strain engineering of graphene: a review," *Nanoscale*, vol. 8, pp. 3207 - 3217, 2016.
- [132] A. K. Geim, "Graphene prehistory," *Physica Scripta*, vol. 2012, no. T146, pp. 1 - 4, 2012.
- [133] M. A. Rafiee, J. Rafiee, Z. Wang, H. Song, Z.-Z. Yu and N. Koratkar, "Enhanced Mechanical Properties of Nanocomposites at Low Graphene Content," *ACS Nano*, vol. 3, no. 12, pp. 3884 - 3890, 2009.
- [134] C.-L. Huang, C.-W. Lou, C.-F. Liu, C.-H. Huang, X.-M. Song and J.-H. Lin, "Polypropylene/graphene and polypropylene/carbon fiber conductive composites: Mechanical, crystallization and electromagnetic properties," *Applied Sciences*, vol. 5, no. 4, pp. 1196 - 1210, 2015.
- [135] CNT Composites, "Structure of CNTs," CNT Composites, [Online]. Available: <https://sites.google.com/site/cntcomposites/structure-of-cnts>. [Accessed 18 July 2020].
- [136] A. Eatemadi, H. Daraee, H. Karimkhanloo, M. Kouhi, N. Zarghami, A. Akbarzadeh, M. Abasi, Y. Hanifehpour and S. W. Joo, "Carbon nanotubes: properties, synthesis, purification, and medical applications," *Nanoscale Research Letters*, vol. 9, no. 393, pp. 1 - 13, 2014.
- [137] S. Iijima, "Helical microtubules of graphitic carbon," *Nature*, vol. 354, pp. 56 - 58, 1991.
- [138] S. Iijima and T. Ichihashi, "Single-shell carbon nanotubes of 1-nm diameter," *Nature*, vol. 363, pp. 603 - 605, 1993.
- [139] G. Ren, "Carbon nanotube," Encyclopædia Britannica, inc., 16 November 2018. [Online]. Available: <https://www.britannica.com/science/carbon-nanotube>. [Accessed 16 July 2020].
- [140] B. Jurková, *Carbon nanomaterials and their interactions with bacteria*, Prague: Charles University, Faculty of Science, 2013.
- [141] J. N. Coleman, U. Khan, W. J. Blau and Y. K. Gun'ko, "Small but strong: A review of the mechanical properties of carbon nanotube-polymer composite," *Carbon*, vol. 44, no. 9, pp. 1624 - 1652, 2006.
- [142] CNT Composites, "Mechanical Properties," CNT Composites, [Online]. Available: <https://sites.google.com/site/cntcomposites/mechanical-properties>. [Accessed 11 January 2021].

- [143] X. Tong, C. Liu, H.-M. Cheng, H. Zhao, F. Yang and X. Zhang, "Surface Modification of Single-Walled Carbon Nanotubes with Polyethylene via In Situ Ziegler–Natta Polymerization," *Journal of Applied Polymer Science*, vol. 92, pp. 3697 - 3700, 2004.
- [144] F. Guo, S. Aryana, Y. Han and Y. Jiao, "A Review of the Synthesis and Applications of Polymer–Nanoclay Composites," *Applied Sciences*, vol. 8, no. 1696, pp. 1 - 29, 2018.
- [145] F. Uddin, "Clays, Nanoclays, and Montmorillonite Minerals," *Metallurgical and Materials Transactions A*, vol. 39, p. 2804 – 2814, 2008.
- [146] C. Zhou, D. Tong and W. Yu, "Smectite Nanomaterials: Preparation, Properties, and Functional Applications," in *Nanomaterials from Clay Minerals - A New Approach to Green Functional Materials*, Oxford, Elsevier Inc., 2019, pp. 335 - 364.
- [147] D. Donatella, C. Silvestre, S. Cimmino, A. Marra and M. Pezzuto, "Processing, Structure, and Morphology in Polymer Nanocomposites," in *Polymer Morphology: Principles, Characterization, and Processing*, Canada, John Wiley & Sons, 2016, pp. 374 - 396.
- [148] H. Heinz, "Clay minerals for nanocomposites and biotechnology: surface modification, dynamics and responses to stimuli," *Clay Minerals*, vol. 47, pp. 205 - 230, 2012.
- [149] T. D. Fornes, D. L. Hunter and D. R. Paul, "Nylon-6 Nanocomposites from Alkylammonium-Modified Clay: The Role of Alkyl Tails on Exfoliation," *Macromolecules*, vol. 37, no. 5, pp. 1793 - 1798, 2004.
- [150] K. Wang, L. Chen, J. Wu, M. L. Toh, C. He and A. F. Yee, "Epoxy Nanocomposites with Highly Exfoliated Clay: Mechanical Properties and Fracture Mechanisms," *Macromolecules*, vol. 38, no. 3, pp. 788 - 800, 2005.
- [151] C. Tezara, J. P. Siregar, H. Y. Lim, F. A. Fauzi, M. H. Yazdi, L. K. Moey and J. W. Lim, "Factors that affect the mechanical properties of kenaf fiber reinforced polymer: A review," *Journal of Mechanical Engineering and Sciences*, vol. 10, no. 2, pp. 2159 - 2175, 2016.
- [152] M. F. Ashby, "Hybrids to fill holes in material property space," *Philosophical Magazine*, vol. 85, no. 26 - 27, pp. 3235 - 3257, 2005.
- [153] S.-M. Choi and H. Awaji, "Nanocomposites—a new material design concept," *Science and Technology of Advanced Materials*, vol. 6, p. 2–10, 2005.
- [154] J. H. Park and G. C. Rutledge, "50th Anniversary Perspective: Advanced Polymer Fibers: High Performance and Ultrafine," *Macromolecules*, vol. 50, no. 15, p. 5627–5642, 2017.
- [155] Committee on High-Performance Structural Fibres for Advanced Polymer Matrix Composites National Research Council, High-Performance Structural Fibres for Advanced Polymer Matrix Composites, Washington, D.C.: The National Academies Press, 2005.

- [156] M. L. Minus and S. Kumar, "The processing, properties, and structure of carbon fibers," *JOM*, vol. 57, p. 52 – 58, 2005.
- [157] W. Watt, " Production and properties of high modulus carbon fibres," *Proc. Roy. Soc. Lond. A*, vol. 319, pp. 5 - 15, 1970.
- [158] V. A. Mikhailova, N. A. Savost'yanova, N. V. Bondarenko, A. V. Khorkhorin and V. M. Chermashentseva , "High-modulus, high-strength carbon fibre based on polyacrylonitrile," *Fibre Chemistry*, vol. 23, pp. 186 - 188, 1992.
- [159] X. Huang, "Fabrication and Properties of Carbon Fibers," *Materials (Basel)*, vol. 2, no. 4, p. 2369–2403, 2009.
- [160] Y. Arai, "Pitch Based Carbon Fibre with Low Modulus and High Heat Conduction," *Nippon Steel Technical Report*, vol. 84, no. UDC 661. 666-487, pp. 12 - 17, 2001.
- [161] J. E. McIntyre, *Synthetic Fibres: Nylon, Polyester, Acrylic, Polyolefin*, 1st ed., Cambridge: Woodhead Publishing Ltd, 2005.
- [162] P. Smith and P. J. Lemstra, "Ultra high strength polyethylene filaments by solution spinning/drawing," *Journal of Materials Science*, vol. 15, no. 2, p. 505 – 514, 1980.
- [163] C. J. Kuo and W. L. Lan, "Gel spinning of synthetic polymer fibres," in *Advances in Filament Yarn Spinning of Textiles and Polymers*, Cambridge, Woodhead Publishing Limited, 2014, pp. 100 - 112.
- [164] T. Kitagawa, M. Ishitobi and K. Yabuki, "An analysis of deformation process on poly-p-phenylenebenzobisoxazole fiber and a structural study of the new high modulus type PBO HM+ fiber," *Journal of Polymer Science: Part B: Polymer Physics*, vol. 38, pp. 1605 - 1611, 2000.
- [165] W. H. Otto, "Relationship of Tensile Strength of Glass Fibres to Diameter," *Journal of the American Ceramic Society*, vol. 38, no. 3, p. 122 – 125, 1955.
- [166] A. W. Rajput, A. u. Aleem and F. A. Arain, "An environmentally friendly process for the preparation of UHMWPE as spun fibres," *International Journal of Polymer Science*, vol. 2014, pp. 1 - 5, 2014.
- [167] R. Schaller, K. Feldman, P. Smith and T. A. Tervoort, "High-Performance Polyethylene Fibers "Al Dente": Improved GelSpinning of Ultrahigh Molecular Weight Polyethylene Using Vegetable Oils," *Macromolecules*, vol. 48, p. 8877 – 8884, 2015.
- [168] F. O. Anderegg, "1939," *Industrial and Engineering Chemistry*, vol. 31, no. 3, pp. 290 - 298, 1939.

- [169] B. A. Newcomb and H. G. Chae, "The Properties of Carbon Fibers," in *Handbook of Properties of Textile and Technical Fibres (Second Edition)*, Kidlington, Elsevier Ltd, 2018, pp. 841-871.
- [170] Y. T. Zhu, W. R. Blumenthal, S. T. Taylor and T. C. Lowe, "Analysis of Size Dependence of Ceramic Fiber and Whisker Strength," *Journal of the American Ceramic Society*, vol. 80, no. 6, p. 1447 – 1452 , 1997.
- [171] Materials Today, "Novel ultrafine polymer fibers stronger and tougher than Kevlar," Elsevier Ltd., 22 January 2018. [Online]. Available: <https://www.materialstoday.com/mechanical-properties/news/ultrafine-polymer-fibers-stronger-tougher/>. [Accessed 16 April 2020].
- [172] Massachusetts Institute of Technology, "Ultrafine Fibers have exceptional Strength," Science Daily, 5 January 2018. [Online]. Available: <https://www.sciencedaily.com/releases/2018/01/180105123949.htm>. [Accessed 16 April 2020].
- [173] E. P. Tan, S. Y. Ng and C. T. Lim, "Tensile testing of a single ultrafine polymeric fiber," *Biomaterials*, vol. 26, no. 13, pp. 1453 - 1456, 2005.
- [174] J. Rösler, M. Bäker and H. Harders, "Mechanical behaviour of fibre reinforced composites," in *Mechanical Behaviour of Engineering Materials*, Berlin Heidelberg New York, Springer, 2007, pp. 295 - 331.
- [175] F. C. Campbell, *Structural Composite Materials*, Ohio: ASM International, 2010.
- [176] S. C. Buddi, P. P. Prasanthi and P. Srikanth, "Mechanical Properties o Fibre Reinforced Composite using Finite Element Method," *International Journal of Mechanical Engineering and Robotics Research*, vol. 4, no. 1, pp. 80 - 90, 2015.
- [177] Y. Swolfs, L. Gorbatikh and I. Verpoest, "Fibre hybridisation in polymer composites: a review," *Composites Part A: Applied Science and Manufacturing*, vol. 67, pp. 181 - 200, 2014.
- [178] D. R. Paul and L. M. Robeson, "Polymer nanotechnology: Nanocomposites," *Polymer*, vol. 49, no. 15, pp. 3187 - 3204, 2008.
- [179] A. J. Clancy, D. B. Anthony and Francois De Luca, "Metal Mimics: Lightweight, Strong, and Tough Nanocomposites and Nanomaterial Assemblies," *ACS Appl. Mater. Interfaces*, vol. 12, p. 15955 – 15975, 2020.
- [180] Y. J. Liu and X. L. Chen, "Evaluations of the effective material properties of carbon nanotube-based composites using a nanoscale representative volume element," *Mechanics of Materials*, vol. 35, no. 1-2, pp. 69 - 81, 2003.
- [181] O. Breuer and U. Sundararaj, "Big Returns From Small Fibers: A Review of Polymer/Carbon Nanotube Composites," *Polymer Composites*, vol. 25, no. 6, pp. 630 - 645, 2004.

- [182] S. Kumar, Sarita, M. Nehra, N. Dilbaghi, K. Tankeshwar and K.-H. Kim, "Recent advances and remaining challenges for polymeric nanocomposites in healthcare applications," *Progress in Polymer Science*, vol. 80, pp. 1 - 38, 2018.
- [183] K. Müller, E. Bugnicourt, M. Latorre, M. Jorda, Y. E. Sanz, J. M. Lagaron, O. Miesbauer, A. Bianchin, S. Hankin, U. Bölz, G. Pérez, M. Jesdinszki, M. Lindner, Z. Scheuerer, S. Castelló and M. Schmid, "Review on the Processing and Properties of Polymer Nanocomposites and Nanocoatings and Their Applications in the Packaging, Automotive and Solar Energy Fields," *Nanomaterials (Basel)*, vol. 7, no. 4, pp. 1 - 47, 2017.
- [184] M. Mariano, N. E. Kissi and A. Dufresne, "Cellulose Nanocrystals and Related Nanocomposites: Review of some Properties and Challenges," *Journal of Polymer Science, Part B: Polymer Physics*, vol. 52, pp. 791 - 806, 2014.
- [185] W. J. Boo, L. Sun, G. L. Warren, E. Moghbelli, H. Pham, A. Clearfield and H. J. Sue, "Effect of nanoplatelet aspect ratio on mechanical properties of epoxy nanocomposites," *Polymer*, vol. 48, no. 4, pp. 1075 -1082, 2007.
- [186] R. O. Ritchie, "The conflicts between strength and toughness," *Nature Materials volume*, vol. 10, pp. 817 - 822, 2011.
- [187] N. Domun, H. Hadavinia, T. Zhang, T. Sainsbury, G. H. Liaghat and S. Vahid, "Improving the fracture toughness and the strength of epoxy using nanomaterials – a review of the current status," *Nanoscale*, vol. 7, p. 10294 – 10329, 2015.
- [188] J.-K. Kim and Y.-W. Mai, *Engineered Interfaces in Fiber Reinforced Composites*, Oxford: Elsevier Science Ltd, 1998.
- [189] M. S. Ghoraishi, J. E. Hawk, M. Ghoreishi and A. Zadhoush, "The role of interface in improving fracture toughness of shaped steel fiber-reinforced Composites," *Journal of Composite Materials*, vol. 52, no. 7, p. 981 – 987, 2018.
- [190] L.-G. Tang and J. L. Kardos, "A review of methods for improving the interfacial adhesion between carbon fiber and polymer matrix," *Polymer Composites*, vol. 18, no. 1, pp. 100 - 113, 1997.
- [191] T. W. Clyne and D. Hull, "Fracture Mechanics and the Toughness of Composites," in *An Introduction to Composite Materials*, Cambridge, Cambridge University Press, 2019, pp. 142 - 177.
- [192] Q. H. Qin, "Introduction to the composite and its toughening mechanisms," in *Toughening Mechanisms in Composite Materials*, Cambridge, Woodhead Publishing, 2015, pp. 1 - 32.
- [193] D. D. Cicco, Z. Asaee and F. Taheri, "Use of Nanoparticles for Enhancing the Interlaminar Properties of Fiber-Reinforced Composites and Adhesively Bonded Joints—A Review," *Nanomaterials (Basel)*, vol. 7, no. 11, pp. 1 - 29, 2017.

- [194] D. M. Laura, H. Keskkula, J. W. Barlow and D. R. Paul, "Effect of glass fiber surface chemistry on the mechanical properties of glass fiber reinforced, rubber-toughened nylon 6," *Polymer*, vol. 43, no. 17, pp. 4673 - 4687, 2002.
- [195] M. R. Dadfar and F. Ghadami, "Effect of rubber modification on fracture toughness properties of glass reinforced hot cured epoxy composites," *Materials and Design*, vol. 47, pp. 16 - 20, 2013.
- [196] D. Carolan, A. Ivankovic, A. J. Kinloch, S. Sprenger and A. C. Taylor, "Toughened carbon fibre-reinforced polymer composites with nanoparticle-modified epoxy matrices," *Journal of Materials Science*, vol. 52, pp. 1767 - 1788, 2016.
- [197] R. F. Gibson, "A review of recent research on mechanics of multifunctional composite materials and structures," *Composite Structures*, vol. 92, no. 12, pp. 2793 - 2810, 2010.
- [198] M. K. Shin, B. Lee, S. H. Kim, J. A. Lee, G. M. Spinks, S. Gambhir, G. G. Wallace, M. E. Kozlov, R. H. Baughman and S. J. Kim, "Synergistic toughening of composite fibres by self-alignment of reduced graphene oxide and carbon nanotubes," *Nature Communications*, vol. 3, no. 650, pp. 1 - 8, 2012.
- [199] A. Warriar, A. Godara, O. Rochez, L. Mezzo, F. Luizi, L. Gorbatikh, S. V. Lomov, W. A. VanVuure and I. Verpoest, "The effect of adding carbon nanotubes to glass/epoxy composites in the fibre sizing and/or the matrix," *Composites Part A: Applied Science and Manufacturing*, vol. 41, no. 4, pp. 532 - 538, 2010.
- [200] H. Zhang, Y. Liu, M. Kuwata, E. Bilotti and T. Peijs, "Improved fracture toughness and integrated damage sensing capability by spray coated CNTs on carbon fibre prepreg," *Composites Part A: Applied Science and Manufacturing*, vol. 70, pp. 102 - 110, 2015.
- [201] R. Nagalingam, S. Sundaram, B. Stanly and J. Retnam, "Effect of nanoparticles on tensile, impact and fatigue properties of fibre reinforced plastics," *Bulletin of Materials Science*, vol. 33, no. 5, pp. 525 - 528, 2011.
- [202] K. Shivakumar and R. Panduranga, "Interleaved Polymer Matrix Composites - A Review," in *AIAA*, Boston, Massachusetts, 2013.
- [203] S. F. Chen and B. Z. Jang, "Fracture behaviour of interleaved fiber-resin composites," *Composites Science and Technology*, vol. 41, no. 1, pp. 77 - 97, 1991.
- [204] J. Sun and B. Bhushan, "Hierarchical structure and mechanical properties of nacre: a review," *RSC Advances*, vol. 2, no. 20, pp. 7617 - 7632, 2012.
- [205] K. Livanov, L. Yang, A. Nissenbaum and D. H. Wagner, "Interphase tuning for stronger and tougher composites," *Scientific reports*, vol. 6, no. 26305, pp. 1 - 9, 2016.

- [206] H. Kakisawa and T. Sumitomo, "The toughening mechanism of nacre and structural materials inspired by nacre," *Science and Technology of Advanced Materials*, vol. 12, no. 6, pp. 1 - 14, 2011.
- [207] G. Mayer, "Rigid Biological Systems as Models for Synthetic Composites," *Science*, vol. 310, no. 5751, pp. 1144 - 1147, 2005.
- [208] H. Pettermann, *Continuum Mechanics Modeling of Composite Materials*, Vienna: Vienna University of Technology, 2003.
- [209] R. K. Behera, D. Pinisetty and D. D. Luong, "Modeling and Simulation of Composite Materials," *JOM*, vol. 71, no. 11, p. 3949 – 3950, 2019.
- [210] Y. A. Bahei-El-Din and A. M. Elrafei, "Mechanics of fracture in fibrous metal matrix composite," in *Current Advances in Mechanical Design and Production VII: Proceedings of the Seventh Cairo University International MDP Conference*, Oxford, Elsevier Science Ltd., 2000, pp. 271 - 280.
- [211] H. G. Kim and L. K. Kwac, "Evaluation of elastic modulus for unidirectionally aligned short fiber composites," *Journal of Mechanical Science and Technology*, vol. 23, pp. 54 - 63, 2009.
- [212] J. Aboudi, S. M. Arnold and B. A. Bednarczyk, *Micromechanics of Composite Materials: A Generalized Multiscale Analysis Approach*, Oxford: Butterworth-Heinemann, Elsevier, 2013.
- [213] L. J. Mishnaevsky, "Micromechanical modelling of wind turbine blade materials," in *Advances in Wind Turbine Blade Design and Materials*, Cambridge, Woodhead Publishing, 2013, pp. 298 - 324.
- [214] C. M. Landis and R. M. McMeeking, "A shear-lag model for a broken fiber embedded in a composite with a ductile matrix," *Composites Science and Technology*, vol. 59, no. 3, pp. 447 - 457, 1999.
- [215] S. Mahesh, J. C. Hanan, E. Üstündag and I. J. Beyerlein, "Shear-Lag Model for a Single Fiber Metal Matrix Composite with an Elasto-Plastic Matrix and a Slipping Interface," *International Journal of Solids and Structures*, vol. 41, no. 15, pp. 4197 - 4218, 2004.
- [216] M. J. Starink and S. Syngellakis, "Shear lag models for discontinuous composites: fibre end stresses and weak interface layers," *Materials Science and Engineering: A*, vol. 270, no. 2, pp. 270 - 277, 1999.
- [217] Y. Yu, M. Lu, M. H. Chen, L. S. Wang, Z. X. Bu, G. Song and L. Sun, "Modeling of dynamic mechanical properties of polymer composites reinforced by one dimensional nanofillers," *Journal of Applied Physics*, vol. 120, no. 17, pp. 175103 (1 - 12), 2016.

- [218] L. J. Bonderer, A. R. Studart, J. Woltersdorf, E. Pippel and L. J. Gauckler, "Strong and ductile platelet-reinforced polymer films inspired by nature: Microstructure and mechanical properties," *Journal of Materials Research*, vol. 24, no. 9, pp. 2741 - 2754, 2009.
- [219] J. G. Michopoulos, J. C. Hermanson, A. Lliopoulos, S. G. Lambrakos and T. Furukawa, "Data-Driven Design Optimization for Composite Material Characterization," *Journal of Computing and Information Science in Engineering*, vol. 11, no. 021009, pp. 1 - 11, 2011.
- [220] A. C. Orifici, I. Herszberg and R. S. Thomson, "Review of methodologies for composite material modelling incorporating failure," *Composite Structures*, vol. 86, no. 1 - 3, pp. 194 - 210, 2008.
- [221] L. Himanen, A. Geurts, A. S. Foster and P. Rinke, "Data-Driven Materials Science: Status, Challenges, and Perspectives," *Advanced Science*, vol. 6, no. 21, pp. 1900808 (1 - 23), 2019.
- [222] V. Moreno-Maldonado, L. S. Acosta-Torres, F. H. Barcelo-Santana, R. D. Vanegas-Lancon, M. E. Plata-Rodriguez and V. M. Castano, "Fiber-Reinforced Nanopigmented Poly(methylmethacrylate) as Improved Denture Base," *Journal of Applied Polymer Science*, vol. 126, pp. 289 - 296, 2012.
- [223] N. Primeau, C. Vautey and M. Langlet, "The effect of thermal annealing on aerosol-gel deposited SiO₂ films: a FTIR deconvolution study," *Thin Solid Films*, vol. 310, no. 1-2, pp. 47 - 56, 1997.
- [224] J. M. Whitney, *Analysis of the Test Methods for High Modulus Fibers and Composites: A Symposium Presented at a Meeting of Committee D-30 on High Modulus Fibers and Their Composites*, Philadelphia: American Society for Testing and Materials, 1973.
- [225] H. Schuerch, "Effect of diameter upon elastic properties in thin fibers," *AIAA Journal*, vol. 2, no. 3, pp. 569 - 571, 1964.
- [226] A. Rohatgi, "WebPlotDigitizer," August 2021. [Online]. Available: <https://automeris.io/WebPlotDigitizer>. [Accessed 13 October 2021].
- [227] S. Cuenot, C. Fretigny, S. Demoustier-Champagne and B. Nysten, "Surface tension effect on the mechanical properties of nanomaterials measured by atomic force microscopy," *The American Physical Society*, vol. 69, pp. 165410 (1 - 5), 2004.
- [228] V. Veer and R. Kumar, "Size and Shape Dependent Young Modulus and Vibrational Frequency of Nanomaterials," *International Journal for Research in Applied Science & Engineering Technology*, vol. 3, no. IX, pp. 22 - 28, 2015.
- [229] C. Lee, X. Wei, J. W. Kysar and J. Hone, "Measurement of the Elastic Properties and Intrinsic Strength of Monolayer Graphene," *Science*, vol. 321, no. 5887, pp. 385 - 388, 2008.

- [230] M.-F. Yu, B. S. Files, S. Arepalli and R. S. Ruoff, "Tensile Loading of Ropes of Single Wall Carbon Nanotubes and their Mechanical Properties," *Physical Review Letters*, vol. 84, no. 24, pp. 5552 - 5555, 2000.
- [231] Smiths; "Polyethylene (HD-PE & UHMW-PE) Technical Datasheet," Smiths Metal, 2018. [Online]. Available: <https://www.smithmetal.com/pdf/plastics/polyethylene.pdf>. [Accessed 28 January 2021].
- [232] F. Zhao and N. Takeda, "Effect of interfacial adhesion and statistical fiber strength on tensile strength of unidirectional glass fiber/epoxy composites. Part I: experiment results," *Composites Part A: Applied Science and Manufacturing*, vol. 31, no. 11, pp. 1203 - 1214, 2000.
- [233] S. Keusch, H. Queck and K. Gliesche, "Influence of glass fibre/epoxy resin interface on static mechanical properties of unidirectional composites and on fatigue performance of cross ply composites," *Composites Part A*, vol. 29A, pp. 701 - 705, 1998.
- [234] T. H. Cheng, F. R. Jones and D. Wang, "Effect of Fibre Conditioning on the Interfacial Shear Strength of Glass-Fibre Composite," *Composites Science and Technology*, vol. 48, no. 1-4, pp. 89 - 96, 1993.
- [235] Z. Zhai, Z. Liu, L. Feng and S. Liu, "Interfacial adhesion of glass fibre reinforced polypropylene-maleic anhydride modified polypropylene copolymer composites," *Reinforced Plastics and Composites*, vol. 33, no. 8, pp. 785 - 793, 2014.
- [236] J. Rausch, R. C. Zhuang and E. Mäder, "Systematically varied interfaces of continuously reinforced glass fibre/polypropylene composites: Comparative evaluation of relevant interfacial aspects," *EXPRESS Polymer Letters*, vol. 4, no. 9, pp. 576 - 588, 2010.
- [237] P. Nygård, . K. Redford and . C.-G. Gustafson, "Interfacial strength in glass fibre-polypropylene composites: influence of chemical bonding and physical entanglement," *Composite Interfaces* , vol. 9, no. 4, p. 365–388, 2002.
- [238] A. Pegoretti, M. Fidanza, C. Migliaresi and A. T. DiBenedetto, "Toughness of the fibre/matrix interface in nylon 6/glass composites," *Composit Part A*, vol. 29A, pp. 283 - 291, 1998.
- [239] . N. Takeda, D. Song, K. Nakat and T. Shioya, "The effect of fibre surface treatment on the micro-fracture progress in glass fibre/Nylon 6 composites," *Composite Interfaces*, vol. 2, no. 2, pp. 143 - 155 , 1994.
- [240] A. DiBenedetto, "Evaluation of fiber surface treatments in composite materials," *Pure & Appl. Chem.* , vol. 57, no. 11, pp. 1659 - 1665 , 1985.
- [241] X. S. Bian, L. Ambrosio, J. M. Kenny, L. Nicolais and A. DiBenedetto, "Effect of Water Absorption on the Behaviour of E-Glass Fibre/Nylon-6 Composites," *Polymer Composites*, vol. 12, no. 5, pp. 333 - 337, 1991.

- [242] C. K. Moon, J.-o. Lee, H. H. Cho and K. S. Kim, "Effect of diameter and surface treatment of fibre on interfacial shear strength in glass fibre/epoxy and HDPE," *Journal of Applied Polymer Science*, vol. 45, no. 3, pp. 443 - 450, 1992.
- [243] M. Nardin and J. Schultz, "Relationship between fibre-matrix adhesion and the interfacial shear strength in polymer-based composites," *Composite Interfaces*, vol. 1, no. 2, pp. 177 - 192, 1993.
- [244] . C. Wang, X. Ji, A. Roy, V. V. Silberschmidt and Z. Chen, "Shear strength and fracture toughness of carbon fibre/epoxy interface:effect of surface treatment," *Materials and Design*, vol. 85, p. 800–807, 2015.
- [245] D. S. Varma, S. Saxena, N. Gupta and I. K. Varma, "Carbon fibre/epoxy composites: Effect of epoxy network and surface treatment of fibres on interfacial shear strength," *Indian Journal of Engineering and Materials Sciences*, vol. 4, no. 6, pp. 266-270, 1997.
- [246] Y. Yusong, Z. Yan, L. Ye, D. Qi and C. Da , "Effect of sizing on the interfacial shear strength of carbon fiber/epoxy resin monofilament composite," *Journal of Wuhan University of Technology-Mater. Sci. Ed*, vol. 29, p. 483–487, 2014.
- [247] J. Park, . J. Lee and . T. Park, "Improved interfacial shear strength and durability of single carbon fiber reinforced isotactic polypropylene composites using water-dispersible graft copolymer as a coupling agent," *Polymer Composites*, vol. 17, no. 3, pp. 375-383, 1996.
- [248] S. Yumitori, Y. Arao, T. Tanaka, K. Naito, K. Tanaka and T. Katayama, "Increasing the interfacial strength in carbonfiber/polypropylene composites by growing CNTs on the fibers," *Computational Methods and Experimental Measurements XVI*, vol. 55, pp. 275-284, 2013.
- [249] D. T. Burn, . L. T. Harper, M. Johnson, N. Warrior, . L. Yang and J. Thomason, "The influence of coupling agent, fibre sizing and matrix degradation on the interfacial shear strength between carbon fibre and polypropylene," in *ECCM-16TH European Conference on Composite Mateials*, Seville, Spain, 2014.
- [250] K. Tanaka, K. Ohno and T. Katayama, "Effects of PP modification and processing time on fiber/matrix interfacial strength for carbon fiber reinforced polypropylene," *WIT Conferences: 2nd International Conference on High Performance and Optimum Design of Structures and Materials*, vol. 166, pp. 329-334, 2016.
- [251] J. Li, "Interfacial features of polyamide 6 composites filled with oxidation modified carbon fibres," *Proc. IMechE*, vol. 223, no. 9, pp. 2135-2141, 2009.
- [252] K. Tanaka, S. Mizuno, H. Honda, T. Katayama and S. Enoki, "Effect of water absorption on the mechanical properties of carbon fiber/polyamide composites," *Journal of Solid Mechanics and Materials Engineering* , vol. 7, no. 5, pp. 520-529, 2013.

- [253] K. Tanaka, S. Okuda, Y. Hinoue and T. Katayama, "Effects of water absorption on the fiber–matrix interfacial shear strength of carbon nanotube-grafted carbon fiber reinforced polyamide resin," *Journal of Composites Science*, vol. 3, pp. 1-9, 2019.
- [254] M. H. Gabr and K. Uzawa, "Effect of different types of nano/micro fillers on the interfacial shear properties of polyamide 6 with de-sized carbon fiber," *World Academy of Science, Engineering and Technology International Journal of Materials and Metallurgical Engineering*, vol. 11, no. 1, pp. 82-87, 2017.
- [255] E. Pisanova, S. Zhandarov and E. Mäder, "Adhesive interactions in interphases: competition between acid-base and diffusion mechanisms," in *Institute of Polymer Research, Germany*, 1999.
- [256] E. V. Pisanova, S. F. Zhandarov and V. A. Dovgyalo, "Interfacial adhesion and failure modes in single filament thermoplastic composites," *Polymer Composites*, vol. 15, pp. 147-155, 1994.
- [257] P. K. Vallittu, "High-aspect ratio fillers: Fiber-reinforced composites and their anisotropic properties," *Dental Materials*, vol. 31, no. 1, pp. 1 - 7, 2015.
- [258] H. G. Kim, "Effects of fiber aspect ratio evaluated by elastic analysis in discontinuous composites," *Journal of Mechanical Science and Technology*, vol. 22, pp. 411 - 419, 2008.
- [259] C. J. R. Verbeek, "The influence of interfacial adhesion, particle size and size distribution on the predicted mechanical properties of particulate thermoplastic composites," *Materials Letters*, vol. 57, no. 13-14, pp. 1919 - 1924, 2003.
- [260] G. Yerbolat, S. Amangeldi, M. H. Ali, N. Badanova, A. Ashirbeok and G. Islam, "Composite Materials Property Determination by Rule of Mixture and Monte Carlo Simulation," in *IEEE International Conference on Advanced Manufacturing (ICAM)*, Yunlin, 2018.
- [261] DoITPoMS, "Derivation of the rule of mixtures and inverse rule of mixtures," University of Cambridge, 2020. [Online]. Available: https://www.doitpoms.ac.uk/tlplib/bones/derivation_mixture_rules.php. [Accessed 18 August 2020].
- [262] J. C. Halpin and J. L. Kardos, "The Halpin-Tsai Equations: A Review," *Polymer Engineering and Science*, vol. 16, no. 5, pp. 344 - 352, 1976.
- [263] W. A. Curtin, "Exact theory of fibre fragmentation in a single-filament composite," *Journal of Materials Science*, vol. 26, pp. 5239 - 5253 , 1991.
- [264] D. Tripathi and F. R. Jones, "Review Single fibre fragmentation test for assessing adhesion in fibre reinforced composites," *Journal of Materials Science*, vol. 33, pp. 1 - 16, 1998.
- [265] K. G. Dassios, "A Review of the Pull-Out Mechanism in the Fracture of Brittle Matrix Fibre Reinforced Composites," *Advanced Composites Letters*, vol. 16, no. 1, pp. 17 - 24, 2007.

- [266] A. Kelly and W. R. Tyson, "Tensile properties of fibre-reinforced metals: Copper/tungsten and copper/molybdenum," *Journal of the Mechanics and Physics of Solids*, vol. 13, no. 6, pp. 329 - 338, 1965.
- [267] B. F. Jones and R. G. Duncan, "The effect of fibre diameter on the mechanical properties of graphite fibres manufactured from polyacrylonitrile and rayon," *Journal of Material Science*, vol. 6, pp. 289 - 293 , 1971.
- [268] Saint-Gobain Vetrotex, "E, R and D glass properties - Technical data sheet," Deutschland GmbH, March 2020. [Online]. Available: https://glassproperties.com/glasses/E_R_and_D_glass_properties.pdf. [Accessed 31 August 2020].
- [269] P. K. Mallick, "Thermoplastics and thermoplastic–matrix composites for lightweight automotive structures," in *Materials, Design and Manufacturing for Lightweight Vehicles*, Cambridge, Woodhead Publishing Limited, 2010, pp. 174 - 207.
- [270] B. Fei, "High-performance fibers for textiles," in *Engineering of High-Performance Textiles*, Duxford, Woodhead Publishing, 2018, pp. 27 - 58.
- [271] L. T. Harper, D. T. Burn, M. S. Johnson and N. A. Warrior, "Long discontinuous carbon fibre/polypropylene composites for high volume structural applications," *Journal of Composite Materials*, vol. 52, no. 9, pp. 1155 - 1170, 2018.
- [272] A. D. Evans, C. C. Qian, T. A. Turner, L. T. Harper and N. A. Warrior, "Flow characteristics of carbon fibre moulding compounds," *Composites Part A: Applied Science and Manufacturing*, vol. 90, pp. 1 - 12, 2016.
- [273] J. L. Thomason, "The influence of fibre length and concentration on the properties of glass fibre reinforced polypropylene. 6. The properties of injection moulded long fibre PP at high fibre content," *Composites Part A: Applied Science and Manufacturing*, vol. 36, no. 7, pp. 995 - 1003, 2005.
- [274] J. J. Murray, C. Robert, K. Gleich, E. D. McCarthy and C. M. Ó. Brádaigh, "Manufacturing of unidirectional stitched glass fabric reinforced polyamide 6 by thermoplastic resin transfer moulding," *Materials & Design*, vol. 189, no. 108512, pp. 1 - 14, 2020.
- [275] S. Francis, T. Bru, L. E. Asp, M. Wysocki and C. Cameron, "Characterisation of tape-based carbon fibre thermoplastic discontinuous composites for energy absorption," *Plastics, Rubber and Composites - Macromolecular Engineering*, vol. 50, no. 7, pp. 351 - 361, 2021.
- [276] Y. Wan and T. Jun, "Tensile and compressive properties of chopped carbon fiber tapes reinforced thermoplastics with different fiber lengths and molding pressures," *Composites Part A: Applied Science and Manufacturing*, vol. 87, pp. 271 - 281, 2016.

- [277] E. C. Botelho, L. Figiel, M. C. Rezende and B. Lauke, "Mechanical behavior of carbon fiber reinforced polyamide composites," *Composites Science and Technology*, vol. 63, no. 13, pp. 1843 - 1855, 2003.
- [278] H. Ramezani-Dana, M. Gomina, J. Bréard and G. Orange, "Experimental investigation of the mechanical behavior of glass fiber/high fluidity polyamide-based composites for automotive market," *Journal of Reinforced Plastics and Composites*, vol. 40, no. 21-22, p. 827 – 844, 2021 .
- [279] H. Iba, T. Chang and Y. Kagawa, "Optically transparent continuous glass fibre-reinforced epoxy matrix composite: fabrication, optical and mechanical properties," *Composites Science and Technology*, vol. 62, no. 15, pp. 2043 - 2052, 2002.
- [280] Z. P. Chow, Z. Ahmad and K. J. Wong, "Experimental Study on the Mechanical Properties of Glass Fibre Reinforced Epoxy at Elevated Temperature," *International Journal of Automotive and Mechanical Engineering*, vol. 16, no. 3, pp. 7108 - 7120, 2019.
- [281] Y. Dobah, Y. Ghazzawi and M. Bourchak, "Mechanical properties of hybrid carbon fiber reinforced polyethylene and epoxy composites," *Journal of Engineering and Applied Sciences*, vol. 10, no. 16, pp. 7053 - 7057, 2015.
- [282] L. A. Savas, U. Tayfun and M. Dogan, "The use of polyethylene copolymers as compatibilizers in carbon fiber reinforced high density polyethylene composites," *Composites Part B*, vol. 99, pp. 188 - 195, 2016.
- [283] E. Scippa and K. Piekarski, "Carbon fiber reinforced polyethylene for possible orthopedic uses," *Journal of Biomedical Materials Research*, vol. 7, no. 1, pp. 59 - 70, 1973.
- [284] R. Huang, X. Xu, S. Lee, Y. Zhang, B.-J. Kim and Q. Wu, "High Density Polyethylene Composites Reinforced with Hybrid Inorganic Fillers: Morphology, Mechanical and Thermal Expansion Performance," *Materials*, vol. 6, pp. 4122 - 4138, 2013.
- [285] Z. Xu and C. Gao, "Graphene fiber: a new trend in carbon fibers," *Materials Today*, vol. 18, no. 9, pp. 480 - 492, 2015.
- [286] R. W. Fairbridge, "Silica, silicate," in *Encyclopedia of Planetary Science. Encyclopedia of Earth Science*, Germany, Springer, 1997, p. 737.
- [287] O. Aydın, A. Kocaveli, Ö. Gürsoy , E. Erzi and D. Dışpınar, "Aluminum Matrix Graphene-Reinforced Composite Materials," in *Shape Casting*, Cham, Springer, 2019, pp. 365 - 371.
- [288] N. Connor, "Graphene – Density – Strength – Melting Point," Material Properties, 11 May 2021. [Online]. Available: <https://material-properties.org/graphene-density-strength-melting-point/>. [Accessed 15 January 2022].

- [289] N. Saifuddin, A. Z. Raziah and A. R. Junizah, "Carbon Nanotubes: A Review on Structure and Their Interaction with Proteins," *Journal of Chemistry*, vol. 13, pp. 1 - 18, 2012.
- [290] P. G. Collins and P. Avouris, "Nanotubes for Electronics," *Scientific American*, vol. 283, no. 6, pp. 62 - 69, 2000.
- [291] C. Laurent, E. Flahaut and A. Peigney, "The weight and density of carbon nanotubes versus the number of walls and diameter," *Carbon*, vol. 48, no. 10, pp. 2994 - 2996, 2010.
- [292] K. Fujii and H. Fujisaki, "Flow Properties and Yield Stresses of Dilute Sodium-Montmorillonite Suspensions," *Clay Science*, vol. 11, pp. 271 - 283, 2000.
- [293] "Montmorillonite," Mindat.org, 2022. [Online]. Available: <https://www.mindat.org/min-2821.html>. [Accessed 20 January 2022].
- [294] A. R. Schwyter and K. L. Vaughan, "Particle Density," in *Introduction to Soil Science Laboratory Manual*, USA, Libretexts, University of Wyoming, 2020, p. 5.4.
- [295] O. L. Manevitch and G. C. Rutledge, "Elastic Properties of a Single Lamella of Montmorillonite by Molecular Dynamics Simulation," *J. Phys. Chem. B*, vol. 108, no. 4, pp. 1428 - 1435, 2004.
- [296] S. Lowell, J. E. Shields, M. A. Thomas and M. Thommes, "Density Measurement," in *Characterization of Porous Solids and Powders: Surface Area, Pore Size and Density*, Netherlands, Kluwer Academic, 2004, pp. 326 - 338.
- [297] Y. H. Hu and E. Ruckenstein, "Pore Size Distribution of Single-Walled Carbon Nanotubes," *Ind. Eng. Chem. Res.*, vol. 43, no. 3, pp. 708 - 711, 2004.
- [298] Z. Zhang, H. Jin, C. Wu and J. Ji, "Efficient production of high-quality few-layer graphene using a simple hydrodynamic-assisted exfoliation method," *Nanoscale Research Letters*, vol. 13, no. 416, pp. 1-8, 2018.
- [299] J. Gigault, I. L. Hécho, S. Dubascoux, M. Potin-Gautier and G. Lespes, "Single walled carbon nanotube length determination by asymmetrical-flow field-flow fractionation hyphenated to multi-angle laser-light scattering," *Journal of Chromatography A*, vol. 1217, no. 50, pp. 7891 - 7897, 2010.
- [300] I. Zaman, T. T. Phan, H.-C. Kuan, Q. Meng, L. T. B. La, L. Luong, O. Yousf and J. Ma, "Epoxy/graphene platelets nanocomposites with two levels of interface strength," *Polymer*, vol. 52, no. 7, pp. 1603 - 1611, 2011.
- [301] C. Salom, M. G. Prolongo, A. Toribio, A. J. Martínez-Martínez, I. Aguirrede Cárcer and S. G. Prolongo, "Mechanical properties and adhesive behavior of epoxy-graphene nanocomposites," *International Journal of Adhesion and Adhesives*, vol. 84, pp. 119 - 125, 2018.

- [302] Q. Cheng, J. Bao, J. Park, Z. Liang, C. Zhang and B. Wang, "High Mechanical Performance Composite Conductor: Multi-Walled Carbon Nanotube Sheet/Bismaleimide Nanocomposites," *Advanced Functional Materials*, vol. 19, pp. 3219 - 3225, 2009.
- [303] R. J. Mora, J. J. Vilatela and A. H. Windle, "Properties of composites of carbon nanotube fibres," *Composites Science and Technology*, vol. 69, no. 10, pp. 1558 - 1563, 2009.
- [304] X. Wang, P. D. Bradford, W. Liu, H. Zhao, Y. Inoue, J.-P. Maria, Q. Li, F.-G. Yuan and Y. Zhu, "Mechanical and electrical property improvement in CNT/Nylon composites through drawing and stretching," *Composites Science and Technology*, vol. 71, pp. 1677 - 1683, 2011.
- [305] T. H. Nam, K. Goto, Y. Yamaguchi, E. V. A. Premalal, Y. Shimamura, Y. Inoue, S. Arikawa, S. Yoneyama and S. Ogihara, "Improving mechanical properties of high volume fraction aligned multi-walled carbon nanotube/epoxy composites by stretching and pressing," *Composites Part B: Engineering*, vol. 85, pp. 15 - 23, 2016.
- [306] C. A. Cooper, S. R. Cohen, A. H. Barber and H. D. Wagner, "Detachment of nanotubes from a polymer matrix," *Applied Physics Letters*, vol. 81, no. 20, pp. 3873 - 3875, 2002.
- [307] Q. Zhang, S. Rastogi, D. Chen, D. Lippits and P. J. Lemstra, "Low percolation threshold in single-walled carbon nanotube/high density polyethylene composites prepared by melt processing technique," *Carbon*, vol. 44, no. 4, pp. 778 - 785, 2006.
- [308] G. Zhang, T. Wu, W. Lin, Y. Tan, R. Chen, Z. Huang, X. Yin and J. Qu, "Preparation of polymer/clay nanocomposites via melt intercalation under continuous elongation flow," *Composites Science and Technology*, vol. 145, pp. 157 - 164, 2017.
- [309] V. Pettarin, P. M. Frontini, V. J. R. R. Pita, M. L. Dias and V. F. Diaz, "Polyethylene/(organo-montmorillonite) composites modified with ethylene/methacrylic acid copolymer: Morphology and mechanical properties," *Composites Part A: Applied Science and Manufacturing*, vol. 39, no. 12, pp. 1822 - 1828, 2008.
- [310] S. K. Samal, S. K. Nayak and S. Mohanty, "Polypropylene Nanocomposites: Effect of Organo-modified Layered Silicates on Mechanical, Thermal & Morphological Performance," *Journal of Thermoplastic Composite Materials*, vol. 21, no. 3, pp. 243 - 263, 2008.
- [311] L. A. Novokshonova, P. N. Brevnov, V. G. Grinev, S. N. Chvalun, S. M. Lomakin, A. N. Shchegolikhin and S. P. Kuznetsov, "Polyethylene-Layered Silicate Nanocomposites: Synthesis, Structure, and Properties," *Nanotechnologies in Russia*, vol. 3, no. Nos 5-6, pp. 330 - 343, 2008.
- [312] R. T. Tebeta, A. M. Fattahi and N. A. Ahmed, "Experimental and numerical study on HDPE/SWCNT nanocomposite elastic properties considering the processing techniques effect," *Microsystem Technologies*, vol. 26, pp. 2423 - 2441, 2020.

- [313] B. Qi, Q. X. Zhang, M. Bannister and Y. W. Mai, "Investigation of the mechanical properties of DGEBA-based epoxy resin with nanoclay additives," *Composite Structures*, vol. 75, no. 1-4, pp. 514 - 519, 2006.
- [314] M. A. L. Machado, L. Valentini, J. Biagiotti and J. M. Kenny, "Thermal and mechanical properties of single-walled carbon nanotubes–polypropylene composites prepared by melt processing," *Carbon*, vol. 43, no. 7, pp. 1499 - 1505, 2005.
- [315] D. McIntosh, V. N. Khabashesku and E. V. Barrera, "Benzoyl Peroxide Initiated In Situ Functionalization, Processing, and Mechanical Properties of Single-Walled Carbon Nanotube–Polypropylene Composite Fibers," *J. Phys. Chem. C*, vol. 111, pp. 1592 - 1600, 2007.
- [316] M. Moniruzzaman, J. Chattopadhyay, E. W. Billups and K. I. Winey, "Tuning the Mechanical Properties of SWNT/Nylon 6,10 Composites with Flexible Spacers at the Interface," *Nano Letters*, vol. 7, no. 5, pp. 1178 - 1185, 2007.
- [317] J. Gao, B. Zhao, M. E. Itkis, E. Bekyarova, H. Hu, A. Yu and R. C. Haddon, "Chemical Engineering of the Single-Walled Carbon Nanotube–Nylon 6 Interface," *J. Am. Chem. Soc.*, vol. 128, no. 23, pp. 7492 - 7496, 2006.
- [318] J. Zhu, J. Kim, H. Peng, J. L. Margrave, V. N. Khabashesku and E. V. Barrera, "Improving the Dispersion and Integration of Single-Walled Carbon Nanotubes in Epoxy Composites through Functionalization," *Nano Letters*, vol. 3, no. 8, pp. 1107 - 1113, 2003.
- [319] D. Penumadu, A. Dutta, G. M. Pharr and B. Files, "Mechanical properties of blended single-wall carbon nanotube composites," *Journal of Materials Research*, vol. 18, no. 8, pp. 1849 - 1853, 2003.
- [320] J. A. King, D. R. Klimek, I. Miskioglu and G. M. Odegard, "Mechanical Properties of Graphene Nanoplatelet/Epoxy Composites," *Journal of Applied Polymer Science*, vol. 128, no. 6, pp. 4217 - 4223, 2013.
- [321] C. Vallés, A. M. Abdelkader, R. J. Young and I. A. Kinloch, "Few layer graphene–polypropylene nanocomposites: the role of flake diameter," *Faraday Discuss*, vol. 173, pp. 379 - 390, 2014.
- [322] J.-Z. Liang, Q. Du, G. C.-P. Tsui and C.-Y. Tang, "Tensile properties of graphene nano-platelets reinforced polypropylene composites," *Composites Part B: Engineering*, vol. 95, pp. 166 - 171, 2016.
- [323] T. Bansala, P. Verma, A. Vashisth, J. T. Hope, S. Yakovlev, S. Uppili, M. J. Green and R. A. Hule, "High-density polyethylene reinforced by low loadings of electrochemically exfoliated graphene via melt recirculation approach," *Journal of Applied Polymer Science*, vol. 138, no. 20, pp. 1 - 12, 2021.

- [324] N. L. Batista, E. Helal, R. S. Kurusu, N. Moghimian, E. David, N. R. Demarquette and P. Hubert, "Mass-Produced Graphene—HDPE Nanocomposites: Thermal, Rheological, Electrical, and Mechanical Properties," *Polymer Engineering and Science*, vol. 59, no. 4, pp. 675 - 682, 2019.
- [325] N. Yesildag, C. Hopmann, M. Adamy and C. Windeck, "Properties of Polyamide 6-Graphene-Composites Produced and Processed on Industrial Scale," *AIP Conference Proceedings*, vol. 1914, no. 1, pp. 150001(1- 5), 2017.
- [326] R. Wang, L. Wu, D. Zhuo, J. Zhang and Y. Zheng, "Fabrication of Polyamide 6 Nanocomposite with Improved Thermal Conductivity and Mechanical Properties via Incorporation of Low Graphene Content," *Industrial and Engineering Chemistry Research*, vol. 57, no. 32, pp. 10967 - 10976, 2018.